Master thesis in Acoustics

# Reciprocity calibration method for ultrasonic piezoelectric transducers in air

Eivind Mosland

June 2013

Department of Physics and Technology

UNIVERSITY OF BERGEN

# Preface

The experimental setup used is based on work by PhD student Espen Storheim [1] and master student Ørnulf Svan Amundsen [2]. It has been developed further by the present author in close collaboration with my fellow master student Rune Hauge [3, 4] and PhD student Storheim. The experiments and FE simulations have been performed in cooperation with Hauge. Parts of this thesis have been co-written with Hauge and are also included in [4], but in a slightly altered form. This include Chapters 3, 4, 5 and 6, as well as a section of Chapter 2. Chapters 3 and 4 are mainly written by the present author, except Section 3.7. Chapter 5 and Section 2.8 are mainly written by Hauge. Chapter 6 is co-written by Hauge and the present author.

This master thesis was performed as part of the project "Ultrasonic instrumentation for gas characterisation" under The Michelsen Centre for Industrial Measurement Science and Technology (MIMT).

Rune Hauge, I am extremely grateful for the possibility to work together with you throughout my time as a master student. Thank you for interesting discussions about professional and personal subjects, and for the possibility to share my anguish and happiness with you.

I would like to express my gratitude to my supervisor Magne Vestrheim and co-supervisors Per Lunde and Jan Kocbach for their insight and valuable feedback.

The help from Espen Storheim, partially funded by MIMT, have been invaluable. Thank you for your tips, tricks and skills when life is hard and problems arise in MATLAB, FEMP, LaTeX, or in the experimental setup.

It is greatly appreciate that Magne Aanes readily has shared his knowledge and answered many questions, especially with regard to the design and construction of the piezoelectric transducers.

I would also like to thank the rest of the Acoustics group at the University of Bergen. It has been a pleasure, and I'm looking forward to keeping in touch with you through Christmas parties (Julebord) and other social or professional events.

Staff engineer Per Heradstveit has been friendly and helpful when things need to be soldered, and the staff at the engineering workshop at the Department of Physics and Technology have been essential in the construction of the piezoelectric transducers and in the development of the measurement setup.

Most of all I would like to thank my fiancée Gunnhild Jette, forever my Goldcrest. If not for you...

Eivind Mosland, Bergen 17. June 2013

# Contents


**1 Introduction** **1**
- 1.1 Background and motivation . . . 1
- 1.2 Previous work . . . 2
- 1.3 Objectives . . . 3
- 1.4 Thesis outline . . . 3

**2 Theory** **5**
- 2.1 Three-transducer reciprocity calibration . . . 5
  - 2.1.1 Transmitting voltage response . . . 5
  - 2.1.2 Receiving voltage sensitivity . . . 6
  - 2.1.3 Spherical wave reciprocity . . . 6
  - 2.1.4 Measurement conditions and corrections . . . 6
  - 2.1.5 Derivation of the method at ideal measurement conditions . . . 7
  - 2.1.6 Corrections . . . 9
- 2.2 Absorption in air . . . 10
- 2.3 Diffraction correction . . . 11
  - 2.3.1 Khimunin's diffraction correction . . . 11
  - 2.3.2 Correction term . . . 11
- 2.4 Electronics . . . 13
  - 2.4.1 Cables . . . 13
  - 2.4.2 Transmitting electronics . . . 14
  - 2.4.3 Receiving electronics . . . 16
- 2.5 Reciprocity check . . . 18
- 2.6 Two-transducer reciprocity calibration . . . 18
- 2.7 Measurements with a calibrated microphone . . . 18
- 2.8 Finite element model . . . 19

**3 Experimental setup and measurement methods** **23**
- 3.1 Equipment . . . 24
- 3.2 Electrical measurement setup . . . 24
- 3.3 Acoustical measurement setup . . . 28
  - 3.3.1 Transmitting electronics . . . 29
  - 3.3.2 Cables . . . 30
  - 3.3.3 Transducers and positioning . . . 31
  - 3.3.4 Receiving electronics . . . 34
  - 3.3.5 The oscilloscope . . . 35
  - 3.3.6 Environmental parameters . . . 36
  - 3.3.7 Noise measurements . . . 37
  - 3.3.8 Data acquisition . . . 37
- 3.4 Measurements of dimension and mass . . . 38
- 3.5 Brüel & Kjær 4138 microphone systems . . . 38
  - 3.5.1 Calibration of the microphones using a pistonphone . . . 41
- 3.6 Piezoelectric ceramic disks . . . 42
- 3.7 Signal processing . . . 43
  - 3.7.1 Recorded waveforms . . . 43
  - 3.7.2 Calculation of $V_{pp}^{rec}$ - Fourier transform method . . . 44
  - 3.7.3 Calculation of $V_{pp}^{rec}$ - direct method . . . 45
  - 3.7.4 Calculation of SNR . . . 45

**4 Finite element simulation setup** **49**
4.1 FEMP 5.0 . . . 49
4.2 Simulation parameters . . . 49
4.3 Transducer meshing structures . . . 50
4.4 Material parameters . . . 52
4.4.1 The piezoelectric ceramic, Pz27 . . . 52
4.4.2 Air . . . 53
4.4.3 Matching layer . . . 53
4.4.4 Glue . . . 55
4.4.5 Housing . . . 55
4.4.6 Backing . . . 56

**5 Matching layer characterization** **59**
5.1 Theory . . . 59
5.1.1 Calculating the sound speed . . . 59
5.1.2 Characteristic impedance . . . 60
5.2 Measurement setup and methods . . . 61
5.3 Signal processing . . . 62
5.3.1 Zero crossing detection . . . 62
5.3.2 Measured waveforms, R3 . . . 63
5.3.3 Measured waveforms, R7 . . . 64
5.4 Results . . . 66
5.4.1 Sound speed . . . 66
5.4.2 Density - characteristic impedance . . . 67
5.5 Discussion . . . 67

**6 Transducer construction** **69**
6.1 Transducer design . . . 69
6.1.1 Piezoelectric ceramic disk . . . 70
6.1.2 Matching layer . . . 72
6.1.3 Backing layer and transducer housing . . . 78
6.2 The assembly process . . . 81

**7 Results - Piezoelectric ceramic disks** **85**
7.1 Electrical quantities . . . 85
7.2 Three-transducer reciprocity calibration . . . 90
7.2.1 Peak to peak detection . . . 91
7.2.2 SNR . . . 92
7.2.3 Generator voltage . . . 93
7.2.4 Effect of corrections . . . 93
7.2.5 Reciprocity check . . . 97
7.2.6 Measurement results and comparison with FE simulations . . . 98
7.3 Two-transducer calibration . . . 102
7.4 Measurement with a calibrated microphone . . . 102
7.4.1 SNR . . . 103
7.4.2 Results . . . 103
7.5 The modified method applied to the microphone systems . . . 105

**8 Results - Piezoelectric transducers** **109**
8.1 Three-transducer reciprocity calibration . . . 109
8.1.1 Peak to peak detection . . . 110
8.1.2 SNR . . . 110
8.1.3 Generator voltage . . . 111
8.1.4 Effect of corrections . . . 112
8.1.5 Reciprocity check . . . 115
8.1.6 Measurement results and comparison with FE simulations . . . 115
8.2 Measurement with a calibrated microphone . . . 118
8.2.1 SNR . . . 119
8.2.2 Results and comparison . . . 120
8.3 The modified method applied to the microphone system . . . 121

**9 Conclusions and further work** **125**

**Bibliography** **127**

**A MATLAB-scripts** **A-1**
A.1 Electrical measurements . . . A-1
A.1.1 impanal.m . . . A-1
A.2 Acoustical measurements . . . A-2
A.2.1 main.m . . . A-2
A.2.2 measurement_parameters.m . . . A-4
A.2.3 init_instruments.m . . . A-6
A.2.4 instruments.m . . . A-7
A.2.5 adjustAmplitude.m . . . A-9
A.2.6 adjustTime.m . . . A-10
A.2.7 DPO_les.m . . . A-11
A.2.8 instrument_shutdown.m . . . A-12
A.2.9 VaisalaHMT313.m . . . A-12
A.3 Signal processing . . . A-13
A.3.1 Khimunin_diffractioncorrection.m . . . A-13
A.3.2 absorpsjonluft.m . . . A-13
A.3.3 findPeakToPeak.m . . . A-14
A.3.4 findpeakToPeak_FFT.m . . . A-15
A.3.5 threeTransducerCalibration.m . . . A-15
A.3.6 calculateHvv.m . . . A-16
A.3.7 calculateHvvMic.m . . . A-18
A.3.8 correctionReceivingElectronics.m . . . A-20
A.3.9 correctionTransmittingElectronics.m . . . A-21
A.3.10 calculateJ.m . . . A-22
A.3.11 calculateY.m . . . A-22
A.3.12 correctionDiffraction.m . . . A-22
A.3.13 performCalibrationElm.m . . . A-23
A.3.14 performCalibrationMic.m . . . A-23
A.3.15 frequencyresponse_new.m . . . A-24
A.3.16 frequencyresponse_old.m . . . A-26
A.3.17 calculateSNR.m . . . A-27

**B FEMP-structures** **B-1**
B.1 `piezodiskwidefrontglue` . . . B-1
B.2 `transducervacuum` . . . B-2
B.3 `piezodiskwidefrontfluid` . . . B-4
B.4 `transducerfluid` . . . B-6

**C Paper submitted for the proceedings of the 36th Scandinavian Symposium on Physical Acoustics at Geilo, Norway, 3-6 February 2013** **C-1**

# List of Figures


2.1 Acoustic measurement required in the calibration . . . 7
2.2 Sketch of a piston source model . . . 11
2.3 Example plot - correction for diffraction . . . 12
2.4 A circuit description of a coaxial cable . . . 14
2.5 A circuit description of the transmitting electronics . . . 15
2.6 Circuit - signal generator to transmitting transducer . . . 15
2.7 A circuit description of the receiving electronics . . . 17

3.1 HP 4192A impedance analyzer used to measure the admittance of the transducers. . . . 25
3.2 Conductance and susceptance of a Pz27 piezoelectric ceramic disk at R1 . . . 25
3.3 As Fig. 3.2, but for R2 . . . 26
3.4 Holder for electrical measurement on a single piezoelectric disk . . . 26
3.5 Conductance and susceptance of a Pz27 piezoelectric ceramic disk at R1 . . . 27
3.6 As Fig. 3.5, but for R2 . . . 27
3.7 Holder for electrical measurement on a piezoelectric transducer . . . 28
3.8 An overview of the acoustical measurement setup. . . . 28
3.9 Block diagram of the acoustical measurement setup. . . . 29
3.10 Instruments used in the acoustic measurements . . . 30
3.11 The acoustical measurement setup . . . 32
3.12 A Brüel & Kjær 4138-A-015 microphone system mounted on an aluminium rod. . . . 32
3.13 A piezoelectric ceramic disk acting as a transmitting transducer. . . . 33
3.14 Two piezoelectric transducers developed during the present work . . . 33
3.15 Typical frequency response of B&K 2636 measurement amplifier. . . . 34
3.16 Amplifier correction. . . . 34
3.17 Example measured output voltage with 10 mV/div vertical scaling . . . 35
3.18 As Fig. 3.17, but with 2 mV/div vertical scaling. . . . 36
3.19 Calibration chart, Brüel & Kjær 4138 pressure-field microphone, serial no. 1832479 . . . 39
3.20 Calibration chart, Brüel & Kjær 4138 pressure-field microphone, serial no. 2784915 . . . 39
3.21 Comparison of calibrations of B&K 4138 and B&K 4138-A-015 . . . 40
3.22 Free-field correction curves for eighth-inch Condenser Microphone Type 4138 . . . 40
3.23 Open-circuit free-field frequency response for the two Brüel & Kjær 4138 . . . 41
3.24 Pz27 piezoelectric ceramic disk with and without wires . . . 42
3.25 An example waveform. . . . 43
3.26 An example waveform. . . . 44
3.27 The frequency spectra of the waveform in Fig. 3.25 . . . 45

4.1 Decimated meshes of `transducerfluid` and `piezodiskwidefrontfluid` . . . 51
4.2 An example mesh from `transducervacuum` . . . 52
4.3 Attenuation coefficient and mechanical quality factor for Aptflex R3 . . . 54
4.4 Mechanical quality factor, $Q_m$, of Aptflex R3 . . . 54

5.1 Illustration of the sound speed measurement cell. . . . 60
5.2 Block diagram of the measurement setup used in the sound speed measurements . . . 61
5.3 Transmitted voltage for case (1), $V_{el}^{(1)}$. Zero crossing marked with ×. . . . 63
5.4 Received voltage for case (1), $V_{ac}^{(1)}$. Zero crossing marked with ×. . . . 63
5.5 Transmitted voltage for case (2), $V_{el}^{(2)}$. Zero crossing marked with ×. . . . 63
5.6 Received voltage for case (2), $V_{ac}^{(2)}$. Zero crossing marked with ×. . . . 64
5.7 Transmitted voltage, $V_{el}$, for case (1). Zero crossing marked with ×. . . . 64
5.8 Received voltage, $V_{ac}$, for case (1). Zero crossing marked with ×. . . . 65

5.9 Transmitted voltage, $V_{el}$, for case (2). Zero crossing marked with ×. . . . . 65
5.10 Received voltage, $V_{ac}$, for case (2). Zero crossing marked with ×. . . . . 65
5.11 The calculated sound speed for R3, $c_{l,R3}$ . . . . . 66
5.12 The calculated sound speed for R7, $c_{l,R7}$ . . . . . 66

6.1 Sketch of (a) the assembled transducer and (b) transparent view of the assembled transducer. 69
6.2 Sketch of the assembled transducer. Side view cross section. . . . . 70
6.3 Measured and FE simulated conductance of Element #5, Element #15 and Element #20 71
6.4 Matching layer alternatives. Aptflex R3 is shown in (a) and Aptflex R7 is shown in (b). . 72
6.5 Simulated magnitude of (a) $H_{15}^{VV}$ and (b) $S_V$ for the frequency range 70 to 150 kHz . . . 73
6.6 Comparison of the magnitude of (a) $H_{15}^{VV}$ and (b) $S_V$ for a Pz27 piezoelectric ceramic disk 74
6.7 Comparison of of the simulated conductance of a Pz27 piezoelectric ceramic disk of dimensions 20 mm × 2 mm with an Aptflex R3 matching layer of dimensions 23.8 mm × 3.9 mm. Simulated with the structure vibrating in air and in vacuum. No silver conductive epoxy layer. `piezodiskwidefrontfluid` and `piezodiskwidefrontglue` is used (see Section 4.3). 75
6.8 Measured conductance and susceptance of the piezoelectric disk with attached front layer of Transducer No. 2. Check of repeatability. . . . . 75
6.9 Measured conductance and susceptance of the piezoelectric disk with attached front layer of Transducer No. 2 compared to FE simulations with the structure vibrating in vacuum, with a layer of silver conductive epoxy. The material data for Aptflex R3 supplied by PA [89] are used in FEM a), and adjusted material data for R3 are used in FEM b). Using `piezodiskwidefrontglue` in the simulations (see Section 4.3). . . . . 76
6.10 As Fig. 6.9, but for the element and matching layer of Transducer No. 1 and only simulations with the adjusted material data. . . . . 77
6.11 As Fig. 6.10, but for the element and matching layer of Transducer No. 3. . . . . 77
6.12 Comparison of measured conductance and susceptance of the Element #5 with matching layer (used in Transducer No. 1), Element #15 with matching layer (used in Transducer No. 2) and Element #20 with matching layer (used in Transducer No. 3). . . . . 78
6.13 Measured conductance of Transducer No. 1 compared to FE simulations of the transducer vibrating in vacuum. The simulations are performed for a simplified transducer, without the backing layer and the stainless steel lid. The adjusted material data for the Aptflex R3 matching layer and `transducervacuum` are used in the simulation (see Section 4.3. . . 79
6.14 As in Fig. 6.13, but for Transducer No. 2. . . . . 79
6.15 As in Fig. 6.13, but for Transducer No. 3. . . . . 80
6.16 Comparison of measured conductance and susceptance of Transducer No. 1, Transducer No. 2, and Transducer No. 3. . . . . 80
6.17 Picture of (a) the PVC mould used for centering the piezoelectric element on the matching layer and (b) the piezoelectric element with the soldered wire on one electrode and the matching layer fastened on the other electrode. . . . . 81
6.18 Picture of the Divinycell H130 backing layer. Machined out to be assembled into the steel casing. Figure (a) shows the rearmost side of the backing layer, with the cone visible. (b) shows the face of the backing layer which is connected to the piezoelectric element. . . . . 82
6.19 Picture showing the rear of the housing, with the H130 backing material inserted. The wire from the piezoelectric element is seen extended through the middle of the backing. Picture showing the steel lid containing the BNC connector. The connector is hindered from rotating by use of a screw. . . . . 82
6.20 Picture of the assembled Transducer No. 1 suspended in the measurement setup. (a) shows the front of the transducer, while (b) shows the back of the transducer, with the coaxial cable connected to the BNC connector. . . . . 83

7.1 Conductance and susceptance of Element #6 for the frequency range 50 kHz to 300 kHz. Measured before and after the wires are soldered onto the element. Compared with FE simulations of the element vibrating in air. . . . . 86
7.2 As Fig. 7.1, but for the frequency range 94 kHz to 103 kHz, around R1. . . . . 86
7.3 As Fig. 7.1, but for the frequency range 240 kHz to 260 kHz, around R2. . . . . 87
7.4 Conductance and susceptance of Element #10 for the frequency range 50 kHz to 300 kHz. Measured before and after the wires are soldered onto the element. Compared with FE simulations of the element vibrating in air. . . . . 87
7.5 As Fig. 7.4, but for the frequency range 94 kHz to 103 kHz, around R1. . . . . 88
7.6 As Fig. 7.4, but for the frequency range 240 kHz to 260 kHz, around R2. . . . . 88

7.7 Conductance and susceptance of Element #16 for the frequency range 50 kHz to 300 kHz. Measured before and after the wires are soldered onto the element. Compared with FE simulations of the element vibrating in air. . . . . 89
7.8 As Fig. 7.7, but for the frequency range 94 kHz to 103 kHz, around R1. . . . . 89
7.9 As Fig. 7.7, but for the frequency range 240 kHz to 260 kHz, around R2. . . . . 90
7.10 Measured $H_{1m5m}^{VV}$ for measurement No. 1. Result obtained by the direct method and the FFT method, with open-circuit generator voltages $V_{pp}$ = 2 V (upper) and $V_{pp}$ = 20 (lower). 91
7.11 SNR for a measurement No. 4, where Element #16 transmits to Element #6 with a separation distance of 77 cm. . . . . 92
7.12 Measured voltage to voltage transfer function for measurement No. 1. Obtained with two different generator voltages. In the following, measurements with the two different generator voltages are combined using the frequencies shown with the symbol '×' as limits. 93
7.13 Transmitting voltage response of Element #16. $S_V^{T3}$ calculated with all corrections compared to $S_V^{T3}$ calculated with all correction and $C_\alpha$ = 1. The difference observed between these two calculations is shown in the lower plot. The demarcations between the use of $V_{pp}$ = 20 V and $V_{pp}$ = 2 V open-circuit generator voltage are shown using the symbol '×'. 94
7.14 As Fig. 7.13, but for the voltage to voltage transfer function accounting for receiving electronics, $H_{5m5}^{VV}$. . . . . 95
7.15 As Fig. 7.13, but for the voltage to voltage transfer function accounting for transmitting electronics, $H_{1m1}^{VV}$. . . . . 95
7.16 As Fig. 7.13, but for the correction for diffraction correction and near-field effects, $C_{dif}$. . 96
7.17 The magnitude and phase of $p_{ax}$ for Element #16 radiating at the peak frequency of R1, $f$ = 98.2 kHz. Simulated in FEMP 5.0. The Rayleigh length of 9.2 cm is shown, as well as the far-field values to which the magnitude (multiplied by $z$) and phase converge. . . . . 97
7.18 As Fig. 7.17, but for the peak frequency of R2 in the simulation, $f$ = 249.2 kHz, with $r_R$ = 18.8 cm. . . . . 97
7.19 Reciprocity check of a the transducer pair Element #6 and Element #16. Showing the electrical transfer impedances of two measurements performed with the transducers interchanged (See Eq. (2.70)). The upper plot is for measurements with an open-circuit generator voltage of $V_{pp}$ = 2 V, while $V_{pp}$ = 20 V is used in the lower plot. . . . . 98
7.20 Comparison of $S_V$ and $M_V$ for Element #6, Element #10, and Element #16, determined by the modified three-transducer reciprocity calibration method. . . . . 99
7.21 Transmitting voltage response and free-field open-circuit receiving voltage sensitivity for Element #6, obtained through the modified three-tranducer reciprocity calibration and compared to FE simulations of Element #6. . . . . 100
7.22 As Fig. 7.21, but for Element #10. . . . . 101
7.23 As Fig. 7.21, but for Element #16. . . . . 101
7.24 The results for $S_V$ and $M_V$ for Element #16, obtained using the modified three-transducer reciprocity calibration method and the modified two-transducer reciprocity calibration method. Two-trans a) is the result for measurement No. 2, and Two-trans b) is the result for measurement No. 3. . . . . 102
7.25 SNR for Element #16 transmitting to B&K 4138-A-015 with a separation distance of 44 cm. Measurements with open-circuit generator voltages of $V_{pp}$ = 2 V and $V_{pp}$ = 20 V are shown. . . . . 103
7.26 The transmitting voltage response of Element #10, obtained with measurement with B&K 4138 + B&K 2633. Two different open-circuit generator voltages are used. Compared to measurements using the modified three-transducer reciprocity calibration method. . . . . 104
7.27 The transmitting voltage response of Element #6, obtained by measurements with an open-circuit generator voltage of $V_{pp}$ = 2 V and the two different microphone systems. Compared to measurements using the modified three-transducer reciprocity calibration method. . . . . 104
7.28 As Fig. 7.27, but for Element #16. . . . . 105
7.29 Free-field open-circuit receiving voltage response of B&K 4138 + B&K 2633. Comparison of results from the modified three-transducer reciprocity calibration method and calibration data supplied by B&K. . . . . 105
7.30 As Fig. 7.29, but for the microphone system B&K 4138-A-015. The calibration supplied by B&K only extends to 200 kHz. . . . . 106

8.1 The measured $H_{1m5m}^{VV}$ of measurement No. 1, calculated using either the direct method or FFT method to determine the peak to peak voltage. The upper part is with a open-circuit generator voltage of $V_{pp}$ = 2 V, and the lower part is with $V_{pp}$ = 20 V. . . . . 110

8.2 SNR for a measurement where Transducer No.2 transmits to Transducer No. 1, with a separation distance of 66 cm and an open-circuit generator voltage of $V_{pp}$ = 2 V and $V_{pp}$ = 20 V. . . . . 110
8.3 Comparison of the SNR obtained in the measurement with Transducer No. 2 to Transducer No.1 (Fig. 8.2) and with Element #16 to Element #6 (Fig. 7.11). The former at a separation distance of 66 cm, and the latter at a separation distance of 77 cm. Both with an open-circuit generator voltage $V_{pp}$ = 20 V. . . . . 111
8.4 The measured $H^{VV}_{1m5m}$ of measurement No. 1, obtained with $V_{pp}$ = 2 V and $V_{pp}$ = 20 V open-circuit generator voltage. Demarcation frequencies, as given in Table 8.2, are indicated by the symbol '×'. . . . . 112
8.5 $S_V$ of Transducer No. 2 calculated with all corrections compared to $S_V$ calculated with all corrections, but with $C_\alpha$ = 1. The effect of this is shown in the lower plot. The demarcation frequencies between the different generator voltages (see Table 8.2) are shown by the symbol '×'. . . . . 113
8.6 As Fig. 8.5, but for $C_{dif}$. . . . . 113
8.7 As Fig. 8.5, but for $H^{VV}_{5m5}$. . . . . 114
8.8 As Fig. 8.5, but for $H^{VV}_{1m1}$. . . . . 114
8.9 Reciprocity check of the transducer pair Transducer No. 2 and Transducer No. 3. Showing the electrical transfer impedances of two measurements performed with the transducers interchanged (See Eq. (2.70)). In the upper plot an open-circuit generator voltage of $V_{pp}$ = 2 V is used, and $V_{pp}$ = 20 V is used in the lower plot. . . . . 115
8.10 Comparison of $S_V$ and $M_V$ for the three piezoelectric transducers, found using the modified three-transducer reciprocity calibration method. . . . . 116
8.11 The magnitude of $S_V$ and $M_V$ of Transducer No. 1, obtained by the modified three-transducer reciprocity calibration method and compared with FE simulations. FEM a) is the transducer vibrating in air and FEM b) is the transducer vibrating in vacuum. . . . . 117
8.12 As Fig. 8.13, but for Transducer No. 2. . . . . 117
8.13 As Fig. 8.13, but for Transducer No. 3. . . . . 118
8.14 Signal to noise ratio for measurements performed with Transducer No.3 as transmitter and B&K 4138-A-015 as receiver, with a separation distance of 44 cm and an open-circuit generator voltage of $V_{pp}$ = 2 V and $V_{pp}$ = 20 V. . . . . 119
8.15 Comparison of the SNR obtained in measurements with Transducer No. 3 to B&K 4138-A-015 (Fig. 8.14) and Element #16 to B&K 4138-A-015 (Fig. 7.25). The former at a separation distance of 55 cm, and the latter at a separation distance of 44 cm. Both with an open-circuit generator voltage $V_{pp}$ = 20 V. . . . . 120
8.16 Transmitting voltage response of Transducer No. 1 (T2) measured by B&K 4138-A-015 for the frequency range 50 kHz to 200 kHz. Two different open-circuit generator voltages, $V_{pp}$ = 2 V and $V_{pp}$ = 20 V. . . . . 120
8.17 As Fig. 8.16, but for Transducer No. 2 (T3). . . . . 121
8.18 As Fig. 8.16, but for Transducer No. 3 (T1). . . . . 121
8.19 Free-field open-circuit receiving voltage sensitivity of B&K 4138-A-015, found by the three-transducer reciprocity calibration method with open-circuit generator voltage $V_{pp}$ = 2 V and $V_{pp}$ = 20 V, compared to $M_V$ supplied by B&K and calibrated by use of a pistonphone. 122
8.20 As Fig. 8.19, but with a combination of the two generator voltages. Transition between the different voltage are denoted by the symbol '×'. . . . . 122
8.21 As Fig. 8.20, but compared to the results obtained from a modified three-transducer calibration method using piezoelectric disks. . . . . 123

# List of Tables


2.1 Description of variables in Eq. (2.75), and reference to the respective equation numbers they are defined at in [24] . . . 19

3.1 Equipment used in the measurements . . . 24
3.2 Output and input impedance of equipment . . . 29
3.3 Coaxial cable type RG58, typical specifications [45] . . . 30
3.4 Overview of the approximate lengths of the RG58 coaxial cables used in the different transducer configurations, see Table 3.5. . . . 31
3.5 Transducer configurations used in measurements. . . . 31
3.6 Microphone systems used in the measurements . . . 38
3.7 Dimensions of Pz27 piezoelectric ceramic disks . . . 43
3.8 Calculation intervals used in the signal processing. . . . 44

4.1 Material data for the piezoelectric material type Pz27. The adjusted data set is used in the FE simulations. . . . 53
4.2 Material data used to model the fluid medium, air. . . . 53
4.3 Material data used when modelling Aptflex R3 and Aptflex R7. . . . 55
4.4 Material data used when modelling the silver conductive epoxy. . . . 55
4.5 Material data used when modelling the stainless steel, grade 316, housing. . . . 56
4.6 Material data used when modelling the Divinycell H130 backing. . . . 56

5.1 The instruments used for the sound speed measurements. . . . 62
5.2 Averaged sound speed results. . . . 67
5.3 The dimensions and mass of the matching layers investigated in the present work. . . . 67

6.1 Dimensions of the constructed transducers. Measured with a Mitutoyo MDH-25M digimatic micrometer (see Section 3.4). . . . 74

7.1 Dimensions of Pz27 piezoelectric ceramic disks . . . 85
7.2 Three-transducer reciprocity calibration of Pz27 piezoelectric ceramic disks. . . . 91
7.3 Demarcation frequencies used when combining measurements with different open-circuit generator voltages. . . . 93
7.4 Measurements on Pz27 piezoelectric ceramic disks with calibrated microphones. . . . 103
7.5 Three-transducer reciprocity calibration of B&K 4138 + B&K 2633. . . . 105
7.6 Three-transducer reciprocity calibration of B&K 4138-A-015. . . . 106

8.1 Three-transducer reciprocity calibration of the piezoelectric transducers developed during this work. . . . 109
8.2 Demarcation frequencies used when combining measurements with different open-circuit generator voltages. . . . 112
8.3 Measurements on the piezoelectric transducer developed as part of the present work with calibrated microphones. . . . 119
8.4 Three-transducer reciprocity calibration of B&K 4138-A-015. . . . 121

# Chapter 1

# Introduction

## 1.1 Background and motivation

Ultrasonic measurement technology is used in many different application areas, such as the petroleum, marine and medical industries. Calibration of the transducers used is essential in order to get reliable and accurate results from the measurements. The present work concerns transducers for use in gas at ultrasonic frequencies, and the calibration of these. It is motivated in part by the use of ultrasonic fiscal flow measurements of gas [5–7] and the need for increased precision in measurement of gas characteristics [8, 9].

A wide range of calibration methods exists for transducers in gas used in the audible frequency range and at lower ultrasonic frequencies. The characteristics of the transducers can for instance be determined by use of a reference condenser microphone, through reciprocity calibration [10–12], or by an electrostatic actuator [13], often in combination with a pistonphone. Other methods used to calibrate ultrasonic transducers for use in gas are [14] impedance measurements, tone burst testing, thermal calorimetry, time delay spectrometry, vector calibration, dynamic calibration, beam profiling, and photoacoustic methods [15]

Difficulties concerning these calibration techniques arise when used to perform calibrations for frequencies exceeding approximately 150 kHz. This is in part due to the short wavelength and high attenuation in gas, and the relatively low sensitivity of many gas-coupled transducers caused by acoustical impedance mismatch between the transducers and gas [14, 16]. In addition are not reference condenser microphones readily available for higher ultrasonic frequencies [16].

Accurate calibration of transducers for use in gas at ultrasonic frequencies exceeding 150 kHz is of interest in applications such as fiscal metering, gas characterization, measurement of calorific value of natural gas, and monitoring of airborne ultrasound sources [5–9, 14, 16–19]. Several alternative calibration techniques for higher frequencies have been presented in the literature. Reference piezopolymer (PVDF) hydrophones for use in gas at higher frequencies have been developed by Hayward and co-workers, e.g. Gachagan *et al.* [14] and Galbraith *et al.* [20]. Preliminary results have been presented by Matar *et al.* [18] using optical tomography, requiring a controlled temperature and a sound path screened from the surroundings. Bashford *et al.* have measured the sound field with a miniature electrostatic probe [21]. The standard free-field reciprocity calibration method, referred to as the three-transducer reciprocity calibration method in the present work, has been extended to frequencies above 100 kHz by Anderson *et al.* [16] for electrostatic transducers, comparing measurements to model predictions. This method has later been used e.g. by Schröder *et al.* [22]. An advantage with the three-transducer reciprocity calibration method is the fact that only three electroacoustic transducers and commonly available laboratory instrumentation are needed to perform the procedure.

In the present work the three-transducer reciprocity calibration method for use in gas at ultrasonic frequencies is investigated further, for frequencies upwards to 300 kHz[1] and using piezoelectric transducers. Piezoelectric transducers are widely used in industrial applications, e.g. due to their chemical resistance and performance at elevated pressures and temperatures.

Advanced theoretical and numerical modelling is frequently used in the development of transducers to predict performance and characteristics. Moreover, mathematical models can be combined with experimental measurements to improve the transducer construction or the measurement methods and setup. As a result of such models a better interpretations of measurements may be achieved, thus increasing the understanding of the physical properties and behaviour of the object under study. One widely used

[1] This upper frequency is chosen due to the increasingly significant impact of absorption at higher frequencies and because of limitations in the current measurement and simulation setups.

method is finite element (FE) modelling. This powerful modelling method has been subject to extensive research for more than forty years, and is well suited for use in ultrasonic applications [23].

The use of piezoelectric transducers enables comparison of measurements to simulations performed in the FE simulation tool FEMP (*Finite element modelling of piezoelectric structures*) [24, 25]. FEMP is developed at UiB[2]/CMR[3] and specifically targeted at modelling axisymmetric piezoelectric transducers.

## 1.2 Previous work

The theoretical basis for the three-transducer reciprocity calibration method for microphones was initially presented by MacLean [26] in 1940. It was soon after implemented experimentally by Rudnick and Stein for frequencies up to 100 kHz [27], correcting for absorption, and expanded theoretically by Wathen-Dunn [28]. The method was standardized by the American National Standards Institute (ANSI) in 1966 [10], and later by the International Electrotechnical Commission (IEC) for 1-inch condenser microphones [29, 30]. The IEC standard [29] was later replaced by [11]. These standards are intended for use on standard laboratory microphones in the audible frequency range.

Several descriptions of experimental methods for reciprocity calibration used by national laboratories of metrology have since been published, e.g. Burnett and Nedzelnitski [31] of the National Bureau of Standards in the United States, which include methods for 1/2-inch microphones.

Standard three-transducer reciprocity calibrations are intended to be performed in an anechoic room using continuous waves [10], but reflections from the walls and possible coupling, with resulting standing waves between the two transducers, may present challenges. The use of a time selective technique to correct for these effects was described by Barrera-Figueroa [12] for laboratory standard microphones operating at audio frequencies.

The three-transducer reciprocity calibration method was performed on 1/4-inch condenser microphones for ultrasonic frequencies up to 160 kHz by Bouaoua [19], using continuous waves and an anechoic room. This study was motivated by the need for monitoring of ultrasonic noise and possible health hazards, and effects of e.g. standing waves and distortion of the driving voltage were examined.

Anderson *et al.* [16] extended the three-transducer reciprocity calibration technique to the frequency range 100-500 kHz, using pulsed sound waves, correcting for the absorption, and accounting for diffraction effects. Measurements were performed on electrostatic transducers and compared to model prediction, reporting an agreement within 2.5 dB and a maximum difference of 7 % between resonance frequencies obtained by admittance measurements and model predictions. The diffraction effects were included in [16] by treating the transmitter and receiver as two circular pistons of equal radius in rigid baffles of infinite extent, thus enabling the use of the diffraction correction in [32].

Circular electrostatic transducers [33] with a diameter of 5.08 cm and a separation distance of approximately 14 cm were used in the measurements in [16], generating tone bursts of 20 cycles to avoid standing waves and minimize reflections. Results were presented for the magnitude of the pressure response and transmit sensitivity. The mathematical model to which the measurements in [16] were compared to make use of a lumped parameter approximation to predict the performance of an electrostatic transducer [33]. The mechanical damping of the model was adjusted in order to improve agreement between model predictions and the transducers' performance near resonance. Only comparison with this mathematical model were used to verify the calibration, with no comparison to results obtained with other experimental methods.

To the author's knowledge, the method implemented by Anderson *et al.* [16] has so far only been compared to model predictions for electrostatic transducers, and it has not been compared to experimental results obtained by use of an independent measurement method. Furthermore, the calibration method does not include phase measurements.

A need is seen for further studies of the three-transducer reciprocity calibration method for use in gas at ultrasonic frequencies, e.g. to include the phase, improve the accuracy of the method, and obtain better correspondence between measurements and FE simulations.

The simulation tool FEMP [24, 25] has been used to investigate piezoelectric structures for more than fifteen years at UiB and CMR. Extensive work has been performed on piezoelectric ceramic disks and transducers, using both the piezoelectric material Pz27 from Ferroperm [34] and PZT-5A from MTC[4]. Acoustical and electrical measurements have been compared to simulations in FEMP, e.g. in [2, 35–39]. Varying agreement between model predictions and acoustical measurements have been reported, with an increasing deviation at higher frequencies reported in [2, 37, 38], and thus further studies are needed.

[2]University of Bergen, Bergen, Norway
[3]Christian Michelsen Research, Bergen, Norway
[4]Morgan Technical Ceramics, Stourport, England

## 1.3 Objectives

The main objectives in the present work is to develop and implement a modified three-transducer reciprocity calibration method for use in air at ultrasonic frequencies, and to compare the experimental results to both model predictions and separate acoustical measurements using calibrated condenser microphones. The magnitude of the transducers' transmitting voltage responses and free-field open-circuit receiving voltage sensitivities are to be measured. The frequency range to be studied is 50 kHz to 300 kHz. It is focused on the frequencies around 100 kHz, where comparison with measurements with calibrated condenser microphones can be made.

Piezoelectric transducers are widely used in industrial applications and are to be studied in the present work, enabling FE analysis in FEMP 5.0 [24, 25]. FE simulations are to be compared to measurements of acoustical and electrical quantities. Circular piezoelectric ceramic disk of the material Pz27 [34] and piezoelectric transducers are to be used. In-house constructed piezoelectric transducers are to be developed for this work with the goal of increasing the signal to noise ratio (SNR) and bandwidth of the first radial mode (R1), thus improving the performed calibrations. The use of piezoelectric transducers where the dimensions and materials are known, are of importance in the FE simulations to be performed in FEMP 5.0 [24, 25].

Corrections for absorption in air and near-field effects are to be included in the modified three-transducer reciprocity calibration method, and in addition effects of the receiving and transmitting electronics are to be studied and accounted for. Effects of receiving and transmitting electronics consisting of essentially the cables connecting the transducers to the instruments, and the finite termination of the receiving transducer, are to be investigated. Near-field effects are accounted for by use of the diffraction correction defined in [40, 41].

Overall further objectives in the Acoustics group at UiB are to quantify the measurement uncertainties in the method, include the phase in the experimental measurements, and develop multiple sets of piezoelectric transducers to improve the accuracy across the whole frequency range. The FE analysis is expected to be even more important in this further development of the method.

## 1.4 Thesis outline

Chapter 2 covers the theoretical basis of this work, focusing on the modifications of the three-transducer reciprocity calibration method. The experimental setup and measurement methods used are described in Chapter 3, as well as the piezoelectric ceramic disks and condenser microphone systems. A brief description of the signal processing is included. In Chapter 4 the finite element simulation setup is discussed, including the simulation tool, structures and material parameters. Chapter 5 covers the material characterization of the matching layers in the transducers. The development and construction of piezoelectric transducers are presented and discussed in Chapter 6. In Chapter 7 and 8 the results from the modified three-transducer reciprocity calibration method are shown and discussed, for piezoelectric ceramic disks and piezoelectric transducers, respectively. This includes comparison with FE simulations and measurements with a calibrated condenser microphones system. Conclusions are drawn in Chapter 9, and suggestions for future work are presented.

The MATLAB-scripts used in the acoustical measurements, electrical measurements and post-processing are included in Appendix A. In Appendix B the files for the FEMP-structures are given. Preliminary results [42] were presented at the 36th Scandinavian Symposium on Physical Acoustics at Geilo, Norway, 3-6 February 2013. A paper submitted for the proceedings is included in Appendix C.

# Chapter 2

# Theory

This chapter presents the theoretical basis needed to perform the experiments and simulations in this work. A modification of the conventional three-transducer reciprocity calibration method described in the standards [10, 11, 43] is conducted, and the modified method is used in the experimental measurements. An important part of the modifications are corrections to account for the lack of ideal measurement conditions.

The modified three-transducer reciprocity calibration method is presented and derived in Section 2.1. The inclusion of the correction factors are also described in this section. In Sections 2.2, 2.3 and 2.4 the correction factors are derived. The effects discussed are absorption, near-field effects and electronics, respectively. A reciprocity check is described in Section 2.5, the two-transducer reciprocity calibration method is presented in Section 2.6, and measurements with a calibrated microphone system are covered in Section 2.7. Finally a brief description of the theoretical basis of the finite element simulation tool FEMP [24, 25] is included in Section 2.8.

Linear theory is used throughout the present work, and it is assumed that all quantities have a harmonic time dependency of $e^{i\omega t}$ when complex notation is used. $\omega = 2\pi f$ is the angular frequency and $t$ is the time.

## 2.1 Three-transducer reciprocity calibration

Three acoustical measurements are needed in a three-transducer reciprocity calibration. The measurements are performed using three electroacoustic transducers: a receiving transducer, a transmitting transducer, and a reciprocal transducer. The reciprocal transducer is used both as transmitter and receiver in the measurements. An absolute calibration of receiving sensitivities and transmitting responses can be achieved, yielding both magnitude and phase of the quantities of interest.

The conventional three-transducer reciprocity method is described in [10, 11] for microphones in air, and in [43] for hydrophones in water[1]. It is based on measurements of the current through the transmitting transducer and the open-circuit output voltage from the receiving transducer, in addition to the axial separation distance.

The method in [10, 11, 43] is modified [17] in order to use measurements of the input voltage to the transmitting transducer instead of current measurements and to account for the lack of ideal measurement conditions. In addition to measurements of voltage and distance, measurements of the transducers' electrical impedances are needed in the modified method.

The definitions of the transmitting responses, the receiving sensitivities and the spherical wave reciprocity are given in Sections 2.1.1, 2.1.2 and 2.1.3, respectively. From the definitions of these quantities, expressions are derived for the transmitting responses and receiving sensitivities of the transducers used.

### 2.1.1 Transmitting voltage response

A transmitting response relates a generated sound pressure to the electrical input to the transducer [44]. The transmitting voltage response yields the axial free-field sound pressure at a reference distance, generated by a given input voltage to a transmitting transducer. For a lossless medium the transmitting

[1]The derivation of the three-transducer reciprocity calibration method performed in the present work is mainly based on [43].

voltage response is defined as[2] [44, 45]

$$S_V(f) \equiv \frac{p_3(z = d_0, f)}{V_1(f)} = |S_V(f)|e^{i\varphi_{S_V}}. \tag{2.1}$$

Here $f$ is the frequency, $p_3$ is the free-field sound pressure, $z$ is the axial distance, $d_0$ is the reference distance and $V_1$ is the input voltage to the transmitting transducer. $|S_V(f)|$ is the magnitude and $\varphi_{S_V}$ is the phase of the transmitting voltage response. The reference distance is the axial distance from the front of the transmitting transducer, and it needs to be in the far-field of the source. If the far-field condition are not fulfilled for a given reference distance, the sound pressure must be extrapolated back to the reference distance from a pressure measured in the far-field [46]. A reference distance of $d_0 = 1$ m is used throughout the present work.

A corresponding transmitting current response, $S_I(f)$, is defined using the current through the transmitting transducer instead of the input voltage. The transmitting current response and the transmitting voltage response are related using the electrical input impedance $Z_T(f)$ of the transmitter, giving [45]

$$S_I(f) = S_V(f)Z_T(f). \tag{2.2}$$

### 2.1.2 Receiving voltage sensitivity

The electrical output from a receiving transducer is related to the pressure at the sensitive area of the receiving transducer by a receiving response. The free-field open-circuit receiving voltage sensitivity is defined as [44, 45]

$$M_V(f) \equiv \frac{V_5(f)}{p_4(f)} = |M_V(f)|e^{i\varphi_{M_V}}, \tag{2.3}$$

where $p_4(f)$ is the free-field sound pressure at the position of the receiving transducer, assuming plane wavefronts [44], and $V_5(f)$ is the open-circuit output voltage of the receiving transducer. The magnitude and phase of the free-field open-circuit receiving voltage sensitivity are denoted $|M_V(f)|$ and $\varphi_{M_V}$, respectively. Throughout the present work the free-field open-circuit receiving voltage sensitivity for normal incidence is considered.

### 2.1.3 Spherical wave reciprocity

The reciprocity principle [44] states that a linear, passive and reversible electroacoustic transducer is reciprocal if the relation between the receiving voltage sensitivity $M_V$ and the transmitting current response $S_I$ only depends on the geometry of the transducer, the frequency and the medium. For a lossless medium and spherical waves (i.e. far-field) the lossless complex spherical wave reciprocity parameter $J$ is given as [43]

$$J \equiv \frac{M_V(f)}{S_I(f)} = \frac{M_V(f)}{S_V(f)Z(f)} = \frac{4\pi d_0}{i\omega\rho}e^{ikd_0} = \frac{2d_0}{if\rho}e^{ikd_0}, \tag{2.4}$$

where $k = \omega/c$ is the wave number, $c$ is the sound velocity in the medium and $\rho$ is the density of the medium.

### 2.1.4 Measurement conditions and corrections

In the derivation of the three-transducer reciprocity calibration method it is assumed that the measurements are performed at ideal conditions [43]. This means that the receiving transducer measures the open-circuit output voltage caused by the free-field pressure in the far-field of the transmitting transducer, that the two transducers are aligned coaxially, and that the air is lossless [43, 44]. The free-field pressure is defined as the sound pressure in a homogenous, isotropic fluid medium without boundaries, or in practice where the effects of boundaries are negligible [44].

The far-field is the distance from the finite sound source where there is spherical wave divergence, i.e. the phase is proportional with the distance and the amplitude is inversely proportional with the distance [43]. The wavefronts are considered to be plane for a finite receiver placed in the far-field of the

[2]The present work has been performed in close cooperation with R. Hauge, and the choice of subscripts to denote the pressure and voltages is influenced by the system model notation used in [4].

source. A commonly used distance to denote the transition between the near-field and far-field regions is the Rayleigh length, defined as [46]

$$r_R = \frac{A}{\lambda} = \frac{\pi a^2}{\lambda}, \tag{2.5}$$

where $A = \pi a^2$ is the front area of a circular transmitting transducer with radius $a$ and $\lambda$ is the wavelength. The chosen distance to the far-field in practical situations depend on the desired accuracy of both the phase and amplitude, as well a the frequency and the geometry of the transducer.

The accuracy of the calibration depends on the signal to noise ratio (SNR) in the measurements. A SNR of at least 20 dB is required in the acoustical measurements for an error of about ± 1 dB in the calibration [43].

An open-circuit receiver measuring the free-field sound pressure in the far-field of the transmitter in a lossless medium is not achieved in a real measurement situation, and therefore corrections are applied to the measured voltages in the modified three-transducer reciprocity calibration method. In Section 2.1.5 the method is derived based on ideal conditions. The use of corrections to relate the ideal voltages to the measured voltages are described in Section 2.1.6, thus yielding the expressions for the fully modified three-transducer reciprocity calibration method.

### 2.1.5 Derivation of the method at ideal measurement conditions

The three transducers used in the calibration are here denoted T1, T2 and T3. T1 is the transmitting transducer, T2 is the receiving transducer, and T3 is the reciprocal transducer. The transmitting voltage response of T1 and T3 and the free-field open-circuit receiving voltage sensitivity of T2 and T3 are to be determined. If T1 is reciprocal, its free-field open-circuit receiving voltage sensitivity can be determined. The transmitting voltage response of T2 can be determined if T2 is reciprocal. A graphical representation of the three acoustical measurements that are to be performed is given in Fig. 2.1.

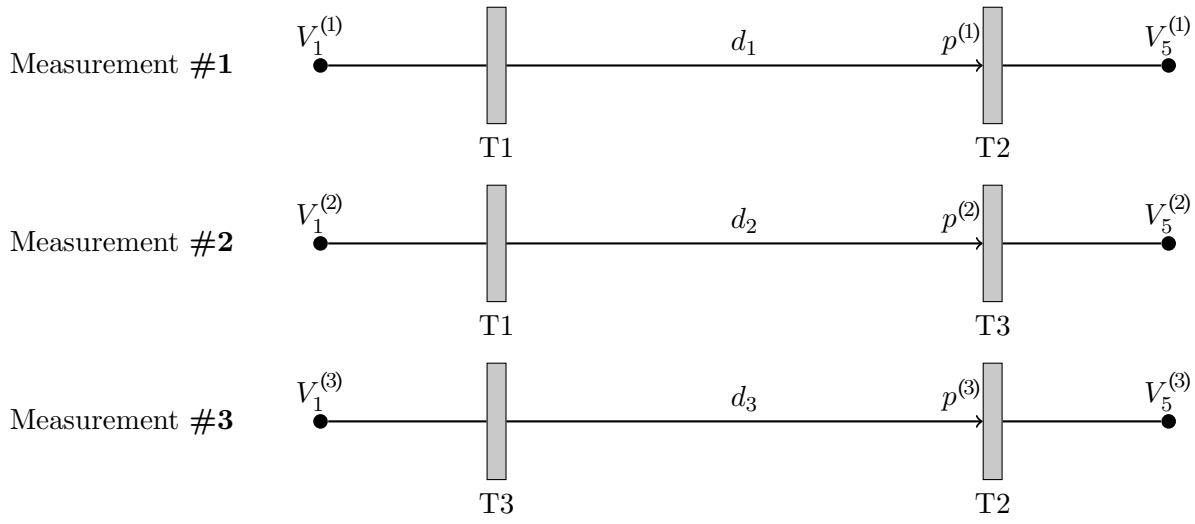


Figure 2.1: Measurements performed in the modified three-transducer reciprocity calibration method.

The quantities in the measurements #1, #2 and #3 are denoted by the superscripts $^{(1)}$, $^{(2)}$, and $^{(3)}$. In the following equations the frequency and distance dependency notation are omitted. For each measurement an input voltage to the transmitting transducer, $V_1$, an axial far-field free-field pressure, $p$, at the center of the receiving transducer's front surface, and an open-circuit output voltage from the receiving transducer, $V_5$, are defined. The separation distances between the two coaxial transducers in measurement #1, #2 and #3 are denoted $d_1$, $d_2$ and $d_3$.

First considering measurement #1, the axial far-field free-field pressure at $d_1$ is given by Eq. (2.1) to be [17]

$$p^{(1)} = V_1^{(1)} S_V^{T1} \frac{d_0}{d_1} e^{ik(d_0 - d_1)}, \tag{2.6}$$

where the $S_V^{T1}$ is the transmitting voltage response of transducer T1, which is used as the transmitting transducer in measurement #1. The pressure is extrapolated from the reference distance $d_0$ used in the

definition in Eq. (2.1) to the measurement distance $d_1$ using spherical far-field theory. The open-circuit voltage from the receiving transducer is found by combining Eqs. (2.6) and (2.3), giving [17]

$$V_5^{(1)} = p^{(1)} M_V^{T2} = V_1^{(1)} S_V^{T1} M_V^{T2} \frac{d_0}{d_1} e^{ik(d_0-d_1)}, \tag{2.7}$$

where $M_V^{T2}$ is the free-field open-circuit receiving voltage sensitivity of the transducer T2 used as receiver. An identical approach on measurement #2 yields

$$V_5^{(2)} = p^{(2)} M_V^{T3} = V_1^{(2)} S_V^{T1} M_V^{T3} \frac{d_0}{d_2} e^{ik(d_0-d_2)}, \tag{2.8}$$

where $M_V^{T3}$ is the free-field open-circuit receiving voltage sensitivity of the transducer T3. For measurement #3 the resulting expression is

$$V_5^{(3)} = p^{(3)} M_V^{T2} = V_1^{(3)} S_V^{T3} M_V^{T2} \frac{d_0}{d_3} e^{ik(d_0-d_3)}, \tag{2.9}$$

where $S_V^{T3}$ is the transmitting voltage response of the transducer T3.

A relative receiving voltage sensitivity for the transducers T2 and T3 is found from Eqs. (2.7) and (2.8) to be

$$\frac{M_V^{T2}}{M_V^{T3}} = \frac{V_5^{(1)}}{V_1^{(1)}} \frac{V_1^{(2)}}{V_5^{(2)}} \frac{d_1}{d_2} e^{ik(d_1-d_2)} = \frac{H_{15}^{VV\,(1)}}{H_{15}^{VV\,(2)}} \frac{d_1}{d_2} e^{ik(d_1-d_2)}, \tag{2.10}$$

where the two open-circuit voltage to voltage transfer functions $H_{15}^{VV\,(1)} = V_5^{(1)}/V_1^{(1)}$ and $H_{15}^{VV\,(2)} = V_5^{(1)}/V_1^{(1)}$ are introduced, respectively denoting the transfer function for measurement #1 and #2. The general voltage to voltage transfer function $H_{ij}^{VV} = V_j/V_i$ is the generated voltage $V_j$ given an input voltage $V_i$.

The reciprocity of transducer T3, using the spherical wave reciprocity parameter defined in Eq. (2.4), gives

$$S_V^{T3} = \frac{M_V^{T3}}{JZ^{T3}}, \tag{2.11}$$

where $Z^{T3}$ is the electrical input impedance of transducer T3, which must be measured as part of the calibration procedure.

Making use of Eq. (2.11) in the expression for the open-circuit output voltage in measurement #3 in Eq. (2.9) yields

$$V_5^{(3)} = V_1^{(3)} \frac{M_V^{T3}}{JZ^{T3}} M_V^{T2} \frac{d_0}{d_3} e^{ik(d_0-d_3)}, \tag{2.12}$$

which, when combined with the relative receiving sensitivity in Eq. (2.10), gives the free-field open-circuit receiving voltage sensitivity of transducer T2 as

$$M_V^{T2} = \left[ JZ^{T3} \frac{H_{15}^{VV\,(1)} H_{15}^{VV\,(3)}}{H_{15}^{VV\,(2)}} \frac{d_1 d_3}{d_0 d_2} e^{ik(d_1+d_3-d_0-d_2)} \right]^{\frac{1}{2}}. \tag{2.13}$$

An expression for the receiving voltage sensitivity of T3 is found by using the relative receiving sensitivity in Eq. (2.10) to insert for $M_V^{T2}$ instead of $M_V^{T3}$ in Eq. (2.12), giving

$$M_V^{T3} = \left[ JZ^{T3} \frac{H_{15}^{VV\,(2)} H_{15}^{VV\,(3)}}{H_{15}^{VV\,(1)}} \frac{d_2 d_3}{d_0 d_1} e^{ik(d_2+d_3-d_0-d_1)} \right]^{\frac{1}{2}} \tag{2.14}$$

Furthermore, using Eq. (2.11), the transmitting voltage response of T3 is found to be

$$S_V^{T3} = \left[ \frac{1}{JZ^{T3}} \frac{H_{15}^{VV\,(2)} H_{15}^{VV\,(3)}}{H_{15}^{VV\,(1)}} \frac{d_2 d_3}{d_0 d_1} e^{ik(d_2+d_3-d_0-d_1)} \right]^{\frac{1}{2}}. \tag{2.15}$$

The transmitting voltage response of T1 is also found for the measurement setup described here and shown in Fig. 2.1. Combining Eqs. (2.7) and (2.9) yields the relative transmitting response

$$\frac{S_V^{T1}}{S_V^{T3}} = \frac{V_5^{(1)}}{V_1^{(1)}} \frac{V_1^{(3)}}{V_5^{(3)}} \frac{d_1}{d_3} e^{ik(d_1-d_3)} = \frac{H_{15}^{VV\,(1)}}{H_{15}^{VV\,(3)}} \frac{d_1}{d_3} e^{ik(d_1-d_3)}. \tag{2.16}$$

Using this relation together with the reciprocity of transducer T3 in Eq. (2.11) and the open-circuit output voltage of measurement #2 in Eq. (2.8) yields

$$S_V^{T1} = \left[ \frac{1}{JZ^{T3}} \frac{H_{15}^{VV\,(1)} H_{15}^{VV\,(2)}}{H_{15}^{VV\,(3)}} \frac{d_1 d_2}{d_0 d_3} e^{ik(d_1+d_2-d_0-d_3)} \right]^{\frac{1}{2}}. \tag{2.17}$$

Additional quantities can be determined if either T1 or T2 is a reciprocal transducer. If T1 is assumed to be reciprocal and Eq. (2.17) is inserted into Eq. (2.4), the receiving voltage sensitivity of T1 is given as

$$M_V^{T1} = \left[ \frac{J\left(Z^{T1}\right)^2}{Z^{T3}} \frac{H_{15}^{VV\,(1)} H_{15}^{VV\,(2)}}{H_{15}^{VV\,(3)}} \frac{d_1 d_2}{d_0 d_3} e^{ik(d_1+d_2-d_0-d_3)} \right]^{\frac{1}{2}}, \tag{2.18}$$

where $Z^{T1}$ is the electrical impedance of T1. This means that one additional electrical measurement is needed to find $M_V^{T3}$. In a similar manner the transmitting voltage response of T2 is found by assuming that T2 is reciprocal and inserting the receiving voltage sensitivity in Eq. (2.13) into (2.4), giving

$$S_V^{T2} = \left[ \frac{Z^{T3}}{J\left(Z^{T2}\right)^2} \frac{H_{15}^{VV\,(1)} H_{15}^{VV\,(3)}}{H_{15}^{VV\,(2)}} \frac{d_1 d_3}{d_0 d_2} e^{ik(d_1+d_3-d_0-d_2)} \right]^{\frac{1}{2}}, \tag{2.19}$$

where $Z^{T2}$ is the electrical impedance of T2. Also here one additional electrical measurement is needed.

### 2.1.6 Corrections

Four corrections are introduced to account for the lack of ideal measurement conditions: $C_\alpha$, $C_{dif}$, $H_{1m1}^{VV}$, and $H_{5m5}^{VV}$. The derivation of the corrections are given in Sections 2.2, 2.3, 2.4.2 and 2.4.3, respectively.

$C_\alpha$ is the correction for the absorption in air and $C_{dif}$ is the correction for near-field effects, derived by use of diffraction correction. $H_{1m1}^{VV}$ accounts for the finite impedance of the recording oscilloscope and the cable connecting the oscilloscope to the transmitting transducer, denoted the transmitting electronics. Similarly, $H_{5m5}^{VV}$ accounts for the cable connecting the receiving transducer to the measurement amplifier and the finite impedance of the measurement amplifier.

The recorded voltages are denoted $V_{1m}$ and $V_{5m}$ for the transmitting and receiving[3] side, respectively. The corrections are applied to the two measured voltages to approximate ideal measurement conditions. The input voltage to the transmitting transducer is found by

$$V_1 \simeq V_{1,m} H_{1m1}^{VV}, \tag{2.20}$$

and the open-circuit output voltage from the receiving transducer is found by

$$V_5 \simeq V_{5,m} H_{5m5}^{VV} C_\alpha C_{dif}, \tag{2.21}$$

The voltage to voltage transfer functions in Eqs. (2.13) to (2.15) and (2.17) to (2.19) are thus determined from measurements by

$$H_{15}^{VV} = \frac{V_{5,m} H_{5m5}^{VV} C_\alpha C_{dif}}{V_{1,m} H_{1m1}^{VV}} = H_{1m5m}^{VV} \frac{H_{5m5}^{VV} C_\alpha C_{dif}}{H_{1m1}^{VV}}, \tag{2.22}$$

where $H_{5m5}^{VV} = V_{1,m}/V_{5,m}$ is the measured voltage to voltage transfer function.

Considering $S_V^{T3}$ as an example, combining Eqs. (2.15) and (2.22) yield

$$\left|S_V^{T3}\right| = \left[ \frac{1}{JZ^{T3}} \frac{H_{1m5m}^{VV\ (2)} H_{1m5m}^{VV\ (3)}}{H_{1m5m}^{VV\ (1)}} \frac{d_2 d_3}{d_0 d_1} \right]^{\frac{1}{2}} \frac{C_\alpha{}^{(T3)} C_{dif}{}^{(T3)} H_{5m5}^{VV\,(T3)}}{H_{1m1}^{VV\,(T3)}}, \tag{2.23}$$

[3]Note that the amplification performed by the measurement amplifier must be deducted to find $V_{5m}$, as described in Section 2.4.3.

where ${C_\alpha}^{(T3)}$, ${C_{dif}}^{(T3)}$, ${H_{5m5}^{VV}}^{(T3)}$ and ${H_{1m1}^{VV}}^{(T3)}$ are the effective correction factors in the calculation of $S_V^{T3}$, defined as

$${C_\alpha}^{(T3)} \equiv \sqrt{\frac{{C_\alpha}^{(2)}{C_\alpha}^{(3)}}{{C_\alpha}^{(1)}}}, \tag{2.24}$$

$${C_{dif}}^{(T3)} \equiv \sqrt{\frac{{C_{dif}}^{(2)}{C_{dif}}^{(3)}}{{C_{dif}}^{(1)}}}, \tag{2.25}$$

$${H_{5m5}^{VV}}^{(T3)} \equiv \sqrt{\frac{{H_{5m5}^{VV}}^{(2)}H_{5m5}^{VV\,(3)}}{H_{5m5}^{VV\,(1)}}}, \tag{2.26}$$

and

$${H_{1m1}^{VV}}^{(T3)} \equiv \sqrt{\frac{{H_{1m1}^{VV}}^{(2)}H_{1m1}^{VV\,(3)}}{H_{1m1}^{VV\,(1)}}}. \tag{2.27}$$

The superscripts $^{(1)}$, $^{(2)}$, and $^{(3)}$ refer to measurement #1, #2 and #3, as mentioned above.

## 2.2 Absorption in air

The medium is assumed to be lossless in the theory used to derive the expressions in the three-transducer reciprocity calibration method, although losses in air at the frequencies of interest in the present work can be significant. To correct for absorption in air, the measured pressure at the receiving transducer is corrected to account for losses, or rather the measured output voltage. Several factors contribute to the losses in air, but only the atmospheric absorption is accounted for in this section. Other factors, such as refraction, scattering by turbulence and non-linear propagation effects [47], are not considered here.

The absorption in air at atmospheric conditions is calculated in accordance with [47], assuming single frequency plane waves. A plane pressure wave propagating a distance $s$ in air is attenuated from the initial sound pressure $p_i$ to the sound pressure $p_t$ as

$$p_t = p_i e^{-\alpha_{dB/m} s/20\log_{10}(e)} \simeq p_i e^{-0{,}1151\alpha_{dB/m} s}, \tag{2.28}$$

where $\alpha_{dB/m}$ is the pure-tone sound-attenuation coefficient for atmospheric conditions in dB per metre, in the following termed the attenuation coefficient. The attenuation is caused by shear viscosity, thermal conductivity, mass diffusion, thermal diffusion and molecular relaxation, and can hence be expressed as a sum of absorption coefficients [47],

$$\alpha = \alpha_{cl} + \alpha_{rot} + \alpha_{vib,O} + \alpha_{vib,N}. \tag{2.29}$$

The classic absorption coefficient, $\alpha_{cl}$, is caused by the viscosity of the fluid, heat conduction and diffusion, and the rotational relaxation of the molecules is described by $\alpha_{rot}$. In addition the molecular relaxation of the two main components of air, oxygen and nitrogen, are the cause of the absorption coefficients $\alpha_{vib,O}$ and $\alpha_{vib,N}$, respectively [47].

Analytical expressions are given in [47] to calculate the absorption coefficient $\alpha_{dB/m}$, when the ambient atmospheric temperature $T$ in K, the ambient atmospheric pressure $p_a$ in kPa, the molar concentration of water vapour $h$ in percent, and the frequency $f$ in Hz are known. Expressions are also supplied to convert from relative humidity to the molar concentration of water vapour.

When a calculated absorption coefficient for the current environmental conditions, a correction factor is needed to obtain the output voltage measured in a lossless medium. The open-circuit output voltage from the receiving transducer is proportional to the free-field pressure at the transducers sensitive area, by the definition of free-field open-circuit receiving voltage sensitivity in Eq. (2.3). Therefore the ratio of the pressures with and without loss equals the ratio of voltages, expressed as

$$\frac{V_i}{V_t} = \frac{p_i}{p_t} = e^{\alpha_{dB/m} s/20\log_{10}(e)} = 10^{\alpha_{dB/m} s/20}, \tag{2.30}$$

where $V_i$ is the output generated by the pressure $p_i$ and $V_t$ is the output generated by the pressure $p_t$, and $p_i$ and $p_t$ are the pressure without and with absorption, respectively. This is defined as the absorption correction factor

$$C_\alpha \equiv 10^{\alpha_{dB/m} s/20}. \tag{2.31}$$

## 2.3 Diffraction correction

It is of interest to find a way to compensate for the lack of far-field conditions in the measurements, since conducting measurements in the far-field in air proves difficult due to the significant absorption in air and the practical limitations of the experimental setup. Diffraction correction is a way to quantify the distance dependent effects of diffraction when a sound wave is received by a receiving transducer placed in the near-field of a transmitting transducer, as the incoming wave will not have a plane wavefront. For a finite receiver this will cause deviations in both magnitude and phase in the measured pressure compared to a theoretical measurement with a point source or with a finite receiver in a plane wave sound field.

At far-field conditions, as is required in the three-transducer reciprocity calibration method, it is assumed that the wavefronts are plane with respect to a finite receiving transducer. The demarcation between the near-field and the far-field is chosen based on the details of the measurement setup and the required accuracy. For instance will the distance to the far-field increase with the frequency and the size of the receiving transducer. The distance chosen will also depend on which quantities are of interest.

### 2.3.1 Khimunin's diffraction correction

A diffraction correction is defined by Khimunin [40, 41] as

$$H^{dif}(z,f) = \frac{\langle p(z,f)\rangle_A}{p_p(z,f)}, \tag{2.32}$$

for a uniformly vibrating circular plane piston source in a rigid baffle of infinite extent, hereafter denoted the piston source model. $\langle p(z,f)\rangle_A$ is the free-field pressure generated by piston source model at an axial distance $z$, averaged over the area $A$. The area $A$ corresponds to an acoustically transparent receiver of equal size as, and placed coaxially with, the piston source. $p_p(z,f)$ is the corresponding plane wave pressure at the axial distance $z$. A sketch of this setup is shown in Fig. 2.2.


Figure 2.2: Sketch of a piston source model, where the piston has radius $a$. A circular acoustically transparent circular receiver, also with radius $a$, is placed coaxially to the source at a distance $z$.

The diffraction correction for both the phase [41] and the magnitude [40] can be expressed as [48]

$$H^{dif}(ka,S) = 1 - \frac{4}{\pi}\int_0^{\pi/2} \exp\left[-i\frac{(ka)^2 S}{2\pi}\sqrt{1+\left(\frac{4\pi}{Ska}\right)^2\cos^2(\theta)}\right]\sin^2(\theta)\mathrm{d}\theta, \tag{2.33}$$

where the dimensionless quantities $ka$ and $S = z/(a^2/\lambda)$ are used, and $\theta$ is an integration variable. In the present work $H^{dif}$ is calculated numerically using the MATLAB-script `Khimunin_diffractioncorrection.m`, implemented by Storheim [49] (see Appendix A.3).

### 2.3.2 Correction term

All acoustical measurements in the present work are performed with the receiving transducer placed well outside the Rayleigh length, but it is assumed that some near-field effects still are present. As a result

the measured output voltage will not correspond to the output voltage found under far-field conditions. It is the far-field output voltage that is assumed measured in e.g. [43] and in the initial derivation in Section 2.1.5.

Khimunin's diffraction correction is used to find an approximate correction factor, $C_{dif}$, that relates the measured pressure to the equivalent pressure found under far-field conditions [17], and thus also relate the corresponding output voltages.

Let $p_{meas}(d, f)$ be the measured sound pressure at the axial distance $d$ in the near-field, and let $p_{corr}(d, f)$ be the far-field equivalent pressure at the same axial distance $d$, found by use of the correction factor. A graphic example is shown in Fig. 2.3.

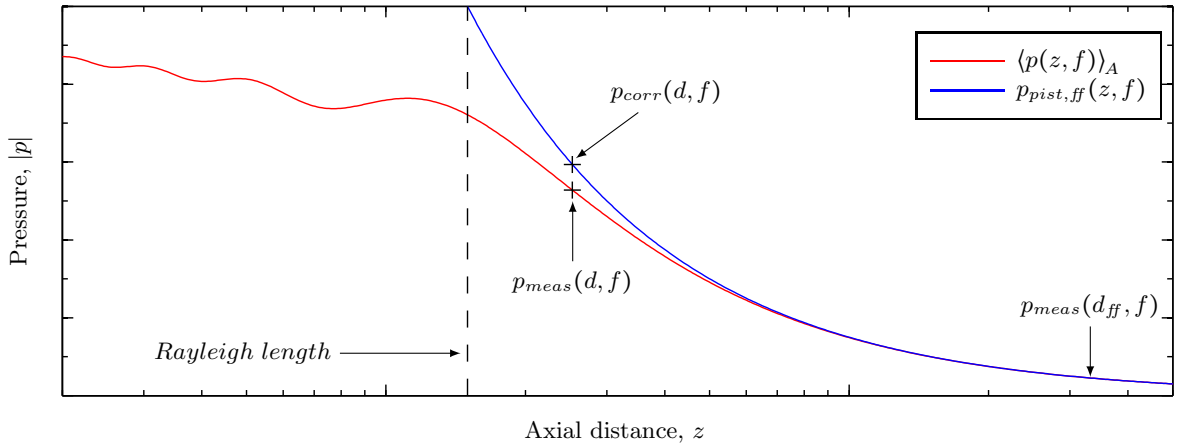


Figure 2.3: Example plot, showing the correction from a measured pressure, $p_{meas}(d, f)$, to a far-field equivalent measured pressure, $p_{corr}(d, f)$, both at a distance $d$. Shown for the piston source model with $ka = 30$, where $k$ is the wavenumber and $a$ is the radius of the transmitter and receiver. $p_{pist,ff}(z, f)$ is given in Eq. (2.37). The Rayleigh length, $\pi a^2/\lambda$, is 15 cm.

In the derivation of the correction factor it is assumed that the pressure measured with a finite transducer has similar distance dependency for distances well outside the Rayleigh length as the averaged pressure $\langle p(z, f)\rangle_A$ [17]. It is also assumed that the transmitting and receiving transducer are circular and of nearly equal size. Thus $p_{corr}(d, f)$ is found from $p_{meas}(d, f)$ by first extrapolating out to the far-field distance $d_{ff}$ using the distance dependency of $\langle p(z, f)\rangle_A$ and then extrapolating back in again to the near-field distance $d$ using the distance dependency of $p_{pist,ff}(z, f)$, where $p_{pist,ff}(z, f)$ is the axial far-field pressure in the piston source model. The pressure $\langle p(z, f)\rangle_A$ converges to $p_{pist,ff}(z, f)$ for sufficiently large distances. A $d_{ff}$ of 1000 m is used in the calculations.

The outward extrapolation of the measured pressure to the far-field axial distance $d_{ff}$ is expressed by [17]

$$p_{meas}(d_{ff}, f) = p_{meas}(d, f)\frac{\langle p(d_{ff}, f)\rangle_A}{\langle p(d, f)\rangle_A}. \tag{2.34}$$

The inward extrapolation from the far-field to the corrected pressure at the near-field axial distance $d$ is given by [17]

$$p_{corr}(d, f) = p_{meas}(d_{ff}, f)\frac{p_{pist,ff}(d, f)}{p_{pist,ff}(d_{ff}, f)}. \tag{2.35}$$

Combining Eqs. (2.34) and (2.35) gives the correction $C_{dif}$ as

$$C_{dif} \equiv \frac{p_{corr}(d, f)}{p_{meas}(d, f)} = \frac{\langle p(d_{ff}, f)\rangle_A}{\langle p(d, f)\rangle_A}\frac{p_{pist,ff}(d, f)}{p_{pist,ff}(d_{ff}, f)}. \tag{2.36}$$

It is desired to express the correction factor by use of Khimunin's diffraction factor. The axial far-field pressure generated by a piston source model is given as [46]

$$p_{pist,ff}(z, f) = \frac{\rho c k a^2 v}{2z}e^{-i(kz+\varphi)}, \tag{2.37}$$

where $v$ is the particle velocity of the piston and $\varphi$ is a phase factor. Introducing this expression in Eq. (2.36) yields [17]

$$C_{dif} = \frac{\langle p(d_{ff}, f)\rangle_A}{\langle p(d, f)\rangle_A} \frac{\frac{\rho c k a^2 v}{2d} e^{-i(kd+\varphi)}}{\frac{\rho c k a^2 v}{2d_{ff}} e^{-i(kd_{ff}+\varphi)}} = \frac{\langle p(d_{ff}, f)\rangle_A}{\langle p(d, f)\rangle_A} \frac{d_{ff}}{d} e^{-ik(d-d_{ff})}. \tag{2.38}$$

In order to introduce Khimunin's diffraction correction from Eq. (2.32), plane waves must be included. The pressure in a plane wave is expressed as [46]

$$p_p(z, f) = \rho c v_p e^{-ikz}, \tag{2.39}$$

where $v_p$ is the particle velocity of the plane wave. Dividing the plane wave pressure at axial distance $d$ with the plane wave pressure at axial distance $d_{ff}$ yields [17]

$$\frac{p_p(d, f)}{p_p(d_{ff}, f)} = \frac{\rho c v_p e^{-ikd}}{\rho c v_p e^{-ikd_{ff}}} = e^{-ik(d-d_{ff})}, \tag{2.40}$$

which is used to include plane waves in Eq. (2.38), giving [17]

$$C_{dif} = \frac{\langle p(d_{ff}, f)\rangle_A}{\langle p(d, f)\rangle_A} \frac{d_{ff}}{d} \frac{p_p(d, f)}{p_p(d_{ff}, f)}. \tag{2.41}$$

Reorganizing the terms and using Eq. (2.32) yields [17]

$$C_{dif} = \frac{d_{ff}}{d} \frac{H^{dif}(d_{ff}, f)}{H^{dif}(d, f)}, \tag{2.42}$$

which is used to correct the measured output voltage at near-field conditions to a far-field equivalent (see Eq. (2.22)).

The use of Khimunin's diffraction correction to determine $C_{dif}$ in the present work is an initial approach. It is based on theory for a uniformly vibrating piston source in a rigid baffle of infinite extent, and is therefore a simplification with regard to the piezoelectric transducers used in the experiments. It is, however, utilized e.g. in [50].

It is possible to derive similar correction factors based on other definitions of the diffraction correction. One possible approach in future work is to use finite element modelling to determine a diffraction correction, as in e.g. [1, 51–53].

## 2.4 Electronics

The input voltage to the transmitting transducer, $V_1$, and the open-circuit output voltage of the receiving transducer, $V_5$, are needed in order to perform the three-transducer reciprocity calibration as described above. In general these ideal voltages cannot be measured directly due to the finite impedance of the measurement equipment and the cables used to connect the transducers to the instruments. Transfer functions are derived to transform the measured voltages to the ideal input and output voltages needed, mainly correcting for the effects of the cables.

In the following a model used to describe the connecting cables is shown and a transfer function for the transmitting electronics is calculated. The receiving electronics are handled in a similar manner.

Measurements of the impedance of all the transducers used in the modified three-transducer reciprocity calibration method are needed in order to correct for the electronics in the system.

### 2.4.1 Cables

Experimental results have shown that the effect of cables on the measurements is significant, thus stressing the importance of modelling of the cables in the electric transfer functions. In the present work the cables are modelled as ideal uniform transmission lines, using distributed elements [54]. For a coaxial cable terminated in a load impedance $Z_L$, an equivalent circuit [45] is shown in Fig. 2.4.

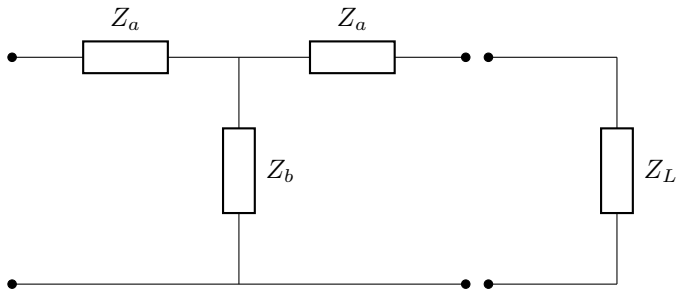


Figure 2.4: A coaxial cable described as an ideal lossless transmission line using distributed elements, terminated in $Z_L$.

The two impedances used to describe the coaxial cable in the equivalent circuit in Fig. 2.4 are given as [45]

$$Z_a = iZ_0 \tan\left(k_{em}\frac{l}{2}\right) \qquad \text{and} \qquad Z_b = \frac{Z_0}{i\sin(k_{em}l)}, \tag{2.43}$$

where $Z_0$ is the characteristic impedance of the cable, $k_{em}$ is the electromagnetic wavenumber and $l$ is the length of the coaxial cable. $Z_0$ and $k_{em}$ can in turn be determined by

$$Z_0 = \sqrt{\frac{L_x}{C_x}} \qquad \text{and} \qquad k_{em} = \omega\sqrt{L_x C_x}, \tag{2.44}$$

where $\omega$ is the angular frequency and $L_x$ and $C_x$ are inductance and capacitance per metre, respectively.

### 2.4.2 Transmitting electronics

The present measurement setup (see Chapter 3) consists of a waveform generator, a transmitting transducer and an oscilloscope on the transmitting side, in addition to the connecting coaxial cables. A circuit diagram of the transmitting electronics is shown in Fig. 2.5. The voltage recorded by the oscilloscope is denoted $V_{1,m}$. A transfer function relating the measured voltage to the input voltage to the transmitting transducer, $V_1$, is defined as

$$H_{1m1}^{VV} \equiv \frac{V_1}{V_{1,m}}. \tag{2.45}$$

The circuit diagram describes the signal generator as a Thévenin generator, where $V_{gen}$ is the Thévenin equivalent voltage, $Z_{gen}$ is the Thévenin equivalent impedance, and $V'$ is the output voltage from the generator. The two lengths of coaxial cable are described by the impedances $Z_{a1}$, $Z_{b1}$, $Z_{a2}$, and $Z_{b2}$, as given in (2.43). The lower branch of the circuit diagram is terminated in the transmitting transducer with the electrical impedance $Z_T$ and the upper branch is terminated in the oscilloscope with the impedance $Z_{OSC}$. The Thévenin representation of the signal generator is included for completeness, as $H_{1m1}^{VV}$ is independent of $V_{gen}$ and $Z_{gen}$.

Using Kirchhoff's circuit laws on the upper and lower branches of the circuit diagram in Fig. 2.5 yield the ratios $V_{1,m}/V'$ and $V_1/V'$, respectively, which are combined to give $H_{1m1}^{VV}$. Since the circuits used to find $V_1/V'$ and $V_{1,m}/V'$ are almost identical, only one of the calculations is shown in detail.

Fig. 2.6 shows the lower branch of Fig. 2.5, including the currents in the circuit.

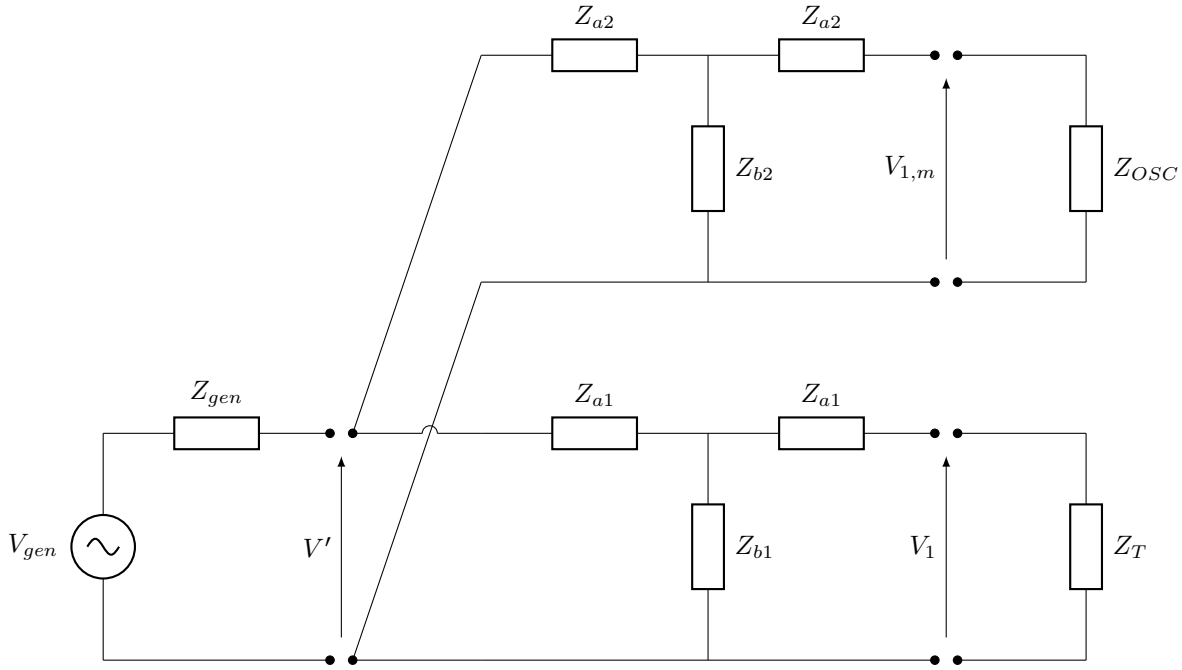


Figure 2.5: A circuit description of the transmitting electronics. The signal generator is described as a Thévenin generator, connected in parallel to the oscilloscope and the transmitting transducer. The connecting cables are described as ideal transmission lines.

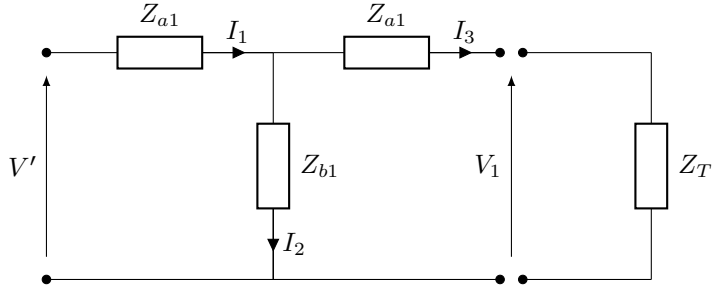


Figure 2.6: A circuit description of the coaxial cable connecting the generator to the transmitting transducer.

Using Kirchhoff's voltage law on three closed loops in the circuit, and Kirchhoff's current law, yields

$$V' = I_1 Z_{a1} + I_2 Z_{b1}, \tag{2.46}$$
$$V_1 = -I_3 Z_{a1} + I_2 Z_{b1}, \tag{2.47}$$
$$V_1 = I_3 Z_T, \tag{2.48}$$
$$I_1 = I_2 + I_3. \tag{2.49}$$

$I_1$, $I_2$, and $I_3$ are the currents shown in Fig. 2.6. Manipulating Eqs. (2.47) and (2.48) to get expressions for the currents $I_2$ and $I_3$, respectively, yields

$$I_2 = \frac{V_1}{Z_{b1}} + I_3 \frac{Z_{a1}}{Z_{b1}} \tag{2.50}$$

and

$$I_3 = \frac{V_1}{Z_T}. \tag{2.51}$$

Combining Eq. (2.49) with Eq. (2.46) eliminates the current $I_1$, and $V'$ is then given as

$$V' = I_2(Z_{a1} + Z_{b1}) + I_3 Z_{a1}. \tag{2.52}$$

Inserting for $I_2$ using Eq. (2.50) yields

$$V' = \left(\frac{V_1}{Z_{b1}} + I_3\frac{Z_{a1}}{Z_{b1}}\right)(Z_{a1} + Z_{b1}) + I_3 Z_{a1} = V_1\frac{Z_{a1} + Z_{b1}}{Z_{b1}} + I_3\frac{{Z_{a1}}^2 + 2Z_{a1}Z_{b1}}{Z_{b1}}. \tag{2.53}$$

The current $I_3$ is then eliminated by Eq. (2.51) and the resulting expression for the ratio $V_1/V'$ is then found to be

$$\frac{V_1}{V'} = \frac{Z_{b1}Z_T}{Z_T(Z_{a1} + Z_{b1}) + (Z_{a1} + Z_{b1})^2 - {Z_{b1}}^2}. \tag{2.54}$$

A similar approach applied on the upper part of the circuit in Fig. 2.5 yields

$$\frac{V_{1,m}}{V'} = \frac{Z_{b2}Z_{OSC}}{Z_{OSC}(Z_{a2} + Z_{b2}) + (Z_{a2} + Z_{b2})^2 - {Z_{b2}}^2}. \tag{2.55}$$

The final voltage to voltage transfer function, transforming the voltage measured by the oscilloscope to the input voltage to the transmitting transducer, is found by combining Eqs. (2.54) and (2.55) to be

$$H_{1m1}^{VV} \equiv \frac{V_1}{V_{1,m}} = \frac{V_1}{V'}\frac{V'}{V_{1,m}} = \frac{Z_{b1}Z_T}{Z_{b2}Z_{OSC}}\frac{Z_{OSC}(Z_{a2} + Z_{b2}) + (Z_{a2} + Z_{b2})^2 - {Z_{b2}}^2}{Z_T(Z_{a1} + Z_{b1}) + (Z_{a1} + Z_{b1})^2 - {Z_{b1}}^2}. \tag{2.56}$$

The impedance of the transmitting transducer $Z_T$ is in the present work determined by either measurements or FE simulations. The impedance of the oscilloscope, $Z_{OSC}$, is stated by the manufacturer as a resistance, $R_{OSC}$, in parallel with an ideal capacitor with capacitance $C_{OSC}$, giving

$$Z_{SCO} = \frac{1}{i\omega C_{OSC} + \dfrac{1}{R_{OSC}}} \tag{2.57}$$

### 2.4.3 Receiving electronics

In the experimental setup, the receiving transducer is connected to an amplifier with an external frequency filter and from there the signal is transmitted to an oscilloscope for recording. The expressions for the three-transducer reciprocity calibration derived in Section 2.1.5 requires that the output voltage from the transducer is found at open-circuit conditions. It is therefore of interest to find the open-circuit voltage from the receiving transducer, $V_5$, expressed by the voltage measured at the oscilloscope.

Investigation of the signal propagation through the coaxial cables between the amplifier and the frequency filter, and from the amplifier to the oscilloscope, indicate that their effect on the measured magnitude is negligible compared to the effects caused by the cable connecting the receiving transducer to the measurement amplifier. It is therefore assumed that the voltage recorded by the oscilloscope equals the voltage at the amplifier input, $V_{5,m}$, if the gain in the amplifier is accounted for and only the magnitude is considered.

The amplification in the measurement amplifier is accounted for by dividing the magnitude of the signal by $10^{G/20}$, where $G$ is the specified gain in dB. For instance if a gain of 60 dB is used, the signal amplitude must be divided by $10^{60/20} = 1000$. Any phase distortion introduced by the amplifier is not considered here.

Three different types of receiving transducers are used in the present work; electrostatic microphones, in-house constructed piezoelectric transducers, and single piezoelectric disks.

The electrostatic microphones and the measurement amplifier are both produced by Brüel & Kjær, and are connected using proprietary preamplifiers, cables and connectors. The open-circuit free-field receiving voltage sensitivity for the microphone is supplied, and the frequency response of the preamplifiers including cables are stated to be flat (see Section 3.5). It is therefore not accounted for the receiving electronics, other than the amplification, when electrostatic microphones are used as receivers in the current experimental setup.

The in-house constructed piezoelectric transducers and single piezoelectric disks are on the other hand connected to the measurement amplifier using coaxial cables, and the $M_V$ is not known. It is therefore of interest to determine the voltage to voltage transfer function

$$H_{5m5}^{VV} \equiv \frac{V_5}{V_{5,m}}, \tag{2.58}$$

in order to find the open-circuit output voltage of the receiving transducer from measurements.

This measurement system is modelled in a similar manner as the transmitting electronics in Section 2.4.2. The resulting circuit diagram is shown in Fig. 2.7.

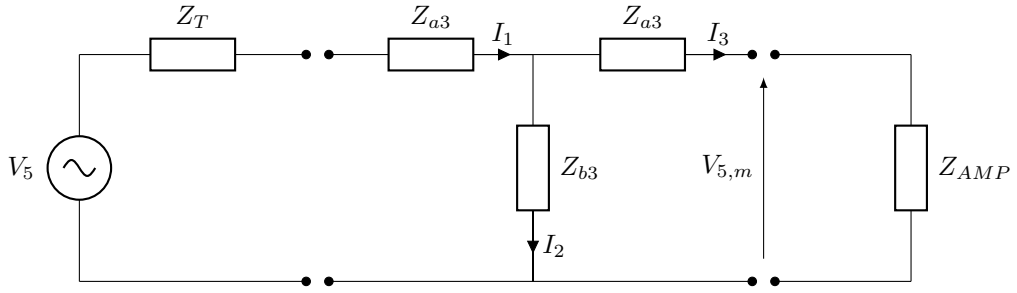


Figure 2.7: Receiving electronics. Modelled with the open-circuit receiving transducer as a Thévenin generator and the coaxial cable as an ideal transmission line, terminated in the amplifier input impedance.

The receiving transducer is modelled as a Thévenin generator with the open-circuit output voltage from the transducer, $V_5$, as the Thévenin equivalent voltage and the output impedance of the transducer, $Z_T$, as the Thévenin equivalent impedance [48]. The coaxial cable is described by the impedances $Z_{a3}$ and $Z_{b3}$, and the cable is terminated in the amplifier with the impedance $Z_{AMP}$ and the input voltage $V_{5,m}$. $I_1$, $I_2$ and $I_3$ are the currents through the system.

Using Kirchhoff's circuit law and current law on the circuit in Fig. 2.7 yields

$$V_5 = I_1(Z_T + Z_{a3}) + I_2 Z_{b3}, \tag{2.59}$$

$$V_{5,m} = I_2 Z_{b3} - I_3 Z_{a3}, \tag{2.60}$$

$$V_{5,m} = I_3 Z_{AMP}, \tag{2.61}$$

$$I_1 = I_2 + I_3. \tag{2.62}$$

The current $I_3$ is expressed using (2.61) as

$$I_3 = \frac{V_{5,m}}{Z_{AMP}}. \tag{2.63}$$

Inserting this into (2.60) yields

$$I_2 = \frac{V_{5,m}}{Z_{b3}} + I_3\frac{Z_{a3}}{Z_{b3}} = \frac{Z_{a3} + Z_{AMP}}{Z_{b3}Z_{AMP}}V_{5,m}. \tag{2.64}$$

Combining Eq. (2.62) with Eq. (2.59) eliminates the current $I_1$, and the open-circuit output voltage is then given as

$$V_5 = I_2(Z_T + Z_{a3} + Z_{b3}) + I_3(Z_T + Z_{a3}). \tag{2.65}$$

Eqs. (2.63) and (2.64) are then inserted for $I_3$ and $I_2$ to yield

$$V_5 = \frac{(Z_{AMP} + Z_{a3})(Z_T + Z_{a3} + Z_{b3})}{Z_{b3}Z_{AMP}}V_{5,m} + \frac{Z_T + Z_{a3}}{Z_{AMP}}V_{5,m}. \tag{2.66}$$

Rearranging the terms and solving for the transfer function yields

$$H_{5m5}^{VV} \equiv \frac{V_5}{V_{5,m}} = \frac{Z_{AMP}(Z_{a3} + Z_{b3}) + (Z_{a3} + Z_{b3})^2 - {Z_{b3}}^2 + Z_T(Z_{a3} + Z_{b3} + Z_{AMP})}{Z_{b3}Z_{AMP}}. \tag{2.67}$$

The impedance of the receiving transducer $Z_T$ is determined by either measurements or FE simulations, and the input impedance of the measurement amplifier for direct input is given as

$$Z_{AMP} = \frac{1}{i\omega C_{AMP} + \dfrac{1}{R_{AMP}}}, \tag{2.68}$$

where $R_{AMP}$ and $C_{AMP}$ are the stated resistance and capacitance of the amplifier, respectively.

## 2.5 Reciprocity check

The reciprocity of a system consisting of two reversible transducers, the medium and boundaries can be verified by two measurements [55]. Consider that the two transducers, for instance T1 and T3, are placed in the same medium at arbitrary positions. If measurements are performed first with T1 as transmitter and T3 as receiver, and then with T3 as transmitter and T1 as receiver, the two measured electrical transfer impedances are equal in a reciprocal system. This is expressed by [55]

$$\frac{V_1^{T3}}{I_5^{T1}} = \frac{V_1^{T1}}{I_5^{T3}}, \tag{2.69}$$

where $V_1^{T1}$ and $V_1^{T3}$ are the input voltages to T1 and T3, respectively. $I_5^{T1}$ and $I_5^{T3}$ are the short-circuit receiving current of T1 and T3, respectively. If the corresponding open-circuit output voltages $V_5^{T1}$ and $V_5^{T3}$ are measured instead, the equality is given as

$$Z_T^{T1}\frac{V_1^{T3}}{V_5^{T1}} = Z_T^{T3}\frac{V_1^{T1}}{V_5^{T3}}. \tag{2.70}$$

There is, however, no guarantee that T1 and T3 are reciprocal even if the system is reciprocal. One possible explanation is that both transducers are close to identically nonlinear [55], but this can be investigated separately.

## 2.6 Two-transducer reciprocity calibration

If two reciprocal transducers have identical sensitivities, then only a single acoustical measurement is needed to determine the transmitting voltage response and the open-circuit receiving voltage sensitivity [55], and thus simplifying the experiments and calculations. The modifications applied to the three-transducer reciprocity calibration method are equally relevant in the two-transducer reciprocity calibration method, and the correction factors are therefore applied to the measured voltages. Using measurement #3 in Fig. 2.1 as the single acoustical measurement yields

$$M_V^{T2} = M_V^{T3} = \left[JZ^{T3}H_{15}^{VV\,(3)}\frac{d_3}{d_0}e^{ik(d_3-d_0)}\right]^{\frac{1}{2}}, \tag{2.71}$$

and

$$S_V^{T2} = S_V^{T3} = \left[\frac{1}{JZ^{T3}}H_{15}^{VV\,(3)}\frac{d_3}{d_0}e^{ik(d_3-d_0)}\right]^{\frac{1}{2}}, \tag{2.72}$$

where the electrical input impedance of the transducer T2, $Z^{T2}$, can be used instead of $Z^{T3}$, as they are assumed to be identical.

The two-transducer reciprocity calibration method can be used as an initial approach or as a test of a prior calibration for two similar reciprocal transducers [55]. It is of interest to compare results obtained using the modified three- and two-transducer reciprocity calibration methods and see if they correspond.

## 2.7 Measurements with a calibrated microphone

A secondary calibration of a transmitting transducer can be performed by measurement with a calibrated microphone [43]. Based on Eq. (2.9) the magnitude of the transmitting voltage response of transducer T3 can be expressed as

$$\left|S_V^{T3}\right| = \frac{\left|H_{15}^{VV}\right|}{|M_{B\&K}|}\frac{d_3}{d_0}, \tag{2.73}$$

where $M_{B\&K}$ is the free-field open-circuit receiving voltage sensitivity of the receiving B&K microphone system. The microphone system consists of the microphone connected to the measurement amplifier through a preamplifier with included cables. The systems used and the calibration of these are described in detail in Section 3.5.

The voltage to voltage transfer function in Eq. (2.73) is found from measurements by

$$H_{15}^{VV} = \frac{V_{5,m}C_\alpha}{V_{1,m}H_{1m1}^{VV}}, \tag{2.74}$$

which corresponds to Eq. (2.22) where $V_{5,m} = V_5$ is assumed for these measurements and no far-field correction is used. This is because $C_{dif}$ is derived for transmitters and receivers of similar size, and the effect of diffraction is less significant for a smaller receiver.

Measurements with a calibrated microphone are compared to measurements with the modified three-transducer reciprocity calibration method.

## 2.8 Finite element model

FE analysis of the piezoelectric ceramic disks and piezoelectric transducers are performed and compared with electrical and acoustical measurements. The simulation tool used is the FE model *Finite Element Modeling of Piezoelectric structures* 5.0 (FEMP 5.0) [24, 25]. A summary of the FE theory is given here, where the notation in [24] is adopted, stating the equations used for calculating the transducer's admittance $Y$, and the sound pressure radiated from the transducer, $p$.

The studied problem is a piezoelectric body, e.g. a piezoelectric disk, polarized in the thickness direction, radiating into a fluid. The symmetry in the disk is utilized, making the problem axisymmetric. The region of interest is approximated by a finite number of smaller volumes, i.e. the elements in the FE method [24]. The elements are separated between finite and infinite elements. The distance from the center of the structure studied to the beginning of the infinite elements is $R_{inf}$ [24]. A number of nodes are defined in each element, where the unknown quantities are to be determined [24]. The FE equations for a piezoelectric disk immersed in an infinite fluid medium is given as [24]

$$-\omega^2\begin{bmatrix} M_{uu} & 0 & 0 \\ 0 & 0 & 0 \\ 0 & 0 & -M_{\psi\psi} \end{bmatrix}\begin{Bmatrix} \hat{u} \\ \hat{\phi} \\ \hat{\psi} \end{Bmatrix}+i\omega\begin{bmatrix} 0 & 0 & C_{u\psi} \\ 0 & 0 & 0 \\ C_{\psi u} & 0 & 0 \end{bmatrix}\begin{Bmatrix} \hat{u} \\ \hat{\phi} \\ \hat{\psi} \end{Bmatrix}+\begin{bmatrix} K_{uu} & K_{u\phi} & 0 \\ K_{\phi u} & K_{\phi\phi} & 0 \\ 0 & 0 & -K_{\psi\psi} \end{bmatrix}\begin{Bmatrix} \hat{u} \\ \hat{\phi} \\ \hat{\psi} \end{Bmatrix}=\begin{Bmatrix} 0 \\ -Q \\ 0 \end{Bmatrix}. \tag{2.75}$$

A description of the variables used in Eq. (2.75) is listed in Table 2.1. Definitions of the variables are found in [24].

Table 2.1: Description of variables in Eq. (2.75), and reference to the respective equation numbers they are defined at in [24]

| Variable | Description | Eq. number in [24] |
|---|---|---|
| $[M_{uu}]$ | Global mass matrix | (3.51) |
| $[M_{\psi\psi}]$ | Global fluid mass matrix | (3.129) |
| $[C_{u\psi}]$ | Global fluid/structure coupling matrix | (3.139) |
| $[C_{\psi u}]$ | Global fluid/structure coupling matrix | (3.139) |
| $[K_{uu}]$ | Global stiffness matrix | (3.76) |
| $[K_{u\phi}]$ | Global piezoelectric stiffness matrix | (3.76) |
| $[K_{\phi u}]$ | Global piezoelectric stiffness matrix | (3.76) |
| $[K_{\phi\phi}]$ | Global dielectric stiffness matrix | (3.76) |
| $[K_{\psi\psi}]$ | Global fluid stiffness matrix | (3.132) |
| $\{Q\}$ | Global charge vector | (3.76) |
| $\{\hat{u}\}$ | Global displacement vector | (3.47) |
| $\{\hat{\phi}\}$ | Global electric potential vector | (3.57) |
| $\{\hat{\psi}\}$ | Global fluid velocity potential vector | (3.119) |
| $\omega$ | Angular frequency | - |

The FE equations in Eq. (2.75) are transformed to H-form, which simplifies the calculation of the response functions of the piezoelectric disk [24]. To transform the equations to H-form, the potential in the nodes of the elements are condensed out of the FE equations, and the potential difference between two electrodes of the piezoelectric disk, $V$, and current going through the non-grounded electrode, $I = dQ/dt = i\omega Q$, are introduced. Eq. (2.75) is then rewritten as [24]

$$-\omega^2\begin{bmatrix} M_{uu} & 0 & 0 \\ 0 & 0 & 0 \\ 0 & 0 & -M_{\psi\psi} \end{bmatrix}\begin{Bmatrix} \hat{u} \\ V \\ \hat{\psi} \end{Bmatrix}+i\omega\begin{bmatrix} 0 & 0 & C_{u\psi} \\ 0 & 0 & 0 \\ C_{\psi u} & 0 & 0 \end{bmatrix}\begin{Bmatrix} \hat{u} \\ V \\ \hat{\psi} \end{Bmatrix}+\begin{bmatrix} H_{uu} & H_{u\phi} & 0 \\ H_{\phi u} & H_{\phi\phi} & 0 \\ 0 & 0 & -K_{\psi\psi} \end{bmatrix}\begin{Bmatrix} \hat{u} \\ V \\ \hat{\psi} \end{Bmatrix}=\begin{Bmatrix} 0 \\ -I/(i\omega) \\ 0 \end{Bmatrix}, \tag{2.76}$$

where $H_{uu}$, $H_{u\phi}$, $H_{\phi u} = H_{u\phi}^T$ and $H_{\phi\phi}$ are given in Eqs. (3.190) - (3.192) in [24], respectively. The response functions of a piezoelectric transducer are calculated directly from Eq. (2.76) by using matrix manipulation [24]. The third equation in Eq. (2.76) is rewritten as

$$\omega^2[M_{\psi\psi}]\{\hat{\psi}\} + i\omega[C_{\psi u}]\{\hat{u}\} - [K_{\psi\psi}]\{\hat{\psi}\} = 0, \tag{2.77}$$

from which the global fluid velocity potential vector is expressed as

$$\{\hat{\psi}\} = -i\omega\left(-[K_{\psi\psi}] + \omega^2[M_{\psi\psi}]\right)^{-1}[C_{\psi u}]\{\hat{u}\}. \tag{2.78}$$

The electrical admittance for the fluid case is expressed as [24]

$$Y = i\omega\left[\{H_{u\phi}\}^T[D]^{-1}\{H_{u\phi}\} - H_{\phi\phi}\right], \tag{2.79}$$

where the matrix $[D]$ is expressed as [24]

$$[D] = [H_{uu}] - \omega^2[M_{uu}] + \omega^2[C_{u\psi}]\left(-[K_{\psi\psi}] + \omega^2[M_{\psi\psi}]\right)^{-1}[C_{\psi u}]. \tag{2.80}$$

For a time harmonic case with an assumed time dependency of $e^{i\omega t}$, the relationship between the velocity potential $\psi$, and the acoustic pressure in the fluid is given as:

$$p = -i\omega\rho_f\psi, \tag{2.81}$$

where $\rho_f$ is the density of the fluid. The admittance $Y$, expressed in Eq. (2.79), is used to express $Z_T$ by the relation

$$Z_T = \frac{1}{Y}. \tag{2.82}$$

To decrease the calculation time of memory-intensive problems, some of the FE simulations are performed without fluid elements, i.e. ignoring the fluid load of air. An approximate solution for the transmitting voltage response is then found using the hybrid FE/Rayleigh integral method, which calculates the Rayleigh integral based on the displacement over the front of the transducer found in the FE simulation [24]. An error is introduced when using the Rayleigh integral, as it assumes that the transmitter is mounted in a rigid baffle of infinite extent [24]. Similarly an error is introduced by neglecting the fluid loading. The method was utilized e.g. in [37], where piezoelectric ceramic disks with a matching layer were simulated. Good qualitative agreement was stated for the case studied.

# Chapter 3

# Experimental setup and measurement methods

The experiments include both electric and acoustic measurements, in addition to measurements of dimensions and mass. In this chapter the measurement setup and measurement methods are described. An overview of the equipment is given in Section 3.1, the dimension and mass measurements are described in Section 3.4, and the electrical measurement setup is covered in Section 3.2. The acoustical measurement setup and methods are described in Section 3.3, covering transmitting electronics, transducers and positioning, receiving electronics, environmental parameters, and data acquisition. The Brüel & Kjær microphones and the piezoelectric ceramic disks used in the acoustic measurements are presented in Sections 3.5 and 3.6, respectively. Finally, the digital signal processing of the recorded data is described in Section 3.7. The piezoelectric transducers developed during the present work and used in the measurements are not covered here, but in Chapter 6.

## 3.1 Equipment

An overview of the equipment used in the measurements is given in Table 3.1.

Table 3.1: Equipment used in the measurements

| Brand/name | Type of equipment | Serial number |
|---|---|---|
| | Physical measurements | |
| Biltema 19-1444 | Digital caliper | - |
| TESA DIGIT-CAL SI | Digital caliper | 4J09704 |
| Mitutoyo MDH-25M | Digimatic micrometer | 15229628 |
| A&D GF-3000-EC | Precision balance | P1826763 |
| | Electrical measurements | |
| HP 4192A | Impedance analyzer | 23423 |
| Vaisala HMI41 | Humidity and temperature indicator | S4030049 |
| | Acoustical measurements - instrumentation | |
| Agilent 33220A | Waveform generator | MY44023589 |
| Brüel & Kjær 2636 | Measurement amplifier | 1615638 |
| Krohn-Hite 3940A | Digital filter | AM2626 |
| Tektronix DPO3012 | Digital oscilloscope | 195539 |
| Vaisala HMT313 | Temperature and relative humidity sensor | F4850018 |
| | Acoustical measurements - positioning | |
| Physik Instrumente M-037 | Compact precision rotation stage | 0912 A |
| Physik Instrumente M-535 | Linear positioning stage | - |
| Physik Instrumente M-531 | Linear positioning stage | 1460497 |
| | Acoustical measurements - transducers | |
| Brüel & Kjær 4138 | 1/8-inch pressure-field microphone | 1832479 |
| Brüel & Kjær UA-0160 | Adaptor - microphone to preamplifier | - |
| Brüel & Kjær 2633 | Preamplifier | - |
| Brüel & Kjær 4138-A-015 | Microphone system | 2795107 |
| - Brüel & Kjær 4138 | 1/8-inch pressure-field microphone | 2784915 |
| - Brüel & Kjær 2670 | Preamplifier | 2799662 |
| Element #6 | Piezoelectric ceramic Pz27 disk | - |
| Element #10 | Piezoelectric ceramic Pz27 disk | - |
| Element #16 | Piezoelectric ceramic Pz27 disk | - |
| Transducer No. 1 | In-house constructed transducer[1] | - |
| Transducer No. 2 | In-house constructed transducer[1] | - |
| Transducer No. 3 | In-house constructed transducer[1] | - |
| | Acoustic measurements - microphone calibration | |
| Brüel & Kjær 4228 | Pistonphone | 1918465 |
| Brüel & Kjær UZ0004 | Correction barometer | 1918465 |

## 3.2 Electrical measurement setup

The electric properties of the piezoelectric ceramic disks and piezoelectric transducers developed during the present work are determined using an HP 4192A impedance analyzer [56], shown in Fig. 3.1. The conductance, $G_T$, and susceptance, $B_T$, are measured and the admittance found by

$$Y_T = G_T + iB_T = \frac{1}{Z_T}. \tag{3.1}$$

[1] Piezoelectric transducers developed during the present work.

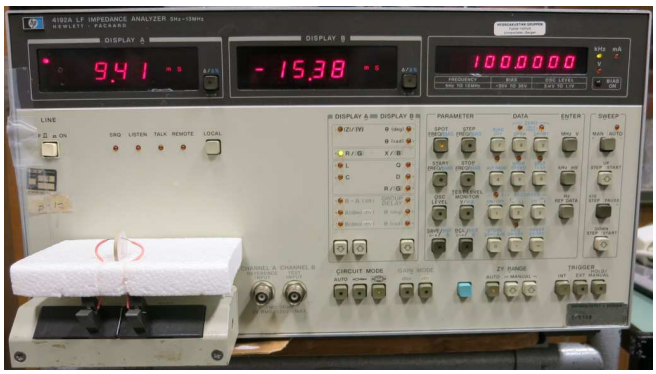

Figure 3.1: HP 4192A impedance analyzer used to measure the admittance of the transducers.

The impedance analyzer is allowed a warmup time of minimum 30 minutes. To account for the wires used in the measurements, a zero offset adjustment of the impedance analyzer (described at page 3-50 in [56]) is conducted for the maximum frequency in the measurement series, before measurements are performed. A drive voltage, referred to a oscillation level in [56], of $V_{rms} = 0.3$ V is used in the presented results. Measurements using different drive voltages, performed on a Pz27 piezoelectric disk of approximate dimensions 20 mm × 2 mm, are shown in Figs. 3.2 and 3.3, for the first and second radial modes of the disk, respectively. Nonlinear effects are seen to cause a downward frequency shift of the resonances and a level reduction of the maximum conductance. $V_{rms} = 0.3$ V is chosen to minimize the nonlinear distortion, while avoiding the resolution limitations observed for the lowest voltage in Fig. 3.3.

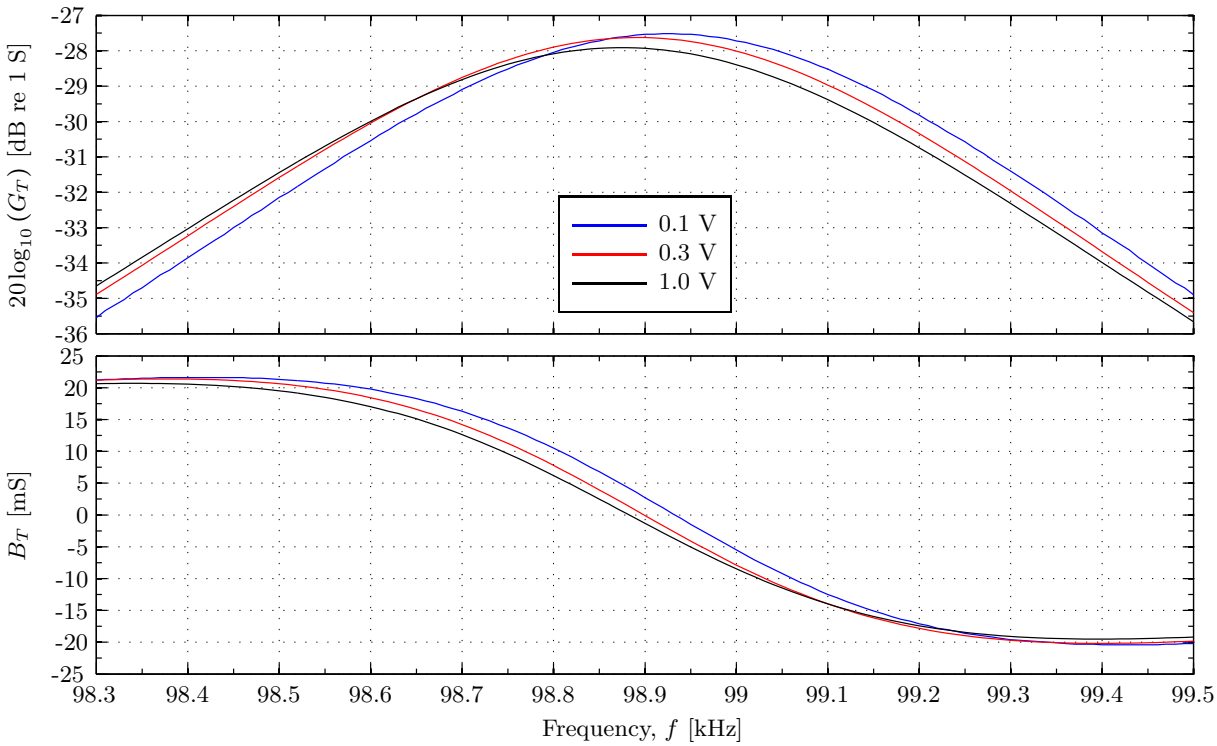


Figure 3.2: Conductance and susceptance of a Pz27 piezoelectric ceramic disk of approximate dimensions 20 mm × 2 mm. Comparison of measurement with different drive voltages. For the frequency range around the first radial mode (R1) of the disk.

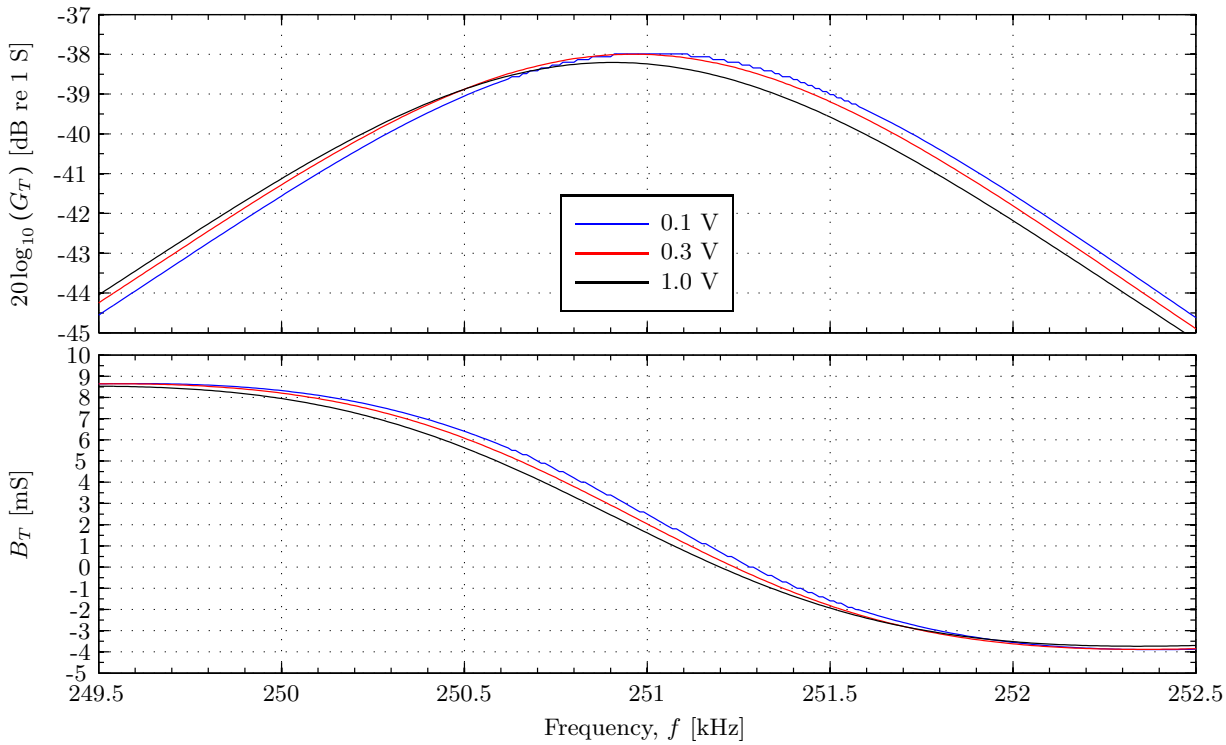


Figure 3.3: As Fig. 3.2, but for the frequency range around the second radial mode (R2) of the disk.

Different wires are used when measuring the admittance, depending on the device measured. Measurements on piezoelectric ceramic disks are performed with the disk placed loosely in a wide groove in a polystyrene holder and held upright by two thin wires connected to the impedance analyzer, as seen in Fig. 3.4.

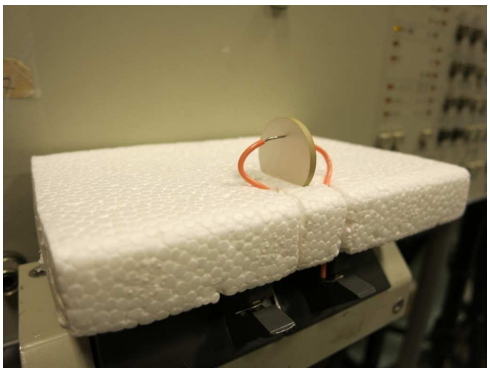

Figure 3.4: A polystyrene holder is used when measuring the admittance of single piezoelectric ceramic disks, with the disk placed loosely in a wide groove in the polystyrene.

This setup is intended to minimize the mechanical load, which is important for comparison with FE simulations. Some repeatability issues are observed at the resonances, as shown for the conductance in Figs. 3.5 and 3.6. A slight change in the magnitude and a shift of the series resonance between any two measurements is seen. One possible reason is the fact that the exact placement of the disk and the wires varies for each measurement. Between each measurement in Figs. 3.5 and 3.6, the disk is removed from the holder and then put back, with the rest of the parameters kept unchanged. A small adjustment of the spring in the wires was performed between measurement #2 and measurement #3, increasing the repeatability issues.

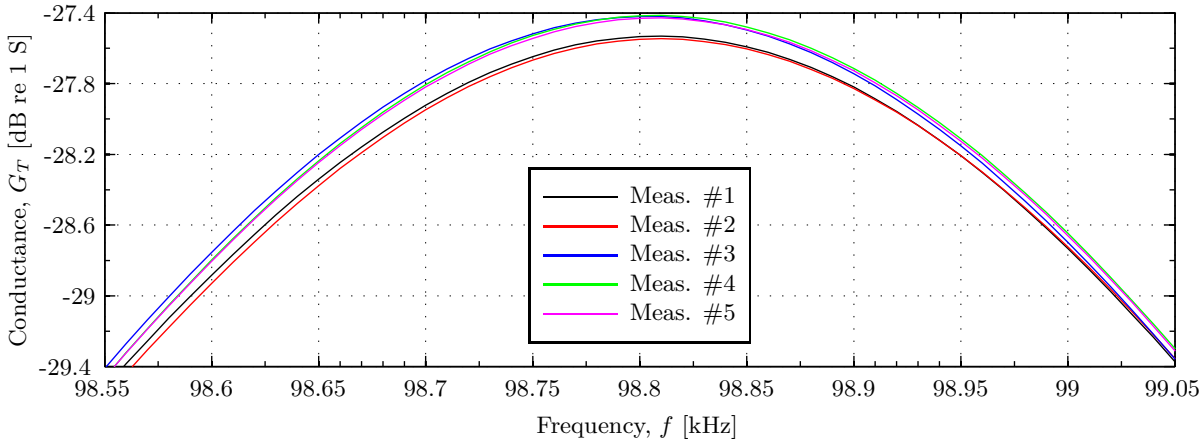


Figure 3.5: Conductance of a Pz27 piezoelectric ceramic disk of approximate dimensions 20 mm × 2 mm. Repeatability measurements. For a frequency range around the first radial mode series resonance.

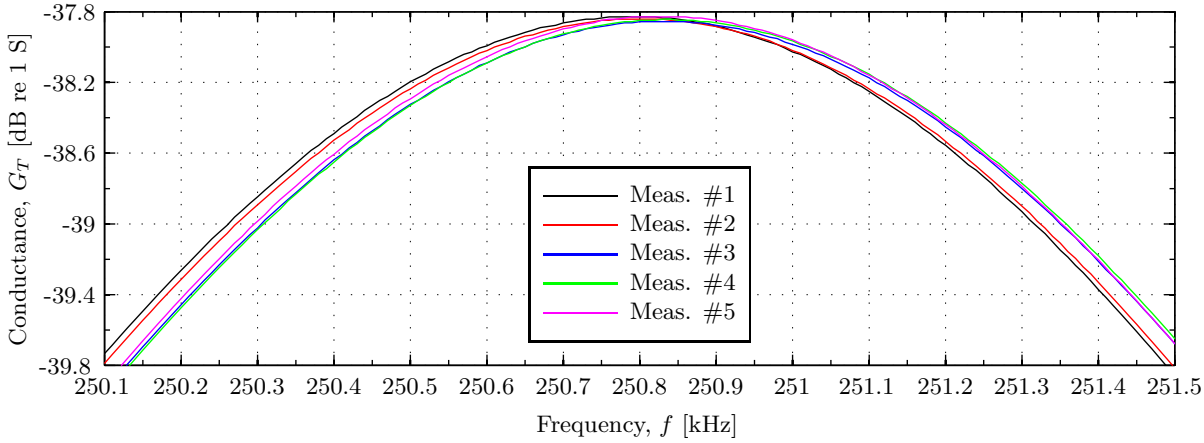


Figure 3.6: As Fig. 3.5, but for a frequency range around the second radial mode series resonance.

When electrical measurements are performed on piezoelectric disks with a matching layer, a different holder constructed of polystyrene and wires is used. The matching layer is wider than the element, which is attached to the matching layer using conductive epoxy, with the conductive epoxy layer extending out to cover remaining rim of the matching layer. A wire is soldered onto the rear electrode on the element. The measurements are performed with the rim of the matching layer, covered in conductive epoxy, resting on a wire tripod. One of the wires in the tripod is connected to the impedance analyzer, as well as the soldered-on wire.

Electrical measurements on the piezoelectric transducers, constructed during this work, are performed as shown in Fig. 3.7.

Environmental parameters are recorded for each measurement series, for use in future work. The temperature and relative humidity are measured with a Vaisala HMP46 probe connected to a Vaisala HMI41 indicator. The measurement uncertainty is ± 2.5 % RH and ± 0.3 °C for the measurement ranges of interest [57]. The ambient pressure is measured using a Brüel & Kjær UZ0004 analog barometer [58].

The measurements are performed by a computer running the MATLAB-script `impanal.m`, given in Appendix A, connected to the impedance analyzer using a GPIB-to-USB adaptor. The measured temperature, relative humidity and pressure, as well as the oscillation level and the measurement frequencies in kHz are specified in the script. Frequency steps ranging from 10 Hz to 1 kHz are used in the measurements. The script is set to pause 250 ms between each query to the impedance analyzer, which is sufficient as one measurement takes approximately 150 ms for frequencies above 400 Hz [56]. The vectors containing conductance, susceptance and frequency (in kHz) are saved to file.

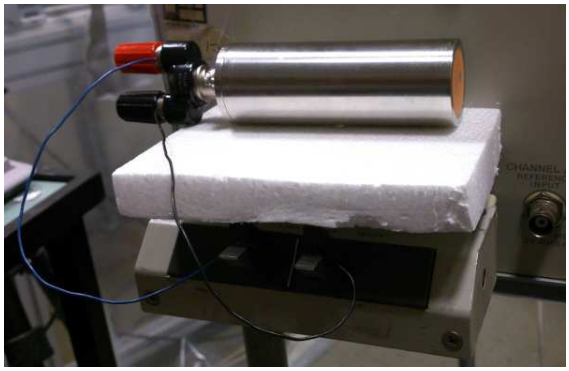

Figure 3.7: Electrical measurement setup for the piezoelectric transducers constructed during this work.

## 3.3 Acoustical measurement setup

An overview of the acoustical experimental setup is given in Fig. 3.8. The acoustical measurement setup is based on the measurement setup developed by Storheim [1] and used by Amundsen in [2]. A pulse is generated by a waveform generator (denoted by (1) in Fig. 3.8) and propagates through air from a transmitting transducer (2) to a receiving transducer (3), where it is amplified by a measurement amplifier (4) with an external filter (5) and recorded by an oscilloscope (6). The oscilloscope also measures the output voltage from the waveform generator. Temperature and relative humidity are recorded. The transmitter and receiver are mounted on carriages on a metal frame inside a plastic measurement chamber, and connected to positioning equipment.

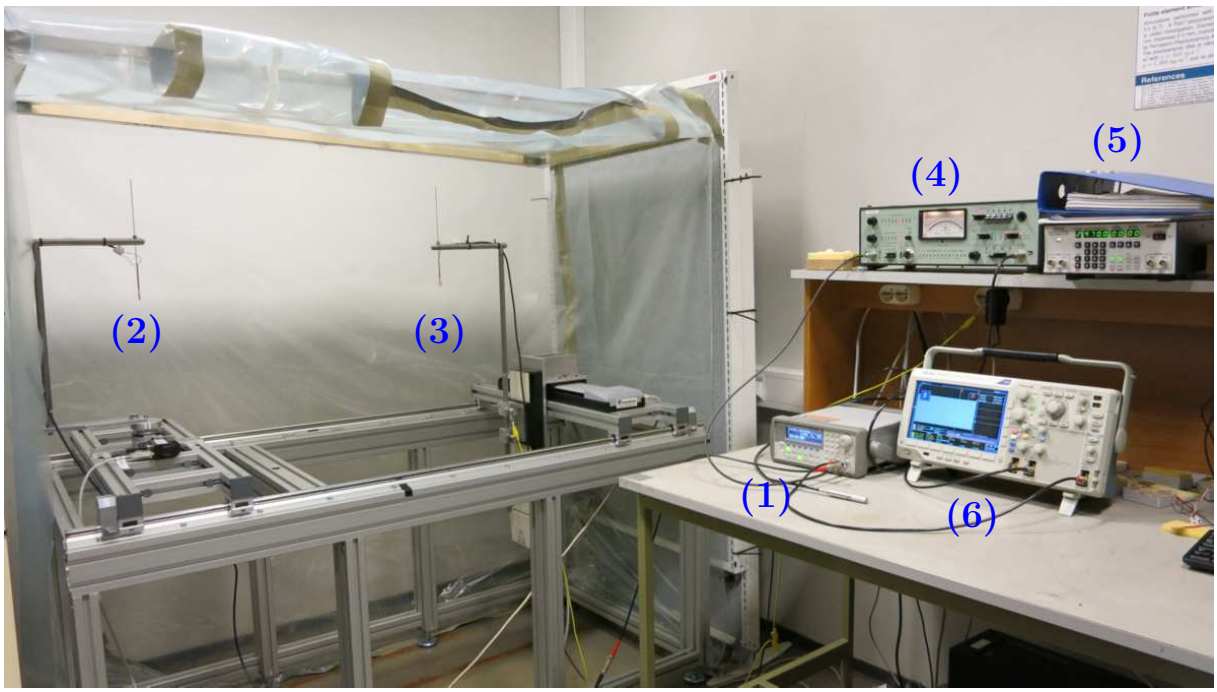


Figure 3.8: An overview of the acoustical measurement setup.

A schematic diagram of the measurement setup is shown in Fig. 3.9. The different parts are described in more detail in the appropriate sections. The input and output impedance of the equipment are needed to account for the instrumentation in the measurements and are given in Table 3.2. The impedance of the instruments are either treated as an ideal resistor, or as an ideal resistor in parallel with an ideal capacitor. The latter is denoted by the symbol "$\|$".

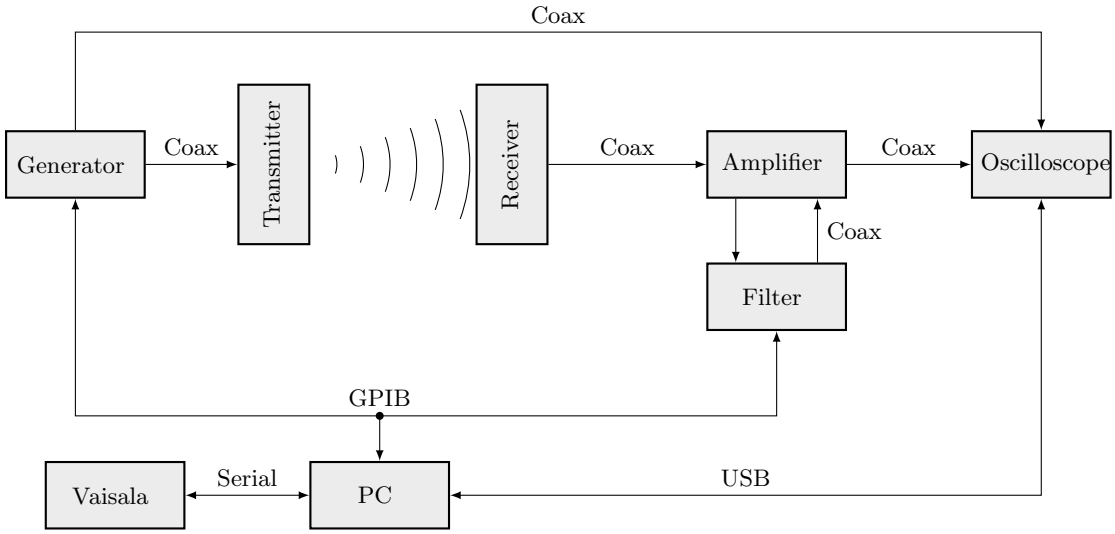


Figure 3.9: Schematic diagram of the measurement setup used in the acoustical measurements.

Table 3.2: Output and input impedance of some of the equipment used in the acoustical measurements

| Brand/name | Type of equipment | Input impedance[2] | Output impedance[3] |
|---|---|---|---|
| Brüel & Kjær 2636 | Measurement amplifier | 1 MΩ ‖ 90 pF | ~100 Ω |
| Tektronix DPO3012 | Digital oscilloscope | 1 MΩ ‖ 11.5 pF | - |
| Agilent 33220A | Waveform generator | - | 50 Ω |
| Krohn-Hite 3940A | Digital filter | 1 MΩ ‖ 100 pF | 50 Ω |

### 3.3.1 Transmitting electronics

A sinusoidal electric burst is generated by an Agilent 33220A waveform generator [59]. The signal is transmitted to the transmitting transducer and to a Textronix DPO3012 digital oscilloscope [60]. A BNC T-connector at the generator output enables parallel connection of the oscilloscope and the transmitting transducer. Coaxial cables with a characteristic impedance of 50 Ω are used to connect the instruments. The oscilloscope is connected to the waveform generator to measure the input voltage to the transmitting transducer, as this varies significantly with the frequency due to impedance changes. The waveform generator and digital oscilloscope are seen in Fig. 3.10

The burst period of the generated signal is set to 40 ms, which corresponds to a burst repetition rate of 25 Hz. A lower burst period is seen to be insufficient for the reverberations to die off between each burst. The amplitude of the sine wave is usually set to either $V_{pp} = 1$ V or $V_{pp} = 10$ V, but can be adjusted from $V_{pp} = 1$ mV to $V_{pp} = 10$ V. The stated voltage is the voltage generated into a 50 Ω load, and it is doubled at open-circuit conditions [59]. Outside resonance the impedance of a single piezoelectric disk is much larger than 50 Ω, and thus the voltage approaches $V_{pp} = 20$ V instead of the specified $V_{pp} = 10$ V. An open-circuit notation is adopted for convenience, e.g. denoting a measurement with a specified voltage of $V_{pp} = 1$ V at 50 Ω load conditions as a $V_{pp} = 2$ V measurement. All voltages used in the calculations are measured voltages and do therefore not necessarily correspond to either $V_{pp} = 1$ V or $V_{pp} = 2$ V.

[2]The input impedance of the B&K 2636 measurement amplifier is given for the direct input, not when using a B&K preamplifier.

[3]The output impedance of the B&K 2636 measurement amplifier is the output impedance of the port connected to the Tektronix DPO3012 oscilloscope.

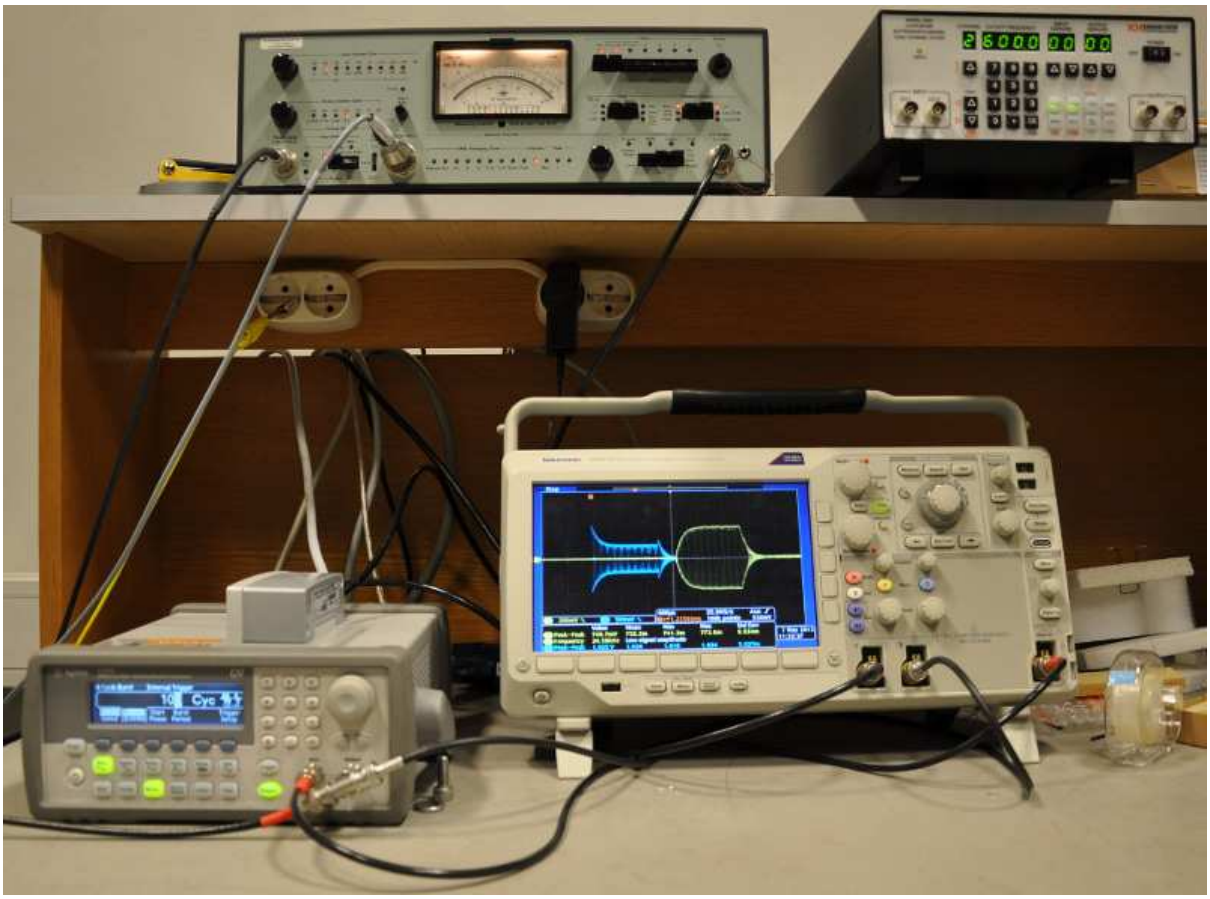

Figure 3.10: Instruments used in the acoustic measurements. The oscilloscope, waveform generator, amplifier and filter, in clockwise order, starting from the bottom right.

The burst length is held constant for each measurement series by adjusting the number of cycles to the current measurement frequency. A burst length of 1.4 ms at a measurement frequency of 100 kHz corresponds to 140 cycles. Burst lengths of 1 ms (~34 cm), 1.4 ms (~48 cm) and 1.6 ms (~55 cm) are used in the measurements, depending on the transmitter, receiver and separation distance. The burst length and separation distance for a given setup is chosen to minimize the effect of electric crosstalk and acoustic reflection from the walls and other nearby protrusions. Separation distances of $z$ = 44 cm, 55 cm, 66 cm and 77 cm are used.

### 3.3.2 Cables

Coaxial cables of type RG58 with a characteristic impedance of approximately 50 Ω are used in the present work. In Section 2.4, the cables are modelled with the typical values of inductance and capacitance shown in Table 3.3.

Table 3.3: Coaxial cable type RG58, typical specifications [45]

| Typical specifications. | |
|---|---|
| Inductance per metre: | $L = 250$ nH/m |
| Capacitance per metre: | $C = 100$ pF/m |

The different cable lengths used in the measurements are specified in Table 3.4. Note that a proprietary cable (not RG58) of 2 m is used when a B&K microphone is connected to the measurement amplifier.

Table 3.4: Overview of the approximate lengths of the RG58 coaxial cables used in the different transducer configurations, see Table 3.5.

| From | To | Length |
|---|---|---|
| Waveform generator | Transmitting piezoelectric disk | 4.0 m |
| Waveform generator | Transmitting piezoelectric transducer | 3.0 m |
| Waveform generator | Oscilloscope | 1.0 m |
| Receiving piezoelectric disk | Measurement amplifier | 3.4 m |
| Receiving piezoelectric transducer | Measurement amplifier | 2.2 m |
| Measurement amplifier | Oscilloscope | 1.0 m |

### 3.3.3 Transducers and positioning

Piezoelectric ceramic disks and piezoelectric transducers developed during the present work are used as transmitting transducers. These transducers are also used as receiving transducer, in addition to two 1/8-inch Brüel & Kjær 4138 condenser microphones [61], one of them with a Brüel & Kjær 2633 preamplifier [62], the other with a Brüel & Kjær 2670 preamplifier [63]. The transducer configurations used in the present work are given in Table 3.5.

Table 3.5: Transducer configurations used in measurements.

| Transmitting transducer type | Receiving transducer type | Separation distance | Burst length |
|---|---|---|---|
| Piezoelectric ceramic disk | B&K 4138 | 44 cm | 1 ms (~34 cm) |
| Piezoelectric ceramic disk | Piezoelectric ceramic disk | 77 cm | 1.4 ms (~48 cm) |
| Piezoelectric transducer | B&K 4138 | 55 cm | 1.4 ms (~48 cm) |
| Piezoelectric transducer | Piezoelectric transducer | 66 cm | 1.6 ms (~55 cm) |

The transmitting transducer and the receiving transducer are mounted on separate carriages to enable adjustment of the separation distance. The carriages are placed on top of a metal frame, with a surrounding plastic measurement chamber to minimize air flow and temperature fluctuations affecting the measurements, see Fig. 3.11.

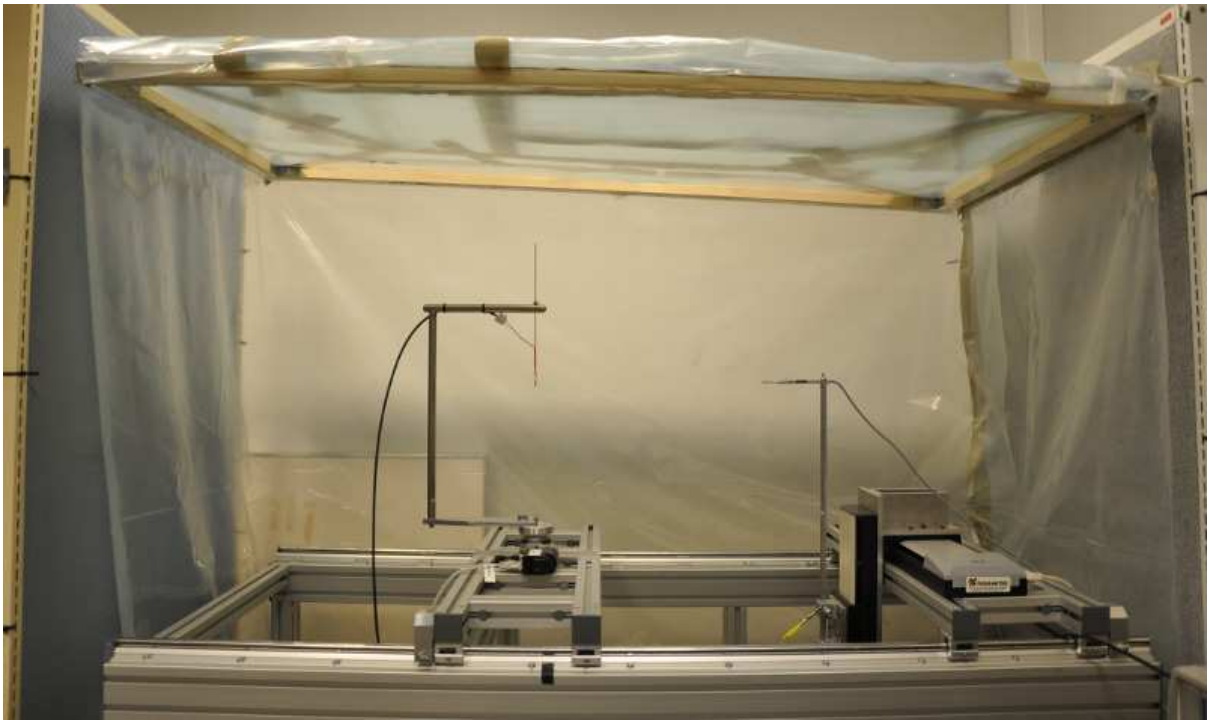

Figure 3.11: The acoustical measurement setup, with a piezoelectric ceramic disk as the transmitting transducer and a Brüel & Kjær 4138 microphone as the receiving transducer. Placed inside the plastic measurement cage with the front flap open.

The transmitter and receiver are first aligned coaxially by visual inspection and a self levelling laser cross level, and then acoustic measurements are performed while the position of the receiver is adjusted in the plane orthogonal to the acoustic axis. It is preferable to perform the positioning at a frequency where a high SNR is observed. The transmitter and receiver are assumed to be coaxial with respect to the acoustic axis when the maximum output voltage is measured. Two computer-controlled [64, 65] linear positioning stages, PI M-531 [66] and PI M-535 [67], are used in the positioning. The transmitting transducer is connected to a PI M-037 rotation stage [68], included in the setup for future use. The separation distance is measured manually with a folding rule, with an estimated total uncertainty of ± 2 mm.

The different types of transducers are mounted in different ways. The Brüel & Kjær microphones are inserted in a hole in an aluminium rod and fastened by a screw at the back, as shown in Fig. 3.12.


Figure 3.12: A Brüel & Kjær 4138-A-015 microphone system mounted on an aluminium rod.

The suspension of the piezoelectric ceramic disks is shown in Fig. 3.13, and the suspension for the piezoelectric transducers developed during the present work is shown in Fig. 3.14. Both types are suspended from a stainless steel structure shaped like an inverted 'L'. Wires are soldered on to the piezoelectric ceramic disk (see Section 3.6) and fastened to a vertical thin metal rod by heat shrink tubing, see Fig. 3.13. The rod is in turn suspended from the horizontal stainless steel rod.

The piezoelectric ceramic disks and the piezoelectric transducers are connected to the instruments

using coaxial cables and BNC-connectors. The Brüel & Kjær microphones are connected by a Brüel & Kjær cable and a 7 pin connector. The suspension of the receiving transducer is connected to electric ground to reduce the electromagnetic noise.

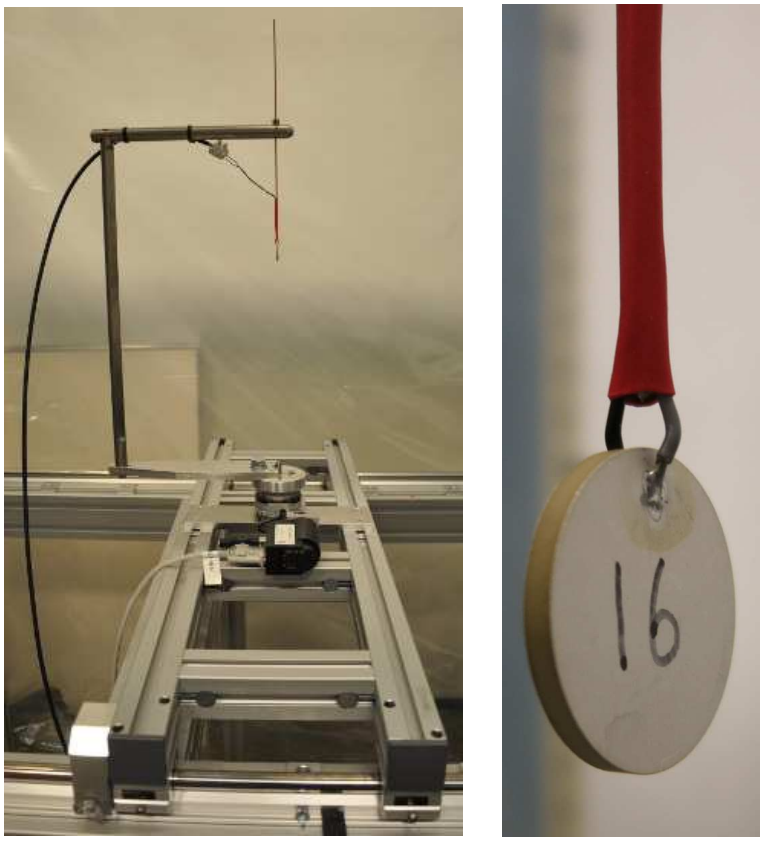


(a) (b)

Figure 3.13: A piezoelectric ceramic disk acting as a transmitting transducer.

Figure 3.14: Two piezoelectric transducers developed during the present work with a separation distance of 66 cm.

### 3.3.4 Receiving electronics

The receiving transducer is connected to a Brüel & Kjær 2636 measurement amplifier [69] with an external Krohn-Hite 3940A digital filter [70]. The measurement amplifier is in turn connected to the Textronix DPO3012 digital oscilloscope where the signal is terminated and recorded.

A maximum total amplification of 100 dB in 10 dB ± 0.05 dB steps is available in the amplifier. A total gain of 60 dB is used in the results presented in the present work; amplifying the signal by 40 dB at the input, prior to the external filter, and 20 dB at the output. The measurement amplifier has an internal high-pass filter turned on with a cutoff frequency at 22.4 Hz and 30 dB per octave attenuation. The linear frequency range of the amplifier is 1 Hz to 200 kHz, and a correction must therefore be introduced when measuring at frequencies above 200 kHz. A typical frequency response of the B&K 2636 measurement amplifier is given in [69] and shown in Fig. 3.15.

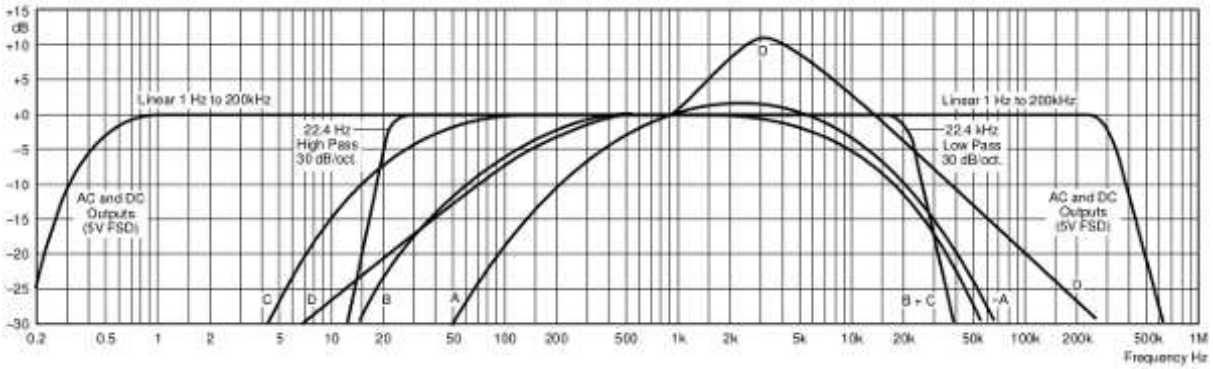


Figure 3.15: The typical frequency response of a B&K 2636 measurement amplifier [69]. The curve to the far right apply to the measurements in the present work.

To investigate the behaviour of the amplifier used in the present work, the output voltage of a sinusoidal wave generated by the waveform generator and amplified by the measurement amplifier is measured. The same amplifier settings are used as in the acoustical measurements. It is assumed that the obtained behaviour is more accurate than that given in Fig. 3.15. The ratio of the voltage at the lowest frequency to the voltage at higher frequencies is shown in Fig. 3.16 and used to correct the measurements.

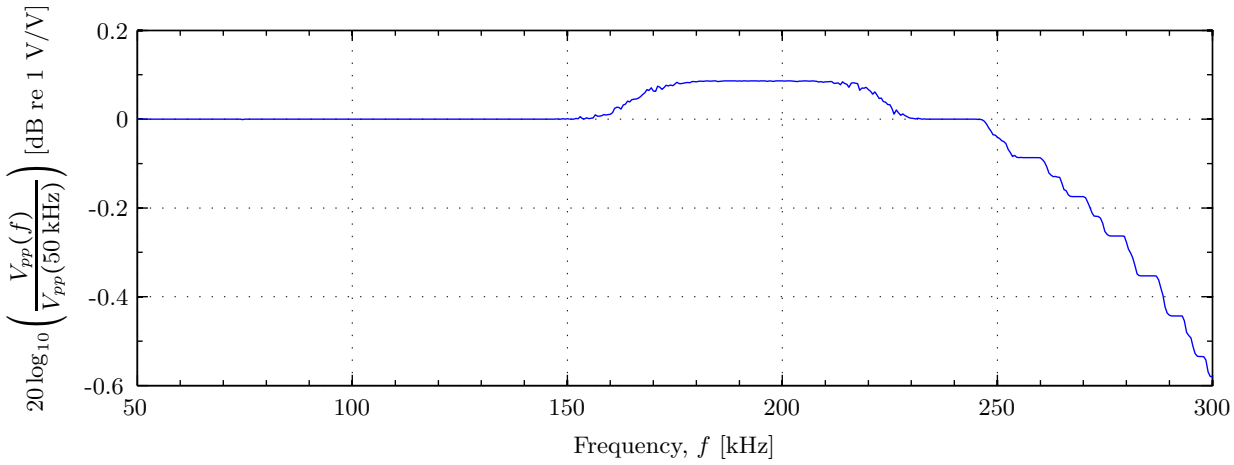


Figure 3.16: The measured peak to peak voltage for the frequency range 50 kHz to 300 kHz, normalized to the measured peak to peak voltage at 50 kHz. This is used to correct the acoustic measurements.

The external digital filter has two separate channels, each with a 24 dB per octave attenuation outside the passband. A bandpass filter is achieved by using one channel as a high-pass filter and the other as a low-pass filter. A computer-controlled bandpass filter is implemented. The cutoff frequency of the high-pass filter is set to 20 kHz. Furthermore, the cutoff frequency of the low-pass filter is set to twice the measurement frequency, and is reset for each frequency step in the measurement series.

### 3.3.5 The oscilloscope

The Textronix DPO3012 digital oscilloscope is used to record both the input voltage to the transmitting transducer and the output voltage from the receiving transducer. The acquisition is triggered by the waveform generator.

An input resistance of 1 MΩ in parallel with a capacitance of 11.5 pF is used. To reduce the random noise in the system, a number of signal bursts are averaged before the received voltage signal is recorded by a computer. Averaging of 128 bursts are used in the measurements presented.

A lowest possible V/div should be chosen when the signal is recorded to get the most out of the 8-bit resolution of the oscilloscope. It is however important not to use a lower V/div than 10 mV/div. This is because a unwanted reduction in the recorded voltage is observed for lower settings due to averaging of the random noise. Fig. 3.17 shows a recorded output voltage waveform with 10 mV/div, both with averaging over 128 bursts and for a single burst.

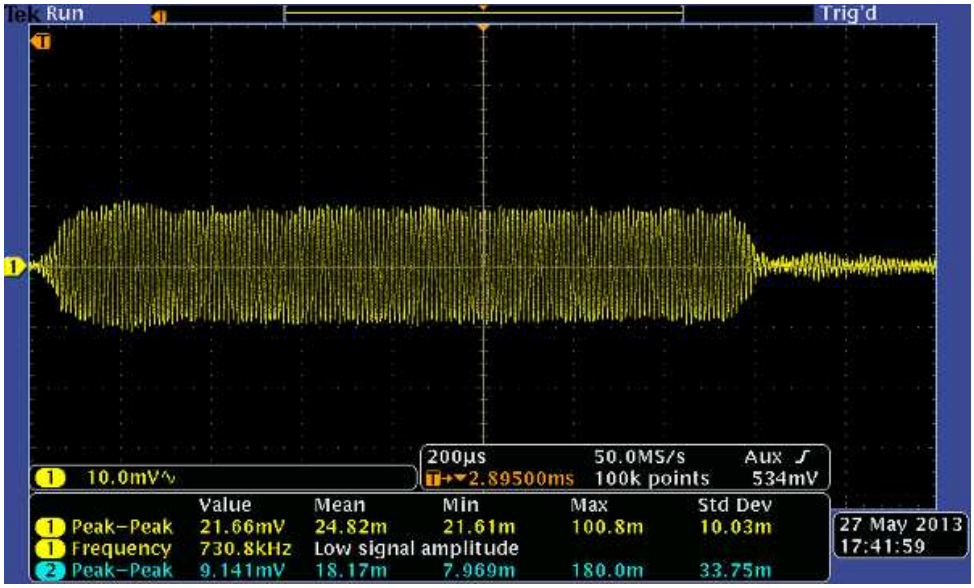


(a)

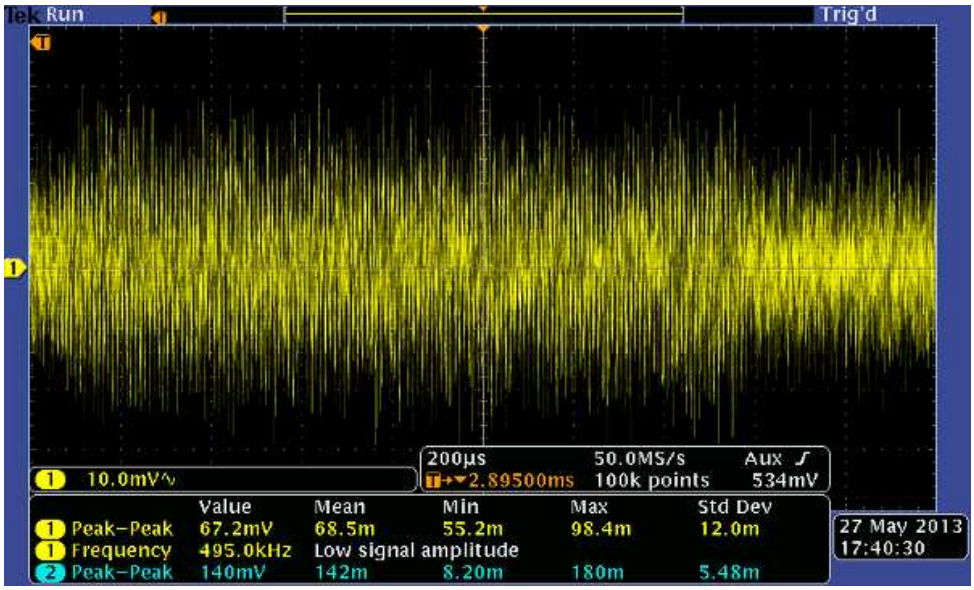


(b)

Figure 3.17: Example measured output voltage with 10 mV/div vertical scaling. (a) averaged over 128 bursts and (b) for a single burst. Transducer No. 2 is used as transmitter and Transducer No. 3 is used as receiver, with a separation distance of 66 cm.

The amplitude of the averaged signal is well within the window frame, and a lower V/div would increase the voltage resolution. The recording of a single burst shows significant amounts of white noise,

which is reduced by averaging multiple bursts. Note that the 8 voltage divisions are visible in the window, but two additional divisions extending above and below the visible view are also recorded by the oscilloscope. Thus the visible window height is 80 mV, while the recorded height is 100 mV.

Fig. 3.18 shows the same signals as in Fig. 3.17, but with 2 mV/div. The peak to peak voltage of the averaged signal now appears to be reduced to under 16 mV, which is the range of the visible window, compared to the 20 mV seen in 3.17. The reason for this discrepancy is seen in Fig. 3.18b, where clipping of the white noise is observed, thus causing the averaging not to fully cancel out noise components. A minimum of 10 mV/div is deemed sufficient to include the vast majority of the white noise in the current measurement setup.

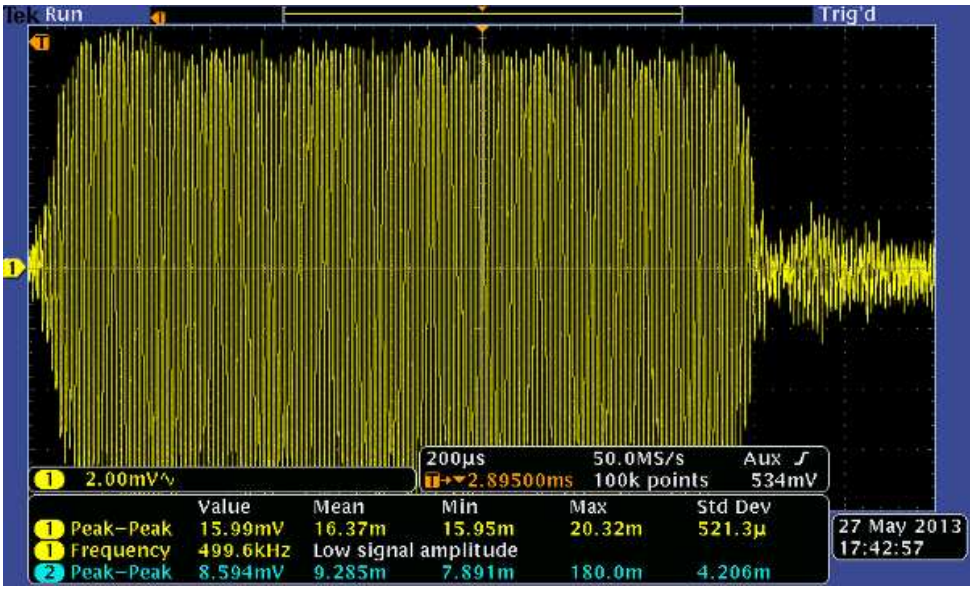


(a)

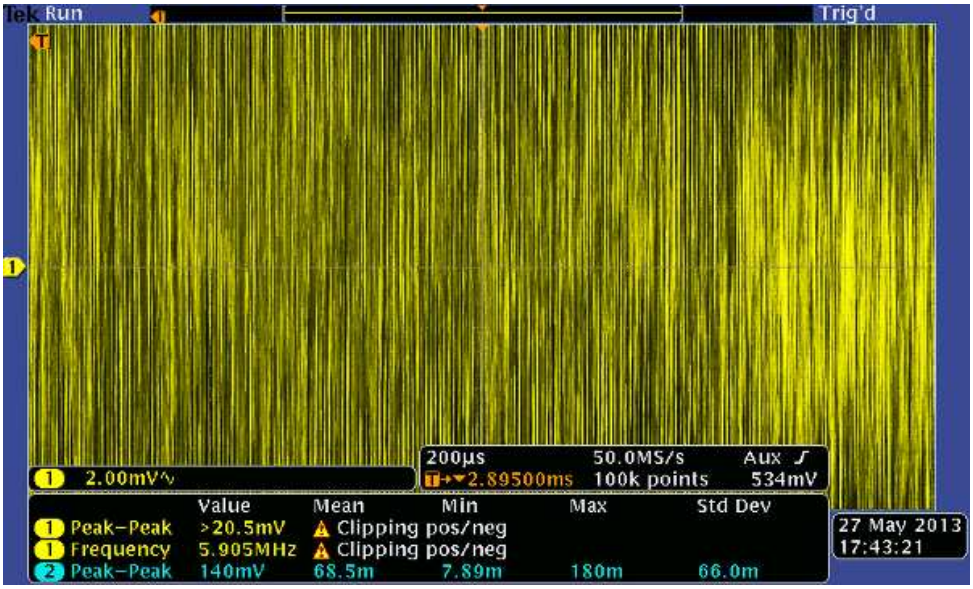


(b)

Figure 3.18: As Fig. 3.17, but with 2 mV/div vertical scaling.

The temporal settings are adjusted so that there are 100 000 samples in the windows, which results in a sample rate of 50 MHz for 200 $\mu$s/div (2 ms window length).

### 3.3.6 Environmental parameters

Relative humidity and temperature are recorded in order to account for absorption in the medium. The relative humidity (RH) and temperature are measured using a Vaisala HMT313 sensor [71]. The sensor

has an uncertainty of ± 0.6 % RH below 40 % RH and an uncertainty of 1.0 % RH above 40 % RH. The uncertainty in the temperature measurements is ± 0.10 °C [72].

### 3.3.7 Noise measurements

The noise in a specific acoustical measurement configuration is determined by an additional measurement series, where the noise is recorded just prior to the arrival of the signal burst, in a time window with a total length of 400 $\mu$s (40 $\mu$s/div) and with 10 mV/div vertical scaling. Only the output voltage from the receiver is recorded. The recorded noise is used to calculate the signal to noise ratio (SNR).

### 3.3.8 Data acquisition

A computer running Windows 7 communicates with the instruments MATLAB -scripts and different communication interfaces: the Tektronix DPO3012 oscilloscope via USB, the Agilent 33220A waveform generator and the Krohn-Hite 3940A filter via a GPIB-to-USB adaptor, and the Vaisala HMT313 temperature and relative humidity sensor via an RS-232-to-USB adaptor (see Fig. 3.9). The scripts are given in Appendix A. Measurements are initiated by the script `main.m` and performed for a measurement series consisting of electrical and acoustical measurements for the specified frequencies. Frequency steps ranging from 0.1 kHz to 0.5 kHz are used, with smallest steps around the resonances at R1 and R2. The following text explains how `main.m` is implemented and which subroutines are called:

- Settings used in the measurements are specified in `measurement_parameters.m`. Important settings used to control the instruments are the frequency vector, input voltage to the transmitting transducer, burst repetition rate, number of averaged bursts and filename. The frequency vector specifies for which frequencies measurements shall be performed. An input voltage of $V_{pp} = 10$ V corresponds to a $V_{pp} = 20$ V open-circuit voltage (see Section 3.3.1). Additional information, such as the separation distance, amplifier gain and the transmitter and receiver used, are entered for use in the post-processing.
- The instruments are initialized by `calibration_parameters.m`.
- Electrical measurements
  - In the electrical measurements the appropriate V/div is assigned to the oscilloscope. Then measurements are performed for each specified frequency.
  - The number of cycles in the signal burst is adjusted for each frequency to keep the temporal signal length constant.
  - The time window is adjusted using `adjustTime.m`.
  - The data acquisition of the scope is turned off, and turned on again after a one second pause. It is necessary to reset the acquisition mode between each frequency, as problems with the averaging have been observed when this routine is omitted.
  - The signal is recorded using `DPO_les.m`, along with the timescale, voltage scale and termination impedance.
- Acoustical measurements
  - The acoustical measurements are performed following the same routine as the electrical measurements, with some alterations.
  - The cutoff frequencies for high- and low-pass filter is set to half and twice the measurement frequency, respectively, thus implementing a moving bandpass filter. Note that an error in the script caused only the low-pass filter cutoff frequency to be adjusted. The high-pass filter cutoff frequency is kept at the initial value.
  - The appropriate voltage scaling is determined automatically for each measurement frequency using `adjustAmplitude.m`, to ensure maximum resolution. The minimum chosen V/div is 10 mV.
  - The script used for recording the signal, `DPO_les.m`, is called from `adjustAmplitude.m` for use in the automatic scaling, and hence an additional calling of `DPO_les.m` is not necessary.
- Everything is saved to a timestamped file.
- The instruments are shut down. Some problems have been observed with the instrument shutdown. Therefore it is recommended to manually run the commands `delete(instrfindall)` and `clear all` between each measurement series.

## 3.4 Measurements of dimension and mass

Accurate measurements of physical dimensions of the piezoelectric ceramic disks and the piezoelectric transducers developed as part of the present work are needed in order to perform accurate FE simulations. Different measurement devices are used to perform the measurements, depending on the dimensions of the sample.

The instruments used to measure the dimensions are:

- Mitutoyo MDH-25 digimatic micrometer [73] with a measurement range of 0 to 25 mm, a resolution of 0.1 $\mu$m and an accuracy of ±0.5 $\mu$m
- TESA DIGIT-CAL SI digital caliper [74] with a measurement range of 0 to 150 mm, a resolution of 0.01 mm and an accuracy of ± 0.03 mm
- Biltema 19-1444 digital caliper with a measurement range of 0 to 150 mm, a resolution of 0.01 mm and an accuracy of ± 0.03 mm

For each dimension, a measurement series consisting of 10 measurements is performed and the mean, $\bar{x}$, and the standard deviation, $\sigma_x$, are calculated. When measuring the thickness of a sample the 10 measured points are distributed across the surface. The diameter of a disk is measured 10 times, rotating the disk between each measurement and thus distributing the measurements across the disk. The total measurement uncertainty is calculated by [75]

$$\sigma_{tot} = \sqrt{\sigma_x^2 + (\sigma_{instr})^2}, \tag{3.2}$$

where $\sigma_{instr}$ is the uncertainty of the measurement device used.

The mass is measured using a A&D GF-3000 precision balance [76] with a stated repeatability (standard deviation) of 0.01 g and linearity of ± 0.02 g.

## 3.5 Brüel & Kjær 4138 microphone systems

Two different Brüel & Kjær microphone systems are used in the measurements. Both consists of a B&K 4138 1/8-inch microphone [61] and a B&K preamplifier, including a proprietary cable of 2 m, where a B&K UA-160 1/8-inch to 1/4-inch adaptor is used connect the microphone to the preamplifier. A preamplifier is used since the microphone requires a 200 V external polarization voltage. Details on the microphone systems are given in Table 3.6. Microphone system No. 1 is assembled in-house and includes a B&K 2633 preamplifier [62]. Microphone system No. 2 is assembled and sealed in a clean environment by B&K [77] and includes a BK2670 preamplifier [63]. Both preamplifiers are stated to have a flat frequency response [62, 63].

Table 3.6: Microphone systems used in the measurements

| Brand/name | Type of equipment | Serial number |
|---|---|---|
| | Microphone system No. 1 | |
| Brüel & Kjær 4138 | 1/8-inch pressure-field microphone | 1832479 |
| Brüel & Kjær UA-160 | Adaptor - microphone to preamplifier | - |
| Brüel & Kjær 2633 | Preamplifier | - |
| | Microphone system No. 2 | |
| Brüel & Kjær 4138-A-015 | Microphone system | 2795107 |
| - Brüel & Kjær 4138 | 1/8-inch pressure-field microphone | 2784915 |
| - Brüel & Kjær UA-160 | Adaptor - microphone to preamplifier | - |
| - Brüel & Kjær 2670 | Preamplifier | 2799662 |

The Brüel & Kjær 4138 1/8-inch pressure-field microphone is designed for "high-level and very high-frequency measurements and measurements in confined spaces" according to the manufacturer [61], with a stated frequency range of 6.5 Hz to 140 kHz. However, the supplied calibration charts of the open-circuit pressure frequency response cover the frequency range from 20 Hz to 200 kHz [78, 79], where the frequency response is measured with an electrostatic actuator and expressed relative to response at 250

Hz. The calibration charts for the microphones in Microphone system No. 1 and Microphone system No. 2 are shown in Figs. 3.19 and 3.20, respectively.

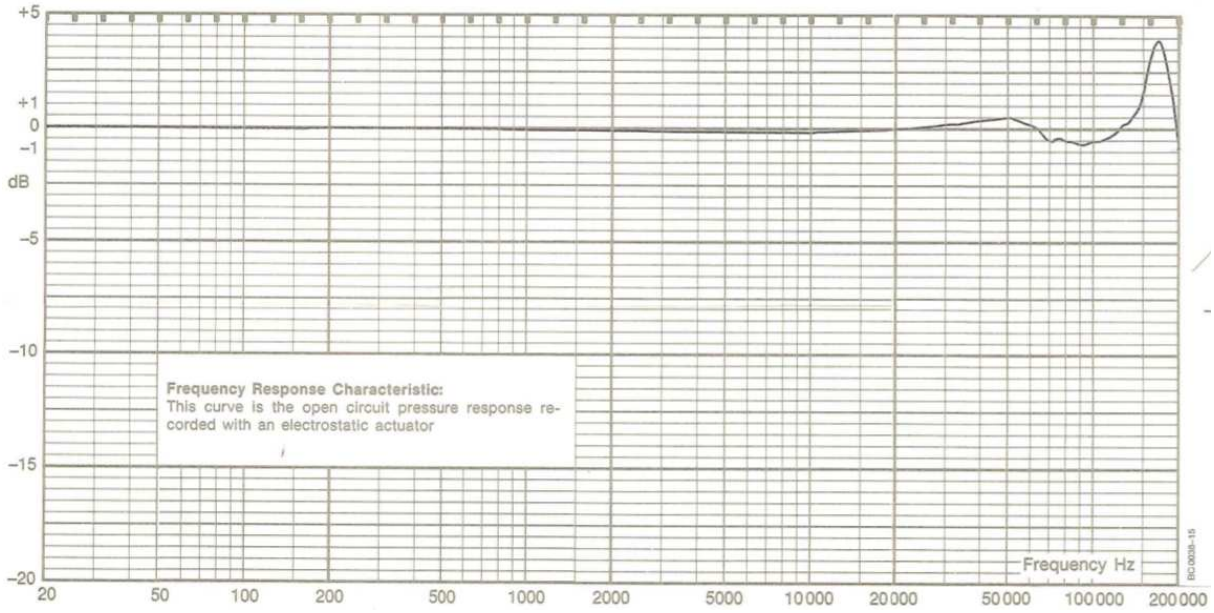


Figure 3.19: Calibration chart of the open-circuit pressure frequency response, relative to 250 Hz, of the Brüel & Kjær 4138 pressure-field microphone [78], serial no. 1832479, as used in Microphone system 1. Measured with an electrostatic actuator.

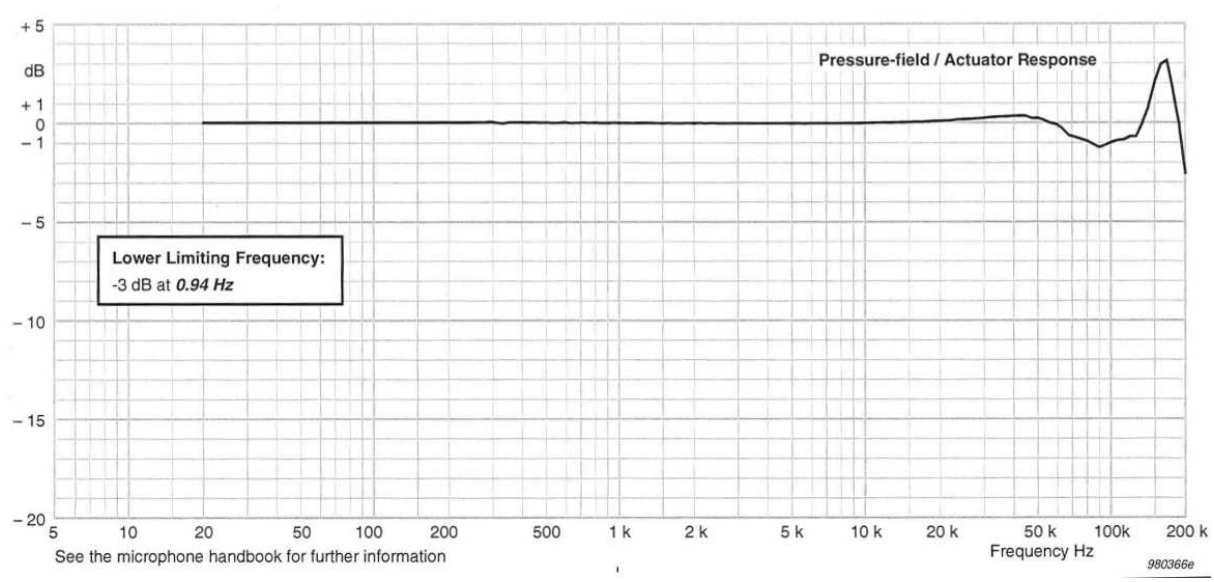


Figure 3.20: As Fig. 3.19, but for Brüel & Kjær 4138 pressure-field microphone [79], serial no. 2784915, as used in Microphone system No. 2.

An additional calibration of Microphone system No. 2, B&K 4138-A-015, is performed by Brüel & Kjær for frequencies up to 100 kHz [80], yielding the open-circuit pressure frequency response, relative to 250 Hz. In Fig.3.21 this calibration of Microphone system No. 2 is compared to the calibration of the microphone as shown in Fig. 3.20. These calibrations should agree, since the preamplifier frequency response is flat [63]. A maximum difference between the two calibrations of about 0.5 dB is observed at 100 kHz, where the uncertainty in the calibration of the system is 0.4 dB [80]. It is seen that the two calibrations agree within the given uncertainties. The calibration of the microphone (Fig. 3.20) is used in the present work, as this provides the largest frequency range and it is assumed that the frequency response of the microphone and of the microphone system agree. This assumption is also applied to Microphone system No. 1.

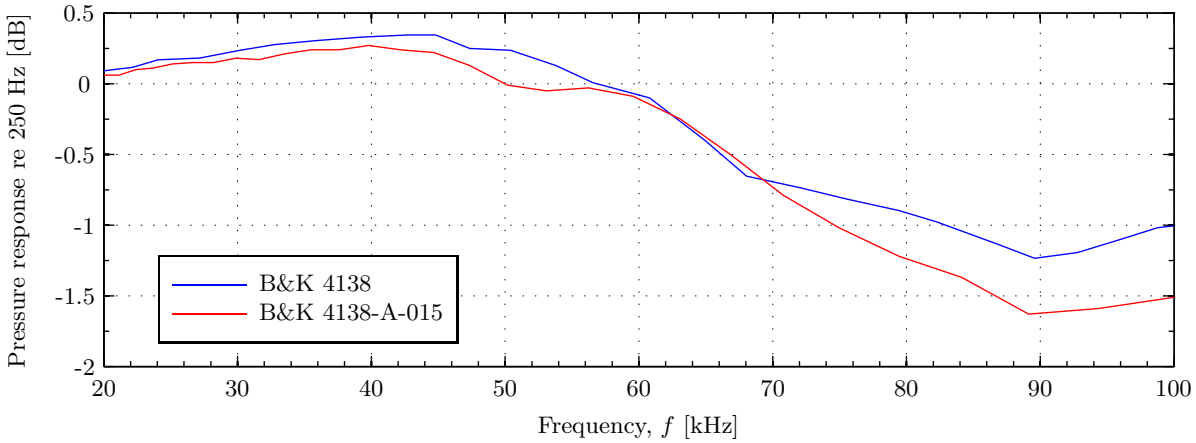


Figure 3.21: Comparison of the calibrated open-circuit pressure frequency responses, relative to 250 Hz, of the B&K 4138 microphone [79] (serial no. 2784915) in Microphone system No. 2 and the complete Microphone system No. 2 [80] (B&K 4138-A-015, serial no. 2795107).

The free-field open-circuit receiving voltage response of the microphone system, relative to 250 Hz, is determined by including a free-field correction to Fig. 3.19 and Fig. 3.20. The typical free-field correction for B&K 4138 microphones with protection grid [81] is given in Fig. 3.22. The curve for 0° incidence is used. It is assumed that the transition to dashed lines after 100 kHz indicates larger uncertainties for these frequencies. The curve for normal incidence is digitalized, as well as the calibration curves in Figs. 3.19 and 3.20, and used to determine $|M_V|$ relative to 250 Hz, shown for both microphone systems in Fig. 3.23.

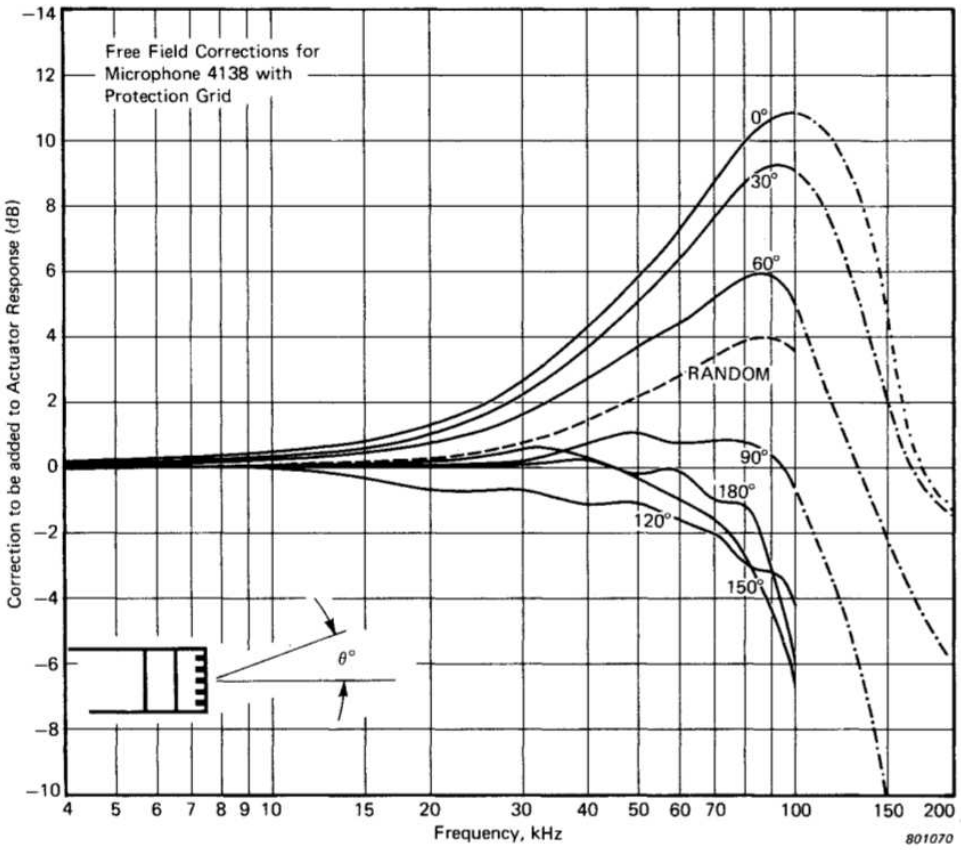


Figure 3.22: "Free-field correction curves for eighth-inch Condenser Microphone Type 4138 fitted with normal protection grid" [81]. Typical values only. The curve for normal incidence is used in the calculations.

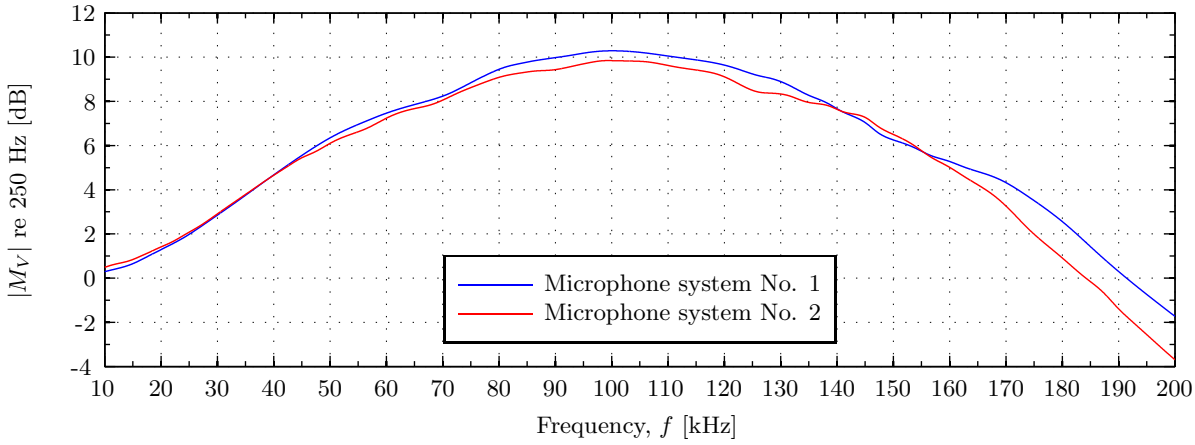


Figure 3.23: $|M_V|$ relative to 250 Hz for the two microphone systems used in the present work.

### 3.5.1 Calibration of the microphones using a pistonphone

The magnitude of the free-field open-circuit receiving voltage response of each of the microphone systems is determined by combining the relative $|M_V|$ (shown in Fig. 3.23) with the free-field open-circuit receiving voltage response at 250 Hz. The latter is found by calibration with a Brüel & Kjær 4228 pistonphone [58] with a DP-0774 adaptor, as no free-field correction is needed at 250 Hz [81].

In the calibration, the microphone system, consisting of a microphone and a preamplifier, is connected to the B&K 2636 measurement amplifier with 20 dB gain, without filters, and recorded by the Tektronix DPO3012 oscilloscope. $|M_V|$ is given by effective quantities as [44]

$$|M_V| = \frac{V_e}{p_e}, \tag{3.3}$$

where $p_e$ is the effective free-field pressure at the position of the receiving transducer, assuming normal incidence and plane wavefronts at the transducer surface [44], and $V_e$ is the effective open-circuit output voltage from the receiving transducer.

The pistonphone generates a known sound pressure level, SPL, which is defined as [46]

$$SPL \equiv 20 \log_{10}\left(\frac{p_e}{p_{ref}}\right), \tag{3.4}$$

where $p_{ref}$ is the reference level, usually set to 20 $\mu$Pa in air. The given SPL for the pistonphone is 124.11 ± 0.09 dB re 20 $\mu$Pa at 251.2 Hz ± 0.1% [82]. The SPL is valid at 1013 hPa, 20°C and a relative humidity (RH) of 65 %. If the calibration of the microphone system is performed under different conditions the sound pressure level is found by [82]

$$\text{Actual } SPL = \text{Stated } SPL + \Delta L_p + \Delta L_V, \tag{3.5}$$

where $\Delta L_V$ is the correction for the load volume, and $\Delta L_p$ is the correction for the ambient pressure, which can be read directly from the supplied correction barometer UZ0004 or calculated using a correction of 0.2 dB per 23 hPa. $\Delta L_V$ is zero for a 1/8-inch microphone with protection grid [82].

Combining Eqs. (3.3), (3.4) and (3.5) and inserting known values yield

$$|M_V(251.2\,\text{Hz})| = \frac{V_e}{10^{\frac{SPL+\Delta L_p}{20}} p_{ref}} = \frac{V_e}{10^{\frac{124.11+\Delta L_p}{20}} 20 \times 10^{-6}}, \tag{3.6}$$

which is $|M_V|$ at 251.2 Hz.

The effective output voltage is found from the measured peak-to-peak voltage, $V_{pp}^{rec}$, by

$$V_e = \frac{V_{pp}^{rec}}{20\sqrt{2}}, \tag{3.7}$$

where it is assumed that the input voltage to the measurement amplifier equals the recorded voltage, when the 20 dB gain in the measurement amplifier is corrected for by dividing the voltage by $10^{20/20} = 10$.

The microphone system with a Brüel & Kjær 4138 microphone, serial no. 1832479, and a Brüel & Kjær 2633 preamplifier, was calibrated at an ambient pressure of 1005 hPa, resulting in a correction factor $\Delta L_p = -0.07$ dB. The measured voltage was $V_{pp}^{rec} = 443.8$ mV, giving

$$|M_V(251.2\,\text{Hz})| = \frac{V_e}{p_e} = \frac{15.6907\,\text{mV}}{31.844\,\text{Pa}} = 0.493\,\text{mV/Pa}. \tag{3.8}$$

The given sensitivity of the microphone is 0.822 mV/Pa [78]. It is stated in [78] that the use of a Brüel & Kjær 2633 preamplifier typically reduces the sensitivity by approximately 6 dB, which corresponds to a total sensitivity of approximately 0.411 mV/Pa for the given configuration. The sensitivity of this microphone system was also calculated in [38] and [2]. The former has calculated it to be 0.3157 mV/Pa, the latter to 0.535 mV/Pa. This discrepancy has not been investigated further.

The Brüel & Kjær 4138-A-015 microphone system, serial no. 2795107, was also calibrated at an ambient pressure of 1005 hPa, resulting in a correction factor $\Delta L_p = -0.07$ dB. The measured voltage was $V_{pp}^{rec} = 470.5$ mV, giving

$$|M_V(251.2\,\text{Hz})| = \frac{V_e}{p_e} = \frac{16.6347\,\text{mV}}{31.844\,\text{Pa}} = 0.522\,\text{mV/Pa}. \tag{3.9}$$

The given sensitivity of the Brüel & Kjær 4138 is 0.925 mV/Pa [79], while it is 0.524 mV/Pa for the microphone system [77]. The sensitivity of the microphone system found by calibration with a pistonphone agrees well within the ± 0.2 dB (approx. 2.3 %) uncertainty of the value stated in [77]

## 3.6 Piezoelectric ceramic disks

Piezoelectric ceramic disks of the material Pz27, manufactured by Ferroperm [34], are used as transmitters and receivers, and as part of the piezoelectric transducers developed during the present work. Pz27 is a soft lead zirconate titanate with a relatively high Curie temperature, exceeding 350 °C, and high electromechanical coupling factors [34].

Disks with stated diameter, $D$, of 20 mm and a stated thickness, $T$, of 2 mm are used. The standard tolerance given by Ferroperm for either of the dimensions is ± 3 %. A batch of 20 disks were ordered and physical and electrical measurements were performed in order to choose which disks to use in the acoustical measurements. The measured dimensions are given in Table 3.7. It is desirable to use similar disks in the measurements, primarily determined based on the frequency of the first radial resonance peak found in the electrical measurements. This is essential to the two-transducer reciprocity calibration method (see Section 2.6). Element #6, Element #10 and Element #16 are chosen for acoustical measurements and Element #5, Element #15 and Element #20 are chosen to be used in the transducer construction.

In order to perform the acoustical measurements, the piezoelectric ceramic disks need to be suspended from a horizontal steel bar, as described in Section 3.3.3. This is made possible by soldering wires to the disks, one wire on each of the electrodes, close to the edge. The disks were preheated to 175 °C and then soldered with 250 °C at the tip of the soldering iron, well below the Curie temperature. The soldering was performed by staff engineer Per Heradstveit. Fig. 3.24 shows a piezoelectric ceramic disk with and without wires connected.

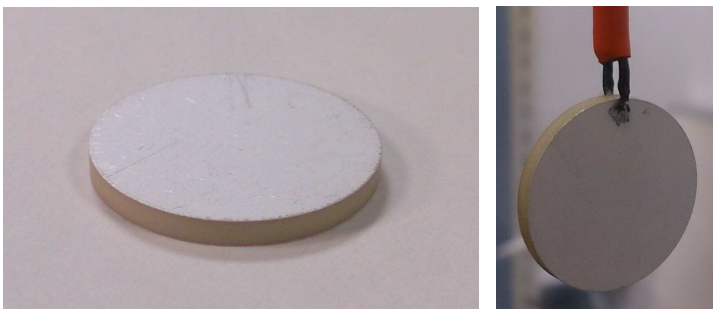

(a) (b)

Figure 3.24: Pz27 piezoelectric ceramic disk of approximate dimensions 20 mm × 2 mm. (a) Without wires. (b) With wires attached.

Table 3.7: Dimensions of Pz27 piezoelectric ceramic disks with stated dimensions 20 mm × 2 mm and a tolerance of ± 3 %, measured with a Mitutoyo MDH-25M digimatic micrometer.

| Disk No. | D [mm] | T [mm] |
|---|---|---|
| #1 | 20.24 ± 0.01 | 2.038 ± 0.001 |
| #2 | 20.229 ± 0.006 | 2.020 ± 0.002 |
| #3 | 20.241 ± 0.007 | 2.025 ± 0.003 |
| #4 | 20.236 ± 0.005 | 2.0241 ± 0.0008 |
| **#5** | 20.24 ± 0.01 | 2.012 ± 0.003 |
| **#6** | 20.25 ± 0.01 | 2.031 ± 0.001 |
| #7 | 20.24 ± 0.01 | 2.041 ± 0.004 |
| #8 | 20.23 ± 0.01 | 2.036 ± 0.002 |
| #9 | 20.206 ± 0.006 | 2.002 ± 0.002 |
| **#10** | 20.234 ± 0.008 | 2.035 ± 0.002 |
| #11 | 20.23 ± 0.01 | 2.0244 ± 0.0008 |
| #12 | 20.246 ± 0.007 | 2.040 ± 0.002 |
| #13 | 20.242 ± 0.008 | 2.031 ± 0.002 |
| #14 | 20.24 ± 0.01 | 2.040 ± 0.002 |
| **#15** | 20.23 ± 0.01 | 2.003 ± 0.001 |
| **#16** | 20.24 ± 0.01 | 2.035 ± 0.001 |
| #17 | 20.23 ± 0.02 | 2.018 ± 0.001 |
| #18 | 20.24 ± 0.01 | 2.037 ± 0.001 |
| #19 | 20.26 ± 0.01 | 2.027 ± 0.001 |
| **#20** | 20.25 ± 0.01 | 2.033 ± 0.002 |

## 3.7 Signal processing

The measured voltage-to-voltage transfer function, $H_{1m5}^{VV}$, is expressed by extracting a voltage value from the measured waveforms $V_{1,m}$ and $V_{5,m}$. The value representing each recorded waveform is the steady-state peak-to-peak voltage, $V_{pp}^{rec}$. $V_{pp}^{rec}$ is calculated post-process, for an interval of samples in the recorded waveform, chosen as the steady-state.

### 3.7.1 Recorded waveforms

The steady-state of a measured waveform is selected by visual inspection. The steady-state is selected as a sample interval, e.g. all samples between sample $n_{start}$ and $n_{stop}$. The measured $V_{5,m}$ is used for determining the steady-state area used for both $V_{5,m}$ and $V_{1,m}$, as the $V_{5,m}$ waveform is the more complex waveform, due to a number of factors inherent in the physical processes of sound wave propagation and reception. The steady-state interval is held constant for all frequencies in one measurement series. A recorded waveform example, using piezoelectric elements as transmitter/receiver, is shown in Fig. 3.25.

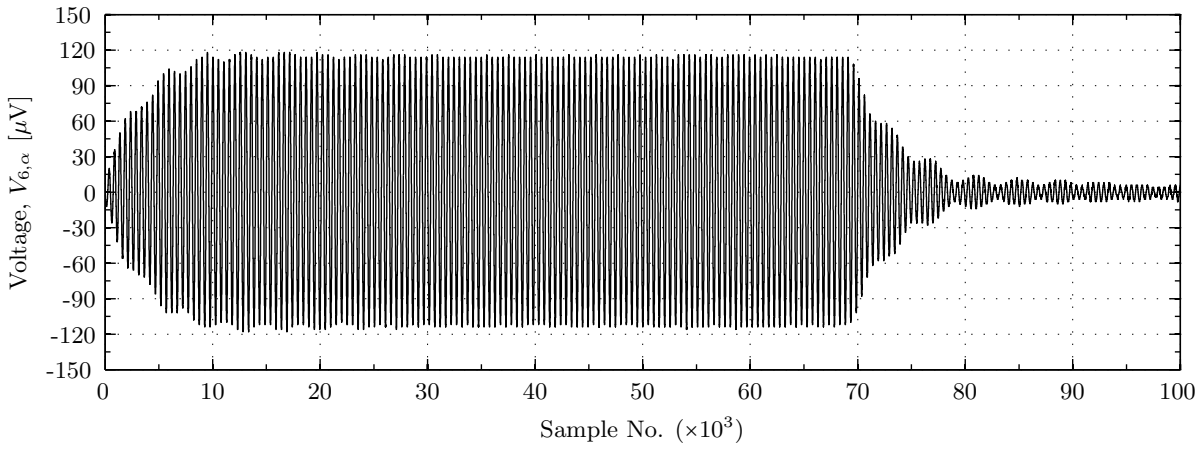


Figure 3.25: An example waveform.

A visual inspection of the waveform in Fig. 3.25 suggests that steady-state is reached somewhere between $n_{start}$ = 20000 and 30000. A waveform from the same measurement, but at another frequency of interest, is shown in Fig. 3.26.

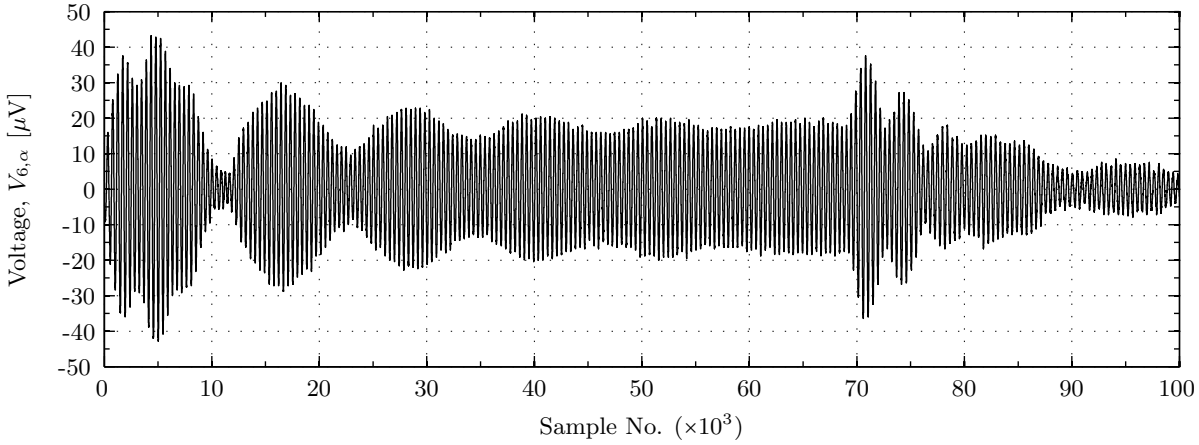


Figure 3.26: An example waveform.

In Fig. 3.26, steady-state is not reached within the applied burst length. An apparent way to reach steady-state for the Fig. 3.26 waveform is to increase the number of cycles in the applied burst. But increasing the burst length, while maintaining a constant separation distance between the transmitter and receiver, might cause effects such as (a) standing waves between the transmitter and receiver, and (b) cause sound waves reflected of other surfaces in the measurement cage to be recorded. To compensate, the measurement distance could also be increased, but that would decrease the SNR. Furthermore, the measurement series for Figs. 3.25 and 3.26 is done with maximum separation distance between the transmitter and receiver possible in the current measurement setup. Thus, the choice of the sample interval where $V_{pp}^{rec}$ is calculated, is a compromise between the number of cycles wanted in the $V_{pp}^{rec}$ calculation for statistical integrity, and whether or not steady-state has been reached. Henceforth, "calculation interval" is used to express the sample interval where $V_{pp}^{rec}$ is calculated.

Calculation of $V_{pp}^{rec}$ for a recorded waveform, either $V_{1m}$ or $V_{5m}$, is done either by Fourier transform of the calculation intervals (see Section 3.7.2) or by direct calculation on the measured waveform (see Section 3.7.3).

The calculation intervals used in the signal processing performed in the present work are shown in Table. 3.8.

Table 3.8: Calculation intervals used in the signal processing.

| Transmit/receive combination | Calculation interval [$10^3$ samples] |
|---|---|
| Element to microphone | 50 - 95 |
| Element to element | 45 - 65 |
| Transducer to microphone | 45 - 68 |
| Transducer to transducer | 50 - 78 |

### 3.7.2 Calculation of $V_{pp}^{rec}$ - Fourier transform method

The MATLAB script `findPeakToPeak_FFT.m` calculates $V_{pp}^{rec}$ for a given sample interval of a recorded waveform (see Appendix A). Let $V_{sig}(t)$ be the discrete voltage signal in the calculation interval of a signal waveform, recorded at the measurement frequency $f_{sig}$. The number of samples in $V_{sig}(t)$ is $N_{sig}$. The Fourier transform of $V_{sig}(t)$ is calculated using the `fft` algorithm in MATLAB, i.e.

$$V_{sig}(t) \xrightarrow{FFT} V_{sig}(f), \tag{3.10}$$

where $V_{sig}(t)$ has been zero-padded to a total length of 200000 samples in the `fft` function. The peak-to-peak voltage is found as

$$V_{pp}^{rec}(f_{sig}) = 2 \cdot 2 \cdot \frac{V_{sig}(f_{sig})}{N_{sig}}. \tag{3.11}$$

The frequency spectrum output of the function `fft` is two-sided, i.e. a spectrum is displayed for both negative and positive frequencies. For a real time response, the two spectra are symmetrical around the DC-component [83]. Parseval's theorem [84], states that the energy of the time and frequency domain must be equal. Hence only half the energy of the time domain is contained in the positive frequencies of the frequency spectra. The frequency spectra is multiplied by 2 to correct for this, as $V_{pp}^{rec}$ is found at the (positive) measurement frequency $f_{sig}$. The peak-to-peak voltage is twice the size of the amplitude, thus $V_{sig}(f_{sig})$ is multiplied by 2 a second time. The frequency spectrum amplitude is dependent of the discrete time domain signal length. For instance, given a discrete sine wave with a whole number of cycles with amplitude $A$, the frequency spectrum amplitude for the sine waves frequency is $|A|/m$ [83], where $m$ is the number of samples in the sine wave[4]. Thus, $V_{sig}(f_{sig})$ is divided by $N_{sig}$, in order to obtain the voltage amplitude of the measured waveform at frequency $f_{sig}$.

As an example, the calculation interval selected for the measurement series from which the waveforms in Figs. 3.25 and 3.26 are extracted, is sample $n_{start}$ = 40000 through $n_{stop}$ = 65000. Fig. 3.27 shows $V_{sig}(f)$ calculated using Eq. (3.10), for the waveform in Fig. 3.25.

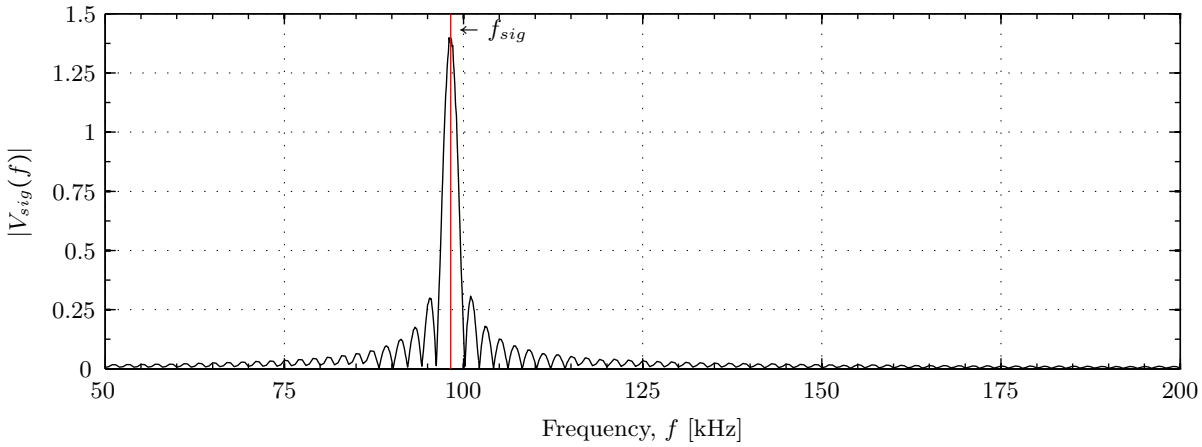


Figure 3.27: The frequency spectra of the waveform in Fig. 3.25. The calculation interval is $n_{start}$ = 40000 through $n_{stop}$ = 65000. The measurement frequency is marked with a red line.

The value of $|V_{sig}(f_{sig})|$ in Fig. 3.27 is 1.397. The number of samples in the calculation interval is $N_{sig} = n_{stop} - n_{start}$ = 25000 samples. Using Eq. (3.11), $V_{pp}^{rec}$ is found as

$$V_{pp}^{rec}(f_{sig}) = 2 \cdot 2 \cdot \frac{1.379}{25000} \approx 220\,\mu\text{V}, \tag{3.12}$$

which is seen to be close to the peak-to-peak voltage of the calculation interval in Fig. 3.25.

### 3.7.3 Calculation of $V_{pp}^{rec}$ - direct method

An alternative, and more straight-forward method for extracting $V_{pp}^{rec}$ from a measured waveform is implemented in the MATLAB script `findpeakToPeak.m` (see Appendix A). The calculation interval zero-crossings are found, equivalent to in Section 5.3.1. The sample length of one period at the measurement frequency is calculated. The $V_{pp}^{rec}$ value is then calculated for each whole periode in the calculation interval, and the output value of the function is the averaged peak-to-peak voltage of each period.

This method is more sensitive to noise than the Fourier transform method described in Section 3.7.2. While the Fourier method filters out the signal frequency from the calculation interval spectrum, the direct method includes the overlaying noise in the calculation. This effect is visualized in Chapters 7 and 8, where the two methods for finding $V_{pp}^{rec}$ are compared.

### 3.7.4 Calculation of SNR

The recorded noise (see Section 3.3.7) is used to determine the noise level. A calculation interval with $n_{start}$ = 50000 and $n_{stop}$ = 90000 is used. The RMS of the noise, with the DC-component subtracted, is calculated by [86]

$$V_{rms}^{noise} = \sqrt{\frac{1}{N}\sum_{i=1}^{N}(V_i - \bar{V})^2}, \tag{3.13}$$

[4]Zero-padding of the time-domain sine wave does not affect this expression [85].

where $N$ is the number of samples in the calculation interval, $V_i$ is the voltage of sample $i$ and $\bar{V}$ is the mean of the noise. The SNR is determined by [86]

$$SNR = 20 \log_{10} \left( \frac{V_{rms}^{rec}}{V_{rms}^{noise}} \right), \tag{3.14}$$

where $V_{rms}^{rec} = V_{pp}^{rec}/(2\sqrt{2})$ is the RMS of the recorded signal in the corresponding acoustical measurement.

# Chapter 4

# Finite element simulation setup

The FE method is used to model the behaviour of the piezoelectric transducers and the surrounding fluid medium. In this chapter a brief description of the FE simulation tool FEMP 5.0, is given in Section 4.1. Section 4.2 covers some important simulation parameters that need to be specified, and the corresponding values used in the present work. The different commands that are used to set up and mesh the modelled piezoelectric structures are described in Section 4.3, and examples of the resulting meshes are shown. An overview of the material parameters needed to define piezoelectric materials, elastic (non-piezoelectric) materials and fluids are given in Section 4.4, as well as all material parameters used in the simulations.

## 4.1 FEMP 5.0

The FE modelling is performed using the latest version of the simulation tool Finite element modelling of piezoelectric transducers, FEMP 5.0 [24, 25]. A brief description of the theory can be found in Section 2.8. FEMP 5.0 is written in MATLAB. The input parameters to FEMP 5.0 are specified in a text file with the file extension `.inn`. The `.inn`-file may contain multiple values assigned to a single variable, allowing parametric simulations. A set of predefined transducer structures are available to specify the geometry of the current problem. Additional structures can be defined by use of the files `read_inn_project.m` and `init_const_project.m` where input parameters, points, areas and boundary conditions for a transducer structure are specified [24, 25].

## 4.2 Simulation parameters

A number of simulation parameters must be given for each FE simulation. Only the simulation parameters used in the present work are covered here.

- The dimensions of the transducer and the fluid domain are specified. When infinite fluid elements are used, the meshing angle in radians is set to 1.3 rad [87].

- A mesh is the spatial distribution of the finite and infinite elements in the FE simulation. The mesh is set up using 5 elements per wavelength, chosen as a compromise between calculation time and accuracy [24], which determines the element size in each material. In the fluid the wavelength for longitudinal waves are used, while the wavelength for shear waves are used in both piezoelectric and non-piezoelectric elastic materials [24]. The maximum frequency in the simulation is used to calculate the wavelength.

- 8 node, corresponding to 2nd order, isoparametric finite elements and 12th order infinite elements are used in the simulations. Note that only finite elements are used if the transducer structure is modelled vibrating in vacuum [24].

- The infinite elements must be set up by defining $R_{inf}$, which is the radial distance from the origin of the mesh to the interface between the finite and infinite fluid elements. The accuracy of the solution are influenced by the choice of $R_{inf}$. For 12th order infinite elements, a minimum distance of $R_{inf} = 0.25a^2/\lambda$ is recommended in [24], where $\lambda$ is the wavelength in the fluid and $a$ is the radius of the front surface of the structure. The radius of the matching layer is used when calculating $R_{inf}$ for the piezoelectric transducer, developed during the present work.

Direct time-harmonic analysis is used to solve the FE problem for a given set of frequencies [24]. It can be quite memory-intensive as the full set of calculations are performed for each frequency. The losses are included as described in Section 4.4. Note that the air is modelled without loss.

When the FE problem is solved using the direct time-harmonic method, several quantities can be computed and saved [87]. The electrical admittance, $Z_T$, and the transmitting voltage response, $S_V$, of the transducer are always calculated in the simulations performed in the present work, using frequency steps of 0.1 kHz. Other quantities that are saved in certain simulations are the axial pressure and the averaged pressure at a plane parallel to the transducer front surface of a specified size and at a specified axial distance.

The transmitting voltage response of the transducer is calculated at a specified axial reference distance from the front of the transducer structure. Here the transmitting voltage response is calculated at 1000 m in the FE simulation, and then extrapolated back to $d_0$ = 1 m by spherical extrapolation, i.e $|S_V(d_0 = 1\,\mathrm{m})| = 1000\,|S_V(1000\,\mathrm{m})|$ since only the magnitude is considered when comparing to the present measurements. This is done to ensure that the transmitting voltage response is determined at far-field conditions.

## 4.3 Transducer meshing structures

A number of different piezoelectric structures are used. Input files for the structures used that are not included as predefined structures in FEMP 5.0 can be found in Appendix B.

- `piezodisk` models a piezoelectric ceramic disk vibrating in vacuum. This structure is included in FEMP 5.0.

- `piezodiskfluid` is used to model a piezoelectric ceramic disk vibrating in air. This structure is included in FEMP 5.0.

- `piezodiskwidefrontfluid` models a piezoelectric ceramic disk with a matching layer of larger radius than the disk, vibrating in air. Square fluid finite elements at the front and back of the transducer are used to enhance the accuracy [49]. Note that this means that $R_{inf}$ must be larger than $\sqrt{2}a$, where a is the radius of the matching layer. A decimated mesh is shown in Fig. 4.1b. Implemented by Storheim [49].

- `piezodiskwidefrontglue` is used to model a piezoelectric ceramic disk with a matching layer attached to the disk with a layer of glue, vibrating in vacuum.

- `transducerfluid` is used to model the piezoelectric transducer developed during the present work, radiating in air (see Chapter 6). The silver conductive epoxy layers are omitted[1]. The complete transducer, i.e. the full length of the backing layer and stainless steel housing, cannot be modelled in the current simulation setup due to insufficient computing power to handle the amount of elements required. A length of approximately 20 mm instead of approximately 80 mm is therefore used as the total length of the transducer. A decimated mesh of `transducerfluid` is shown in Fig. 4.1a. Based on a structure implemented by Storheim [49].

- `transducervacuum` models the piezoelectric transducer vibrating in vacuum, i.e the piezoelectric disk, matching layer, silver conductive epoxy layers, backing layer and housing cylinder. The housing rear lid is omitted. The full length of the stainless steel casing is used, and the short calculation times simplifies multiple simulations to investigate different material parameters. An example mesh is shown in Fig. 4.2, with a short housing for convenience.

In the structures where a backing layer is included, a solid cylinder is modelled, thus omitting the cylindrical hole in the middle of the backing layer, and the coned rear end of the backing layer (see Fig. 6.2).

[1] The structure is based on a structure implemented by Storheim [49]. Some adjustments have been made, but the more time consuming inclusion of the silver conductive epoxy layers has not been given priority.

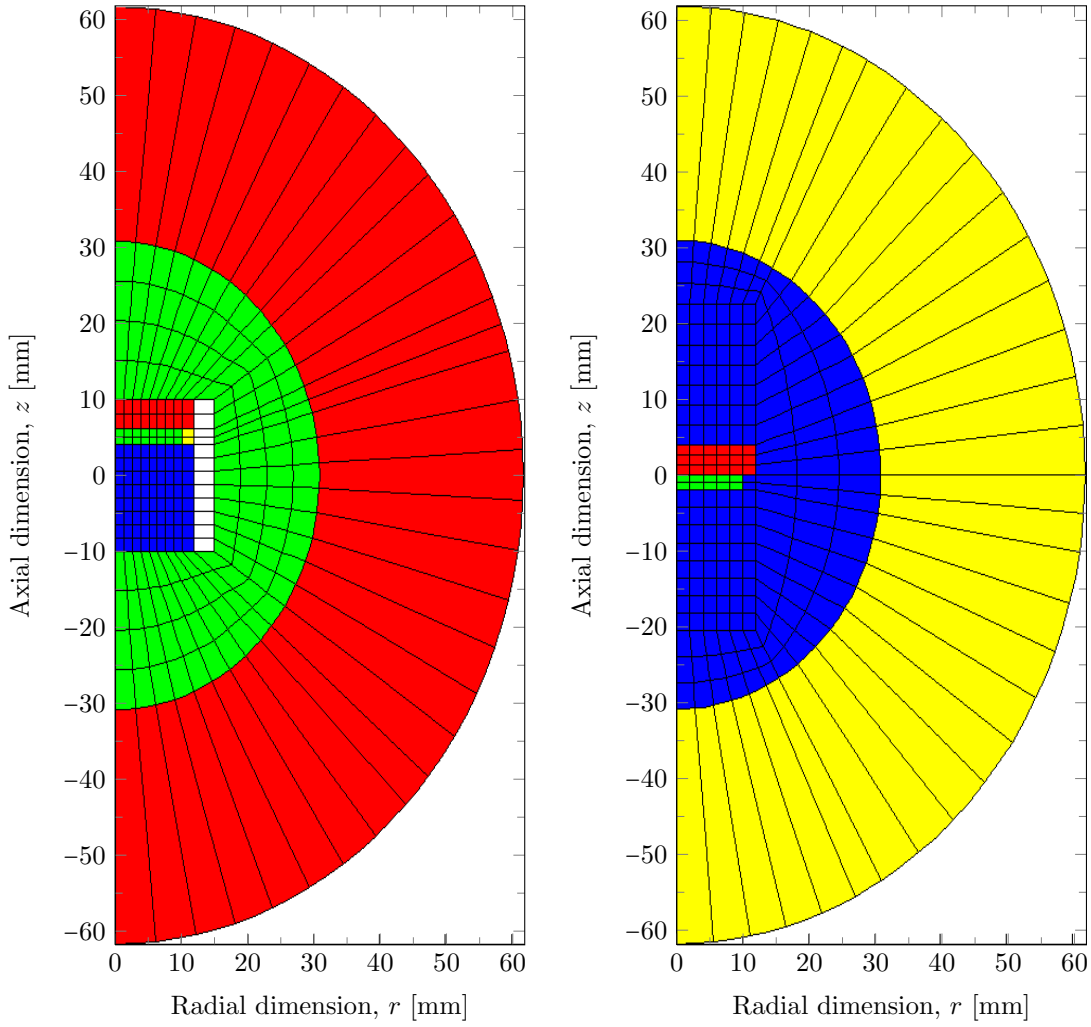


(a) (b)

Figure 4.1: Decimated meshes, with 5 elements per wavelength at 10 kHz and $R_{inf}$ = 30.9 mm (calculated for a maximum frequency of 300 kHz). Silver conductive epoxy are omitted in both models. (a) shows a decimated mesh from `transducerfluid`, where the backing and housing are shorter than for the constructed transducer due to calculation limitations. (b) shows a decimated mesh from `piezodiskwidefrontfluid`.

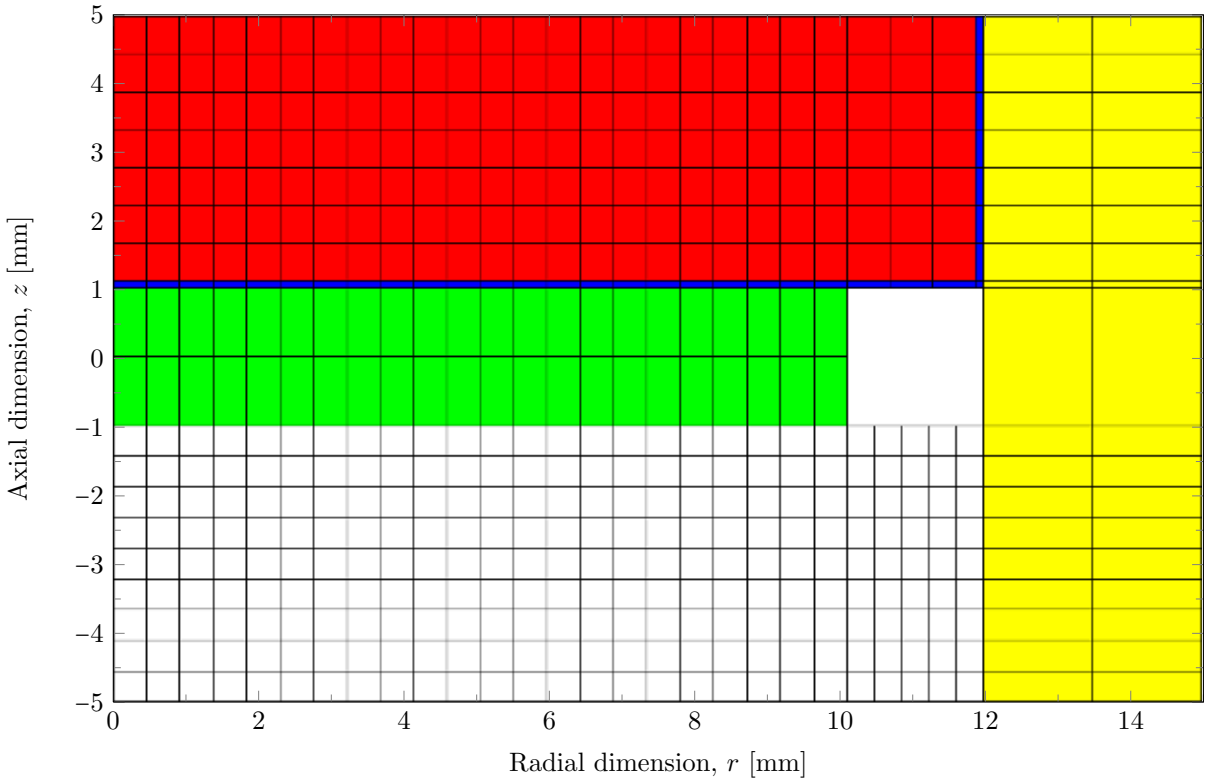


Figure 4.2: An example mesh from `transducervacuum`. The red area is the matching layer, the blue area is the silver epoxy, the green area is the piezoelectric ceramic disk, the yellow area is the stainless steel housing, and the white grid is the backing layer. Note that the length of the housing cylinder is set to 10 mm here to better show the mesh, as opposed to the real length of approximately 80 mm. Meshed with 5 elements per wavelength at 300 kHz.

## 4.4 Material parameters

It is often challenging to obtain accurate material parameters, either due to the incomplete material data supplied by the manufacturer or because of uncertainties in the supplied data, and also batch to batch variations in the materials. In FEMP the material data are stored in a `material.dat`-file. Three different types of materials can be defined: piezoelectric materials, elastic (non-piezoelectric) materials and fluids.

Piezoelectric material are described by mechanical, electromechanical and electrical material parameters, and the density, $\rho$. FEMP uses the elastic stiffness constants at constant electric field, $c_{11}^E$, $c_{12}^E$, $c_{13}^E$, $c_{33}^E$, $c_{44}^E$ and $c_{66}^E$, the piezoelectric stress constants, $e_{31}$, $e_{33}$ and $e_{15}$, and the permittivity at constant strain, $\varepsilon_{11}^S$ and $\varepsilon_{33}^S$. The losses are described by a full set of complex material constants in the simulations performed in the present work, accounting for dielectric, elastic, and piezoelectric losses. A simplified loss model may alternatively be used, where the elastic losses are described by the mechanical quality factor $Q_m$ and the dielectric losses are described by the loss tangent $\delta_e$ [24].

To describe elastic materials with no piezoelectric properties, the density, $\rho$, mechanical quality factor, $Q_m$, sound speed for longitudinal waves, $c_l$, and the sound speed for shear waves, $c_s$, must be given. Poisson's ratio, $\sigma$, may be given instead of $c_s$ [24].

The fluid is modelled without losses and described by its sound speed, $c$, and density, $\rho$ [24].

### 4.4.1 The piezoelectric ceramic, Pz27

The piezoelectric material Pz27 from Ferroperm [34] is used. The material data provided by the manufacturer for Pz27 are specified with an uncertainty of ± 10 % for the dielectric properties, ± 5 % for the electromechanical properties and ± 2.5 % for the mechanical properties. Previous work has shown that a better agreement between measurements and FE simulations is achieved if an adjusted data set is used to model Pz27 [36, 37]. The adjusted material data set found in [37] is used here. This was determined based on the work in [36] and [35], and the material data set was adjusted to improve the agreement between the simulations and measurements at the first radial mode resonances. The measurements in [37] were conducted with piezoelectric elements with similar dimensions as those used in the present work.

It is however emphasized that the adjusted material parameters may not represent the actual material parameters of the piezoelectric ceramic, and will therefore not necessarily fit equally well when used to model different batches or elements of different dimensions [37]. Both the material data from Ferroperm and the adjusted data set from [37] are given in Table. 4.1. Note that the number of digits given does not correspond to the accuracy of the material data.

Table 4.1: Material data for the piezoelectric material type Pz27. The adjusted data set is used in the FE simulations.

| Parameter | Unit | Ferroperm data [34] | Adjusted data set [37] |
|---|---|---|---|
| $c_{11}^E$ | [$10^{10}$ Pa] | 14.70 | $11.875\big(1+i\frac{1}{95.75}\big)$ |
| $c_{12}^E$ | [$10^{10}$ Pa] | 10.50 | $7.430\big(1+i\frac{1}{71.24}\big)$ |
| $c_{13}^E$ | [$10^{10}$ Pa] | 9.37 | $7.425\big(1+i\frac{1}{120.19}\big)$ |
| $c_{33}^E$ | [$10^{10}$ Pa] | 11.30 | $11.205\big(1+i\frac{1}{120.19}\big)$ |
| $c_{44}^E$ | [$10^{10}$ Pa] | 2.30 | $2.110\big(1+i\frac{1}{120.19}\big)$ |
| $e_{31}$ | [C·m$^{-2}$] | -3.09 | $-5.40\big(1-i\frac{1}{166}\big)$ |
| $e_{33}$ | [C·m$^{-2}$] | 16.00 | $16.0389\big(1-i\frac{1}{323.177}\big)$ |
| $e_{15}$ | [C·m$^{-2}$] | 11.60 | $11.20\big(1-i\frac{1}{200}\big)$ |
| $\epsilon_{11}^S$ | [$10^{-p}$ F/m] | 10.0005 | $8.110044\big(1-i\frac{1}{50}\big)$ |
| $\epsilon_{33}^S$ | [$10^{-p}$ F/m] | 8.0927 | $8.14585\big(1-i\frac{1}{86.28}\big)$ |
| $\rho$ | [kg·m$^{-3}$] | 7700 | 7700 |
| $Q_m$ | - | 80 | - |
| $\tan\delta$ | - | 0.017 | - |

### 4.4.2 Air

Air is modelled without losses, using the material parameters given in Table 4.2, corresponding to approximately 20 °C and 1 atm.

Table 4.2: Material data used to model the fluid medium, air.

| Name | Parameter | Unit | Value |
|---|---|---|---|
| Density | $\rho$ | [kg/m$^3$] | 1.21 |
| Sound speed | $c$ | [m/s] | 343 |

### 4.4.3 Matching layer

A matching layer is used in the transducer construction (see Chapter 6) in order to improve the acoustic coupling between the piezoelectric ceramic disk and air. The Aptflex syntactic foams R3 and R7 from Precision Acoustic [88,89] were considered. Aptflex syntactic foam is a composite material made of glass spheres with epoxy resin as the polymeric binder. It is described by the manufacturer to be a tough non-conducting material with a low specific gravity, high hydrostatic compressive strength, and excellent chemical resistance [89]. The microbubbles in the syntactic foam have a diameter size distribution between approximately 10 and 90 $\mu$m [88]. [88,89].

The longitudinal sound speed ($c_l = 2034 \pm 30$ m/s), density ($\rho = 570 \pm 20$ kg/m$^3$) and Poisson's ratio ($\sigma = 0.375 \pm 0.05$) are specified for Aptflex R3. The attenuation coefficient, $\alpha$, is given for frequencies from 1 MHz to 7 MHz [88]. As this is well above the frequencies of interest in the present work, a curve fit is performed to find extrapolated values. The supplied attenuation coefficient is used to calculate the mechanical quality factor, $Q_m$, by [45]

$$Q_m = \frac{k}{2\alpha_{Np/m}}, \tag{4.1}$$

where $\alpha_{Np/m}$ is the attenuation coefficient in Neper per meter, found by $\alpha_{Np/m} = 100\alpha_{dB/cm}/20\log_{10}(e)$. The curve fitting $\alpha_{dB/cm} = 0.42+3.84(f[\text{MHz}])^{1.27}$, supplied by PA [88], does not give physically plausible

values at low frequencies, as is seen in Fig. 4.3. A new curve fitting is therefore performed in the present work, giving $\alpha_{dB/cm} = 4.069(f[\text{MHz}])^{1.24}$. Both the curve of the measured absorption coefficients, the supplied curve fit and the new curve fit are shown in Fig. 4.3, along with the corresponding quality factors. A plot of $Q_m$ resulting from the new curve fit for the frequency range 50 kHz to 300 kHz is shown in Fig. 4.4. From this curve a $Q_m$ of 55 is chosen for use in the simulations, as $Q_m$ varies between 44 and 68 in the plotted frequency range. Note that $Q_m$ is found based on measurements at higher frequencies and that a different curve fit may give a more appropriate value.

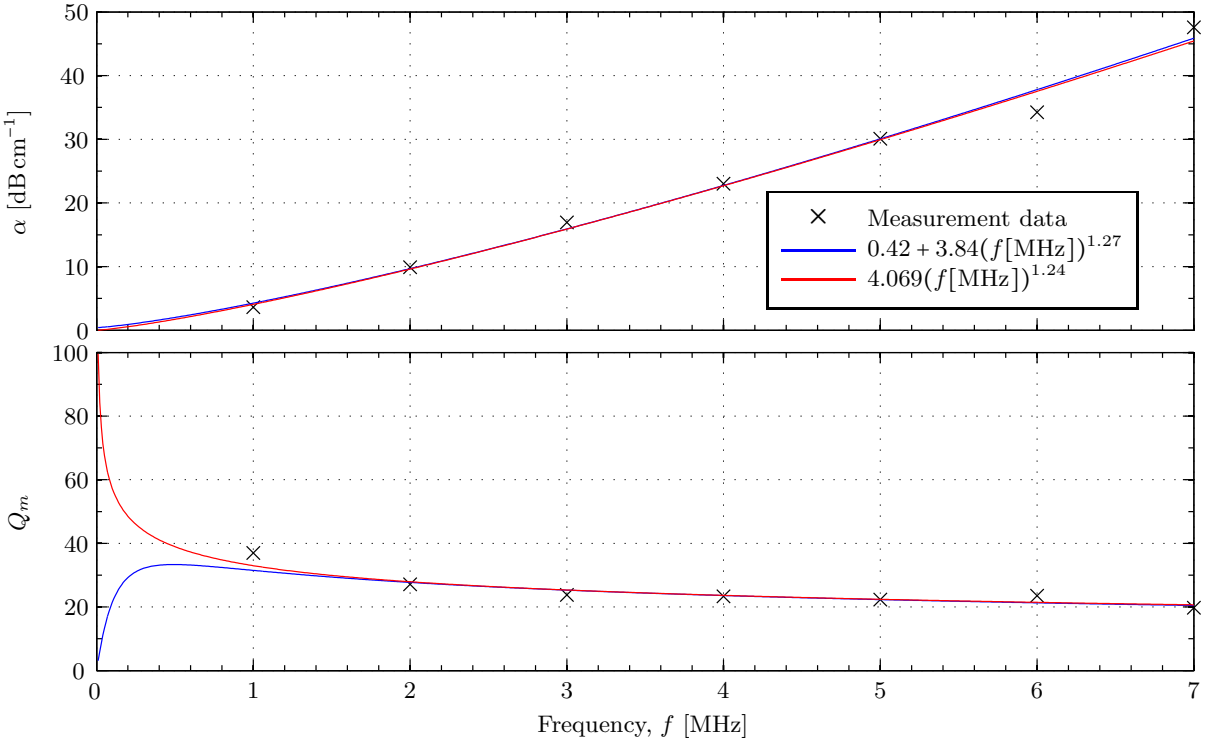


Figure 4.3: Attenuation coefficient, $\alpha_{dB/cm}$, and corresponding mechanical quality factor, $Q_m$, for Aptflex R3. The figure shows sample values measured by Precision Acoustics [88], curve fit performed by Precision Acoustics, $\alpha_{dB/cm} = 0.42 + 3.84(f[\text{MHz}])^{1.27}$ [88], and curve fit performed in the present work, $\alpha_{dB/cm} = 4.069(f[\text{MHz}])^{1.24}$. Plotted for frequencies up to 7 MHz.

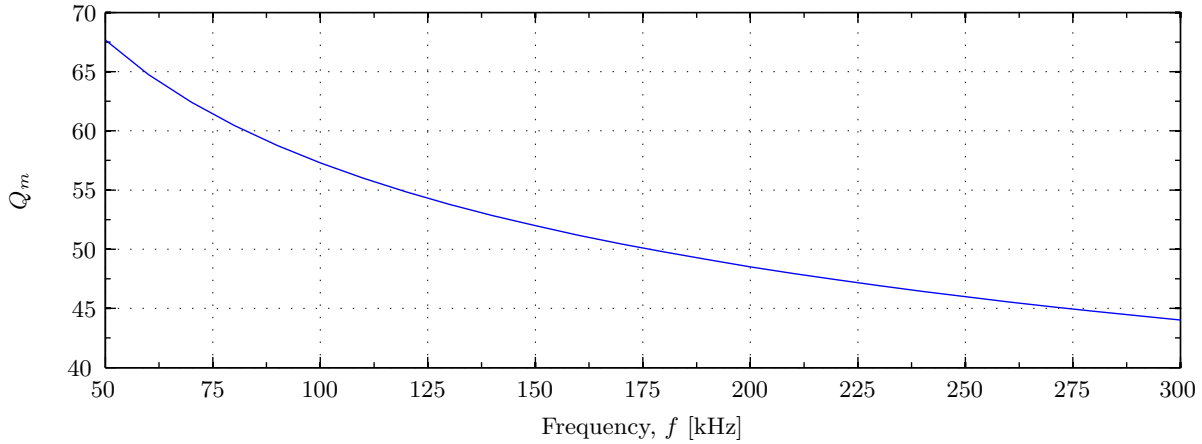


Figure 4.4: Mechanical quality factor, $Q_m$, of Aptflex R3 for the frequency range 50 kHz to 300 kHz. Found by curve fit of measured values, performed in the present work, $\alpha_{dB/cm} = 4.069(f[\text{MHz}])^{1.24}$.

Material data for Aptflex R7 are not available from the manufacturer as it is a quite new material. A density of approximately 450 kg/m$^3$ is indicated, as well as a longitudinal sound speed below that of Aptflex R3 [88]. In the simulations the Poisson's ratio for R7 is assumed to be the same as for the rest

of the Aptflex syntactic foams available, $\sigma = 0.375$ [89]. It is also assumed that $Q_m$ is similar for R3 and R7.

The density and longitudinal sound speed are measured (see Chapter 5), as the material data for Aptflex R7 are uncertain at best. Measurements are also conducted on Aptflex R3, and values exceeding the uncertainties supplied by PA [89] are found.

The different material data for R3 and R7 used in the FE simulations are given in Table 4.3.

Table 4.3: Material data used when modelling Aptflex R3 and Aptflex R7.

| Name | Parameter | Unit | R3 alt. 1[2] | R3 alt. 2[3] | R3 alt. 3[4] | R7[5] |
|---|---|---|---|---|---|---|
| Density | $\rho$ | [kg/m$^3$] | 570 | 598 | 598 | 420 |
| Longitudinal sound speed | $c_l$ | [m/s] | 2034 | 2100 | 2100 | 2266 |
| Poisson's ratio | $\sigma$ | - | 0.375 | 0.375 | 0.35 | 0.375 |
| Mechanical $Q$-factor | $Q_m$ | - | 55 | 55 | 40 | 55 |

### 4.4.4 Glue

A two-component silver conductive epoxy from MG Chemicals [90] is used to glue the matching layer to the piezoelectric ceramic disk and to the metal housing. According to the manufacturer it forms high strength conductive bonds and can be used in place of traditional solder [90]. The stated volume resistivity is 0.38 Ω·cm and the hardness is 65 Shore D [90]. No additional data of interest here is given in the package. The data sheet currently available from the manufacturer contains different values than stated on the packaging of the silver conductive epoxy [90, 91]. There the volume resistivity is stated to be 0.0174 Ω·cm and the hardness to be between 70D and 75D. The density is also included, and it is given as 2440 kg/m$^3$ [91]. This density is used to model the silver conductive epoxy used in the transducer construction.

The longitudinal sound speed and Poisson's ratio are not supplied from the manufacturer. Estimated values must therefore be used in the FE simulations, based on material data for similar materials.

Material parameters for a silver epoxy are found in [92], with a longitudinal sound speed of 1900 m/s, shear sound speed of 980 m/s, density of 2710 kg/m$^3$ and a mechanical quality factor of $Q_m = 18$ at 2 MHz. These material data are used in the simulations, but with the density as given in [91] and an estimated mechanical quality factor of $Q_m = 25$, as it is assumed that the losses are smaller for lower frequencies.

The material data used in the FE simulations to model the two component silver epoxy from MG Chemicals are given in Table 4.4.

Table 4.4: Material data used when modelling the silver conductive epoxy.

| Name | Parameter | Unit | Estimated values |
|---|---|---|---|
| Density [91] | $\rho$ | [kg/m$^3$] | 2440 |
| Longitudinal sound speed | $c_l$ | [m/s] | 1900 |
| Shear sound speed | $c_s$ | [m/s] | 980 |
| Mechanical $Q$-factor | $Q_m$ | - | 25 |

### 4.4.5 Housing

The housing is made of grade 316 stainless steel. The necessary material parameters needed to model stainless steel are not readily available, but the density of a grade 316 stainless steel is given in [93], $\rho = 8000$ kg/m$^3$, and in [94] Young's modulus and Poisson's ratio at 25 °C are given as $Y = 198.6$ GPa and $\sigma = 0.263$, respectively.

[2] Material data supplied by PA [88, 89]
[3] Measured $c_l$ and $\rho$ (see Chapter 5). $\sigma$ and $Q_m$ as stated by PA [88, 89].
[4] Measured $c_l$ and $\rho$ (see Chapter 5). Adjusted $\sigma$ and $Q_m$ (see Chapter 6)
[5] Measured $c_l$ and $\rho$ (see Chapter 5). $\sigma$ and $Q_m$ as stated by PA for R3 [88, 89].

These parameters are used to determine $c_l$ by [45]

$$c_l = \sqrt{\frac{\lambda + 2\mu}{\rho}}, \tag{4.2}$$

and $c_s$ by

$$c_s = \sqrt{\frac{\mu}{\rho}}, \tag{4.3}$$

where $\rho$ is the density and $\lambda$ and $\mu$ are the Lamé parameters, given as

$$\lambda = \frac{\sigma Y}{(1+\sigma)(1-2\sigma)} \qquad \text{and} \qquad \mu = \frac{Y}{2(1+\sigma)}, \tag{4.4}$$

where it is assumed that the material is isotropic.

$Q_m$ for the glue is assumed to be the same as the $Q_m$ estimated for the steel in [95], $Q_m = 100$. The material parameters used in the simulations are given in Table 4.5.

Table 4.5: Material data used when modelling the stainless steel, grade 316, housing.

| Name | Parameter | Unit | Estimated values |
|---|---|---|---|
| Density [93] | $\rho$ | [kg/m$^3$] | 8000 |
| Longitudinal sound speed | $c_l$ | [m/s] | 5528 |
| Shear sound speed | $c_s$ | [m/s] | 3135 |
| Mechanical $Q$-factor | $Q_m$ | - | 100 |

### 4.4.6 Backing

Divinycell H130 [96] is used as backing in the transducer. The longitudinal sound speed is found from the values of Young's modulus, Poisson's ratio ($\sigma = 0.4 \pm 0.045$) and the density ($\rho = 130$ kg/m$^3$ $\pm$ 10 %) given in [96], using Eqs. (4.3) and (4.4). Both a nominal and minimum value for Young's modulus are given in [96], 175 MPa and 135 MPa, respectively. The nominal value is used in the calculations. No data is available on the mechanical loss in Divinycell H130. In [37] $Q_m = 25$ is used for Divinycell H200 and HCP70. An estimated $Q_m = 25$ is used when the full length of backing layer is used in the FEMP-structure `transducerfluid`, while $Q_m = 5$ is used when simulations are performed with the FEMP-structure `transducerfluid` to compensate for the reduced backing layer length. The material data used in the simulations are given in Table 4.6.

Table 4.6: Material data used when modelling the Divinycell H130 backing.

| Name | Parameter | Unit | H130 | H130 |
|---|---|---|---|---|
| Density [96] | $\rho$ | [kg/m$^3$] | 130 | 130 |
| Longitudinal sound speed | $c_l$ | [m/s] | 1698 | 1698 |
| Poisson's ratio [96] | $\sigma$ | - | 0.4 | 0.4 |
| Mechanical $Q$-factor | $Q_m$ | - | 5 | 25 |

# Chapter 5

# Matching layer characterization

Theory, measurement methods and results for matching layer characterization are all presented in this chapter, because the measurement setup used here differs from the setup used elsewhere in the present work.

Matching layers are used to increase the bandwidth and sensitivity of piezoelectric transducers radiating into media with acoustic impedance which is different from the acoustic impedance of the piezoelectric material. Material parameters characterizing the matching layers considered in the transducer construction (see Chapter 6) are needed in order to perform FE simulations. Sound speed measurements are conducted in the measurement cell made by Fosså [97]. The density of the matching layers are determined by volume and weight measurements. Knowing the longitudinal sound speed and density, the characteristic impedance of each matching layer is calculated.

Section 5.1 covers the theory used to find the sound speed and characteristic impedance of a matching layer. The measurement setup is presented in Section 5.2 and the signal processing used to extract the results from the measurements is described in Section 5.3. Results are shown in Section 5.4 and briefly discussed in 5.5.

The theory is used on measurements to calculate the sound speed in the materials Aptflex R3 and R7 from Precision Acoustics (PA). PA provides the longitudinal sound speed and density for R3, given as $c_{l,R3} = 2034 \pm 30$ m/s and $\rho_{R3} = 570 \pm 20$ kg/m$^3$ [88], respectively. These values are compared with the values found experimentally in this chapter. Since no sound speed value is given by PA for the material R7, it is determined here for use in simulations. A density of $\rho_{R7} = 450$ kg/m$^3$ for Aptflex R7, and a sound speed lower than for R3, is indicated by PA [88], and compared to the value measured here.

## 5.1 Theory

In the following, the theory needed for calculating the sound speed in a material sample placed in water is presented. The theory covered in the present work is a simplified version of the theory presented in [97], neglecting the effect of diffraction, and the transit times through the transmitting and receiving transducer and electronics.

### 5.1.1 Calculating the sound speed

In Fig. 5.1 the sound speed measurement cell used for the sound speed measurements is illustrated.

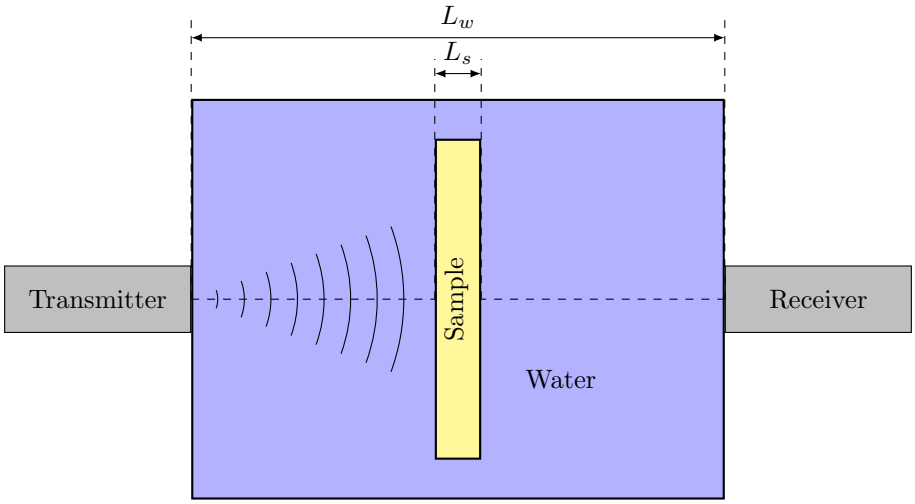


Figure 5.1: Illustration of the sound speed measurement cell. A sample of thickness $L_s$ is immersed in water between a transmitting and a receiving transducer. The sample is orthogonally aligned with the axis of which the two transducers are coaxially aligned. The distance between the front of the transmitter and the front of the receiver is $L_w$.

To calculate the sound speed in the sample, two cases are considered; (1) the sample is not present in the tank, and (2) the sample is present in the tank. The plane wave transit time[1] for case (1), denoted $t^{(1)}$, is expressed as

$$t^{(1)} = \frac{L_w}{c_w^{(1)}}, \tag{5.1}$$

where $L_w$ is the distance between the front of the transmitter and receiver, as seen in Fig. 5.1, and $c_w^{(1)}$ is the sound speed in water for case (1)[2]. The plane wave transit time for case (2), denoted $t^{(2)}$, is expressed as

$$t^{(2)} = \frac{L_w - L_s}{c_w^{(2)}} + \frac{L_s}{c_l}, \tag{5.2}$$

where $L_s$ is the sample thickness, as seen in Fig. 5.1, $c_w^{(2)}$ is the sound speed in water for case (2), and $c_l$ is the longitudinal sound speed in the sample. The difference in transit times between case (1) and (2) is expressed as

$$\Delta t = t_w^{(1)} - t_w^{(2)}. \tag{5.3}$$

By inserting Eqs. (5.1) and (5.2) into Eq. (5.3), the longitudinal speed in the sample, $c_l$, is expressed as

$$c_l = \left[ \frac{L_w}{L_s} \left( \frac{1}{c_w^{(1)}} - \frac{1}{c_w^{(2)}} \right) + \frac{1}{c_w^{(2)}} - \frac{\Delta t}{L_s} \right]^{-1}. \tag{5.4}$$

In Eq. (5.4), , and $L_s$ is measured using a digital caliper (see Section 5.2). $c_w^{(1)}$ and $c_w^{(2)}$ are calculated using Bilaniuk and Wong's 148 point equation for the sound speed in water as a function of temperature [98,99]. The water temperature is measured for each measurement (see Section 5.2).

The transit times $t_w^{(1)}$ and $t_w^{(2)}$ are measured by recording the input voltage to the transmitter, $V_{el}$, and the output voltage from the receiver, $V_{ac}$. By calculating the time difference between corresponding zero crossing pairs in the steady-state of the recorded waveforms, the transit time is measured.

### 5.1.2 Characteristic impedance

The characteristic impedance of a medium is for plane waves defined as [46]

$$z = \rho c, \tag{5.5}$$

where $\rho$ is the density of the medium and $c$ is the longitudinal sound speed in the medium.

[1] The time between the first transmitting wave onset to the first receiving wave onset.

[2] The sound speed in water for case (1) and (2) are considered separately because different water temperatures in the measurements for case (1) and (2), resulted in different sound speeds for the water. The change in the sound speed for the sample with temperature is not considered here.

## 5.2 Measurement setup and methods

A block diagram of the measurement setup is given in Fig. 5.2. The measurement setup closely resembles the setup used in [97].

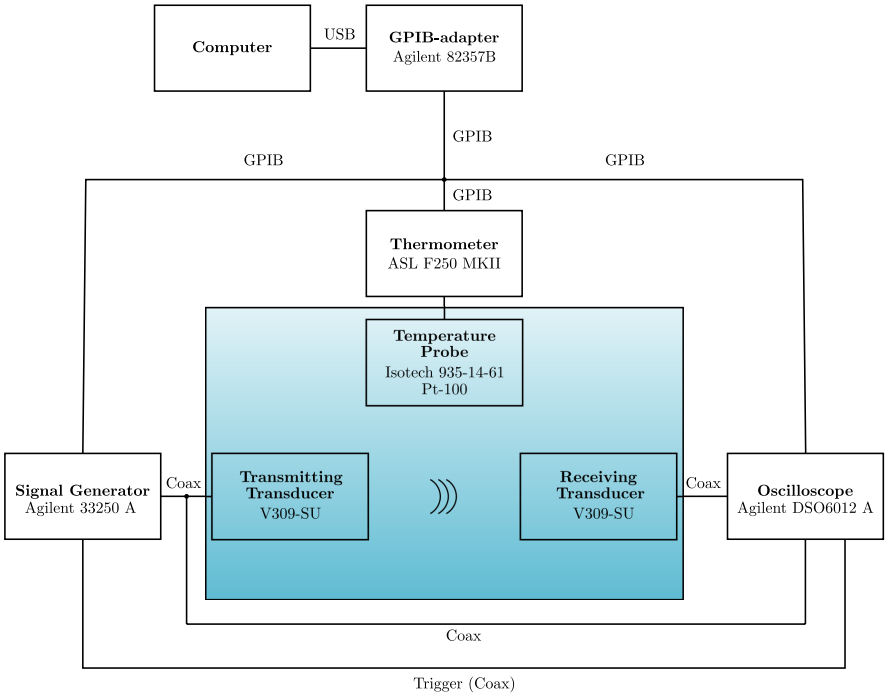


Figure 5.2: Block diagram of the measurement setup used in the sound speed measurements. Borrowed from [97]. Note that the thermometer and temperature probe depicted in this figure was not used during the present work.

An Agilent 33250A signal generator is generating the input voltage to an Olympus V309-SU transmitting transducer [100], which transmits sound into water. The signal is then received by an Olympus V309-SU receiving transducer, and recorded by an Agilent DSO6012A oscilloscope, with vertical resolution of 8 bits. In the oscilloscope, 16 averages are performed for each recorded waveform. The oscilloscope also records the input signal to the transmitting transducer. The measurement cell is filled with Biltema 361769 demineralized water, which is left to stabilize for 48 hours after pouring to minimize the occurrence of air bubbles interfering with the sound field. The temperature in the water during the acoustical measurements is measured using a Hanna Checktemp-1 handheld thermometer [101]. Hanna Checktemp-1 with a resolution of 0.1 °C and an accuracy of ±0.3°C in the temperature range of interest.

An input voltage of 5 Vpp, burst period of 10 ms and 12 cycles were used, as in [97]. Although the Olympus V309-SU transducers used have center frequencies at 4.69 and 5.39 MHz [97], the frequency used for the sound speed measurements is 3.0 MHz. High dampening in Aptflex R7 were observed for frequencies above 3.5 MHz, which resulted in a very low amplitude of the received voltage, $V_{ac}$, rendering post processing futile for the current input voltage.

The measured voltages are shown in Figs. 5.3 - 5.10, along with illustrations of the post process routine.

The volume of the samples are determined by measuring the thickness using a Mitutoyo MDH-25M digimatic micrometer [73], with a resolution of 0.1 $\mu$m and an accuracy of ±0.5 $\mu$m, and the width and length using a Biltema 191444 digital caliper, with a resolution of 0.01 mm and an accuracy of ±0.03 mm. In addition to contribute to determining the volume, the thickness measurement is used to express $L_s$, used in Eq. (5.4). 10 measurement points, evenly distributed over the sample, are collected for each sample's thickness, width and length measurement. See Table 5.3 for the measured dimensions of the two samples used in the present work. The values listed in Table 5.3 are the average value of the 10 measurement points on each sample. $L_w$ is measured by hand using a measuring tape.

The mass of the samples were measured using an A&D GF-3000-EC precision balance [76] with a stated repeatability (standard deviation) of 0.01 g and linearity of ± 0.02 g.

The instruments used in the measurements are listed in Table 5.1.

Table 5.1: The instruments used for the sound speed measurements.

| Brand/name | Type of equipment | Serial number |
|---|---|---|
| Agilent 33250A | Signal generator | MY40014887 |
| Agilent DSO6012A | Oscilloscope | MY45007479 |
| Agilent 82357B | USB/GPIB Interface | 2007/11 (internal ID) |
| Olympus V309SU | Transducer | 725192 |
| Olympus V309SU | Transducer | 721067 |
| Biltema 361769 | Deminearlized water | - |
| Hanna CheckTemp-1 | Handheld thermometer | - |
| Measurement cell | - | - |
| Standa 7R129 | Rotary stage | - |
| Mitutoyo MDH-25M | Digimatic micrometer | 15229628 |
| Biltema 191444 | Digital caliper | - |
| A&D GF-3000-EC | Precision balance | P1826763 |

## 5.3 Signal processing

MATLAB is used to calculate the transit time of the acoustical signal from the transmitter to the receiver. It is assumed that the acoustical signal propagates as a plane wave through both the water and sample material. The transit time is calculated by taking the time difference between a zero crossing pair in the $V_{el}$ and $V_{ac}$ waveforms. A zero crossing pair is the zero crossing of a given period in $V_{el}$ and the zero crossing of a corresponding period in $V_{ac}$.

### 5.3.1 Zero crossing detection

This section covers the method for finding the zero crossings in the measured voltage waveforms $V_{el}$ and $V_{ac}$. In the following, both $V_{el}$ and $V_{ac}$ are treated in the same way, and termed $V$.

The signal is interpolated with 100 points linearly distributed between each point of the original waveform. Then the mean value of the waveform is calculated. The mean value of the voltage waveform $V$ is given as

$$\bar{V} = \frac{1}{N} \cdot \sum_{i=1}^{N} y_i, \tag{5.6}$$

where $y_i$ is the value of sample number $i$ in $V$, consisting of $N$ samples. The sample $y_i$ is regarded as a zero crossing if $\bar{V}$ is between $y_i$ and $y_{i+1}$. In order to detect zero crossings, a new function $C$ is defined as

$$C(y_i) = sgn\left(\bar{V} - y_{i+1}\right) - sgn\left(\bar{V} - y_i\right), \tag{5.7}$$

where $sgn(x)$ is the "sign function", defined as

$$sgn(x) = \begin{cases} -1 & \text{if } x < 0, \\ 0 & \text{if } x = 0, \\ 1 & \text{if } x > 0. \end{cases} \tag{5.8}$$

If $y_i$ is below $\bar{V}$ and $y_{i+1}$ is above, then $C(y_i) = 2$. If $y_i$ is above $\bar{V}$ and $y_{i+1}$ is below, then $C(y_i) = -2$. Zero crossing $n$ is thus found as

$$n = i \,\text{if}: \begin{cases} C(y_i) = 2, \\ C(y_i) = -2. \end{cases} \tag{5.9}$$

The time of zero crossing $n$ is $t_i$, where $t_i$ is the time-value corresponding to $y_i$, i.e. $V(t_i) = y_i$. Only the zero crossings found in the steady state part of the signal is used for calculating the transit time. The time difference for the zero crossings in the steady state is averaged to express the time difference between the transmitted and received signal.

### 5.3.2 Measured waveforms, R3

In Figs. 5.3 - 5.6 the transmitted and received voltage signals for the case without and with a sample present are shown, respectively. The measurement frequency is 3.0 MHz. The figures display the zero crossings used for calculating the transit times for case (1) and (2). The zero crossings are represented by a "×".

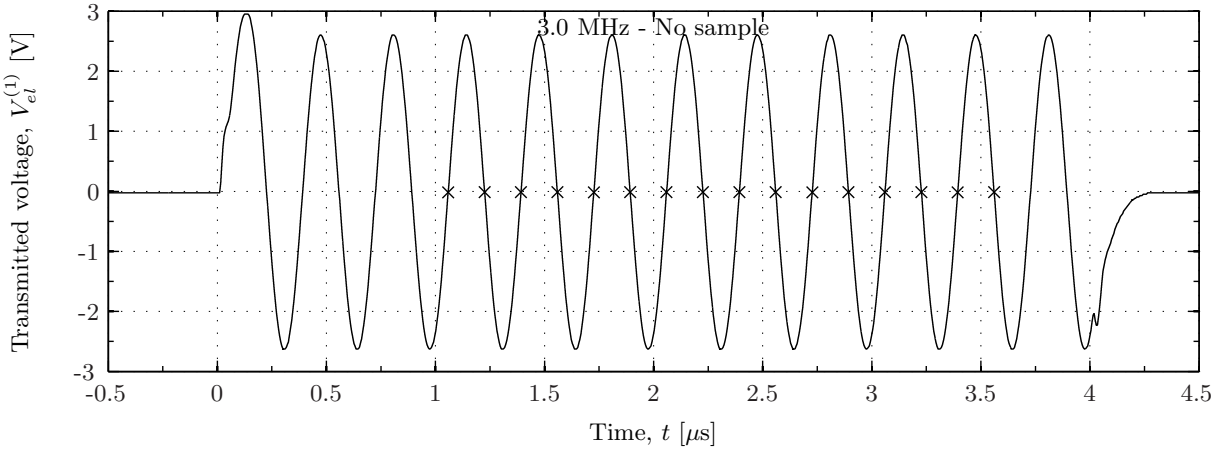


Figure 5.3: Transmitted voltage for case (1), $V_{el}^{(1)}$. Zero crossing marked with ×.

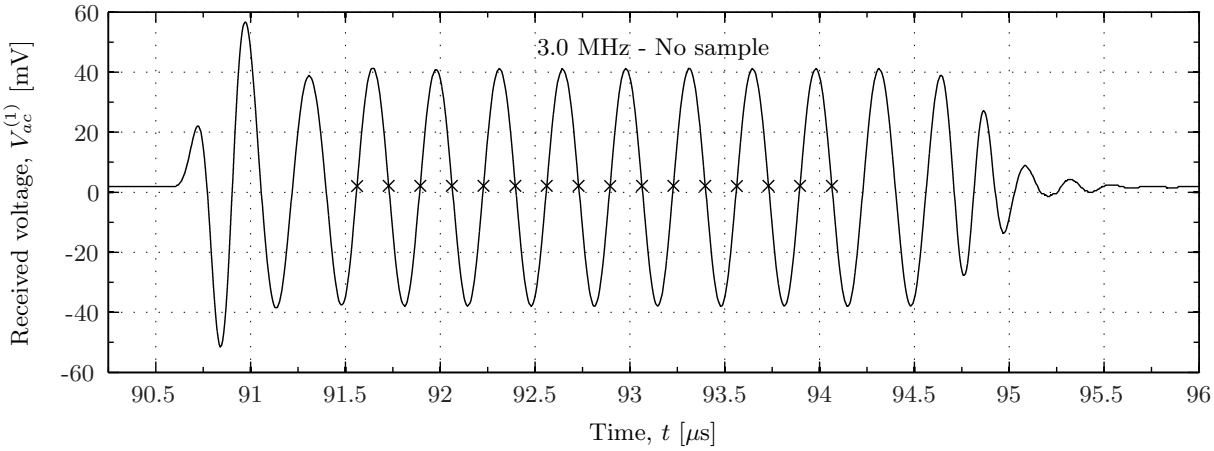


Figure 5.4: Received voltage for case (1), $V_{ac}^{(1)}$. Zero crossing marked with ×.

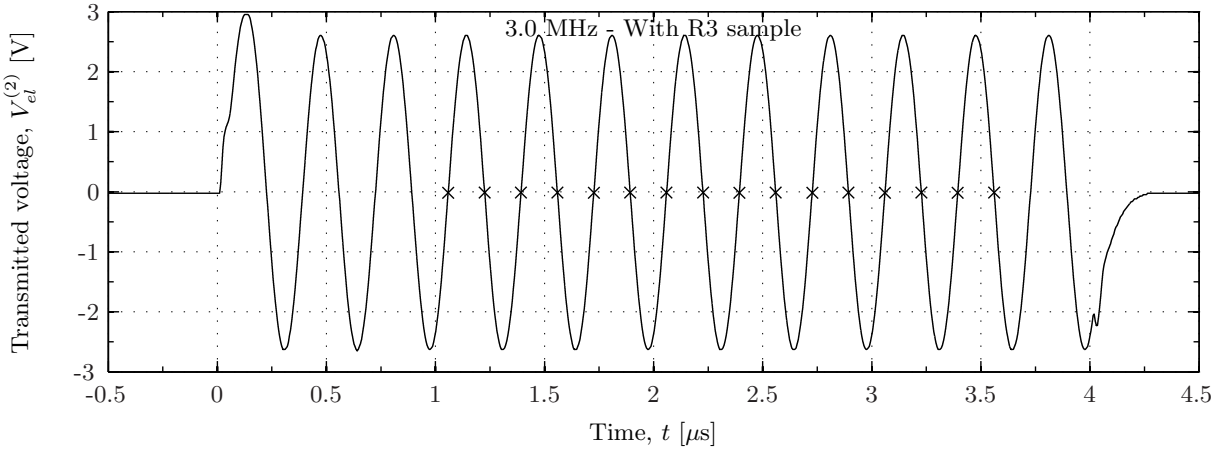


Figure 5.5: Transmitted voltage for case (2), $V_{el}^{(2)}$. Zero crossing marked with ×.

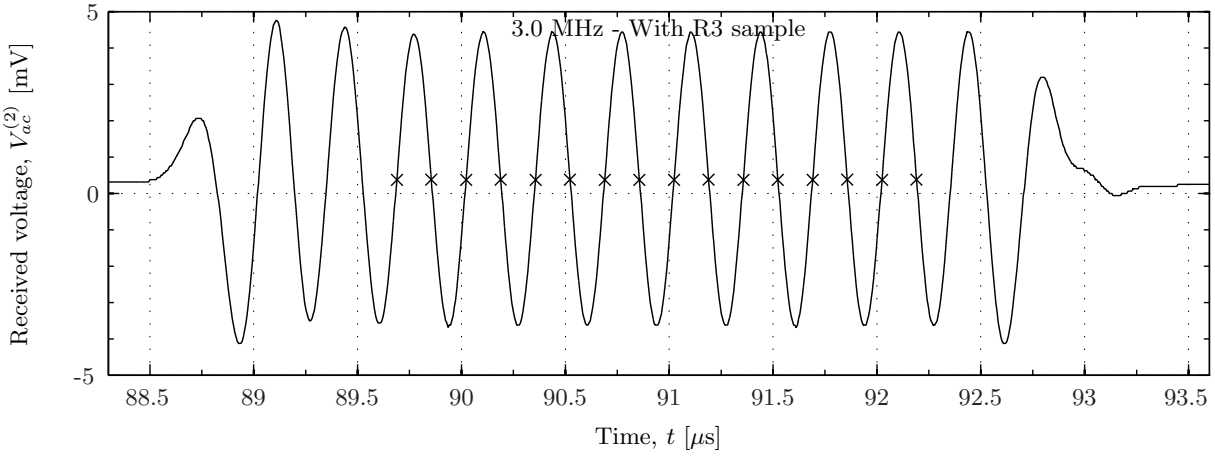


Figure 5.6: Received voltage for case (2), $V_{ac}^{(2)}$. Zero crossing marked with ×.

From Figs. 5.4 - 5.6 it is seen that the onset of the received signal when R3 is present is earlier than when the sound waves only propagates through water. This indicates that the longitudinal sound speed in R3, $c_{l,R3}$, is higher than the sound speed in water, $c_w$. This is as expected based on the material data given by PA.

### 5.3.3 Measured waveforms, R7

As for R3, the Figs. 5.7 - 5.10 show the recorded waveforms of $V_{el}^{(1)}$, $V_{ac}^{(1)}$, $V_{el}^{(2)}$ and $V_{ac}^{(2)}$ when R7 is used as the sample material. The measurement frequency is 3.0 MHz.

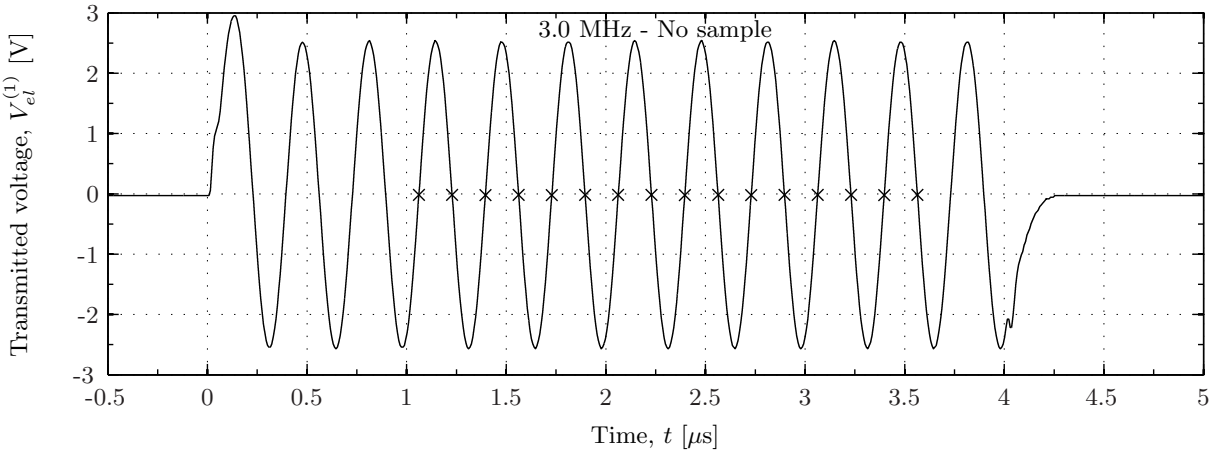


Figure 5.7: Transmitted voltage, $V_{el}$, for case (1). Zero crossing marked with ×.

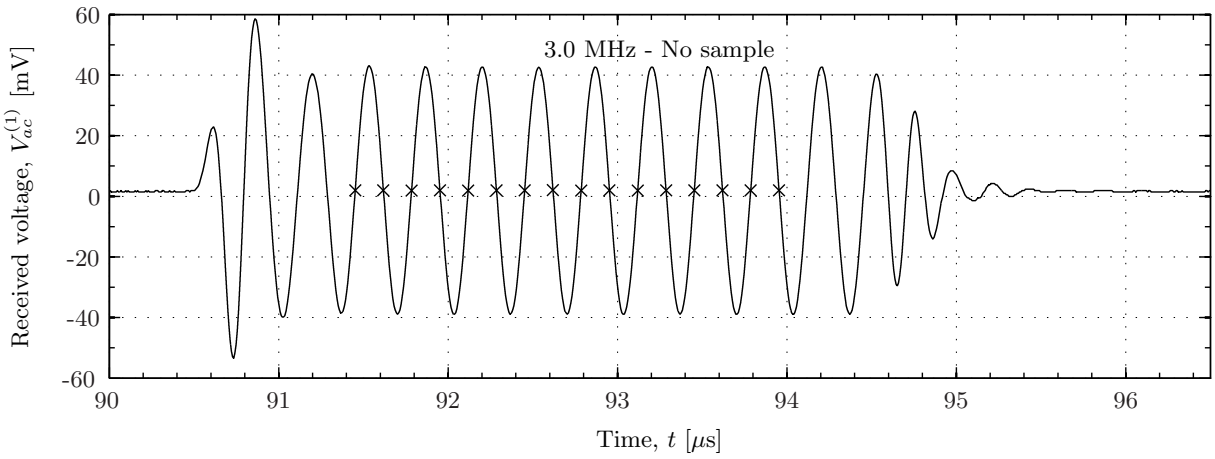


Figure 5.8: Received voltage, $V_{ac}$, for case (1). Zero crossing marked with ×.

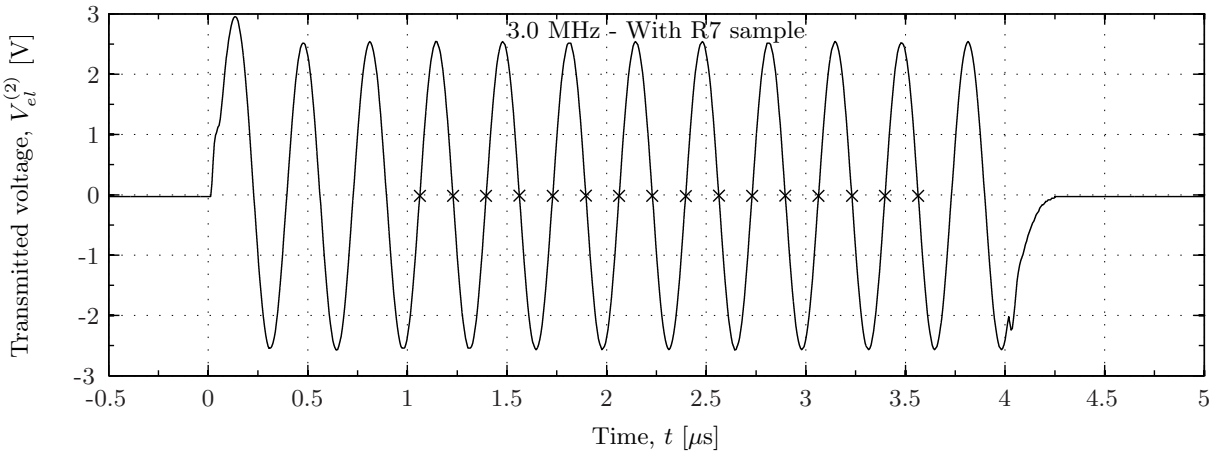


Figure 5.9: Transmitted voltage, $V_{el}$, for case (2). Zero crossing marked with ×.

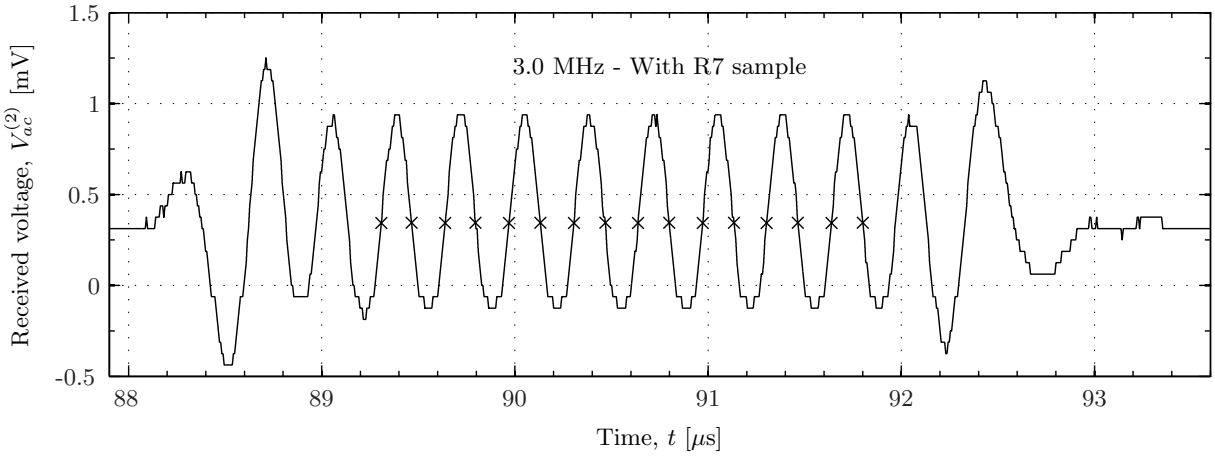


Figure 5.10: Received voltage, $V_{ac}$, for case (2). Zero crossing marked with ×.

It can be seen from Fig. 5.10 that the received signal with a sample present has an onset before the received signal with no sample present, seen in Fig. 5.8. This indicates that the sound speed in the sample is higher than the sound speed in water. It can also be seen that there is a significant decrease in magnitude for $V_{ac}^{(2)}$ compared to $V_{ac}^{(1)}$. This might be a result of the difference in impedance between the sample and water.

## 5.4 Results

In this section the results for sound speed, dimension and weight measurements is presented. The dimension and weight measurements are used to express the density of the matching layers, which together with the measured sound speed are used to calculate the characteristic impedance of the matching layers.

### 5.4.1 Sound speed

In Figs. 5.11 and 5.12 sound speed of Aptflex R3 and R7 are calculated using Eq. (5.4). A measurement is conducted without the sample present in the measurement cell, acting as a reference for 7 subsequent measurements carried out with the sample present.

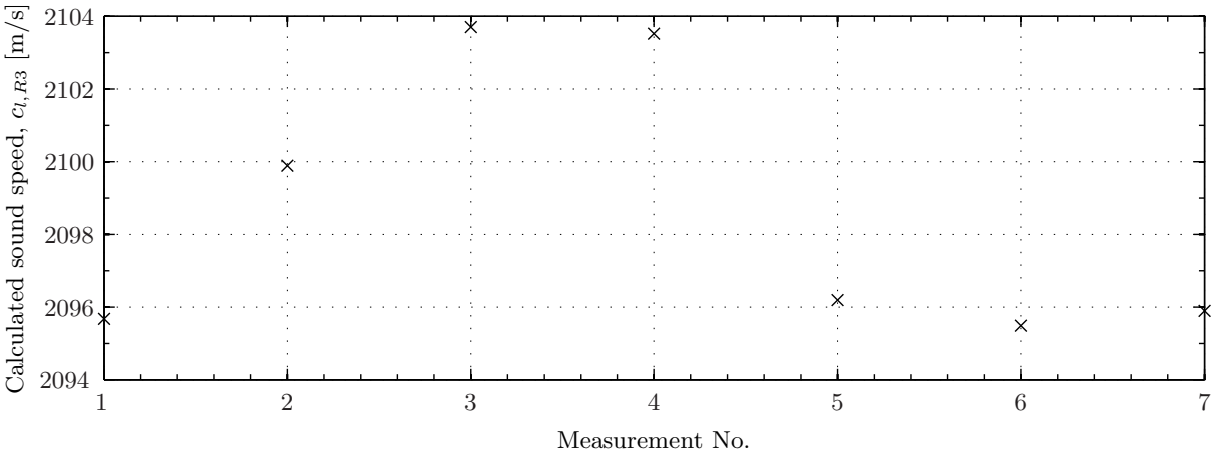


Figure 5.11: The calculated sound speed for R3, $c_{l,R3}$. Measurements done subsequently to each other over a span of 1.5 hours.

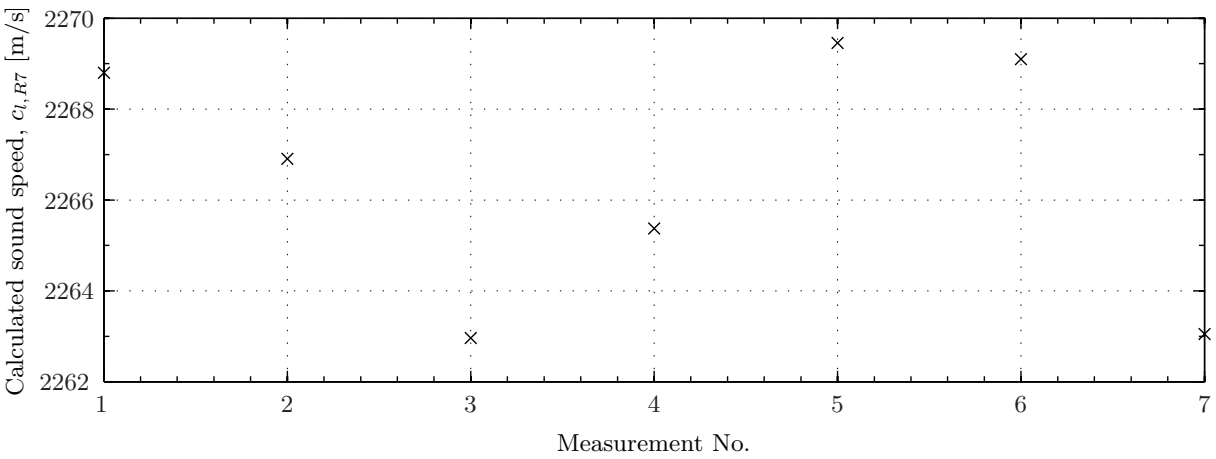


Figure 5.12: The calculated sound speed for R7, $c_{l,R7}$. Measurements done subsequently to each other over a span of 4.5 hours.

The mean sound speeds based on the measurements in Figs. 5.11 and 5.12 are given in Table 5.2 for both R3 and R7. The standard deviation[3] of the 7 measurements for $c_{l,R3}$ is 3.7 m/s, and 2.8 m/s for $c_{l,R7}$.

[3]The standard deviation of the values averaged is given, but not used further, as investigation of uncertainties not are prioritized in the present work.

Table 5.2: Averaged sound speed results.

| Material | Sound speed [m/s] |
|---|---|
| R3 | 2099 |
| R7 | 2267 |

### 5.4.2 Density - characteristic impedance

The averaged results of the dimension measurements, and the mass, of R3 and R7 are given in Table 5.3. The measurements are conducted as described in Section 3.4.

Table 5.3: The dimensions of the samples investigated in the present work.

| Name | Thickness [mm] | Width [mm] | Length [mm] | Mass [g] |
|---|---|---|---|---|
| PA Aptflex R3 | $9.97 \pm 0.03$ | $72.34 \pm 0.02$ | $71.47 \pm 0.04$ | 30.64 |
| PA Aptflex R7 | $9.43 \pm 0.02$ | $70.52 \pm 0.03$ | $70.61 \pm 0.04$ | 19.77 |

The measured values in Table 5.3 translates to densities for Aptflex R3 and R7 of $\rho_{R3} = 595$ kg/m$^3$ and $\rho_{R7} = 420$ kg/m$^3$, respectively. Using Eq. (5.5), the characteristic impedance of Aptflex R3 and R7 are calculated as $z_{R3} = 1.25$ Mrayl and $z_{R7} = 0.95$ Mrayl, respectively.

## 5.5 Discussion

The nominal sound speed and density of Aptflex R3 stated by PA are $2034 \pm 30$ m/s and $570 \pm 20$ kg/m$^3$, respectively. These values are both lower than the values measured here, the sound speed given by PA is approximately 65 m/s lower than the measured, and the density is approximately 30 kg/m$^3$ lower. Measurements are only performed on one sample of R3 and one sample of R7.

A density of 450 kg/m$^3$ is indicated by PA for Aptflex R7. The value measured here is approximately 30 kg/m$^3$ lower. The measured sound speed for R7 is approximately 160 m/s higher than the sound speed measured for R3, which is contrary to the predictions by PA, which suggested a lower sound speed for R7 than for R3.

# Chapter 6

# Transducer construction

This chapter covers the construction of the piezoelectric transducers used in the present work. The transducers are made for use in air, utilizing the first radial mode of a piezoelectric ceramic disk at ~100 kHz. The piezoelectric ceramic disks have approximate dimensions 20 mm × 2 mm. The transducers are built with the goal of obtaining a higher magnitude level of the transmitting voltage response, $S_V$, and the measured voltage to voltage transfer function, $H^{VV}_{1m5m}$, and to increase the bandwidth compared to a single piezoelectric ceramic disk radiating into air. Three piezoelectric transducers are constructed, denoted Transducer No. 1, Transducer No. 2 and Transducer No. 3.

Section 6.1 covers the transducer design, with the subsections covering the piezoelectric element, matching layer, backing layer and housing. Electrical measurements are performed as part of the construction process and are presented and compared to FE simulations. The assembly process is described in Section 6.2.

## 6.1 Transducer design

The fundamental principle for the construction of the transducers in the present work originates from the transducers examined in [95, 102]. Figs. 6.1a and 6.1b show a solid and a transparent drawing of the transducer construction, respectively. The main components of the transducers are a piezoelectric element with a matching- and backing layer, encapsulated in a metal cylinder (transducer housing). The front electrode of the element is grounded into the metal housing by use of a conductive epoxy. The back electrode has a wire soldered onto it, which is connected to a BNC connector. The BNC connector is attached to the back plate of the housing. The metal back plate of the housing is attached to the housing by screws.

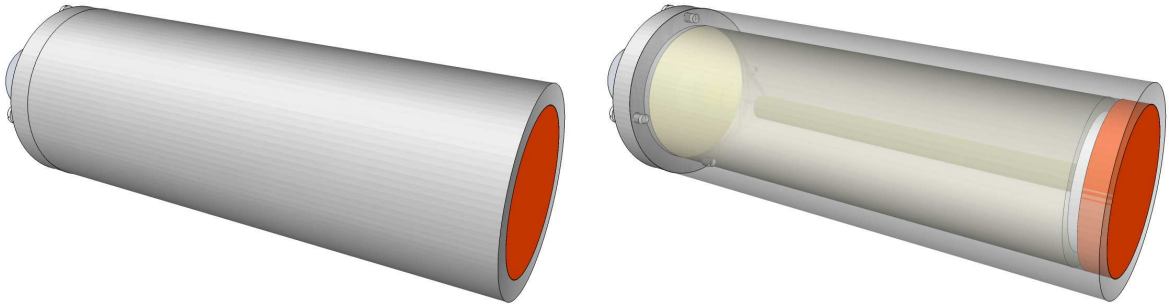

(a) (b)

Figure 6.1: Sketch of (a) the assembled transducer and (b) transparent view of the assembled transducer.

A schematic drawing of the designed transducer is shown in Fig. 6.2, with nominal dimensions given. The dimensions of each transducer may deviate from the nominal values due to inaccuracies in the manufacturing process.

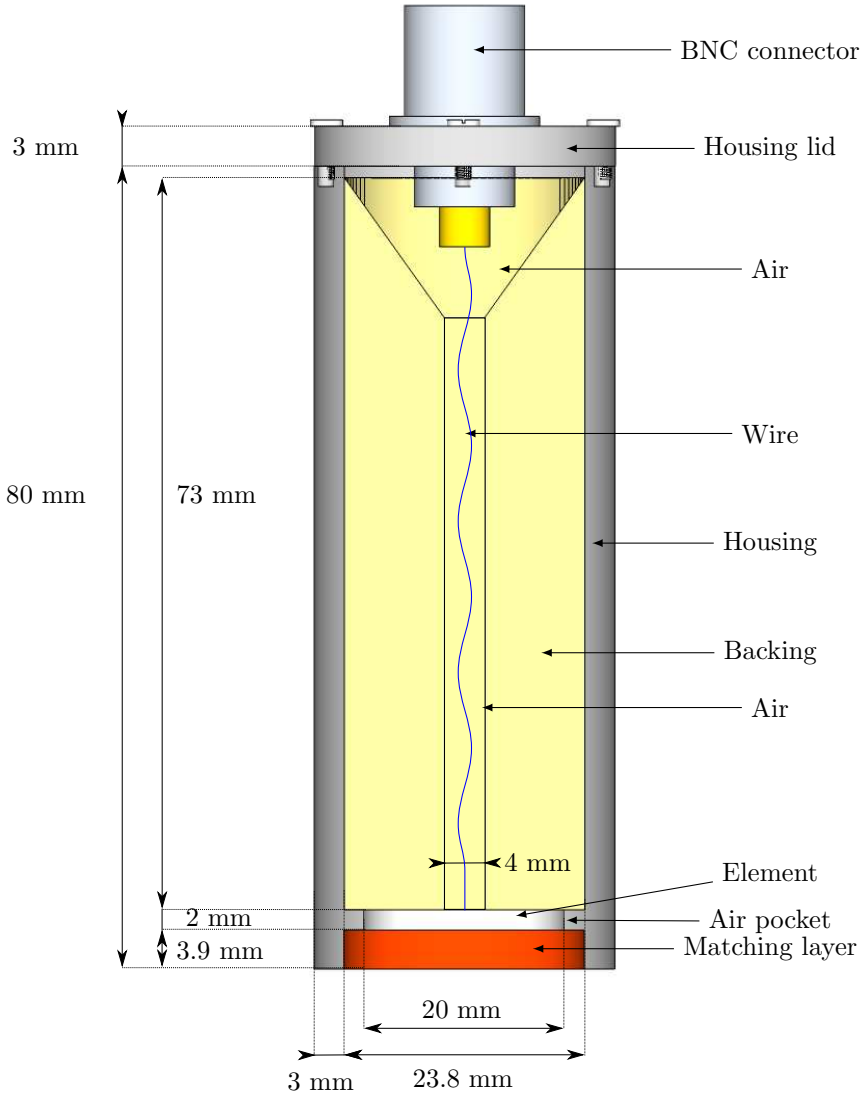


Figure 6.2: Sketch of the assembled transducer. Side view cross section. Showing the piezoelectric disk, matching layer, housing cylinder, backing layer, screwed on housing lid, wire, and BNC connector. The silver conductive epoxy between the piezoelectric disk and the matching layer and between the matching layer and housing wall is not shown.

### 6.1.1 Piezoelectric ceramic disk

The piezoelectric ceramic elements used in the transducer construction are circular disks of the material Pz27 from Ferroperm [34] with approximate[1] dimensions 20 mm × 2 mm (see Section 3.6). The piezoelectric disks are taken from the same batch as the single elements used in the acoustic measurements. Electrical measurements are conducted on all piezoelectric elements of this batch, comparing the magnitude of the conductance and the series resonance frequency of the first radial mode (R1), $f_{R1}$. Elements with similar $f_{R1}$ and maximum conductance are chosen for the transducers: Element #3, Element #15 and Element #20 The measured and simulated conductance of these elements are shown in Fig. 6.3. The simulations are performed with the piezoelectric element vibrating in vacuum, to reduce calculation time (see Section 4.2). It is observed in simulations that the effects of air loading are negligible compared to the difference between simulations and measurements. A frequency difference of approximately 0.6 kHz is observed between the simulated and measured values of $f_{R1}$, and approximately 1 kHz for $f_{R2}$, which is the series resonance frequency of the second radial mode (R2).

[1] See Table 6.1 for accurate dimensions of the elements used.

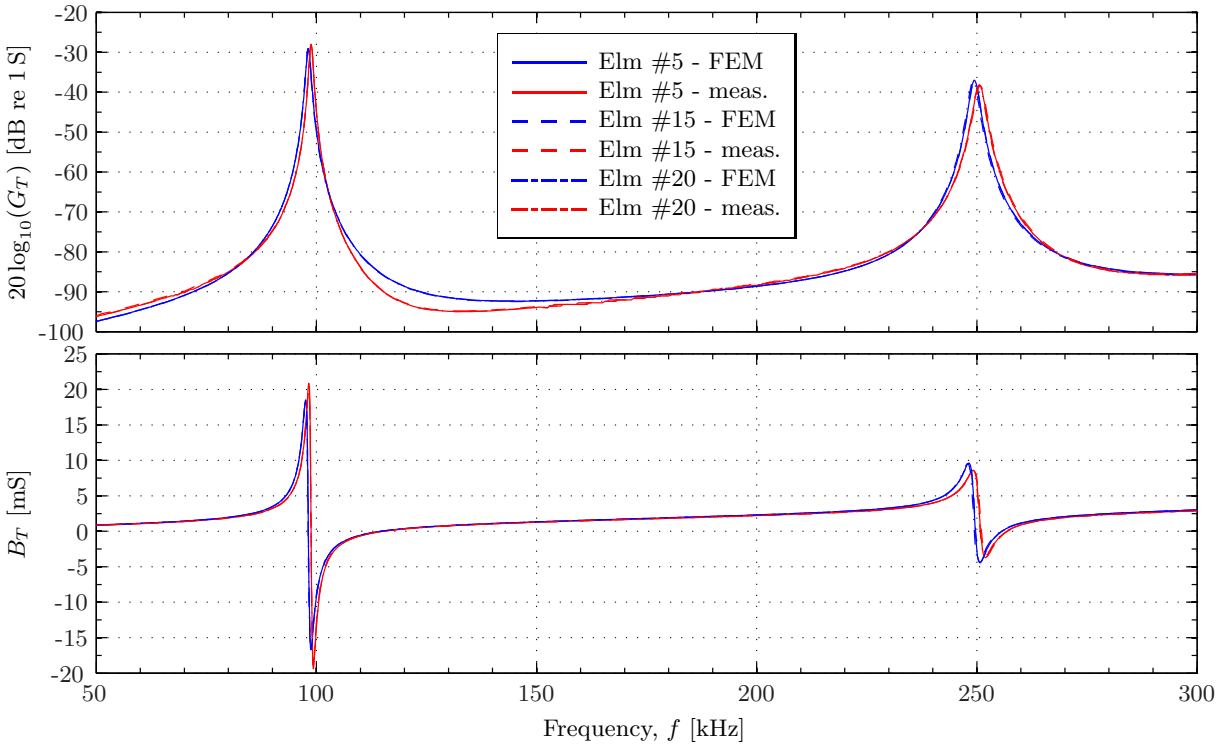


(a)

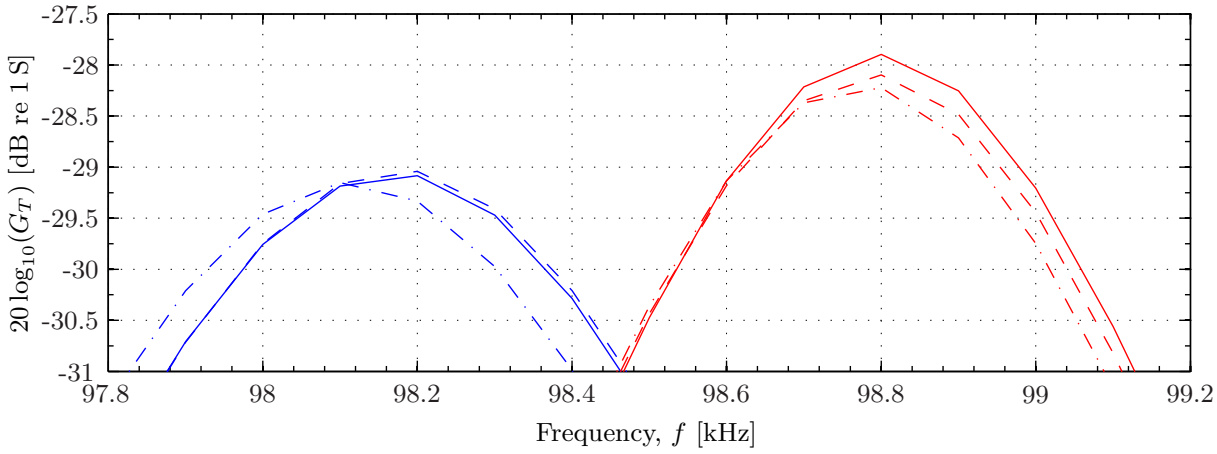


(b)

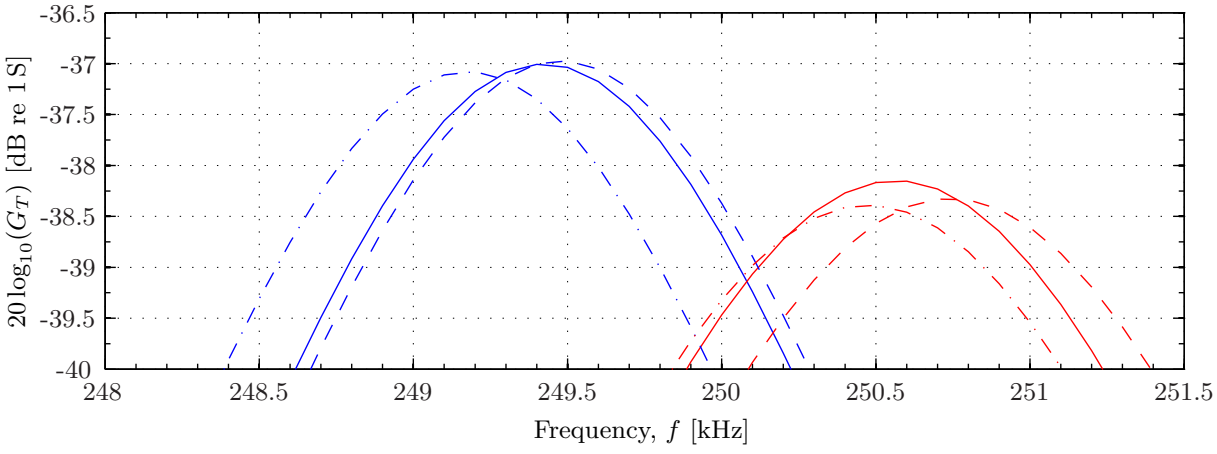


(c)

Figure 6.3: Measured and FE simulated conductance of Element #5, Element #15 and Element #20. Plotted for the frequency range 50 kHz to 300 kHz in (a), and centred around R1 in (b) and R2 in (c). (a) includes the measured and simulated conductance. The simulations are performed with the piezoelectric elements vibrating in vacuum, using `piezodisk` (see Section 4.3).

### 6.1.2 Matching layer

A matching layer is introduced in order to improve the improve the acoustic coupling to air and increase the bandwidth of the transducer. Transmission theory states that there is total transmission of acoustic power if the thickness of the matching layer is $T = \lambda/4$ and the characteristic impedance of the matching layer is the geometric mean of the characteristic impedances of air and Pz27, termed "quarter wavelength matching", [46]. $\lambda$ is the wavelength in the matching layer. The of the characteristic impedance of Pz27, $z_{Pz27}$, is approximately 30 Mrayl[2] and that of air at room temperature the characteristic impedance is approximately $z_{air} = 415$ rayl [46]. This gives an ideal matching layer characteristic impedance of

$$z_m = \sqrt{z_{Pz27} z_{air}} \approx 0.11 \,\text{Mrayl}. \tag{6.1}$$

Two materials are considered for this purpose, the Aptflex syntactic foams R3 and R7 manufactured by Precision Acoustics (PA) [88,89]. Two material samples are shown in Fig. 6.4. These materials have a higher characteristic impedance than the the one found in Eq. (6.1) and than materials used in previous work, e.g. in [37], but they are preferred because they are more mechanically robust.

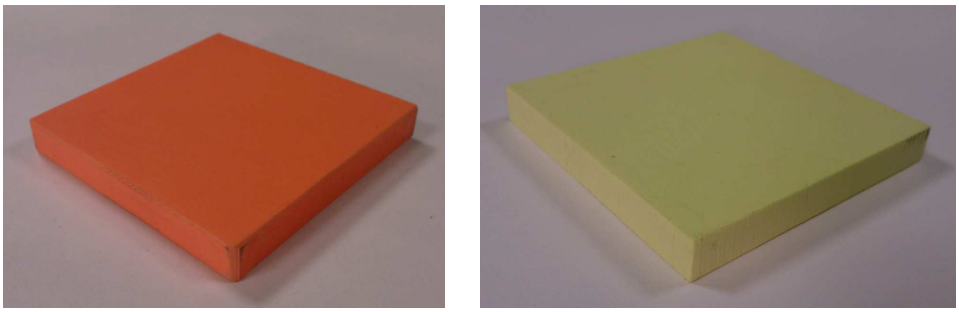

(a) (b)

Figure 6.4: Matching layer alternatives. Aptflex R3 is shown in (a) and Aptflex R7 is shown in (b).

The characteristic impedance of R3, using the material parameters supplied by PA [89], is[3] 1.16 Mrayl. Only indicated material parameters are available for R7, and measurements of $c_l$ and $\rho$ are therefore performed as part of the present work (see Chapter 5). These measured values give a characteristic impedance of 0.95 Mrayl for R7. Based on the characteristic impedances, R7 is the better choice for matching layer, but accurate material parameters are important in the FE simulations. The use of Aptflex R7 in simulations depends on assumptions based on similar materials, in addition to the quantities measured in-house (see Chapters 5 and 4).

In order to compare the behaviour of the two possible matching layers, the quarter wavelength thickness is calculated. Simulation of a piezoelectric element with dimensions[4] 20 mm × 2 mm give $f_{R1} = 99.3$ kHz. The longitudinal sound speed supplied by PA for R3, $c_{l,R3} = 2034$ m/s, and the measured longitudinal sound speed of R7, $c_{l,R7} = 2266$ m/s, are used to calculate the thicknesses

$$T_{R3} = \frac{c_{l,R3}}{4 f_{R1}} \approx 5.12 \,\text{mm} \qquad \text{and} \qquad T_{R7} = \frac{c_{l,R7}}{4 f_{R1}} \approx 5.71 \,\text{mm}. \tag{6.2}$$

To investigate if R7 or R3 offers better coupling to air and higher bandwidth the quantities[5] $H_{15}^{VV}$ and $S_V$ are determined from simulations, using both Aptflex R3 and R7 as matching layer with quarter wavelength thicknesses. The simulations are performed using `piezodiskwidefrontfluid` (see Section 4.3), since the radius of the matching layer exceeds the radius of the piezoelectric disk in the chosen transducer design. A diameter of 22 mm is used for the matching layer in the simulations, and the quarter wavelength thickness found in Eq. (6.2). Results from simulations of $H_{15}^{VV}$ and $S_V$ for the frequency range 70 to 150 kHz for a Pz27 element with matching layer are given in Fig. 6.5. This frequency range covers the first radial mode of the piezoelectric element.

[2] From adjusted material data set, see Section 4.4

[3] The comparison was made prior to the measurements of $c_l$ and $\rho$ were performed on R3 (see Chapter 5).

[4] The choice of matching layer was done prior to determining which elements to use, and nominal dimensions are therefore used in the simulations.

[5] $S_V$ is determined from the FE simulations as described in Section 4.2, and $H_{15}^{VV} = J Z_T S_V^2$ for two identical transducers, with the receiver placed at the reference distance $d_0$ (from Eqs. (2.1), (2.3) and (2.4)).

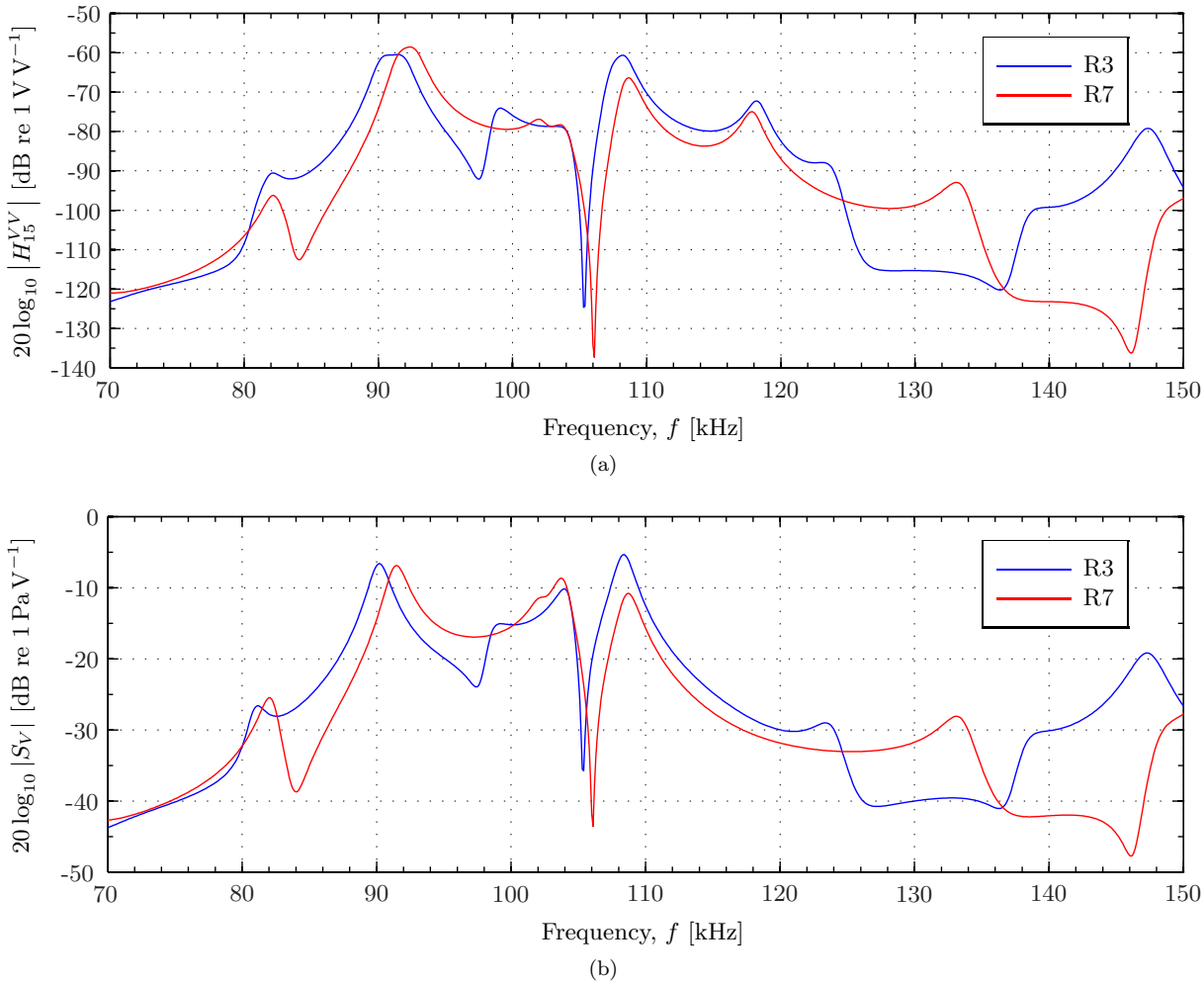


Figure 6.5: Simulated magnitude of (a) $H_{15}^{VV}$ and (b) $S_V$ for the frequency range 70 to 150 kHz for a piezoelectric ceramic disk of the material Pz27 and dimensions 20 mm × 2 mm with an Aptflex matching layer. The dimensions are 22 mm × 5.1 mm for the R3 matching layer, 22 mm × 5.7 mm for the R7 matching layer. $H_{15}^{VV}$ are calculated for a separation distance of 1 m and for two identical reciprocal transducers. The simulations are performed with the structures vibrating in air, using `piezodiskwidefrontfluid` (see Section 4.3).

As seen in Fig. 6.5, using Aptflex R7 as matching layer does not significantly improve the magnitude of neither the $H_{15}^{VV}$ nor $S_V$, compared to R3. Neither R3 or R7 increases the −3 dB bandwidth significantly for the frequency area, since there are several peaks taller than 3 dB for both $H_{15}^{VV}$ and $S_V$.

Since there is no major improvement of the transmitting voltage response when using R7 compared to R3, the latter is chosen as the matching layer to use in the piezoelectric transducers. This is because material data needed to perform FE simulations of R3 are readily available from PA [89], while this is not the case for R7 (see Chapter 4).

A sensitivity analysis with multiple matching layer thicknesses and radiuses have been performed to determine the final dimensions of the Aptflex R3 matching layer, as a the quarter wavelength matching thickness might not be ideal. A relatively flat frequency response and magnitude improvement of $S_V$ are sought. The material data for R3 provided by the manufacturer are used[6], and the piezoelectric disk is simulated with dimensions of 20 mm × 2 mm. The dimensions of the front layer are adjusted with increments of 0.1 mm.

A radius of 11 mm and thickness of 5.1 mm was used as starting points. The thickness was then varied between 3.5 mm and 6.0 mm. A thickness of 3.9 mm was chosen and FE simulations were performed with radiuses varying from 11.0 mm to 12.5 mm. From these simulations the most preferable combination of radius and thickness was seen to be 11.9 mm and 3.9 mm, respectively. In Fig. 6.6 $S_V$ and $H_{15}^{VV}$ are compared for a piezoelectric disk without a matching layer, with an R3 matching layer of 22.0 mm × 5.1 mm (as in Fig. 6.5), and with an R3 matching layer of the chosen dimensions 23.8 mm × 3.9 mm.

[6]The matching layer characterization for R3 had not been performed at this point in the process.

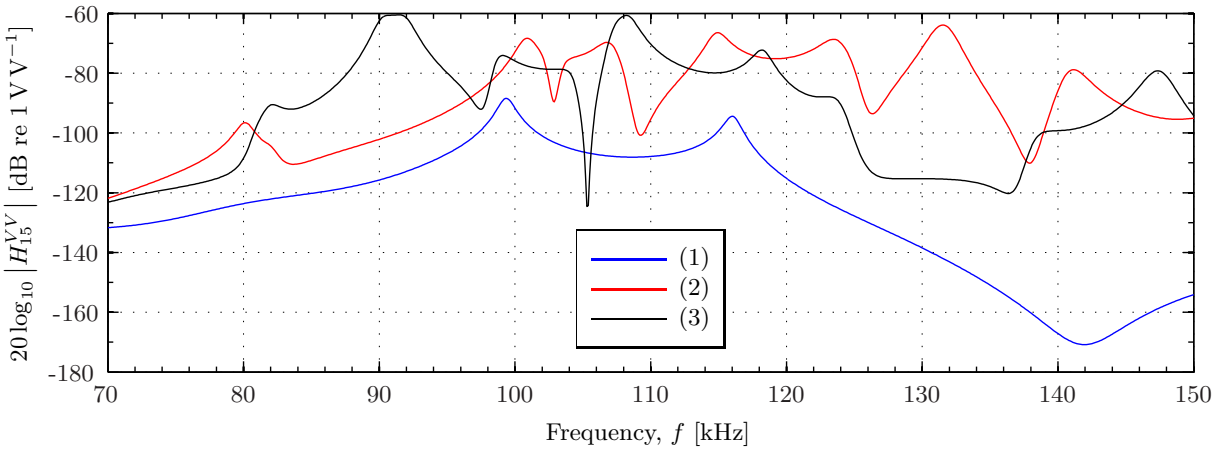


(a)

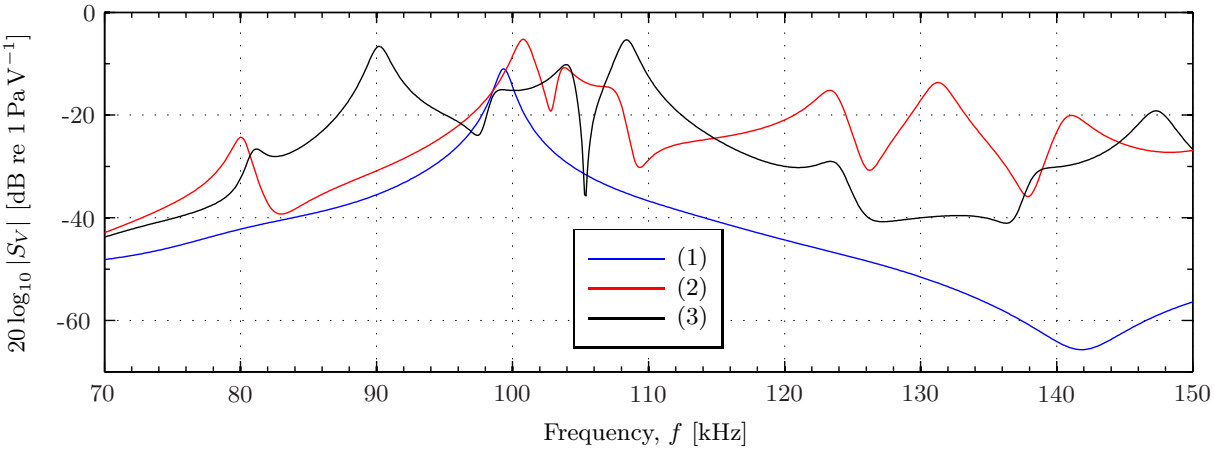


(b)

Figure 6.6: Comparison of the magnitude of (a) $H_{15}^{VV}$ and (b) $S_V$ for a Pz27 piezoelectric ceramic disk of 20 mm × 2 mm. (1) is without a matching layer, (2) is with an R3 matching layer of 23.8 mm × 3.9 mm, and (3) is with an R3 matching layer of 22.0 mm × 5.1 mm. All simulations are performed with the structure vibrating in air, using `piezodiskwidefrontfluid` for (1) and (2), and `piezodiskfluid` for (3) (see Section 4.3).

Three R3 circular matching layers with nominal dimensions 11.9 mm x 3.9 mm were machined out by the in-house workshop and attached to the piezoelectric ceramic disks using silver conductive epoxy (see Sections 6.2 and 4.4.4). The measured dimensions of the piezoelectric ceramic disks and the matching layers are given in Table 6.1.

Table 6.1: Dimensions of the constructed transducers. Measured with a Mitutoyo MDH-25M digimatic micrometer (see Section 3.4).

| Name | Transducer No. 1 | Transducer No. 2 | Transducer No. 3 |
|---|---|---|---|
| Pz27 - Piezoelectric element | #5 | #15 | #20 |
| - radius | 10.12 ± 0.01 mm | 10.12 ± 0.01 mm | 10.125 ± 0.005 mm |
| - thickness | 2.012 ± 0.003 mm | 2.003 ± 0.001 mm | 2.033 ± 0.002 mm |
| Aptflex R3 - Matching layer | | | |
| - radius | 11.895 ± 0.005 mm | 11.895 ± 0.001 mm | 11.904 ± 0.002 mm |
| - thickness | 3.86 ± 0.01 mm | 3.85 ± 0.01 mm | 3.816 ± 0.007 mm |

Electrical measurements were performed at this stage for comparison with FE simulations, i.e. a piezoelectric disk, silver conductive epoxy, a matching layer, and a wire soldered to the rear electrode on the piezoelectric disk. The simulations are performed with the structure vibrating in vacuum for computational reasons, and the wire is neglected. The layer of silver conductive epoxy is assumed to be

0.1 mm and of equal width as the respective matching layer. Fig. 6.7, covering the frequency range 70 kHz to 160 kHz, shows that a frequency shift is observed in some of the resonances when simulations of the structure vibrating in air are compared to simulations of the structure vibrating in vacuum.

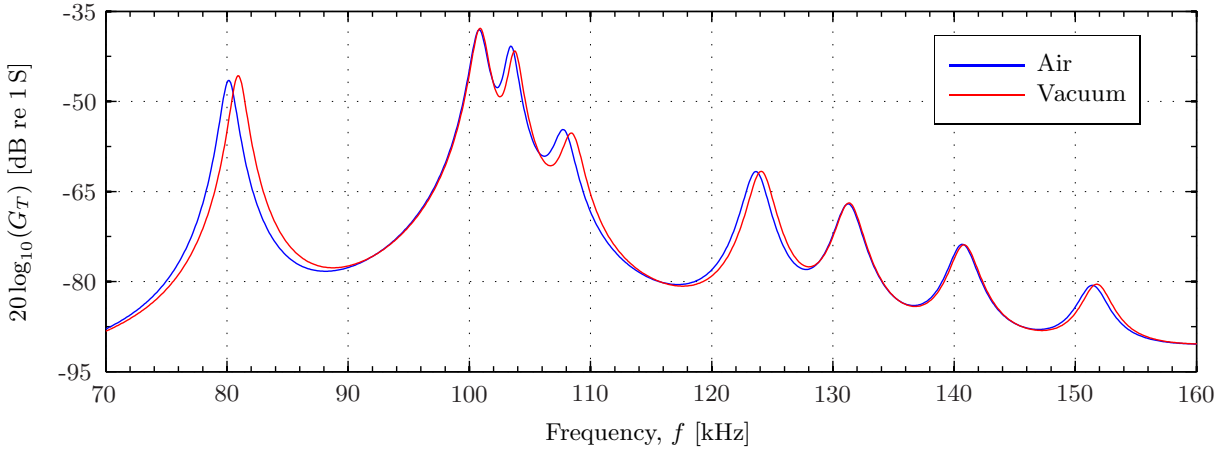


Figure 6.7: Comparison of of the simulated conductance of a Pz27 piezoelectric ceramic disk of dimensions 20 mm × 2 mm with an Aptflex R3 matching layer of dimensions 23.8 mm × 3.9 mm. Simulated with the structure vibrating in air and in vacuum. No silver conductive epoxy layer. `piezodiskwidefrontfluid` and `piezodiskwidefrontglue` is used (see Section 4.3).

Two measurements of the conductance and susceptance of a piezoelectric disk with a matching layer are shown in Fig. 6.8. Some repeatability issues are observed, with a deviation especially for higher frequencies and outside the peaks. There is also a small peak at approximately 70 kHz in the second measurement that does not appear in the first measurement. This may be due to small changes in the electrical measurement setup between each measurement (see Section 3.2 for a description of the setup).

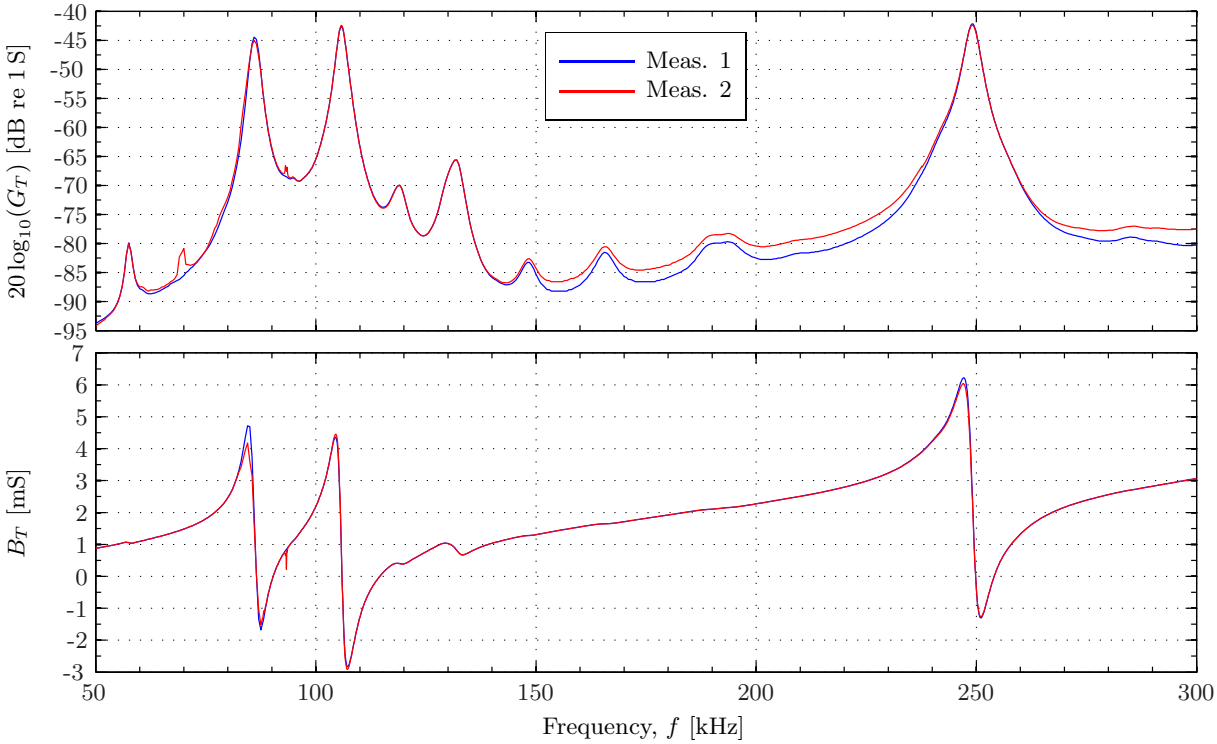


Figure 6.8: Measured conductance and susceptance of the piezoelectric disk with attached front layer of Transducer No. 2. Check of repeatability.

Comparison of measured and simulated conductance and susceptance are shown in Fig. 6.9 for the piezoelectric disk and matching layer used in Transducer No. 2. Better correspondence between the

measured and simulated values are found by adjusting the nominal material data for the R3 matching layer. Measured values are used for the longitudinal sound speed and the density, while both Poisson's ratio and the mechanical quality factor are reduced. The former from 0.375 to 0.35 and the latter from 55 to 40. Figs. 6.10 and 6.11 show measurements and simulations, performed with the adjusted material data set for R3, for the piezoelectric disk and matching layer used in Transducer No. 1 and Transducer No. 3, respectively.

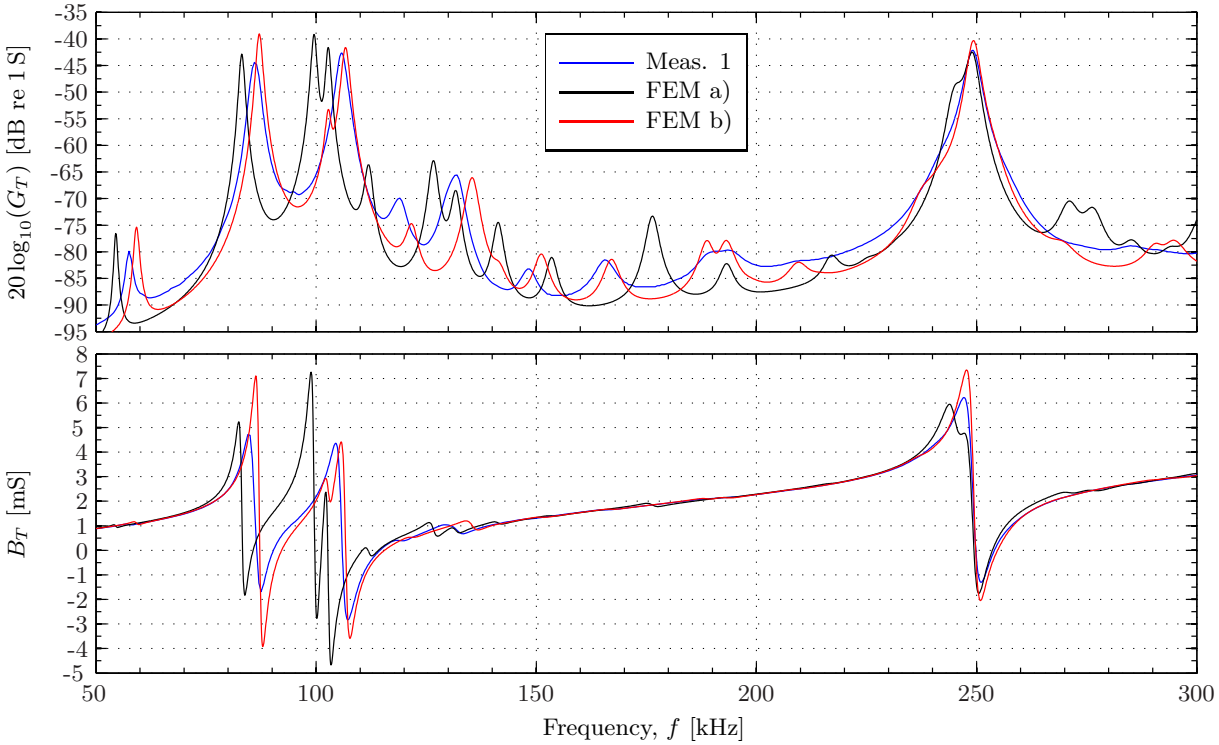


Figure 6.9: Measured conductance and susceptance of the piezoelectric disk with attached front layer of Transducer No. 2 compared to FE simulations with the structure vibrating in vacuum, with a layer of silver conductive epoxy. The material data for Aptflex R3 supplied by PA [89] are used in FEM a), and adjusted material data for R3 are used in FEM b). Using `piezodiskwidefrontglue` in the simulations (see Section 4.3).

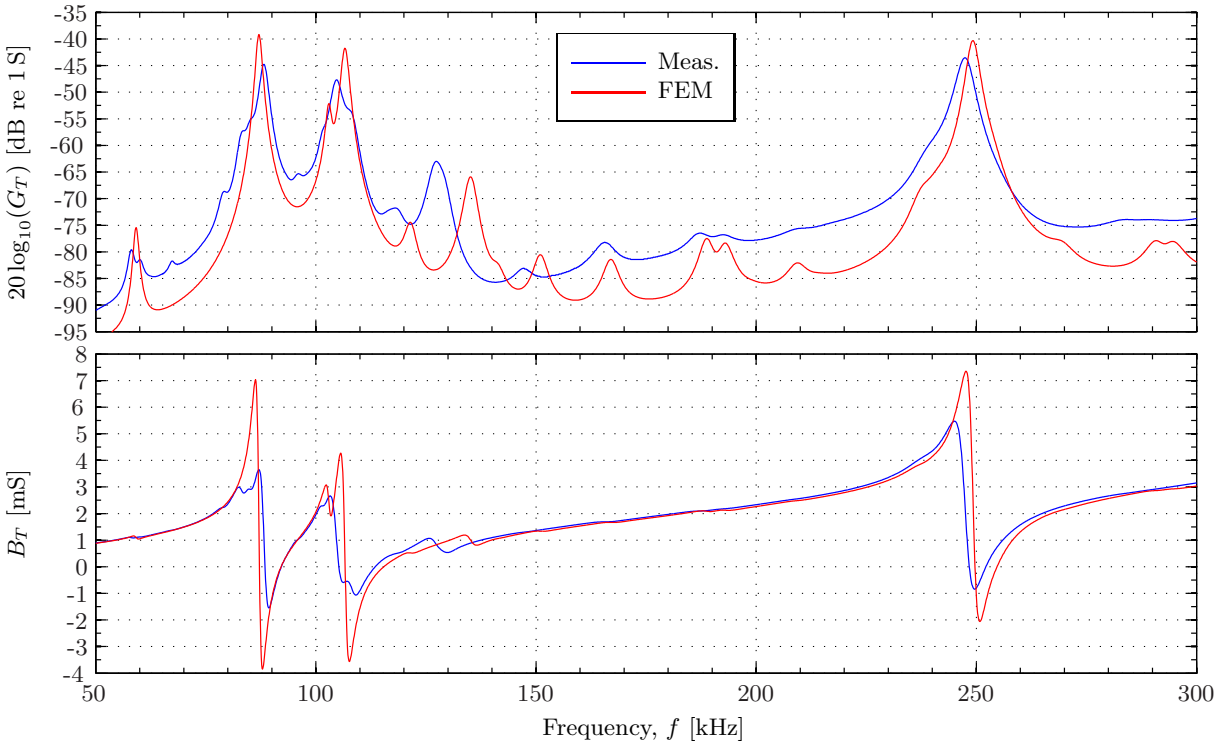


Figure 6.10: As Fig. 6.9, but for the element and matching layer of Transducer No. 1 and only simulations with the adjusted material data.

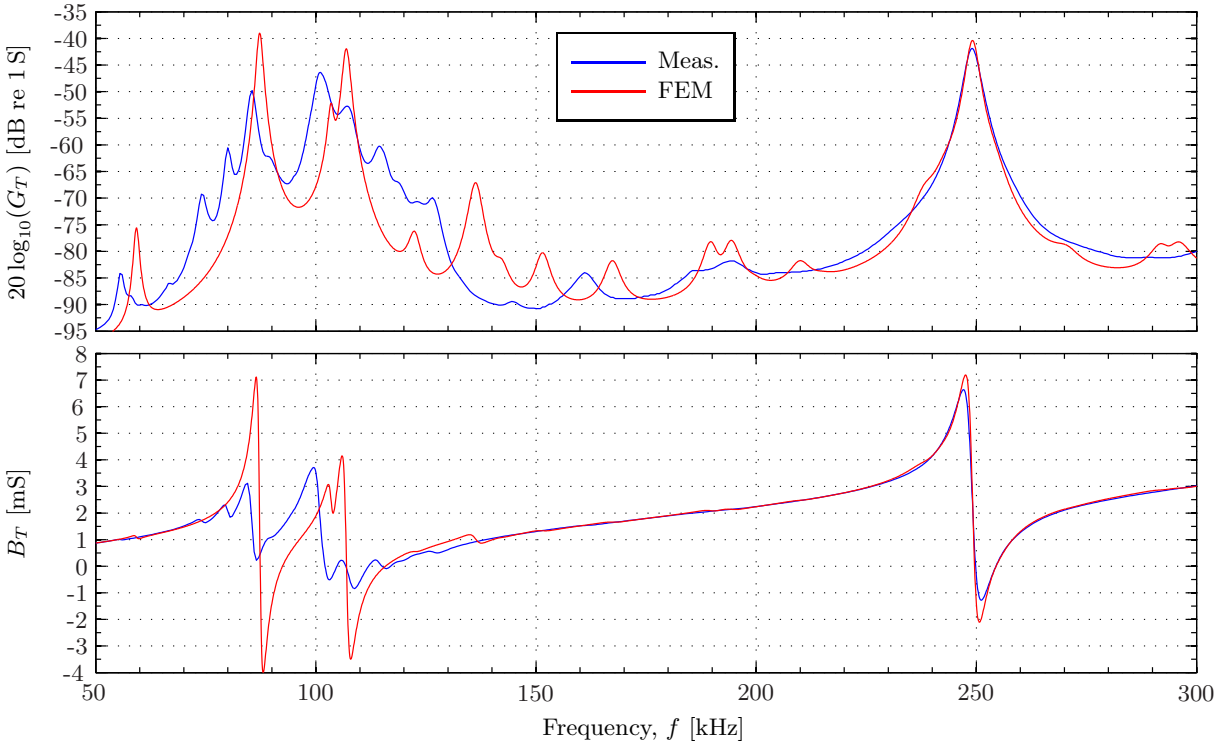


Figure 6.11: As Fig. 6.10, but for the element and matching layer of Transducer No. 3.

Qualitative agreement is observed between measurements and FE simulations in Figs. 6.9, 6.10 and 6.11. Fig. 6.12 compares the measured conductance and susceptance of the three different combinations of element and matching layer.

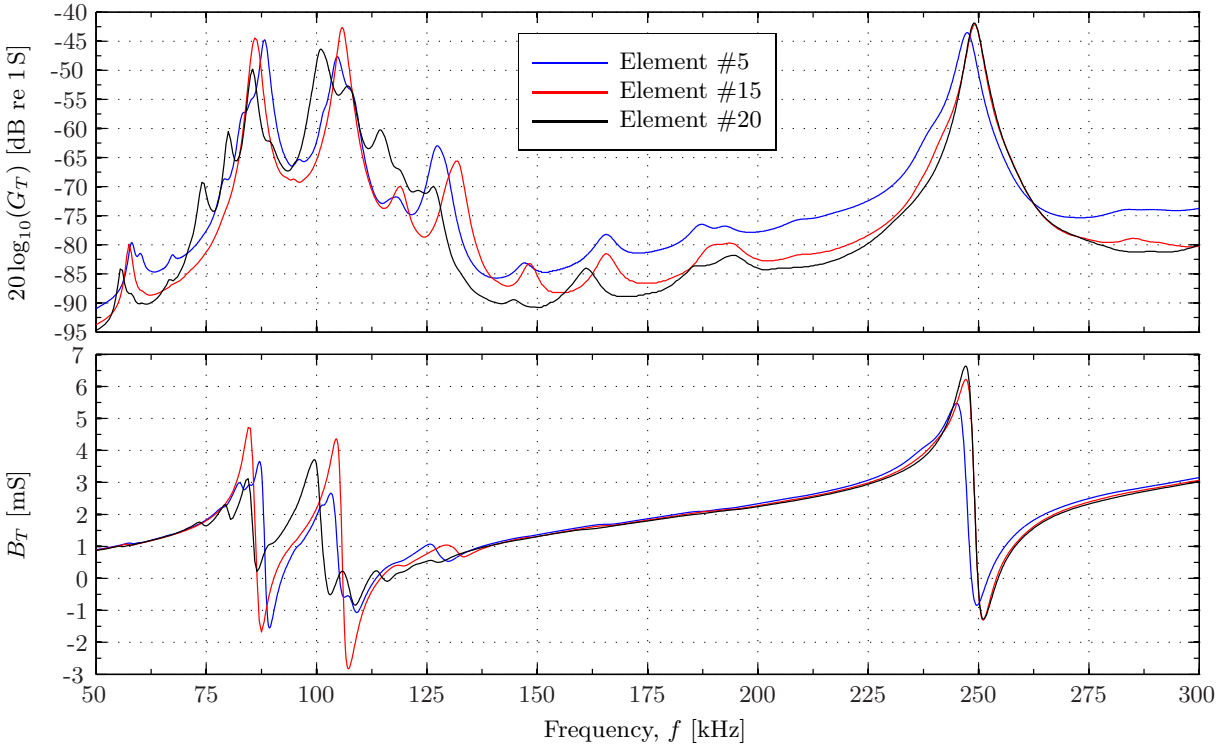


Figure 6.12: Comparison of measured conductance and susceptance of the Element #5 with matching layer (used in Transducer No. 1), Element #15 with matching layer (used in Transducer No. 2) and Element #20 with matching layer (used in Transducer No. 3).

It is seen that the measured conductance of the three sets of piezoelectric disks and matching layers varies more than the repeatability in the measurements and the dimension difference can account for. Possibly a more carefully controlled assembly process can reduce deviations. Better agreement between measurements and simulations may be achieved by further investigation and adjustment of material parameters, but the discrepancies in the measurements limit the attainable accuracy.

### 6.1.3 Backing layer and transducer housing

The material Dinvinycell H130 is used as backing layer [96]. The purpose of the backing layer is to flatten the frequency response of the transducer and to prevent standing waves inside the transducer housing. The backing layer has an equal radius as the matching layer, and a nominal depth of 73 mm. The rearmost side of the backing layer is coned inwards to scatter the backwards propagated soundwave from the element, thus reducing the forming of standing waves inside the backing layer. The depth of the cone is 14 mm, which makes room for the BNC connector fastened in the stainless steel lid. A 4 mm wide hole is made through the length of the backing layer, allowing the wire attached to the element to be extended back and connected to the BNC connector.

The transducer housing is made of grade 316 stainless steel. The stainless steel housing connects the front electrode of the piezoelectric element, through the silver conductive epoxy, to electric ground in the BNC connector. The inner diameter of the housing is 24 mm and the diameter of the matching layer is 23.8 mm, leaving room for the silver conductive epoxy. The housing walls has a thickness of 3 mm. A thinner wall might decrease the resonances in the stainless steel, but the current thickness allows for the housing lid to be fastened mechanically using screws into the housing wall, see Fig. 6.2. The inner length of the housing is 80 mm, which is chosen to have a deep enough backing layer that standing waves inside the housing are sufficiently dampened.

The measured conductance of the constructed transducers are shown in Figs. 6.13, 6.14 and 6.15 for Transducer No. 2, No. 1 and No. 3, respectively. The simulations are performed in with the transducer vibrating vacuum without backing layer and housing lid. The layer of silver conductive epoxy is assumed to be 0.1 mm between the piezoelectric disk and the matching layer and between the matching layer and the stainless steel housing cylinder. The adjusted material data set for the matching layer is used.

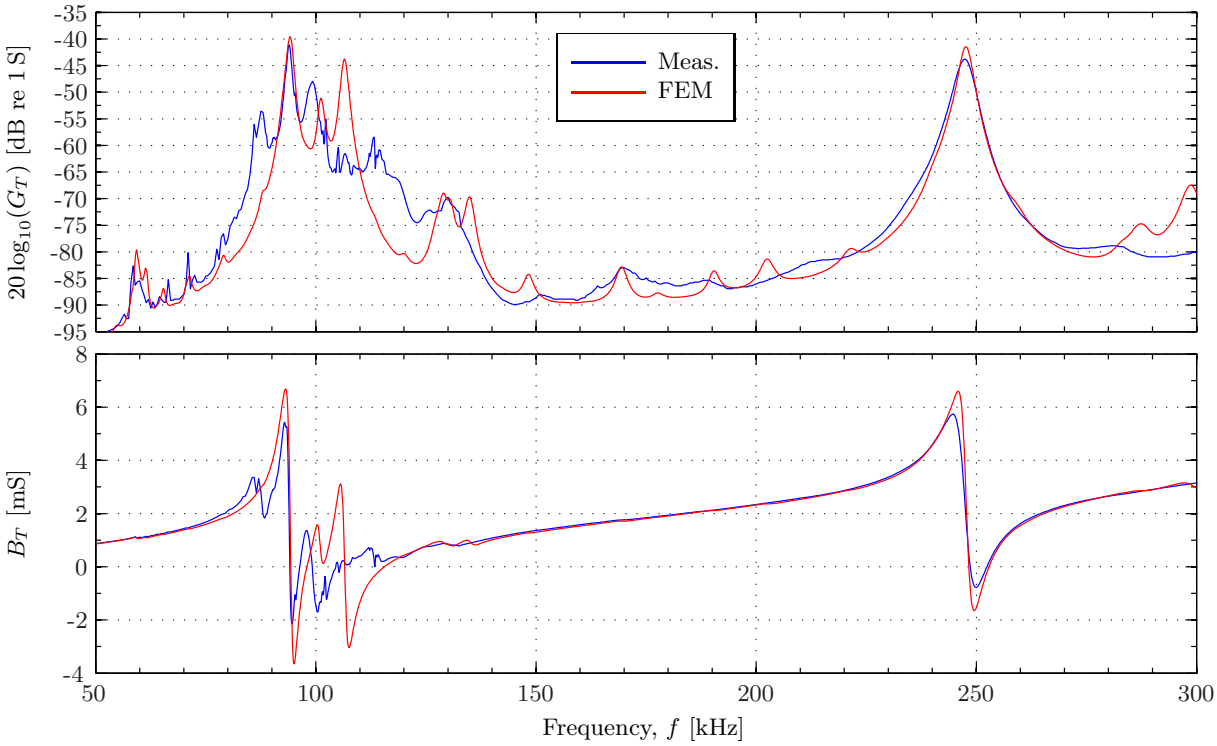


Figure 6.13: Measured conductance of Transducer No. 1 compared to FE simulations of the transducer vibrating in vacuum. The simulations are performed for a simplified transducer, without the backing layer and the stainless steel lid. The adjusted material data for the Aptflex R3 matching layer and `transducervacuum` are used in the simulation (see Section 4.3.

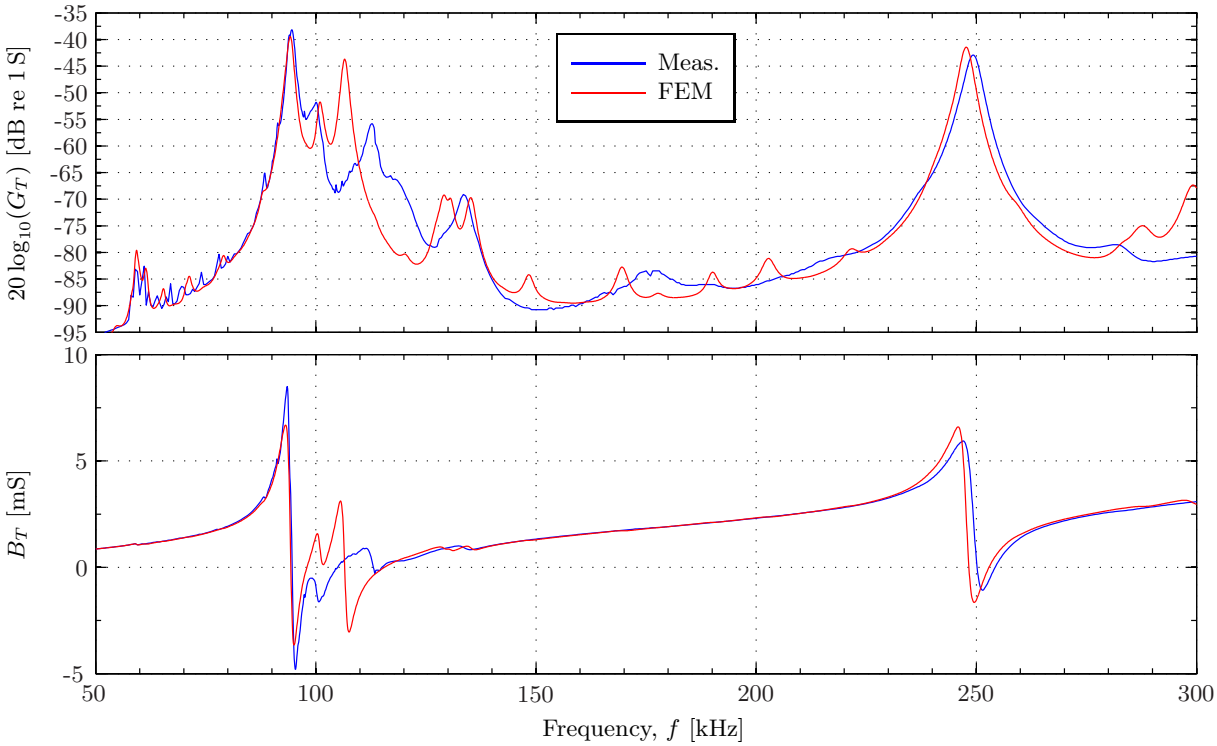


Figure 6.14: As in Fig. 6.13, but for Transducer No. 2.

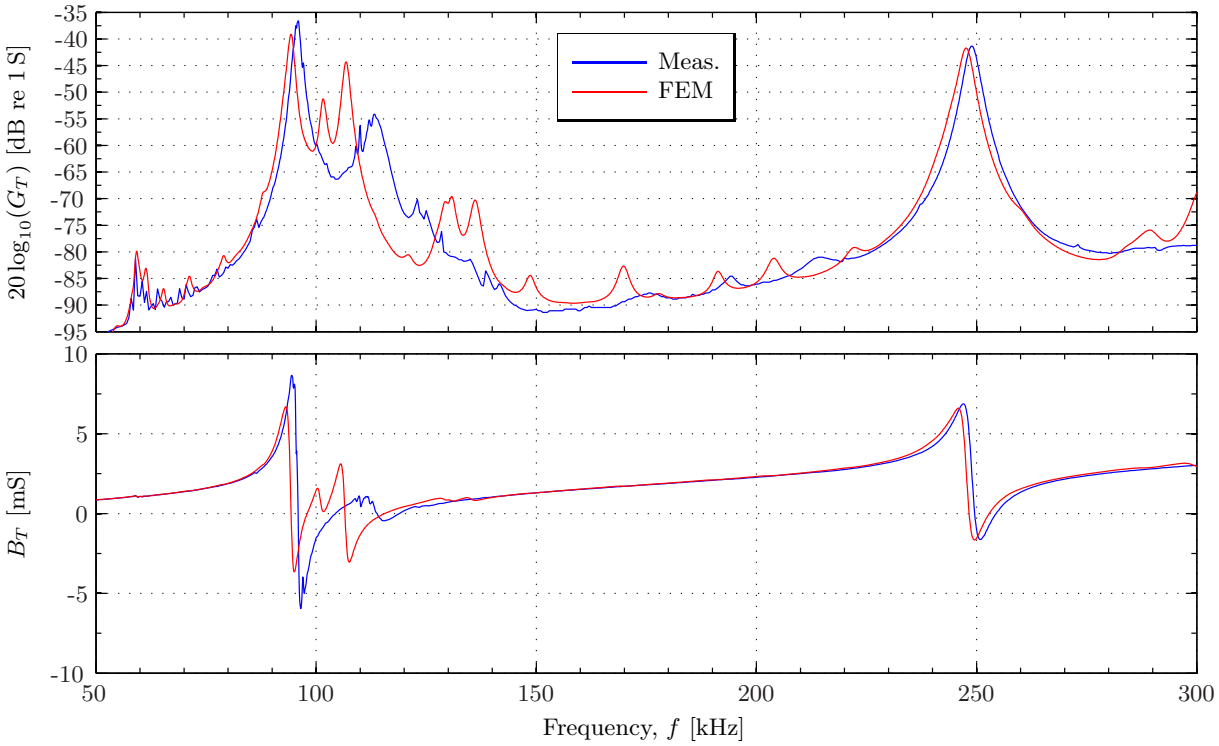


Figure 6.15: As in Fig. 6.13, but for Transducer No. 3.

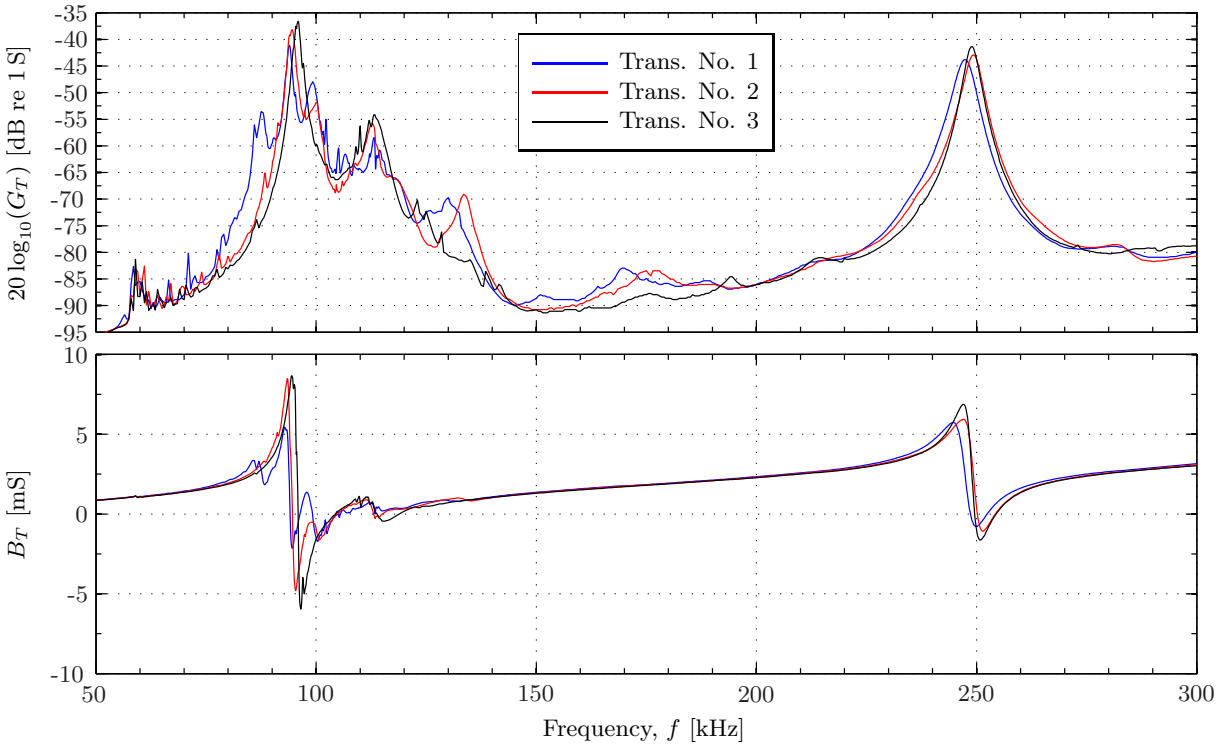


Figure 6.16: Comparison of measured conductance and susceptance of Transducer No. 1, Transducer No. 2, and Transducer No. 3.

Best agreement around the two main resonances are seen for Transducer No. 3 in Fig. 6.15, but the measured conductance lacks a resonance peak at approximately 140 kHz that appears in the simulations and in the measurements in Figs. 6.13 and 6.14.

Possible reasons for the deviations between measurements and simulations are found both in the construction and in the simulations. The simulations are performed with the transducer vibrating in

vacuum, using nominal dimensions for the housing and assumed dimensions of the silver conductive epoxy. A simplified structure, `transducervacuum` (see Section 4.3 ), without the soldered-on wire, the backing layer, and the housing lid, is used in the simulations. Material data for the silver conductive epoxy and stainless steel are not supplied, and material data for similar materials are therefore used (see Section 4.4).

Results of acoustic measurements and comparison with FE simulations are shown in Chapter 8.

## 6.2 The assembly process

Three transducers are built, in order to conduct the three-transducer reciprocity calibration. The first step in the building process is to solder the signal wire onto the piezoelectric element. The soldering requires pre-heating of the element to 175 °C, so that the temperature of the solder iron can be reduced, thus allowing the element to keep a low enough temperature to prevent the polarization of the element being altered through the soldering process. The solder iron temperature is 250 °C. The soldering process is conducted by staff engineer Per Heradstveit, Dept. of Physics and Technology, UiB. The wire used is a multi core electrical wire recommended by staff engineer Heradstveit for its flexibility and mechanical strength.

The PA Aptflex R3 matching layer with nominal dimensions[7] 23.8 mm × 3.9 mm is attached to the front electrode of the piezoelectric element. The matching layer is machined out from a larger sample by the in-house workshop.

The matching layer is attached to the element using a two-component MG Chemicals silver conductive epoxy 8331 [90]. The conductive epoxy has a electrical resistivity of 0.017 Ω·cm. After the two components are mixed with a ratio of 1:1, the working time is 10 min. Eccocoat CC 2 conductive surface coating silver lacquer is applied to the edge of the matching layer, to enhance the electrical coupling to the side of the matching layer, which is attached to the steel wall of the housing later in the process. Conductive epoxy is then applied to the front electrode of the element, and to the backside of the matching layer. The conductive epoxy surfaces is pressed against a smooth PVC surface, and excess conductive epoxy is removed to obtain a thin layer of conductive epoxy on both surfaces. The element is placed on top of the matching layer and centred using a PVC cylindrical mould. A picture of the mould is given in Fig. 6.17a.

The mould is carefully removed and the element and matching layer are cured 12 hours or more before further use. After the conductive epoxy has cured, the electrical resistivity of the conductive epoxy from the edge of the element to the outer edge of the matching layer is measured using a multimeter. A resistance of approximately 10 Ω is measured on the parts used in transducer No. 1, while approximately 2 Ω is measured for transducer No. 2. In Fig. 6.17b, an element with wire soldered at the back electrode and matching layer attached at the front electrode using silver conductive epoxy is shown.

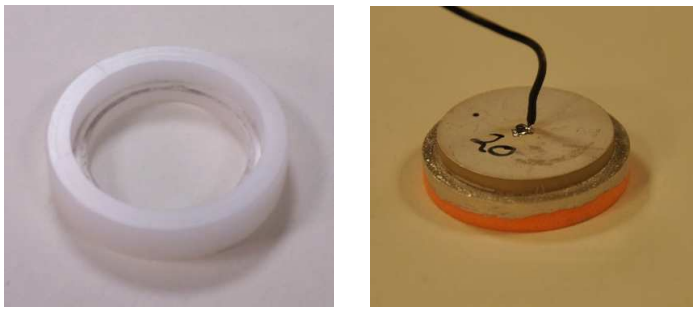

(a) (b)

Figure 6.17: Picture of (a) the PVC mould used for centering the piezoelectric element on the matching layer and (b) the piezoelectric element with the soldered wire on one electrode and the matching layer fastened on the other electrode.

A sandwich construction of the the Divinycell H130 backing layer is made using double-sided tape. A cylinder is then machined by the mechanical workshop to fit inside the housing, with a diameter of 24 mm and a length of 73 mm. The interfaces are aligned parallel to the wall of the housing to reduce the number of reflections. A hole is drilled through the length of the backing layer, allowing the wire attached to the element to be extended back and connected to the BNC connector. The diameter of the hole is 4 mm. Pictures of the backing layer from two different angles can be seen in Fig. 6.18.

[7] See Table 6.1 for accurate dimensions of the elements used.

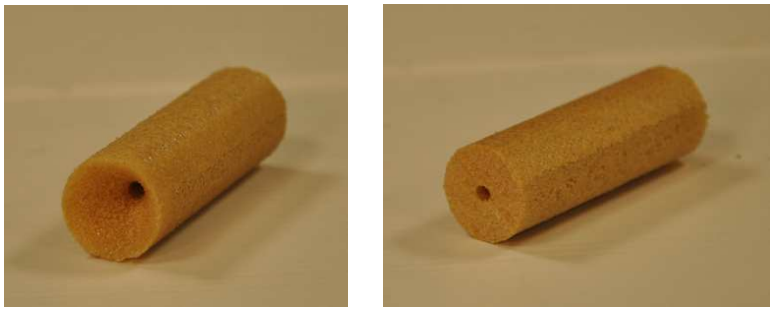

(a) (b)

Figure 6.18: Picture of the Divinycell H130 backing layer. Machined out to be assembled into the steel casing. Figure (a) shows the rearmost side of the backing layer, with the cone visible. (b) shows the face of the backing layer which is connected to the piezoelectric element.

The conductive epoxy used for attaching the element to the matching layer is applied around the edge of the matching layer. The matching layer is then inserted into the front of the housing, aligning the front of the matching layer with the front of the cylinder. The silver conductive epoxy connects the front electrode of the piezoelectric element to the steel housing, which in turn is connected to electric ground in the BNC connector.

The backing layer is inserted into the housing, with the wire soldered onto the element extended through the hole in the middle. No glue is used to attach the backing layer to the piezoelectric element, but it is held in place due to the tight fit of the backing layer in the housing cylinder.

The final step in the assembly of the transducers is installment of the steel lid which contains the BNC connector. To avoid any rotation of the BNC connector when the transducers are in use, the connector is locked in place by a screw from the side of the steel lid, see Fig. 6.19b. If the BNC connector were to rotate, it could cause the wire inside the transducer to break off from either the connector or the element. The signal wire extended back from the element is soldered onto the BNC connector, and the lid is fastened using screws into the steel housing.

(a) (b)

Figure 6.19: Picture showing the rear of the housing, with the H130 backing material inserted. The wire from the piezoelectric element is seen extended through the middle of the backing. Picture showing the steel lid containing the BNC connector. The connector is hindered from rotating by use of a screw.

The finished transducer is seen in Fig. 6.20. The transducer shown is Transducer No. 1, suspended in the measurement chamber with the coaxial cable from the waveform generator connected.

(a) (b)

Figure 6.20: Picture of the assembled Transducer No. 1 suspended in the measurement setup. (a) shows the front of the transducer, while (b) shows the back of the transducer, with the coaxial cable connected to the BNC connector.

# Chapter 7

# Results - Piezoelectric ceramic disks

In this chapter the results obtained by use of the modified three-transducer reciprocity calibration method are presented. The piezoelectric ceramic circular disks Element #6, Element #10 and Element #16 (see Section 3.6) of the material Pz27 [34] are studied. Measured dimensions are given in Table 7.1.

The obtained results are compared to measurements performed with calibrated condenser microphones (see Section 3.5), and to FE simulations performed in FEMP 5.0. The simulations are performed using the measured dimensions and the FEMP-structure `piezodiskfluid` (see Section 4.3).

Table 7.1: Dimensions of the Pz27 piezoelectric ceramic disks studied in this chapter.

| Piezoelectric ceramic disk | D [mm] | T [mm] |
|---|---|---|
| Element #6 | 20.25 ± 0.01 | 2.031 ± 0.001 |
| Element #10 | 20.234 ± 0.008 | 2.035 ± 0.002 |
| Element #16 | 20.24 ± 0.01 | 2.035 ± 0.001 |

The measured conductance and susceptance of the elements are shown in Section 7.1, and compared to FE simulations. Measurements are performed before and after wires are soldered onto the elements, thus showing the effects of the soldering on measured values.

In Section 7.2 the results from the modified three-transducer reciprocity calibration are presented. Effects of the chosen generator voltage and processing method are shown, and the SNR in the measurements are discussed. The effects of each of the corrections introduced in the modified method are described. A reciprocity check is performed on two of the transducer, as the reciprocity of the transducers are assumed in the modified three-transducer reciprocity calibration method. The results for the magnitude of the transmitting voltage response, $S_V$, and free-field open-circuit receiving voltage sensitivity, $M_V$, are presented and compared to FE simulations.

Section 7.3 concerns the use of the two-transducer reciprocity calibration method, and compare example results with the modified three-transducer reciprocity calibration method.

In Section 7.4 the results of $S_V$ obtained using the modified three-transducer reciprocity calibration method are compared to measurements performed using calibrated condenser microphones from B&K.

Two of the elements are used in combination with the calibrated condenser microphones to find $M_{B\&K}$ by the modified three-transducer reciprocity calibration method. Results are shown in Section 7.5, compared to the calibration supplied by the manufacturer.

Only the magnitude is considered in the acoustical measurements at present. A simplified notation is therefore adopted in this chapter, where the modulus of e.g. the transmitting voltage response is denoted $S_V$ instead of $|S_V|$. The essential MATLAB-scripts used to calculate the results from the measurements can be found in Appendix A.3.

## 7.1 Electrical quantities

The electrical measurements are performed as described in Section 3.2. Figs. 7.1, 7.2 and 7.3 shows the conductance and susceptance of Element #6 for the whole frequency range 50 kHz to 300 kHz, the frequency range around R1, and the frequency range around R2, respectively. Similar results are shown for Element #10 in Figs. 7.4, 7.5 and 7.6, and for Element #16 in Figs. 7.7, 7.8 and 7.9.

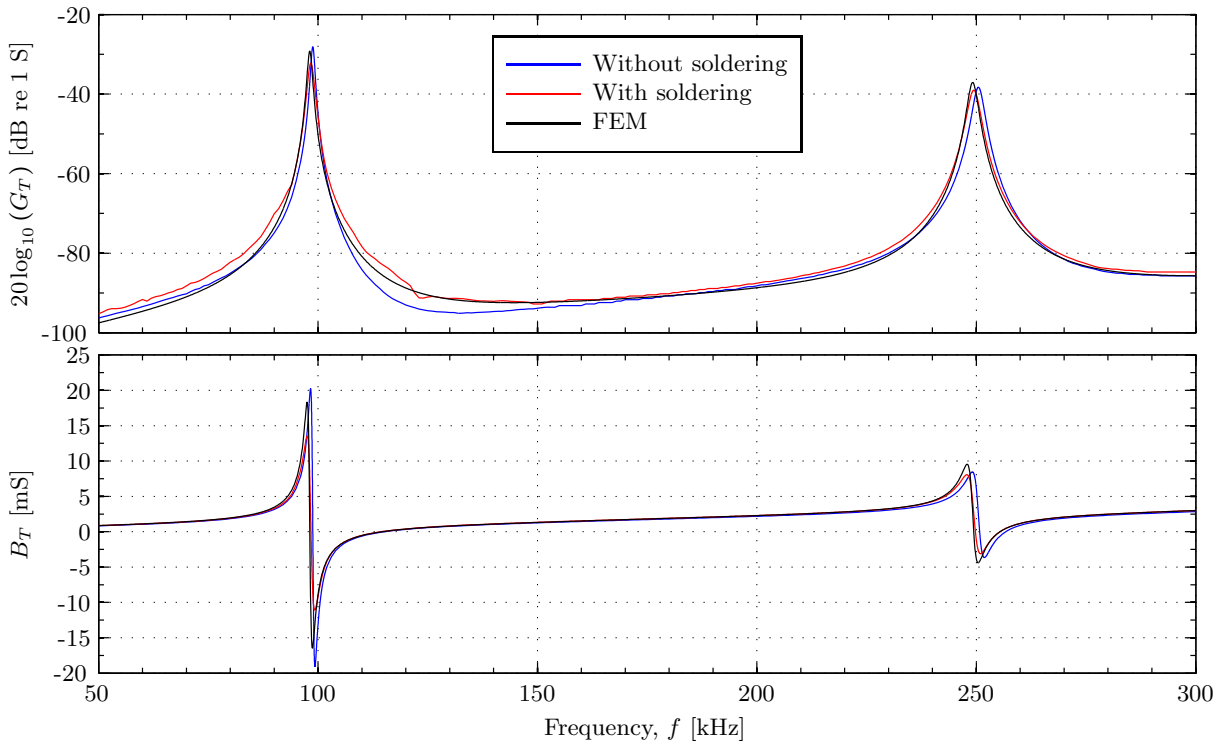


Figure 7.1: Conductance and susceptance of Element #6 for the frequency range 50 kHz to 300 kHz. Measured before and after the wires are soldered onto the element. Compared with FE simulations of the element vibrating in air.

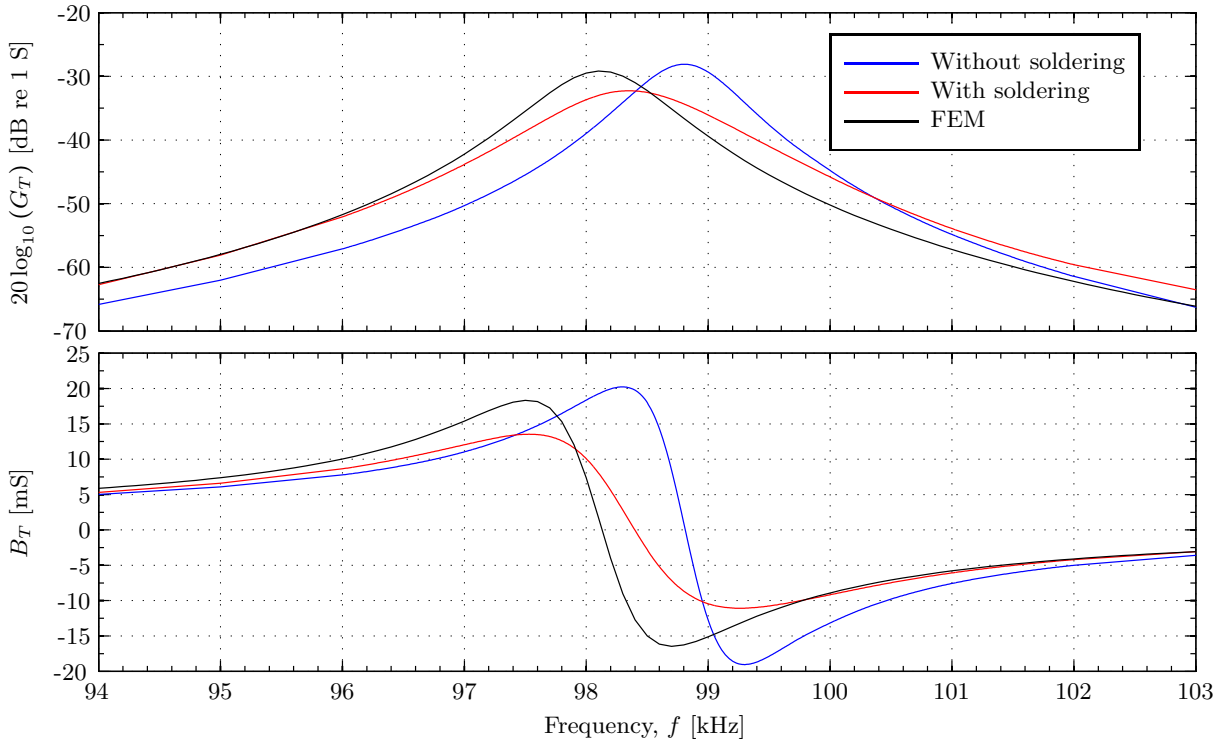


Figure 7.2: As Fig. 7.1, but for the frequency range 94 kHz to 103 kHz, around R1.

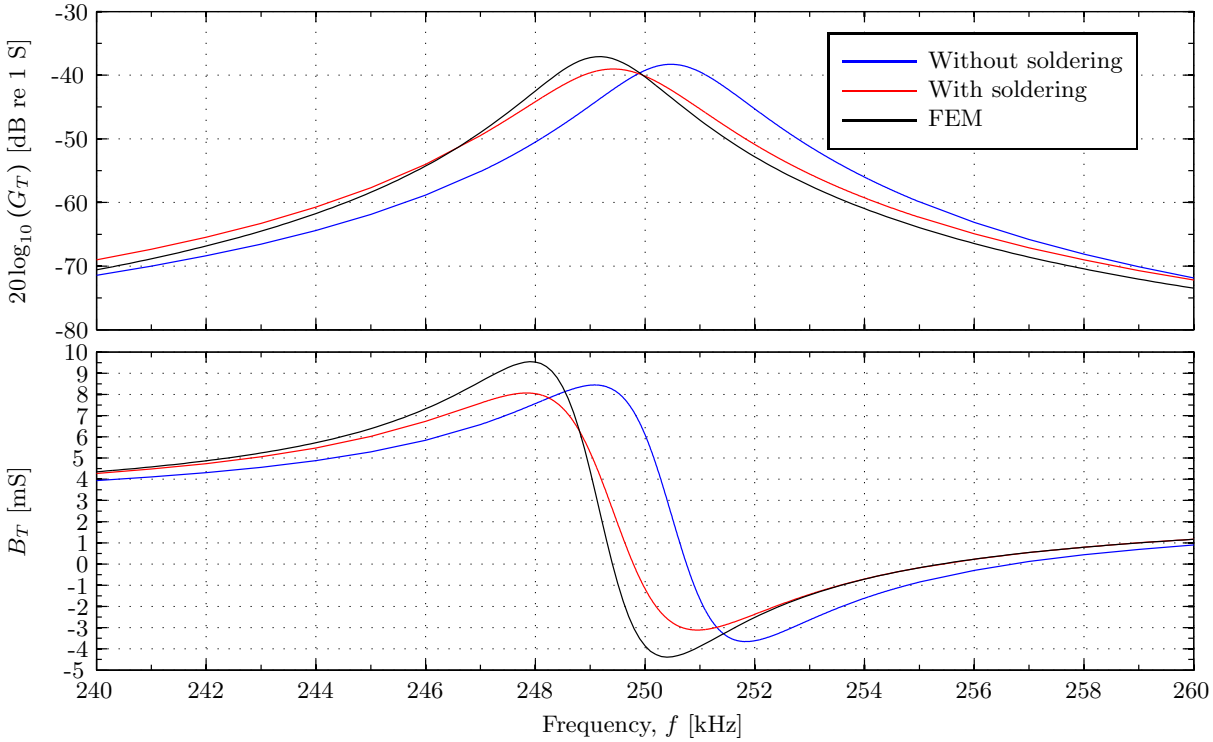


Figure 7.3: As Fig. 7.1, but for the frequency range 240 kHz to 260 kHz, around R2.

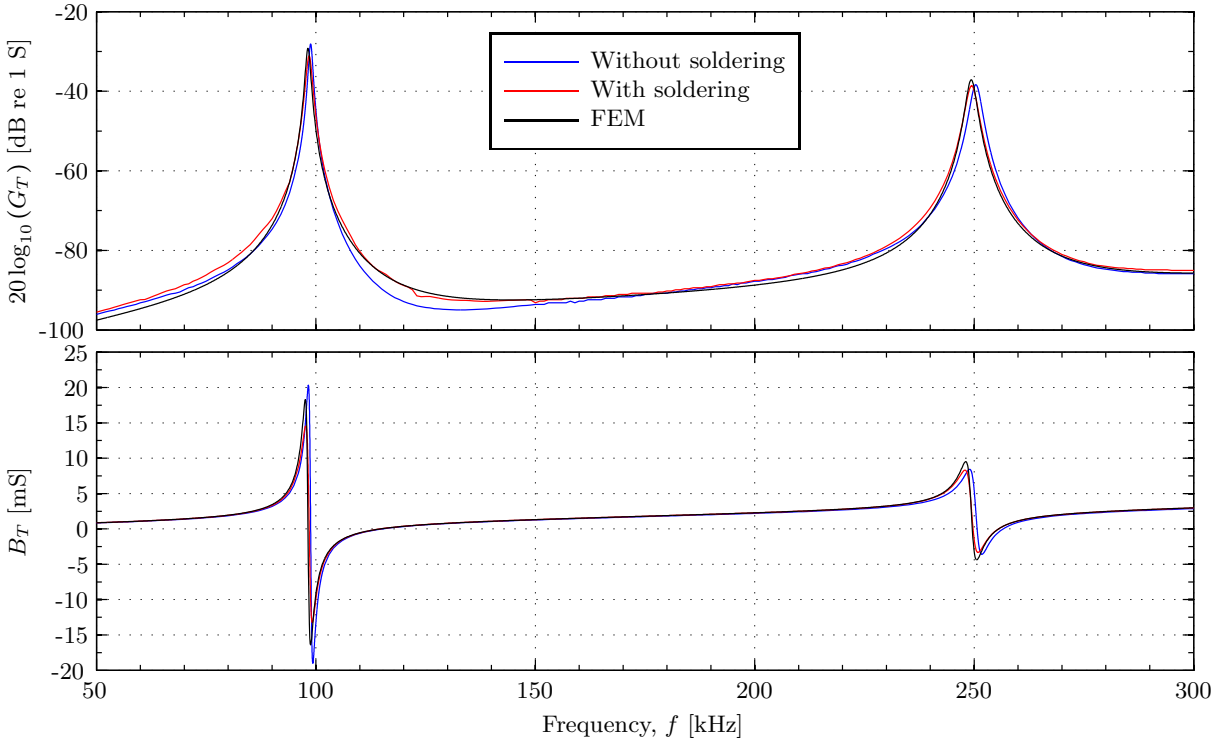


Figure 7.4: Conductance and susceptance of Element #10 for the frequency range 50 kHz to 300 kHz. Measured before and after the wires are soldered onto the element. Compared with FE simulations of the element vibrating in air.

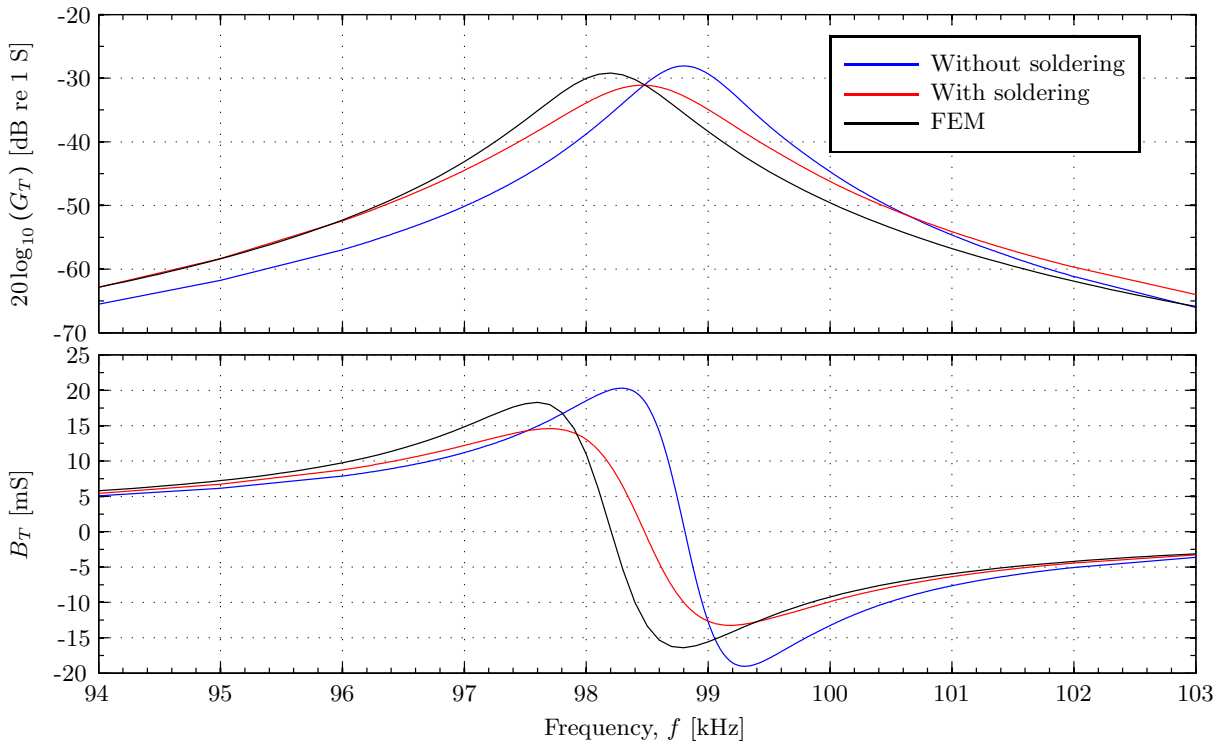


Figure 7.5: As Fig. 7.4, but for the frequency range 94 kHz to 103 kHz, around R1.

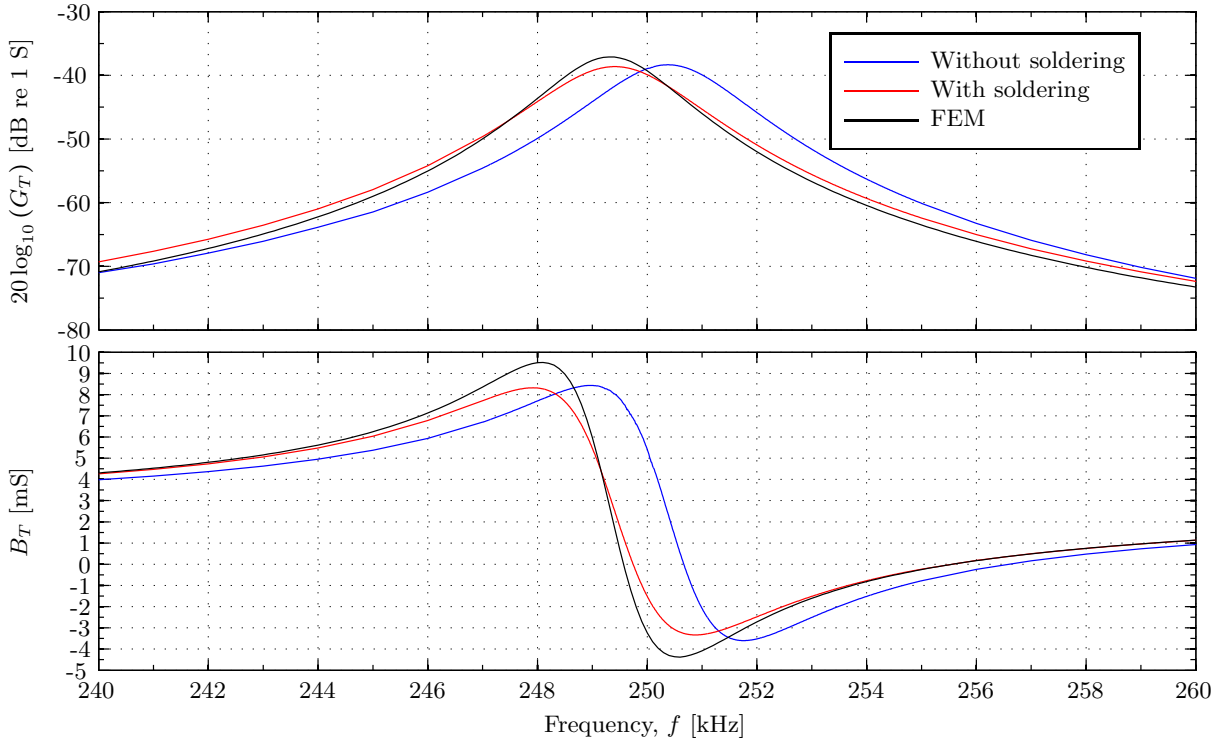


Figure 7.6: As Fig. 7.4, but for the frequency range 240 kHz to 260 kHz, around R2.

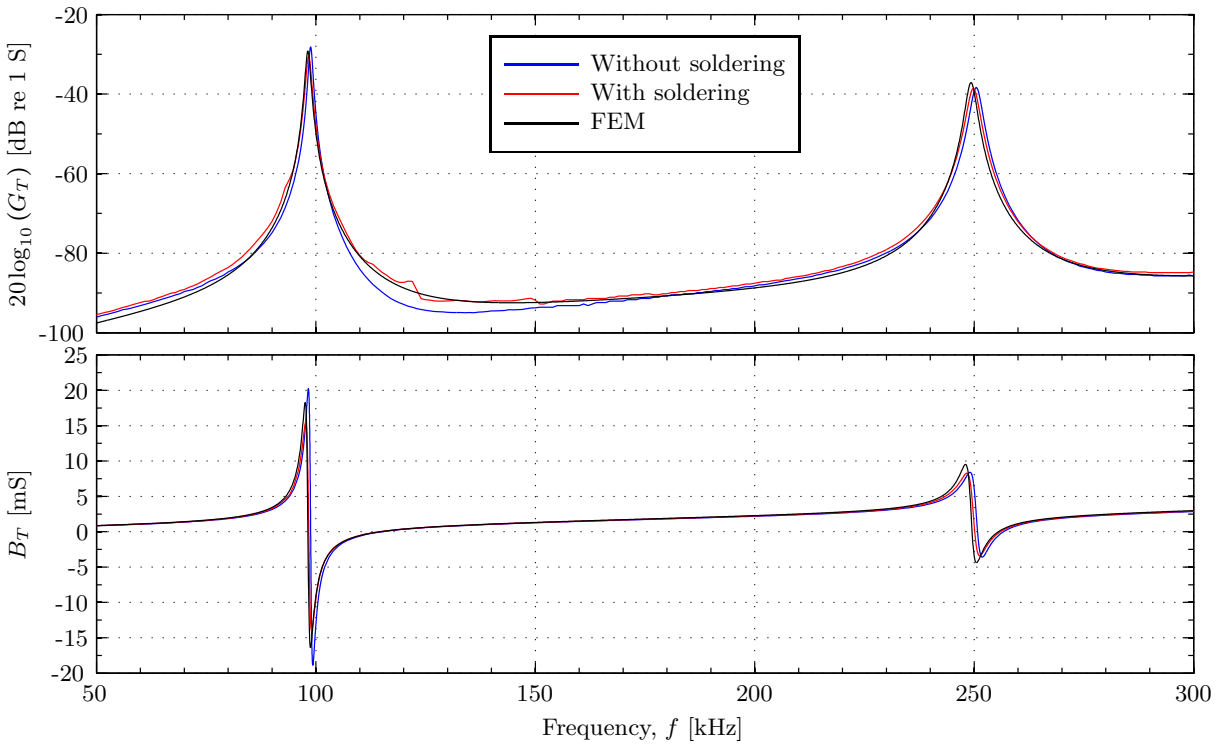


Figure 7.7: Conductance and susceptance of Element #16 for the frequency range 50 kHz to 300 kHz. Measured before and after the wires are soldered onto the element. Compared with FE simulations of the element vibrating in air.

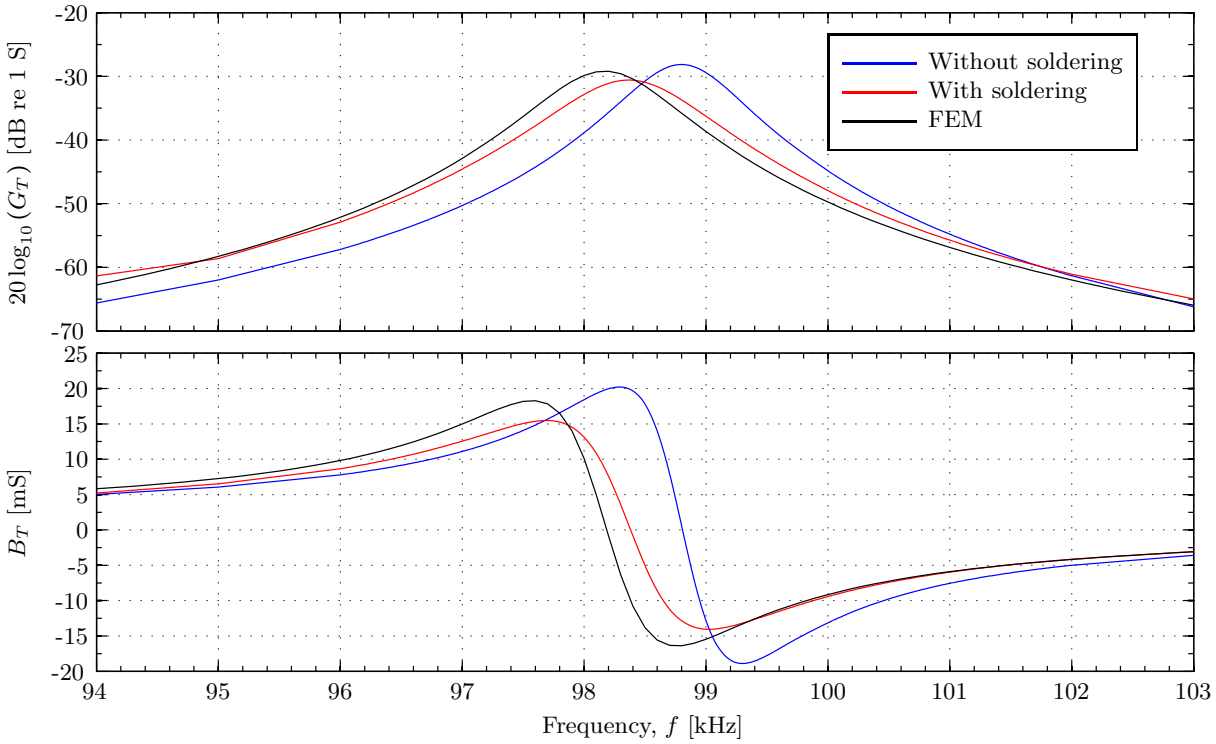


Figure 7.8: As Fig. 7.7, but for the frequency range 94 kHz to 103 kHz, around R1.

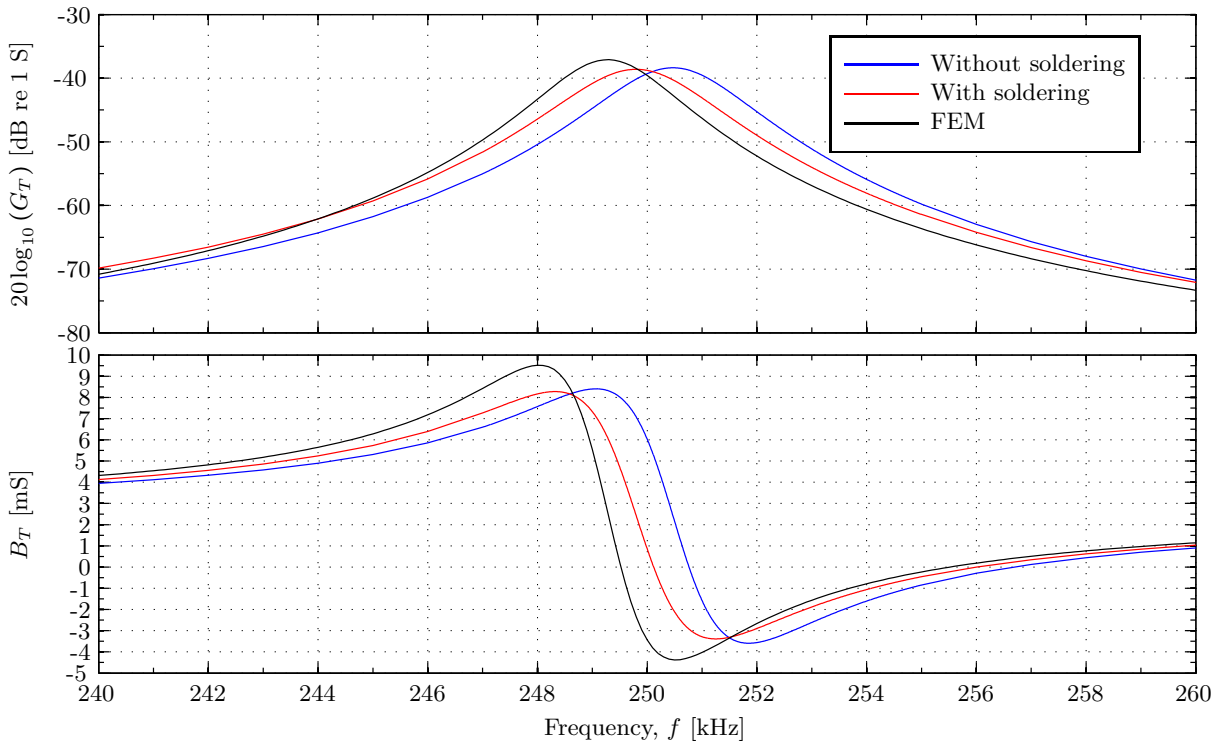


Figure 7.9: As Fig. 7.7, but for the frequency range 240 kHz to 260 kHz, around R2.

A form of suspension is needed when the elements are used in acoustical measurements, thus wires are soldered onto the element as described in Section 3.6. These wires are not included in the FE simulations, and it is of interest to investigate the effect of this, and the agreement between simulations and measurements.

It is seen that the soldering causes an increase in the conductance outside the resonances at R1 and R2 for all three elements. The first radial mode series resonance frequency, $f_{R1}$, and the second radial mode series frequency, $f_{R2}$, are reduced when wires are soldered onto the elements. A decrease in the maximum conductance is observed at the resonances, most significantly at $f_{R1}$. A possible reason for this behaviour is the mass loading introduced by the soldering. It is assumed that the temperature of the soldering iron is sufficiently low compared to the Curie temperature of Pz27, so that the soldering process has not altered the properties of the material. The stated soldering temperature and Cure temperature are (250 °C and 350 °C, respecitively (see Section 3.6). Outside the resonances an increase in the conductance is seen. The repeatability uncertainties at resonance, reported in Section 3.2 for a similar disk, is small compared to the frequency shift and conductance decrease observed here. The susceptance is affected by the soldering in a similar manner as the conductance, with a downward frequency shift and a dampening of the resonances.

When comparison is made with the FE simulations it is seen that the measurements on the elements without wires have higher resonance frequencies, with a frequency difference between 0.5 kHz and 1 kHz for $f_{R1}$ and between 1 kHz and 2 kHz for $f_{R2}$, for all three elements. The measured maximum conductance is slightly higher than the simulated at $f_{R1}$ and slightly lower at $f_{R2}$. Some deviations between simulations and measurements on elements without wires are also seen for the susceptance and for the conductance outside the resonances. The effects caused by the soldering leads coincidentally to a better agreement with the FE simulations when the position of the resonance frequencies and the conductance outside resonance are considered.

## 7.2 Three-transducer reciprocity calibration

The modified three-transducer reciprocity calibration method is used on the Pz27 piezoelectric ceramic disks Element #6, Element #10 and Element #16, as described in Chapters 2 and 3. Specifications for the three performed measurements are given in Table 7.2. A fourth measurement is performed in order to check the reciprocity of two of the elements. Quantities used to model the transmitting and receiving electronics are given in Chapter 3.

In each of the measurements a voltage to voltage transfer function, $H^{VV}_{1m5m}$, is measured. Correction

factors (see Section 2.1.6) are applied to each measured transfer function, and the transfer functions of measurement No. 1, No. 2 and No. 3 are used to calculate $S_V$ and $M_V$ for the transducers.

It is of interest to examine the measurement conditions and measurement methods used in the calibration, and their impact on $H^{VV}_{1m5m}$. The two different methods used to extract the voltage from the measurements are evaluated in Section 7.2.1. The SNR of measurement No. 4 is presented and discussed in Section 7.2.2, and the effects of different generator voltages are shown in Section 7.2.3. The correction factors used in the modified three-transducer reciprocity calibration method are discussed in Section 7.2.4, and the effects of each of the correction factors on the calculated $S_V^{T3}$ are shown. A reciprocity check is performed in Section 7.2.5. Results obtained for $S_V$ and $M_V$ for all elements are presented in Section 7.4.2, and compared to FE simulations.

Table 7.2: Three-transducer reciprocity calibration of Pz27 piezoelectric ceramic disks.

| Measurement parameters | | | | |
|---|---|---|---|---|
| Meas. No. | Transmitter | Receiver | Meas. distance | Burst length |
| 1 | T1 = Element #6 | T2 = Element #10 | 77 cm | 1.4 ms (~48 cm) |
| 2 | T1 = Element #6 | T3 = Element #16 | 77 cm | 1.4 ms (~48 cm) |
| 3 | T3 = Element #16 | T2 = Element #10 | 77 cm | 1.4 ms (~48 cm) |
| Reciprocity check | | | | |
| 4 | T3 = Element #16 | T1 = Element #6 | 77 cm | 1.4 ms (~48 cm) |

### 7.2.1 Peak to peak detection

Two methods are used to determine the voltage of a recorded signal waveform (see Section 3.7). A signal waveform is recorded for each frequency and the peak to peak voltage is extracted from a predetermined calculation interval of the waveform. The direct method determines the voltage directly from the time domain, while the FFT method extracts the voltage from the frequency domain. The different results obtained using the two methods are seen for the measured $H^{VV}_{1m5m}$ in measurement No. 1 in Fig. 7.10. Both an open-circuit generator voltage of $V_{pp}$ = 2 V and of $V_{pp}$ = 20 V are used.

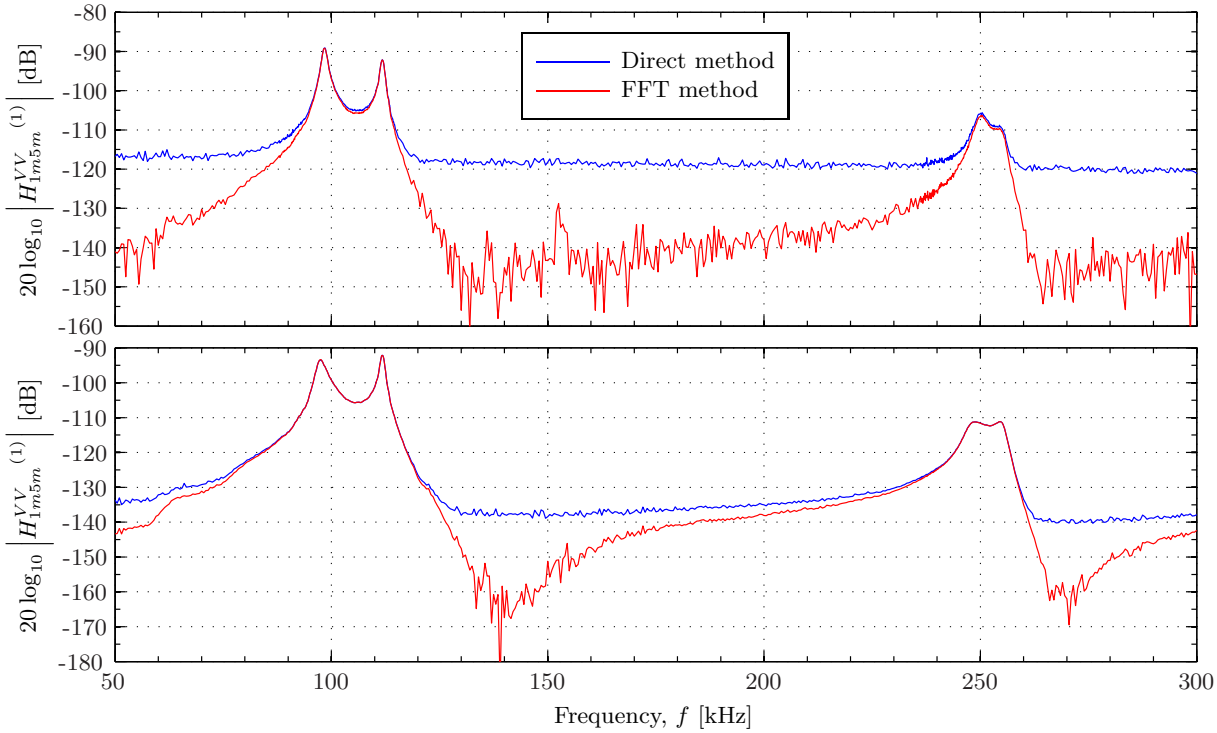


Figure 7.10: Measured $H^{VV}_{1m5m}$ for measurement No. 1. Result obtained by the direct method and the FFT method, with open-circuit generator voltages $V_{pp}$ = 2 V (upper) and $V_{pp}$ = 20 (lower).

The two methods yield agreeing results at the two peaks in R1 for the lower generator voltage. For the higher generator voltage, the frequency range where the two method agree expands outside the peaks at R1, and to the peaks at R2. Outside the peaks it is seen that the two methods part for both generator voltages. It appears that the direct method is more sensitive to noise than the FFT method, i.e. it reaches the noise floor sooner. As a result of this the FFT method is the preferred method, and is therefore used in the following.

### 7.2.2 SNR

The signal to noise ratio is an important parameter in the measurements, and determines the achievable accuracy of the performed calibration. It is stated in [43] that an SNR of at least 20 dB is needed in order to perform a conventional three-transducer reciprocity calibration with an accuracy of ± 1 dB. The SNR is calculated as described in Section 3.7.

The SNR of measurement No. 4, where Element #16 transmits to Element #6, is shown in Fig. 7.11. It is assumed that this SNR is representative for all the measurements listed in Table 7.2.

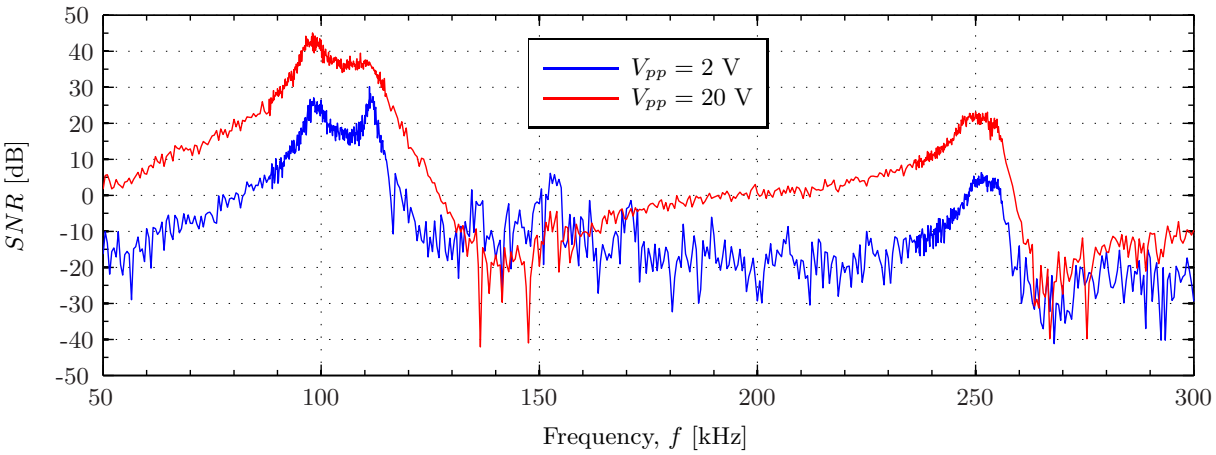


Figure 7.11: SNR for a measurement No. 4, where Element #16 transmits to Element #6 with a separation distance of 77 cm.

For the higher generator voltage an SNR exceeding 20 dB is seen for the approximate frequency range 80 kHz to 120 kHz around R1 and for frequencies at the peak of R2. Similar SNR levels are only observed for the lower generator voltage around the two peaks at R1. Outside resonances a low SNR is observed.

The maximum achieved SNR is nearly 45 dB, at the first peak in R1 for the higher generator voltage. The SNR of the measurement with the higher generator voltage exceeds that seen for the lower generator voltage, as expected. The exception is the frequencies bands around approximately 140 kHz and upwards of 260 kHz, where it seems that both generator voltages are insufficient to rise above the noise floor.

Rapid variations in the curve for the SNR are seen, even for the frequencies where a high SNR is measured, with differences as large as 5 dB. The principal reason for this is the variations in the measured noise. The noise measurements are performed in a separate measurement series from the signal measurements (see Section 3.3.7), and the noise is measured separately for each frequency. Slowly varying noise levels may therefore result in rapid variations as seen in Fig. 7.11. The limitations in the oscilloscope settings are challenging when the noise is measured, as the lowest vertical scaling used is 10 mV/div (see Section 3.3.5). This corresponds to a bit resolution of approximately 0.4 mV, while the typical peak to peak voltage of the noise do not exceed 5 mV. Hence may some of the variations be due to the low bit resolution of the measured noise.

The time window chosen in the noise measurements may be more sensitive to electrical crosstalk than the calculation interval where the signal voltage is extracted (see Section 3.7), and thus be a source of error. It is seen from the measured noise that electrical crosstalk has most impact on the calculated SNR at the frequencies corresponding to the second peak at R1 and for the higher generator voltage. In Fig. 7.11 this causes the second peak at R1 to nearly disappear in the curve for $V_{pp}$ = 20 V. It can be shown that the second peak in R1 corresponds to the peak in the receiving voltage sensitivity, when no corrections are applied.

The effect of electrical crosstalk is assumed to be significantly reduced in the time window where the signal is extracted, compared to the time window where the noise is measured, but this is not investigated.

### 7.2.3 Generator voltage

Fig. 7.12 shows $H_{1m5m}^{VV}$ in measurement No. 1, obtained with the FFT method and two different generator voltages.

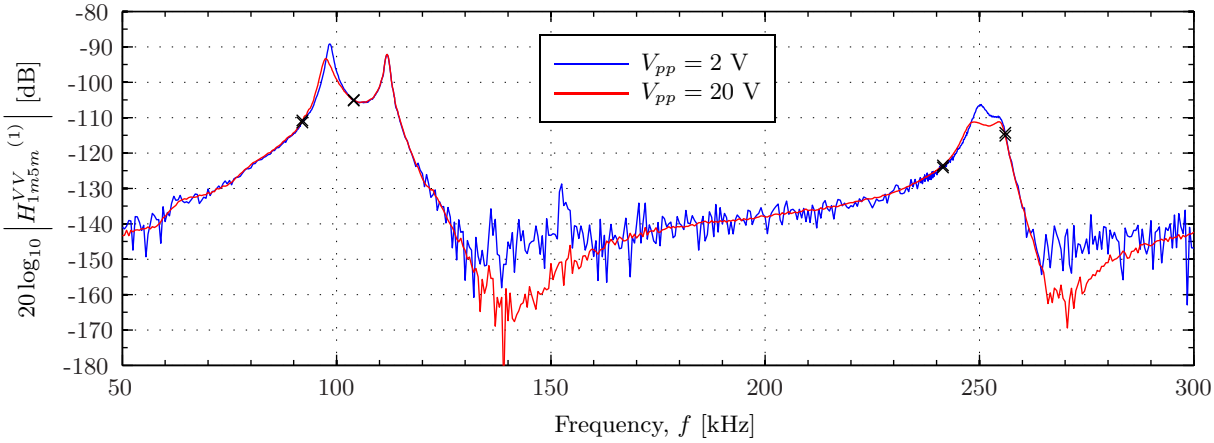


Figure 7.12: Measured voltage to voltage transfer function for measurement No. 1. Obtained with two different generator voltages. In the following, measurements with the two different generator voltages are combined using the frequencies shown with the symbol '×' as limits.

Nonlinear effects are observed in the region around the first peak in R1 and both peaks in R2, when the measurements with a generator voltage of $V_{pp}$ = 20 V is compared to the $V_{pp}$ = 2 V measurements. The magnitudes are reduced and peak frequencies are moved downwards. Note that nonlinear effects on the second peak in R1 are seen to be negligible. This is due to the fact that this peak in $H_{15}^{VV}$ is caused by a peak in sensitivity of the receiving transducer, and not a peak in the transmitting voltage response of the transmitting transducer. The pressure generated by the transmitter are therefore lower in the first peak at R1 than in the second peak at R1. Both the medium and the piezoelectric element may contribute to the nonlinear behaviour. This is discussed further in Section 8.1.3, where similar effects are seen for the piezoelectric transducers. Note that nonlinear behaviour of Pz27 is observed at drive voltages lower than $V_{pp}$ = 2 V in electrical measurements (see Section 3.2). It may therefore also be present in the acoustical measurements at the lower generator voltage, but probably to a small extent.

Outside resonance the nonlinear effects appears to be negligible when comparing the curves for the two different generator voltages, while the advantages of the increased SNR for $V_{pp}$ = 20 V becomes apparent. Because of this a combination of measurements using the two different generator voltages are presented in the following. The chosen frequency limits between the different generator voltages are given in Table 7.3 and shown in the figures using the symbol '×'. These frequencies are denoted demarcation frequencies.

Table 7.3: Demarcation frequencies used when combining measurements with different open-circuit generator voltages.

| Frequency range | | | Open-circuit generator voltage |
|---|---|---|---|
| 50 kHz | - | 92 kHz | $V_{pp}$ = 20 V |
| 92 kHz | - | 104 kHz | $V_{pp}$ = 2 V |
| 104 kHz | - | 241.5 kHz | $V_{pp}$ = 20 V |
| 241.5 kHz | - | 256 kHz | $V_{pp}$ = 2 V |
| 256 kHz | - | 300 kHz | $V_{pp}$ = 20 V |

### 7.2.4 Effect of corrections

In order to account for the lack of ideal measurement conditions correction factors (see Section 2.1.6) are applied to the measured voltage to voltage transfer functions $H_{1m5m}^{VV(1)}$, $H_{1m5m}^{VV(2)}$, and $H_{1m5m}^{VV(3)}$, obtained in measurement No. 1, No. 2 and No. 3, respectively. The resulting corrected transfer functions are in turn used in Eqs. (2.13) to (2.15) and (2.17) to (2.19) to determine the magnitude of $S_V$ and $M_V$ for Element #6, Element #10 and Element #16.

The absorption in air is corrected for by use of $C_\alpha$, which is calculated using the MATLAB-script `absorpsjonluft` (see Appendix A.3), implemented by Knappskog [37]. The coaxial cables connecting the transmitting transducer and the recording oscilloscope are described by the voltage to voltage transfer function for the transmitting electronics, $H^{VV}_{1m1}$, calculated in the MATLAB-script `correctionTransmittingElectronics` (see Appendix A.3). The effects of the cable connecting the receiving transducer to the measurement amplifier and the finite impedance of the measurement amplifier are modelled by the voltage to voltage transfer function for the receiving electronics, $H^{VV}_{5m5}$. It is calculated in the MATLAB-script `correctionReceivingElectronics` (see Appendix A.3). Near-field effects are sought corrected for by $C_{dif}$, where Khimunin's diffraction correction are used. Khimunin's diffraction correction is calculated using `Khimunin_diffractioncorrection` (see Appendix A.3), implemented by Storheim [49].

In this section the effects of each of the corrections are shown. The transmitting voltage response of Element #16, $S^{T3}_V$ is used as an example, calculated by Eq. 2.23. The correction effects shown in the figures describe the effective impact of the correction factor on the calculated $S^{T3}_V$. $S^{T3}_V$ calculated with all corrections is in the figures compared to $S^{T3}_V$ calculated with all corrections except the correction factor studied.

Fig. 7.13 shows the effect of the correction for absorption on $S^{T3}_V$. An ambient pressure of 1 bar is used when $C_\alpha$ is computed. As expected, it is seen that the effect of absorption on the calculated $S^{T3}_V$ increases with the frequency, approaching a maximum 6 dB at 300 kHz. The absorption correction depends on the separation distance, which is approximately 77 cm for the measurements performed in this calibration.

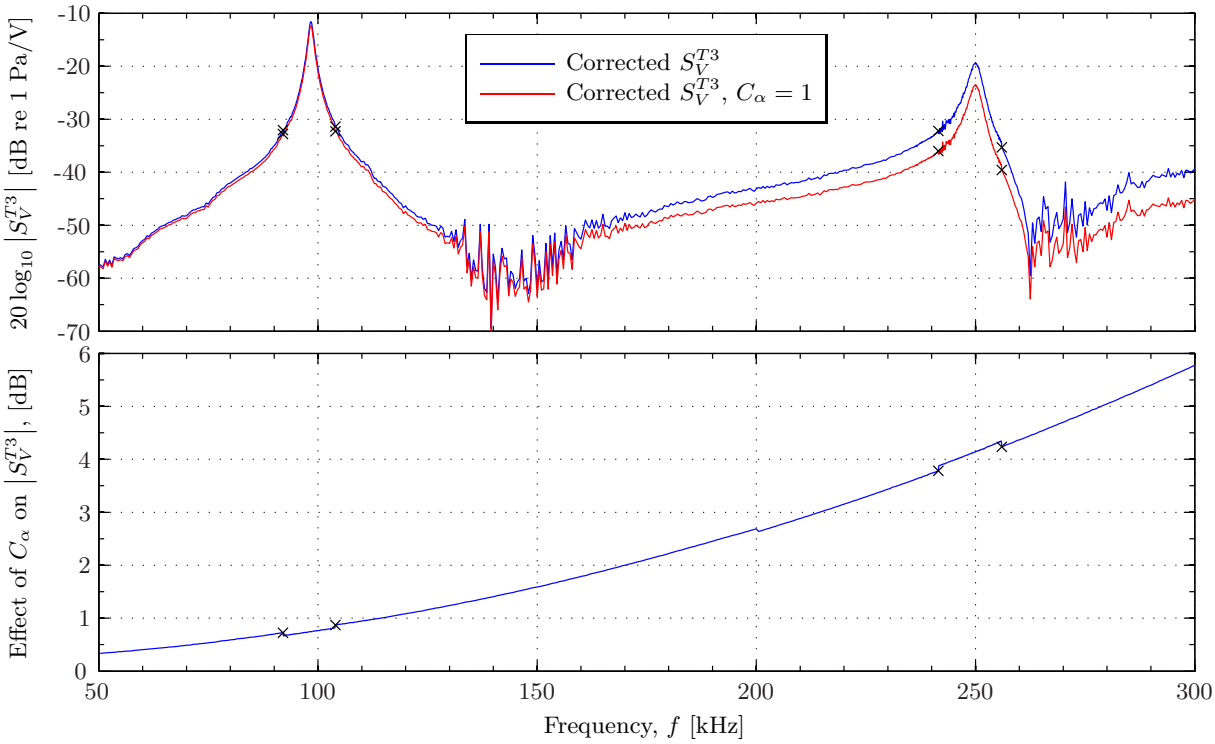


Figure 7.13: Transmitting voltage response of Element #16. $S^{T3}_V$ calculated with all corrections compared to $S^{T3}_V$ calculated with all correction and $C_\alpha = 1$. The difference observed between these two calculations is shown in the lower plot. The demarcations between the use of $V_{pp} = 20$ V and $V_{pp} = 2$ V open-circuit generator voltage are shown using the symbol '×'.

In Fig. 7.14 the effect of the receiving electronics transfer function is shown. The effect of $H^{VV}_{5m5}$ is seen as an overall level increase, with resonances centred at approximately 113 kHz and 256 kHz. These frequencies closely correspond to the second peaks at R1 and R2 for the measured $H^{VV}_{1m5m}$ (e.g. Fig. 7.12). The use of $H^{VV}_{5m5}$ thus shift the peaks to higher frequencies. It can seen that theses peaks are caused by the maximums of $M_V$ for the receiving transducers. The effect is larger at R1 than at R2, with a maximum magnitude approaching 8 dB. Theoretical analysis and measurements have shown that the behaviour of $H^{VV}_{5m5}$ is dominated by the coaxial cable connecting the receiving transducer to the measurement amplifier, not the finite impedance of the measurement amplifier.

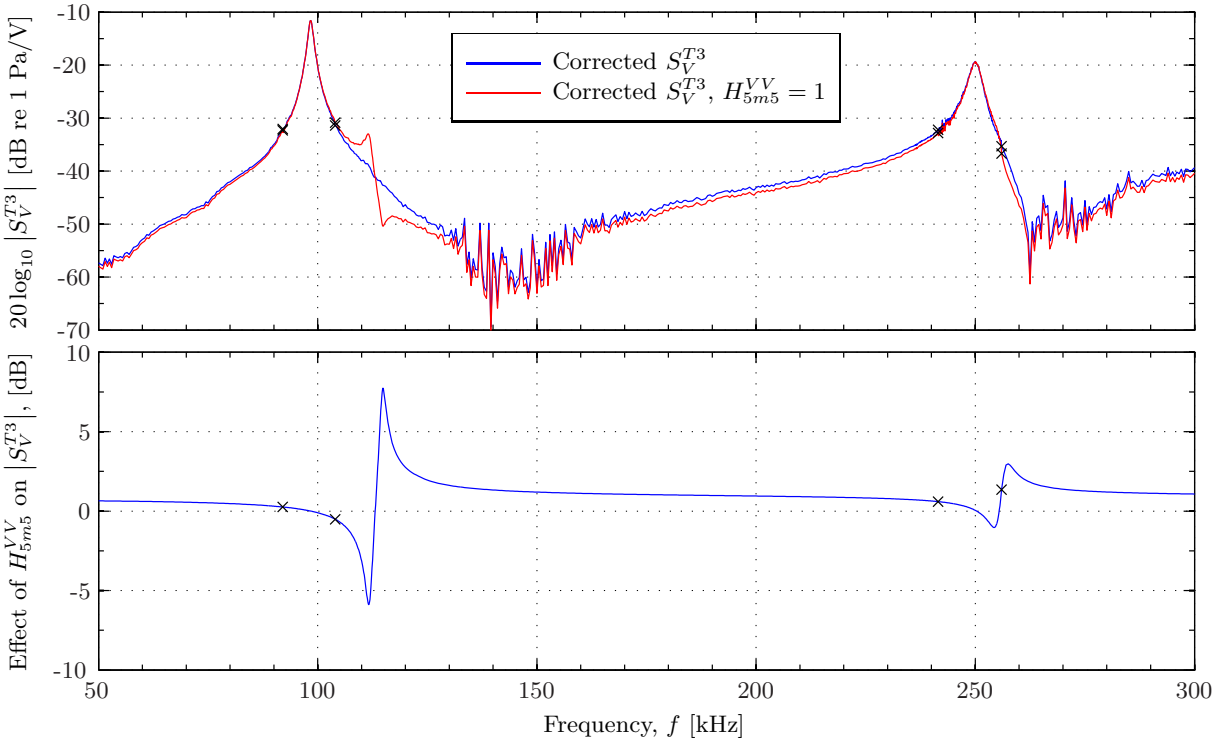


Figure 7.14: As Fig. 7.13, but for the voltage to voltage transfer function accounting for receiving electronics, $H_{5m5}^{VV}$.

The effect of the transmitting electronics, i.e. the coaxial cable connecting the transmitting transducer and the recording oscilloscope, is shown in Fig. 7.15.

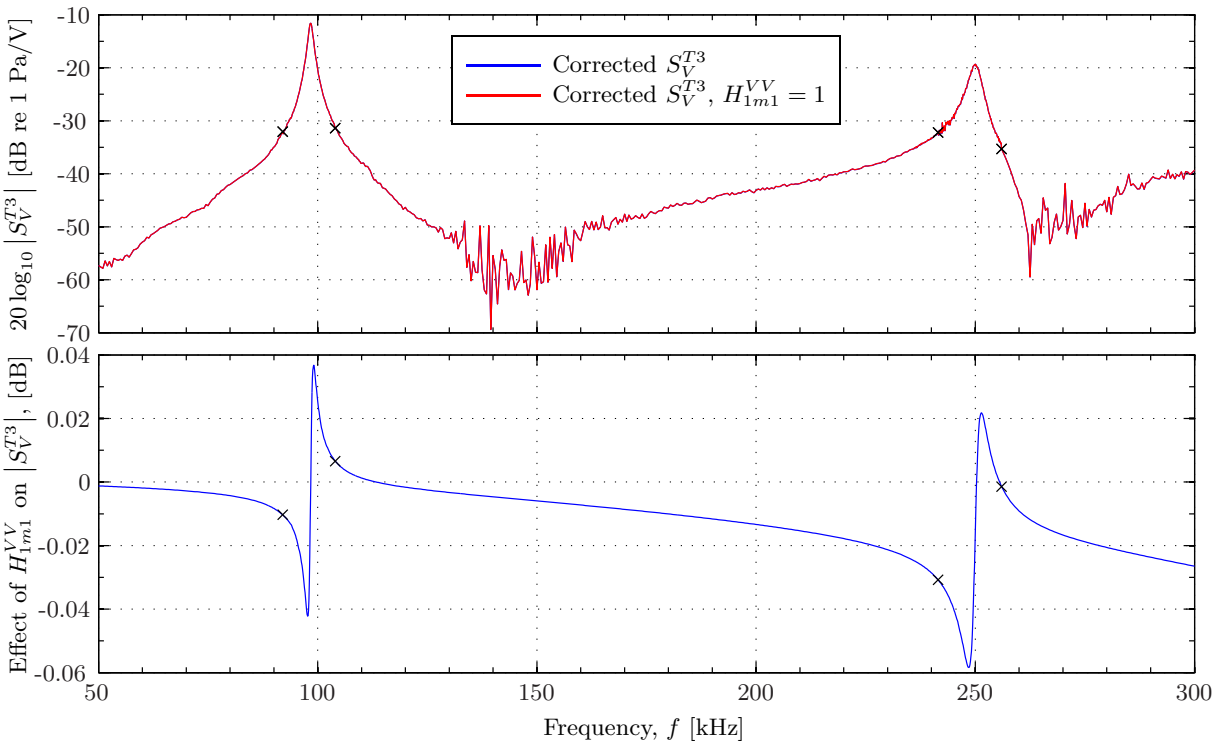


Figure 7.15: As Fig. 7.13, but for the voltage to voltage transfer function accounting for transmitting electronics, $H_{1m1}^{VV}$.

From the figure it is seen that the effect of $H_{1m1}^{VV}$ is small for all frequencies, thus indicating that the effect of the cable connecting the transmitting transducer to the oscilloscope is negligible. Resonances

in $H_{1m1}^{VV}$ are observed at the peaks of $S_V^{T3}$ at R1 and R2, as expected since the correction concerns the transmitting transducer. The effect is never larger than 0.06 dB.

The effect of $C_{dif}$, which corrects for the lack of far-field conditions by use of diffraction correction, is shown in Fig. 7.16.

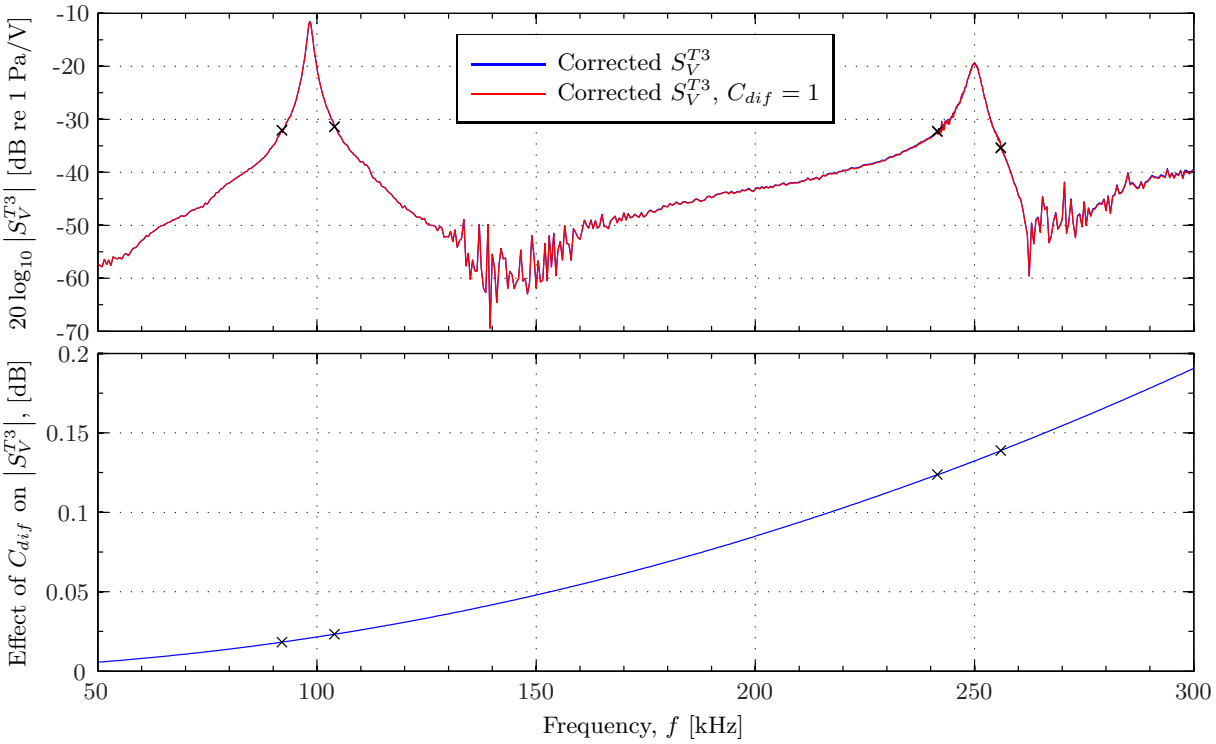


Figure 7.16: As Fig. 7.13, but for the correction for diffraction correction and near-field effects, $C_{dif}$.

For the current separation distance and transducer size the effect of $C_{dif}$ never exceeds 0.2 dB in the calculation of the magnitude of $S_V^{T3}$. The effect increase steadily with the frequency. A slightly more varying frequency behaviour is expected in real measurements, due to the different resonances in the piezoelectric disk.

For the current measurement distance and instrumentation, it is seen that the effects of $C_{dif}$ and $H_{1m1}^{VV}$ are small compared to the effects of $C_\alpha$ and $H_{5m5}^{VV}$. The significance of $C_\alpha$ compared to the other corrections increases at higher frequencies, while the effect of $H_{5m5}^{VV}$ is dominant at a limited frequency range at R1. In general it is seen that the corrections are smallest at the lower frequencies, as expected.

For a shorter separation distance the effects of $C_{dif}$ and $C_\alpha$ would increase, while $H_{5m5}^{VV}$ and $H_{1m1}^{VV}$ would remain unchanged. Figs. 7.17 and 7.18 show the the magnitude (multiplied by $z$) and phase of the axial pressure, $p_{ax}$, for Element #16, calculated in FEMP 5.0. Shown for the peak of R1 at 98.2 kHz and the peak of R2 at 249.2 kHz, respectively. From these plots an estimate can be made for where the far-field is reached, based on the desired level of accuracy for the magnitude and/or phase. At a distance of 50 cm the differences in magnitude (multiplied by $z$) are 0.25 dB and 0.30 dB, and the phase differences are 8° and 25°, for the peaks at R1 and R2, respectively. Note that these figures show the axial pressure, not the pressure measured by a finite receiver, and thus are the deviations larger in a real measurement situation.

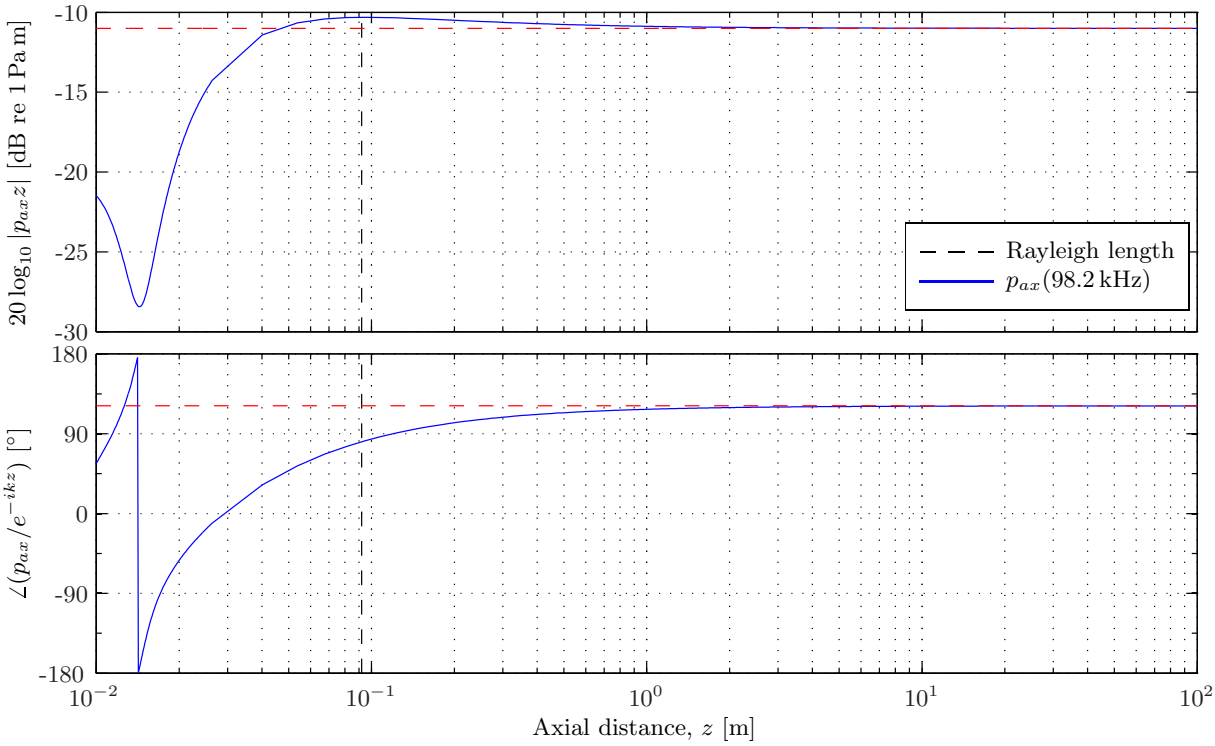


Figure 7.17: The magnitude and phase of $p_{ax}$ for Element #16 radiating at the peak frequency of R1, $f$ = 98.2 kHz. Simulated in FEMP 5.0. The Rayleigh length of 9.2 cm is shown, as well as the far-field values to which the magnitude (multiplied by $z$) and phase converge.

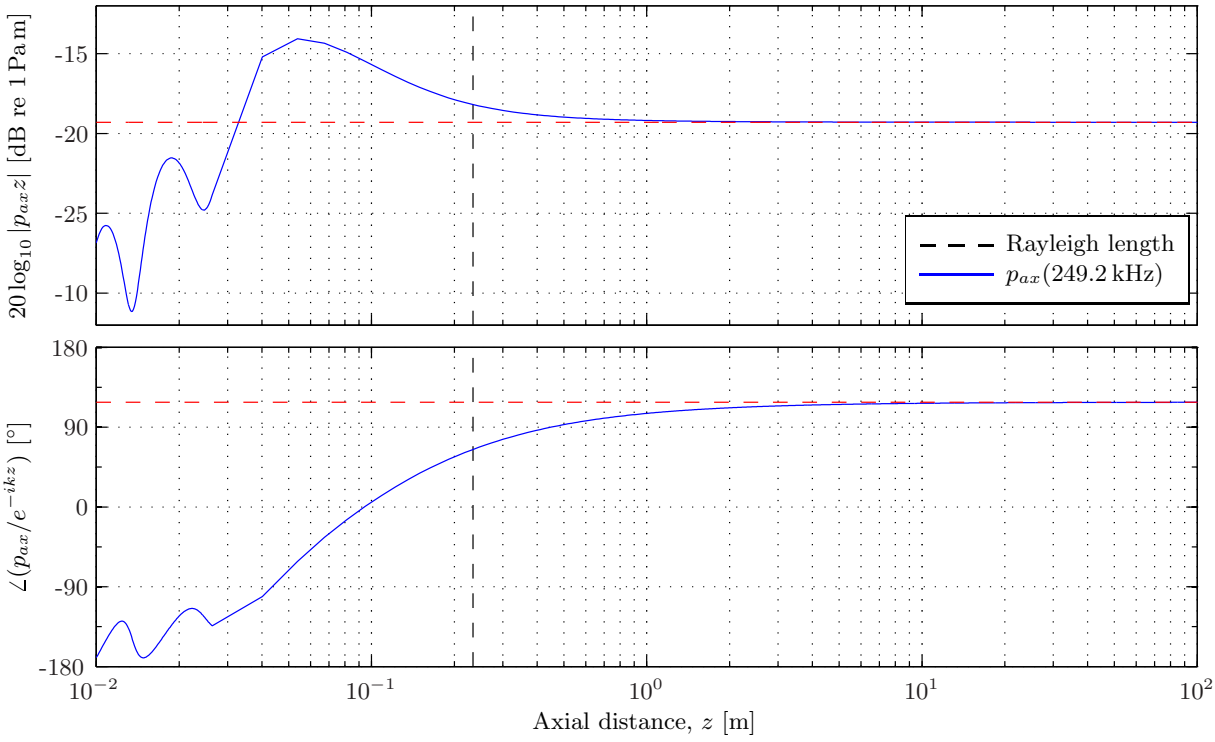


Figure 7.18: As Fig. 7.17, but for the peak frequency of R2 in the simulation, $f$ = 249.2 kHz, with $r_R$ = 18.8 cm.

### 7.2.5 Reciprocity check

The reciprocity of a system consisting of two reversible transducers, the medium and boundaries can be investigated by performing two measurements with the transmitting and receiving transducers inter-

changed (see Section 2.5). If Eq. (2.70) is fulfilled, i.e. the two graphs in Fig. 7.19 coincide, the system is reciprocal [55]. The reciprocity check performed here does not strictly follow this method, as the transmitter and receiver were physically interchanged between the two measurements. Thus altering the boundaries and requiring an additional aligning of the elements. This is, however, the process used in the measurements in Table 7.2. The correction factors (see Section 2.1.6) are applied to the measurements.

The reciprocity check is shown in Fig. 7.19, where measurement No. 2 and measurement No. 4 in Table 7.2 are used.

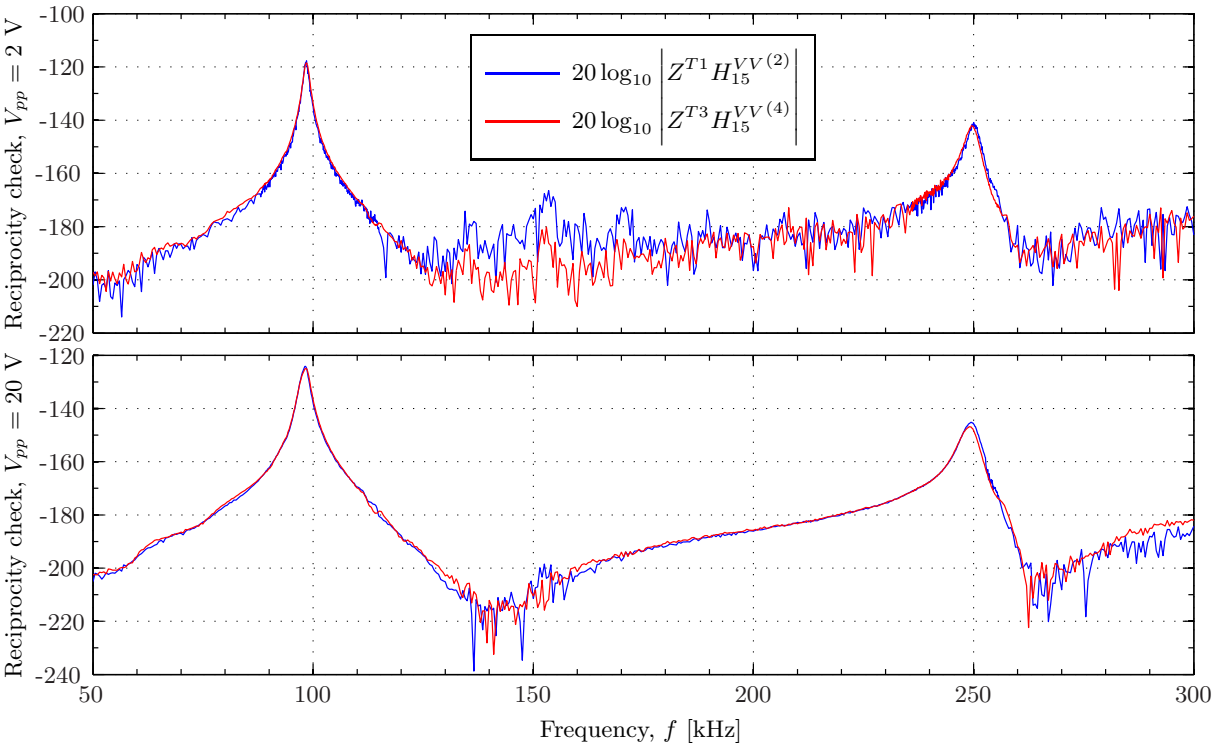


Figure 7.19: Reciprocity check of a the transducer pair Element #6 and Element #16. Showing the electrical transfer impedances of two measurements performed with the transducers interchanged (See Eq. (2.70)). The upper plot is for measurements with an open-circuit generator voltage of $V_{pp} = 2$ V, while $V_{pp} = 20$ V is used in the lower plot.

For the higher generator voltage a deviation of approximately 1 dB and 0.3 kHz is observed for the peak at R1. For the frequency range up to 127 kHz the deviation do not exceeds approximately 2 dB, with deviations below 1 dB for the larger part. The exception is the frequencies around 114 kHz where slightly larger deviations are seen, corresponding to the peak of $M_V$ at R1. For the frequency range 171 kHz to 246 kHz the deviation is less than 1 dB. Outside the stated frequency ranges larger deviations are seen due to insufficient SNR (see Fig. 7.11).

For the lower generator voltage the best agreement is found in the frequency ranges 74 kHz to 113 kHz and 244 kHz to 251 kHz, where the deviations are less than approximately 3 dB and 4 dB, respectively.

This analysis describes the reciprocity of the system, but not necessarily the reciprocity of each transducer [55]. As similar elements are used, they might be equally nonlinear and thus show good agreement in Fig. 7.19. The nonlinear behaviour of the elements at the resonances for the higher generator voltage are seen e.g. in Fig. 7.12, and the observed agreement at the peaks in the lower plot in Fig. 7.19 are therefore not valid.

### 7.2.6 Measurement results and comparison with FE simulations

Results for $S_V$ and $M_V$ are obtained for all three transducers, i.e. Element #6, Element #10 and Element #16. Element #16 is assumed to be reciprocal in all calculations. Element #10 it is assumed to be reciprocal in the calculation of its $S_V$. Similarly, Element #6 is assumed to be reciprocal to calculate its $M_V$. The results from the modified three-transducer reciprocity calibration method are compared to FE simulations. In the simulations, $M_V$ is determined from the simulated $S_V$ and $Z_T$, using Eq. (2.4). The results are obtained by the FFT method (see Section 7.2.1) and are shown for a combination of

generator voltages (see Section 7.2.3). Mainly $S_V$ is discussed in the following, as similar results are seen for both $S_V$ and $M_V$.

In Fig. 7.20 the measured values of $S_V$ and $M_V$ for the three elements are compared.

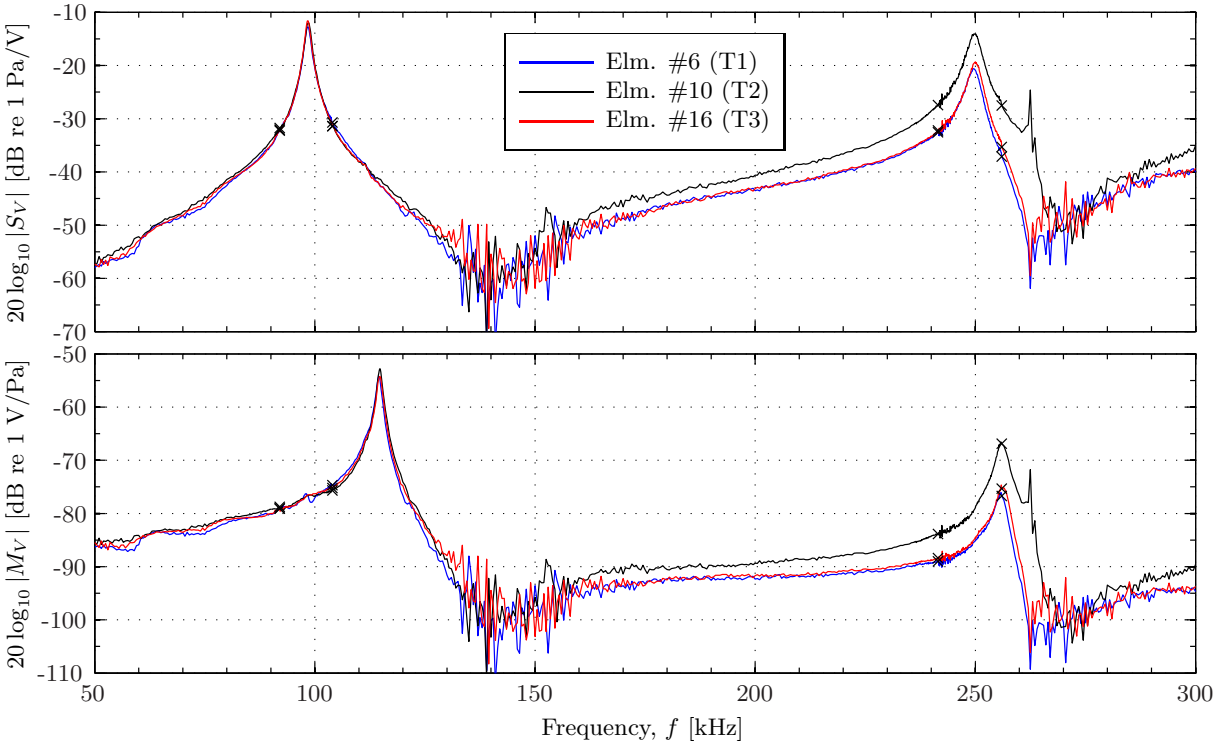


Figure 7.20: Comparison of $S_V$ and $M_V$ for Element #6, Element #10, and Element #16, determined by the modified three-transducer reciprocity calibration method.

An agreement of within 1 dB is seen for $S_V$ for frequencies up to approximately 114 kHz, except around the peak at R1 where the maximum deviation approaches 2 dB. The approximate frequencies for the peak at R1 are 98.4 kHz, 98.6 kHz and 98.4 kHz for Element #6, Element #10 and Element #16, respectively. The corresponding magnitudes are -11.6 dB, -12.0 dB and -12.8 dB. Upwards from approximately 114 kHz the difference between the elements increases, with lower magnitudes observed for Element #6 and Element #16 compared to Element #10. The former two elements agree well within 1 dB from the frequencies where they emerge from the noise to the peak at R2, before it increases to approximately 2 dB and then hits the noise floor at 262 kHz.

The behaviour of $M_V$ is similar to that of $S_V$ and is therefore not be covered in detail. The approximate frequencies of the peak at R1 are 114.5 kHz, 114.8 kHz and 114.8 kHz, with corresponding magnitudes of -54.2 dB, -52.8 dB and -54.2 dB, for Element #6, Element #10 and Element #16, respectively.

For both $S_V$ and $M_V$ an unexpected peak appears at 262.5 kHz for Element #10. A significant dip is seen at the same frequency for Element #6 and Element #16, and investigations show that it is caused by the very low SNR of less than -20 dB (see Fig. 7.11).

The noted magnitude difference between Element #10 to the other two elements for higher frequencies can be traced back to the measured voltage to voltage transfer functions. Examination of these show that a significantly higher magnitude (approximately 6 dB at the peak in R2) is seen for measurement No. 2 compared to measurement No. 1 and measurement No. 3. It is the combination of these three voltage to voltage transfer functions in Eqs. (2.13) to (2.15) and (2.17) to (2.19) that yield the difference seen in Fig. 7.20.

One possible reason for the deviation at higher frequencies is challenges connected to the correct alignment of the transducers (see Section 3.3.3). In brief, an approximate alignment is initially achieved manually, aided by a self levelling laser cross level. Adjustments are then performed, where acoustic measurements are used to determine if the two transducers are aligned coaxially. For the frequencies currently used in the acoustical part of the positioning, it is seen that the spatial differences in the sound field may be small compared to the temporal variations in the recorded voltage, i.e. a relatively wide main lobe. Thus limiting the accuracy of the alignment. Another limiting factor is the initial manual alignment, where the front surface of the transducers must be positioned parallel to each other and to the plane of the computer-controlled linear stages in order to fully utilize the acoustical adjustments.

It can be shown that the width of the main lobe of the transducer decreases at higher frequencies, and it is therefore likely that the alignment primarily effect the measured $H_{1m5m}^{VV}$ at higher frequencies. It is assumed that the deviations between the transfer function obtained through measurement No. 2 compared to measurement No. 1 and measurement No. 3 are mainly caused by differences in the alignment of the transmitting and receiving transducers.

Figs. 7.21, 7.22 and 7.23 show $S_V$ and $M_V$ for Element #6, Element #10 and Element #16, respectively.

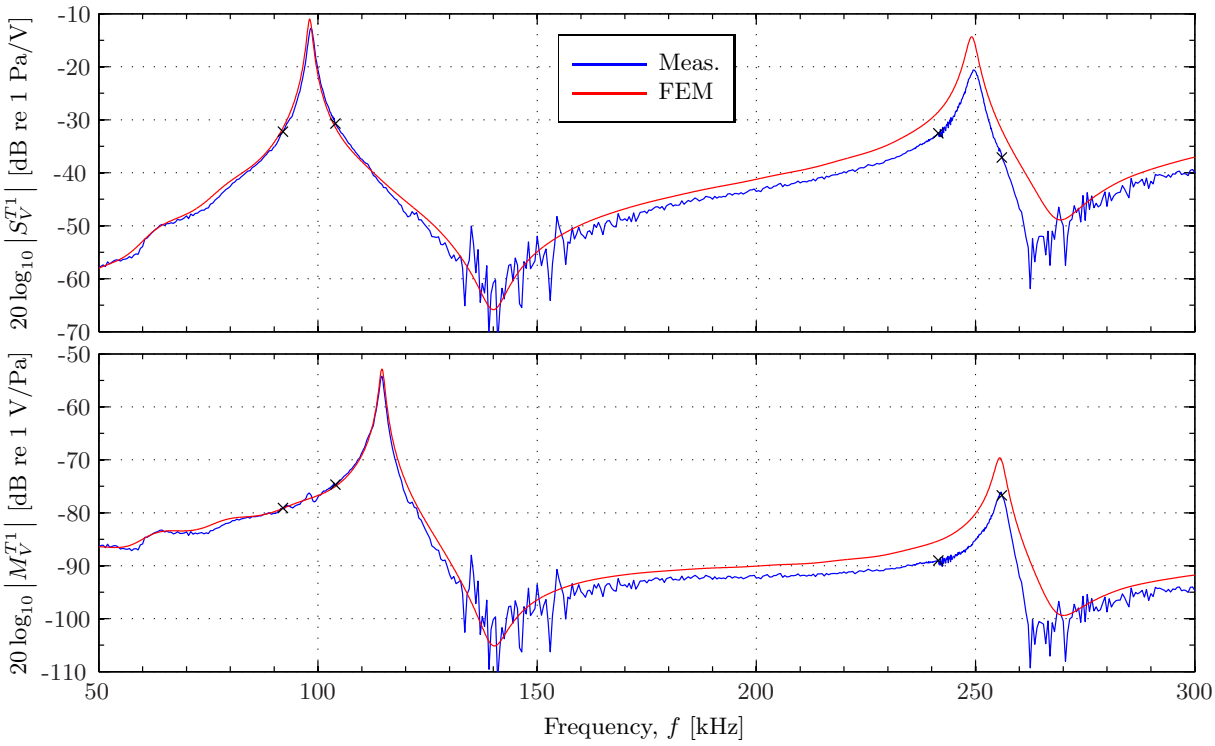


Figure 7.21: Transmitting voltage response and free-field open-circuit receiving voltage sensitivity for Element #6, obtained through the modified three-tranducer reciprocity calibration and compared to FE simulations of Element #6.

Separate simulations are performed for each element using the dimensions given in Table 7.1. Only small differences between the simulations are seen. For instance are the magnitude of the peak at R1 approximately -11.0 dB for all simulations, and the frequencies are 98.2 kHz for Element #10 and Element #16, and 98.1 kHz for element #6. Comparison with the measured values for the peak at R1 stated show that the simulated values are up to 1.8 dB higher and occur at frequencies up to 0.4 kHz below those determined experimentally.

Best agreement is observed in the lower frequency range up to and including R1. Smallest differences are seen for Element #10, with deviations below 0.5 dB for the frequency ranges 60 kHz to 92 kHz and 103 kHz to 126 kHz, increasing to above 2 dB around the peak at R1 (92 kHz to 103 kHz). Similar behaviour is seen for the other two elements, but with slightly increased deviations outside the peak in R1.

Some undulations are observed in the FE simulations for the frequencies below R1, as described by [1]. It is seen in Figs. 7.21, 7.22, and 7.23 that these undulations also are present in the experimental results.

For frequencies upwards from the dip at approximately 140 kHz the simulated values lie below Element #10 and above Element #6 and Element #16. Best agreement is seen for Element #10, except for at the peak at 262.5 kHz which is explained above. This strengthen the assumption stated above about the presumably better alignment in measurement No. 2. Considering Element #10, it is seen that the peak in the measured $S_V$ at R2 is at 249.8 kHz with a level of -14.1 dB, compared to -14.3 dB at 249.3 kHz. The agreement is worse for higher frequencies, e.g. the peak at R2 for $M_V$, due to the decreased SNR (see Fig. 7.11). For the frequencies between the dip at approximately 140 kHz and the peak in $S_V$ at R2, the deviation between measurements and simulations are in the range of 1 dB.

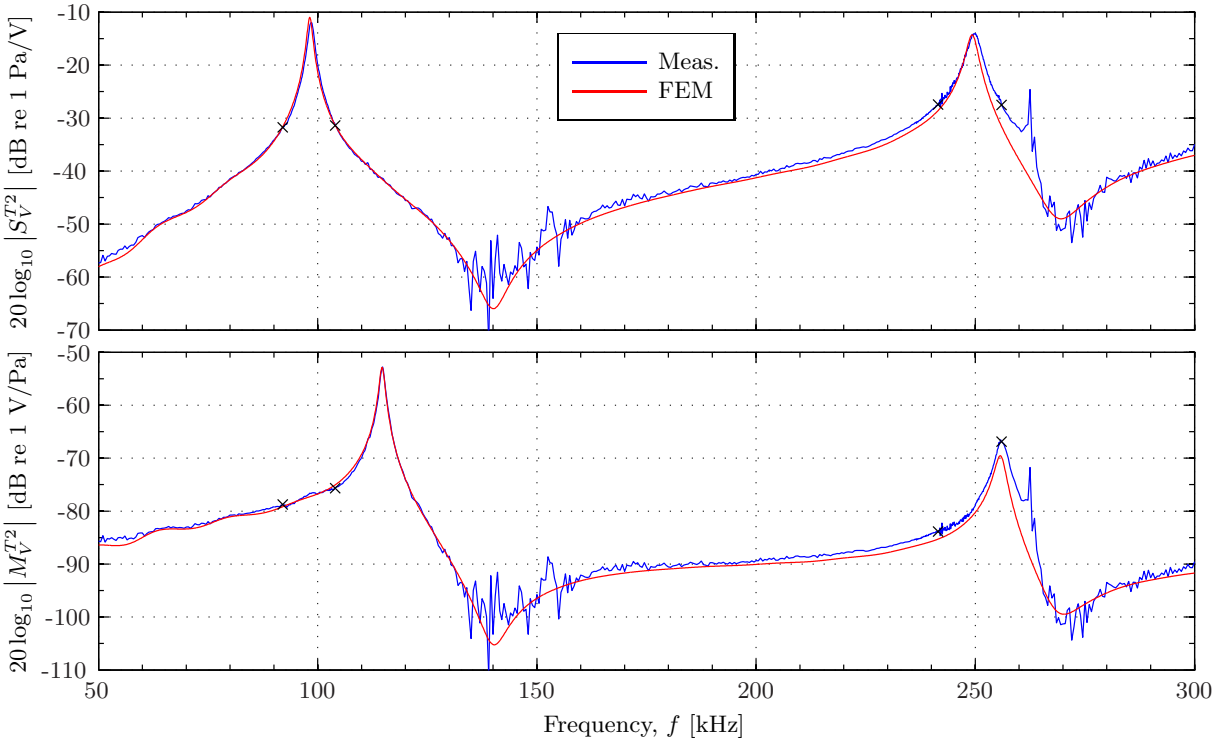


Figure 7.22: As Fig. 7.21, but for Element #10.

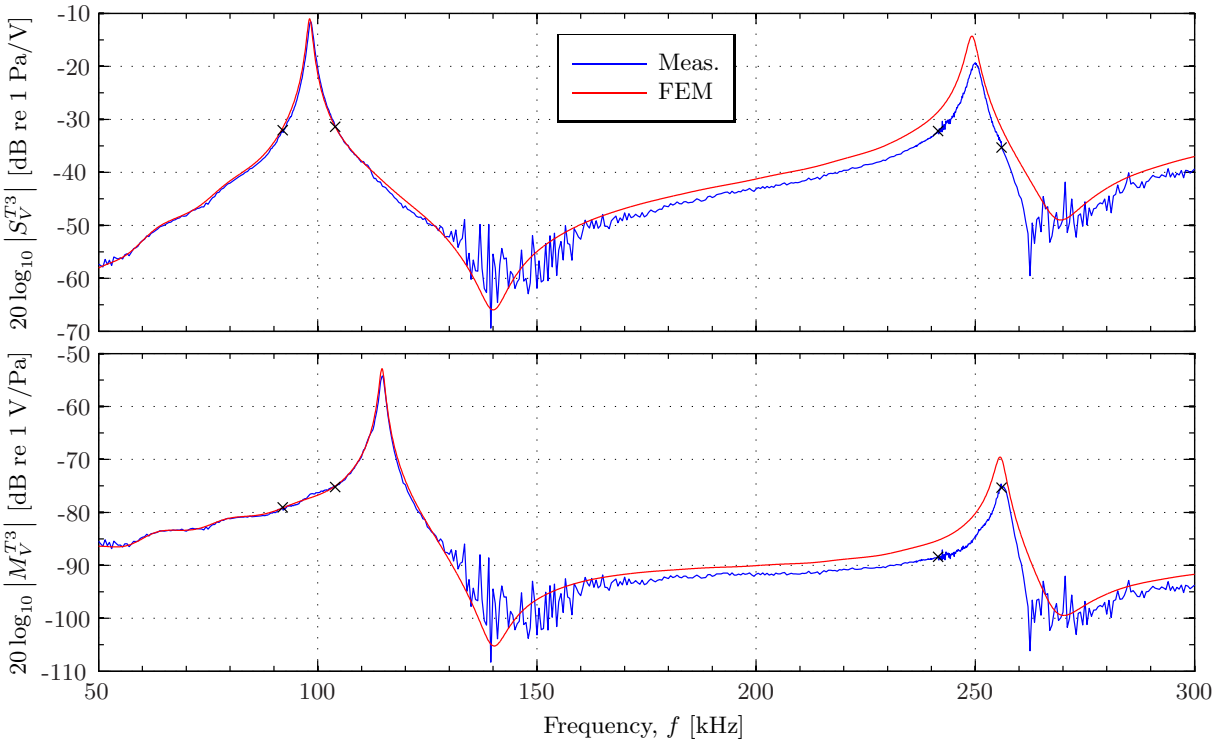


Figure 7.23: As Fig. 7.21, but for Element #16.

Note that the adjusted material parameters of Pz27 are used in the FE simulations. As described in Section 4.4, this data set may not represent the actual material parameters. The adjustment have been performed to provide better agreement with experimental results for circular disks of certain dimensions and from a certain batch [37]. Other geometries, dimensions and batches may not be described equally well.

It is assumed that the uncertainties in the material data available is the largest cause of error in

the FE simulations. There is, however, e.g. the effects of the soldered-on wires used to suspend the piezoelectric disks that must be taken into account (see Section 7.1). Other factors, such as the assumed axial symmetry of the structure modelled, the use of steady-state solutions, and the chosen number of elements per wavelength (5), are assumed to be of less importance for the problems studied.

## 7.3 Two-transducer calibration

The modified three-transducer reciprocity calibration method (see Section 2.6) is used to obtain $S_V$ and $M_V$ for Element #16. The method is performed for measurement No. 2 and measurement No.3 in Table 7.2 and compared to the results from the three-transducer reciprocity calibration method, shown in Fig. 7.24. The impedance of Element #16 is used in the calculations of the Two-transducer reciprocity calibration method.

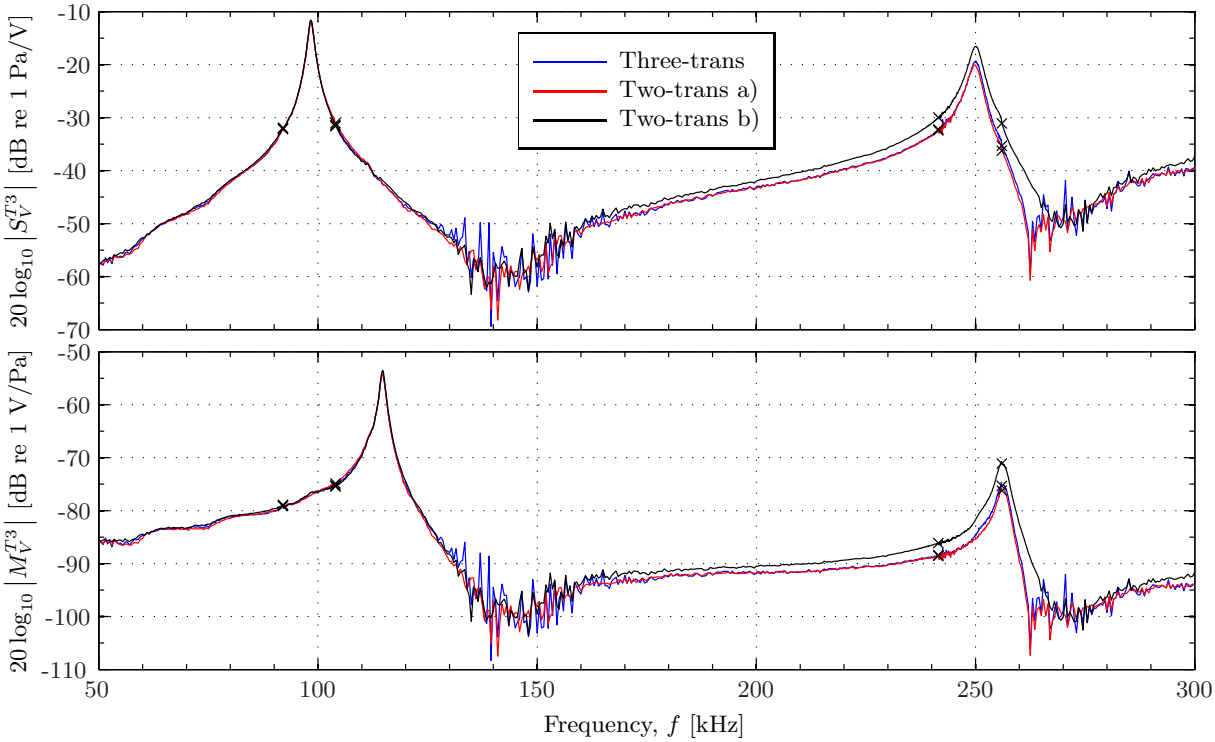


Figure 7.24: The results for $S_V$ and $M_V$ for Element #16, obtained using the modified three-transducer reciprocity calibration method and the modified two-transducer reciprocity calibration method. Two-trans a) is the result for measurement No. 2, and Two-trans b) is the result for measurement No. 3.

An agreement within 1 dB in the frequency range 60 kHz to 120 kHz is observed. Larger deviations are seen at higher frequencies for the values calculated from measurement No. 3 by use of the modified two-transducer reciprocity calibration method. The method seems to be a good predictor of the results from the modified three-transducer reciprocity calibration method for similar disks such as Element #6, Element #10 and Element #16.

## 7.4 Measurement with a calibrated microphone

Measurements with calibrated microphones are used to obtain $S_V$ for Element #6, Element #10 and Element #16 (see Section 2.7) and compared to the results from the modified three-transducer reciprocity calibration method. The calibrated microphones are the two microphone systems from Brüel & Kjære described in Section 3.5. The performed measurements are listed in Table 7.4. Microphone system No. 1 is denoted 'B&K 4138 + B&K 2633' and microphone system No. 2 is denoted 'B&K 4138-A-015' in the following. A representative SNR for the measurements is shown in Section 7.4.1, and the results from the measurements are presented in Section 7.4.2.

Table 7.4: Measurements on Pz27 piezoelectric ceramic disks with calibrated microphones.

| Measurement parameters | | | |
|---|---|---|---|
| Transmitter | Receiver | Meas. distance | Burst length |
| T2 = Element #10 | B&K 4138 + B&K 2633 | 44 cm | 1.0 ms (~34 cm) |
| T1 = Element #6 | B&K 4138 + B&K 2633 | 44 cm | 1.0 ms (~34 cm) |
| T1 = Element #6 | B&K 4138-A-015 | 44 cm | 1.0 ms (~34 cm) |
| T3 = Element #16 | B&K 4138 + B&K 2633 | 44 cm | 1.0 ms (~34 cm) |
| T3 = Element #16 | B&K 4138-A-015 | 44 cm | 1.0 ms (~34 cm) |

### 7.4.1 SNR

The SNR for the measurement where Element #16 transmits to B&K 4138-A-015 is shown in Fig. 7.25. It is assumed to be representative for all microphone measurements listed in Table 7.4.

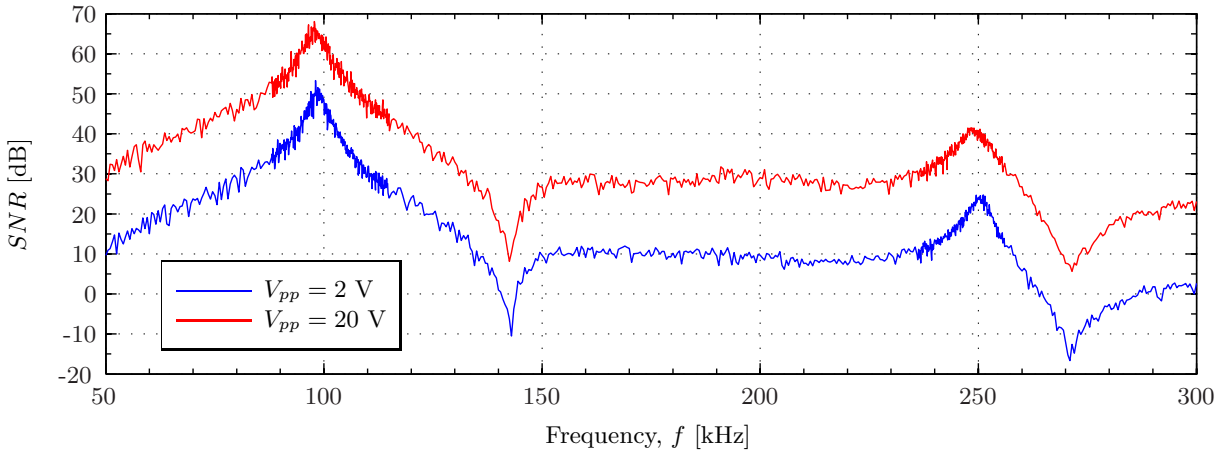


Figure 7.25: SNR for Element #16 transmitting to B&K 4138-A-015 with a separation distance of 44 cm. Measurements with open-circuit generator voltages of $V_{pp} = 2$ V and $V_{pp} = 20$ V are shown.

The to curves obtained with different generator voltages show similar behaviour, but with a the higher generator voltage yielding an SNR increased with 15 to 20 dB. For the higher drive voltage the SNR exceeds 20 dB for the whole frequency range, except at the dips just above 140 kHz and around 270 kHz. Similar levels are achieved for the lower generator voltage in the frequency range 65 kHz to 125 kHz and for a small frequency range centred at 250 kHz. A maximum approaching 70 dB is seen at approximately 98 kHz for the higher generator voltage.

The SNR is improved for the whole frequency range compared to that shown in Fig. 7.11 for measurements where elements are used both as transmitter and receiver. Note that the observed rapid variations in the calculated SNR, even at high SNR values, are also present in Fig. 7.11, and are discussed there.

### 7.4.2 Results

Results of $S_V$ from measurements using a calibrated microphone system is here compared to the results obtained by the modified three-transducer reciprocity calibration method. Element #10 have only been measured with B&K 4138 + B&K 2633, while Element #6 and Element #16 have been measured with both microphone systems.

Fig. 7.26 shows $S_V$ of Element #10, measured with the calibrated microphone system using two different generator voltages and compared to $S_V$ found by the modified method (Fig. 7.22).

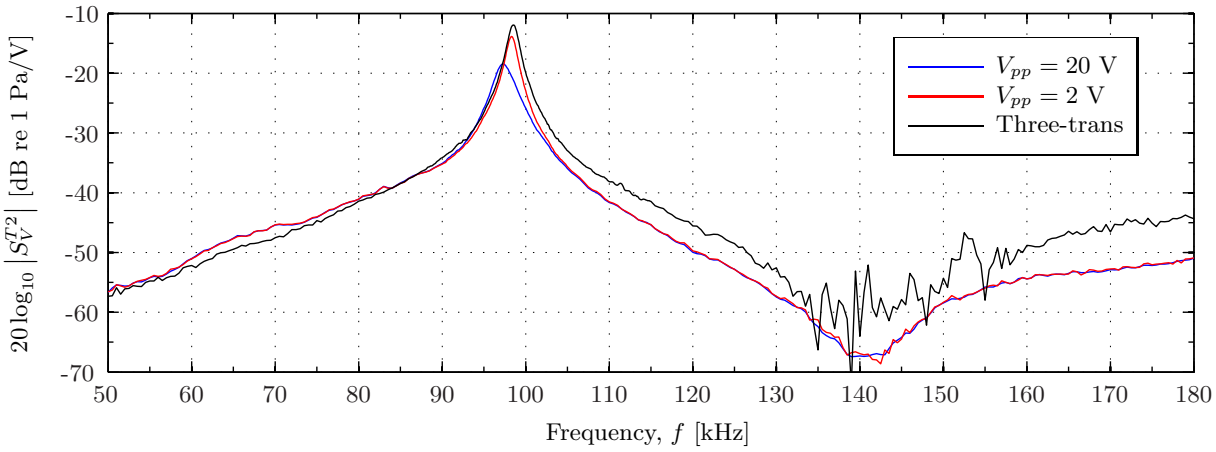


Figure 7.26: The transmitting voltage response of Element #10, obtained with measurement with B&K 4138 + B&K 2633. Two different open-circuit generator voltages are used. Compared to measurements using the modified three-transducer reciprocity calibration method.

When the two different generator voltages are compared, it is seen that nonlinear effects reduce the magnitude and lowers the frequency for the higher generator voltage, as expected. Outside resonance the two generator voltages coincide, and the effect of an increased SNR (see Fig. 7.25) is barely visible for the lower magnitudes. The lower generator voltage is therefore used in the following figures.

The results from the modified three-transducer reciprocity calibration method are higher than the microphone measurements for frequencies above the peak and somewhat lower beneath the peak. The peak in the microphone measurement is 0.2 kHz and 1.9 dB lower than the peak found by the modified method.

Figs. 7.27 and 7.28 show results for $S_V$ for Element #6 and Element #16, respectively.

An overall better agreement is seen for B&K 4138-A-015 and the modified method, than for B&K 4138 + B&K 2633, except for the frequencies below 80 kHz. For Element #6 the peak frequencies coincide at approximately 98.4 kHz, with magnitudes of -14.5 dB, -12.8 dB and -11 dB for B&K 4138 + B&K 2633, the modified method, and B&K 4138-A-015, respectively. Corresponding values for Element #16 are -13.3 dB, -11.6 dB and -10.2 dB. Here the peak is located at 98.2 kHz in the measurements with B&K 4138 + B&K 2633 and 98.4 kHz in the other two graphs.

The largest differences between the two microphone systems is seen in the dip after R1, where the SNR in the modified three-transducer reciprocity calibration measurements is insufficient for comparison. Although only measurements with $V_{pp} = 2$ V are presented, it can be shown that measurements with the two generator voltages agree as seen in Fig. 7.26. It is therefore assumed that the discrepancies are not caused by an insufficient SNR in the measurements.

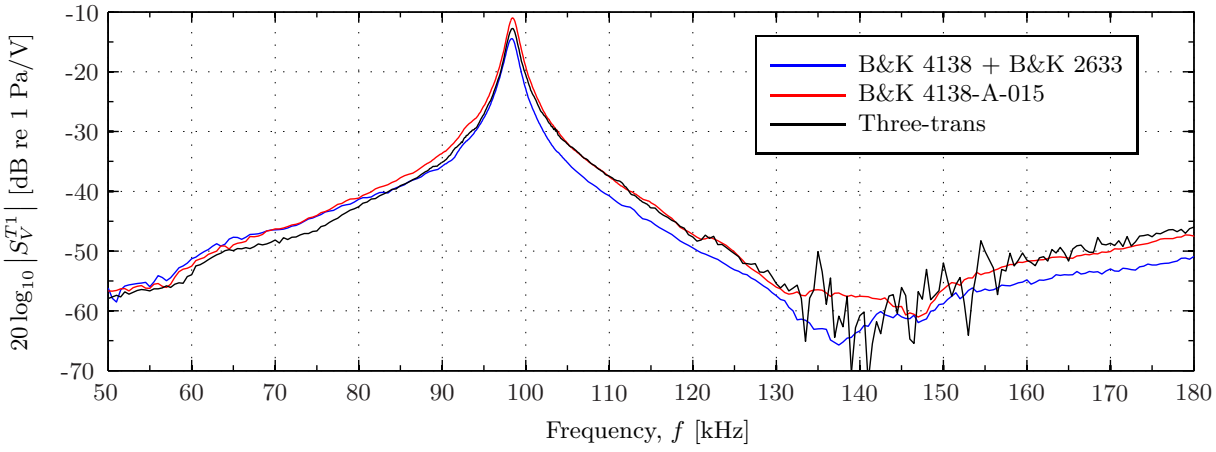


Figure 7.27: The transmitting voltage response of Element #6, obtained by measurements with an open-circuit generator voltage of $V_{pp} = 2$ V and the two different microphone systems. Compared to measurements using the modified three-transducer reciprocity calibration method.

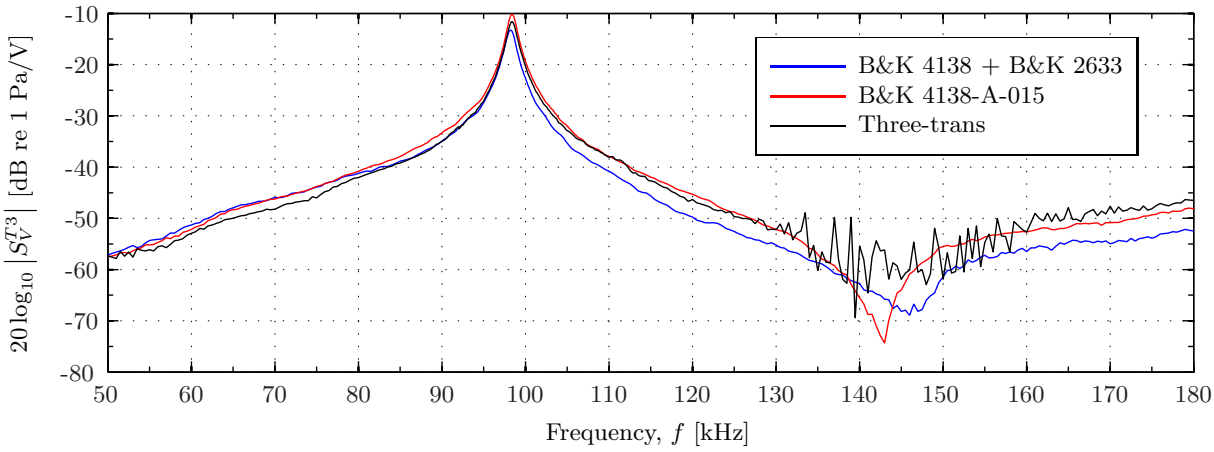


Figure 7.28: As Fig. 7.27, but for Element #16.

## 7.5 The modified method applied to the microphone systems

The modified three-transducer reciprocity calibration method is used to measure $M_V$ for the two microphone systems, using elements as the transducers T1 and T3. The measurements used to find $M_V$ for B&K 4138 + B&K 2633 are listed in Table 7.5. Note that the measurement (No. 2) deemed most trustworthy in Section 7.2.6 is used.

Table 7.5: Three-transducer reciprocity calibration of B&K 4138 + B&K 2633.

| Measurement parameters | | | | |
|---|---|---|---|---|
| Meas. No. | Transmitter | Receiver | Meas. distance | Burst length |
| 1 | T1 = Element #6 | T2 = B&K 4138 + B&K 2633 | 44 cm | 1.0 ms (~34 cm) |
| 2 | T1 = Element #6 | T3 = Element #16 | 77 cm | 1.4 ms (~48 cm) |
| 3 | T3 = Element #16 | T2 = B&K 4138 + B&K 2633 | 44 cm | 1.0 ms (~34 cm) |

Fig. 7.29 shows $M_V$ for B&K 4138 + B&K 2633, obtained through the three-transducer reciprocity calibration using an open-circuit generator voltage of both $V_{pp} = 2$ V and $V_{pp} = 20$ V. Compared to the calibration supplied by B&K (see Section 3.5). Only the frequency range up to 180 kHz has been measured with B&K 4138 + B&K 2633. The demarcation frequencies listed in Table 7.3 are used to merge the measurements with $V_{pp} = 2$ V and $V_{pp} = 20$ V open-circuit generator voltage.

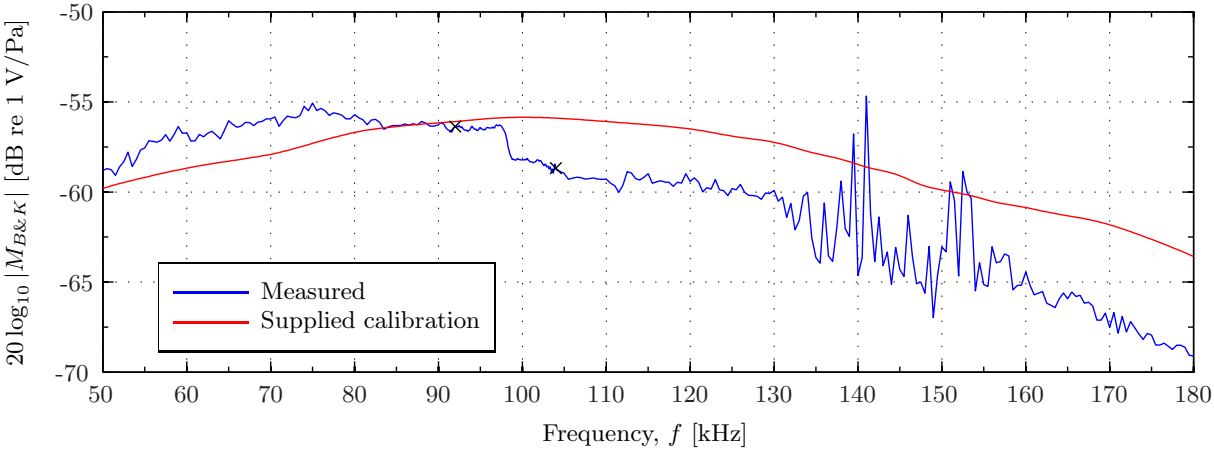


Figure 7.29: Free-field open-circuit receiving voltage response of B&K 4138 + B&K 2633. Comparison of results from the modified three-transducer reciprocity calibration method and calibration data supplied by B&K.

Agreement within 1 dB is seen for the frequency range 80 kHz to 98 kHz. Below these frequencies a higher sensitivity by about 2 dB is indicated by the calibration performed here. The opposite is true for higher frequencies, where the measured $M_V$ is around 2-3 dB lower up to 130 kHz. Then the SNR becomes too low to yield predictable results (see Figs. 7.11 and 7.25). A maximum deviation of approximately 7 dB is seen for the frequencies upwards from 130 kHz. A sudden drop is observed at approximately 98 kHz, close to the peak frequencies of the elements' $S_V$.

The measurements in the modified three-transducer reciprocity calibration method applied to B&K 4138-A-015 are listed in Table 7.6, and the results from the calibration are shown in Fig. 7.30 for the frequency range 50 kHz to 300 kHz. It is compared to the calibration supplied by B&K up to 200 kHz.

Table 7.6: Three-transducer reciprocity calibration of B&K 4138-A-015.

| Measurement parameters | | | | |
|---|---|---|---|---|
| Meas. No. | Transmitter | Receiver | Meas. distance | Burst length |
| 1 | T1 = Element #6 | T2 = B&K 4138-A-015 | 44 cm | 1.0 ms |
| 2 | T1 = Element #6 | T3 = Element #16 | 77 cm | 1.4 ms |
| 3 | T3 = Element #16 | T2 = B&K 4138-A-015 | 44 cm | 1.0 ms |

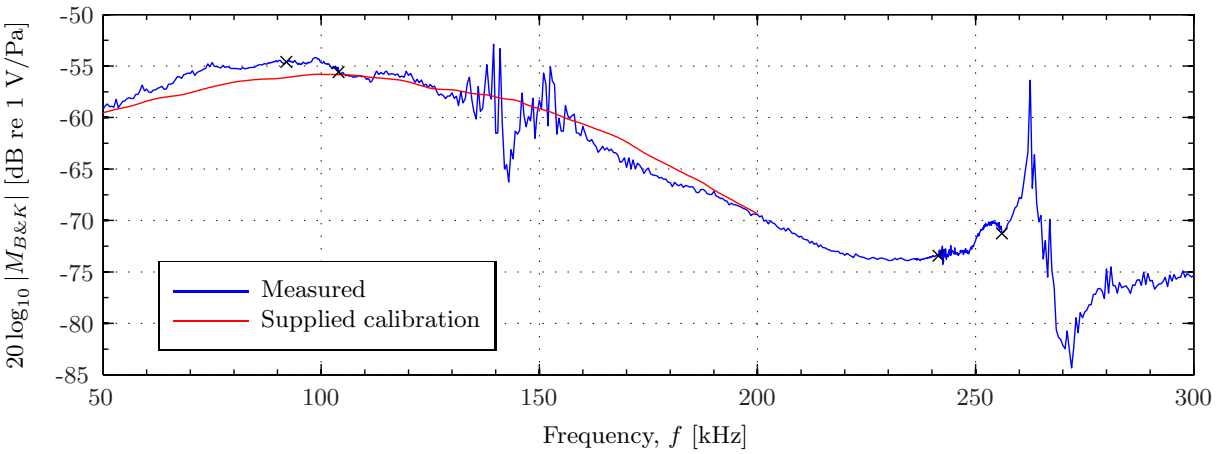


Figure 7.30: As Fig. 7.29, but for the microphone system B&K 4138-A-015. The calibration supplied by B&K only extends to 200 kHz.

Deviations are less than approximately 2 dB for frequencies below 102 kHz, less than 1 dB for the frequency range 102 kHz to 130 kHz, and less than 2 dB in the frequency range 158 kHz to 200 kHz. Between 130 kHz and 158 kHz, and for frequencies above 257 kHz, the low SNR becomes apparent (see Figs. 7.11 and 7.25).

When comparing the measured $M_V$ of the two microphone systems, a better agreement between the measurement and the supplied calibration for B&K 4138-A-015 than for B&K 4138 + B&K 2633. The former agrees within approximately 2 dB and the former within 3 dB, if the areas of very low SNR are omitted. Note that the supplied calibration of the microphone used in B&K 4138 + B&K 2633 was performed in 1995, while that in B&K 4138-A-015 where calibrated in 2012, and that this may explain some of the deviation. There are also uncertainties in the supplied calibrations, estimated to be below approximately ± 0.5 dB for B&K 4138-A-015 based on [80].

# Chapter 8

# Results - Piezoelectric transducers

Piezoelectric transducer are developed as part of this work, with the intent to improve the SNR in the measurements, increase the bandwidth and sensitivity of the transducers, and decrease the nonlinear effects. The first radial mode of the piezoelectric ceramic disks in the transducers is utilized. The development and construction of the transducers are covered in Chapter 6, where also electrical measurements on the complete transducer and its separate parts are shown and compared to FE simulations. The results from the acoustical measurements are presented and discussed in this chapter, closely following the framework of Chapter 7. The three-transducer reciprocity calibration of the three piezoelectric transducers are covered in Section 8.1, Section 8.2 presents results from measurements with the calibrated microphone system B&K 4138-A-015, and in Section 8.3 $M_V$ of the microphone system is measured using the modified three-transducer reciprocity calibration method.

Only magnitude values are considered and therefore a simplified notation is adopted where e.g. the magnitude of the transmitting voltage response is denoted simply by $S_V$ instead of $|S_V|$. The essential MATLAB-scripts used to calculate the presented results from the recorded measurements can be found in Appendix A.3.

## 8.1 Three-transducer reciprocity calibration

The modified three-transducer reciprocity calibration method is performed on the piezoelectric transducers Transducer No.1, Transducer No. 2 and Transducer No. 3. Specifications for the three measurements are given in Table 8.1, as well as a fourth measurement to perform a reciprocity check. Note that T1, T2 and T3 denote the transducers in the modified three-transducer reciprocity calibration method described in Chapter 2, while Transducer No. 1, Transducer No. 2 and Transducer No. 3 are the three transducers developed in Chapter 6.

Table 8.1: Three-transducer reciprocity calibration of the piezoelectric transducers developed during this work.

| Measurement parameters | | | | |
|---|---|---|---|---|
| Meas. No. | Transmitter | Receiver | Meas. distance | Burst length |
| 1 | T1 = Trans. No. 3 | T2 = Trans. No. 1 | 66 cm | 1.6 ms (~55 cm) |
| 2 | T1 = Trans. No. 3 | T3 = Trans. No. 2 | 66 cm | 1.6 ms (~55 cm) |
| 3 | T3 = Trans. No. 2 | T2 = Trans. No. 1 | 66 cm | 1.6 ms (~55 cm) |
| Reciprocity check | | | | |
| 4 | T3 = Trans. No. 2 | T1 = Trans. No. 3 | 66 cm | 1.6 ms (~55 cm) |

The separation distances used in the measurements are chosen with the goal of achieving the best possible SNR. Thus is preferably a short separation distance chosen, but long enough for the signal to reach steady state (see Section 3.7) while the electrical crosstalk is kept at a minimum. In the current measurement setup the maximum distance is approximately 77 cm when measuring with elements as transmitters and receivers, and approximately 66 cm when measuring with piezoelectric transducers.

### 8.1.1 Peak to peak detection

The direct method and FFT method for determining the peak to peak voltage from the recorded signal are used to calculate $H_{1m5m}^{VV}$ for measurement No. 1, and the results are shown in Fig. 8.1. The effects are similar to those seen for piezoelectric disks in Fig. 7.10. It is seen that the two methods coincide at the peaks, while a deviation is observed for the lower magnitude levels. The effects are larger for the lower generator voltage. The FFT method is used in the following.

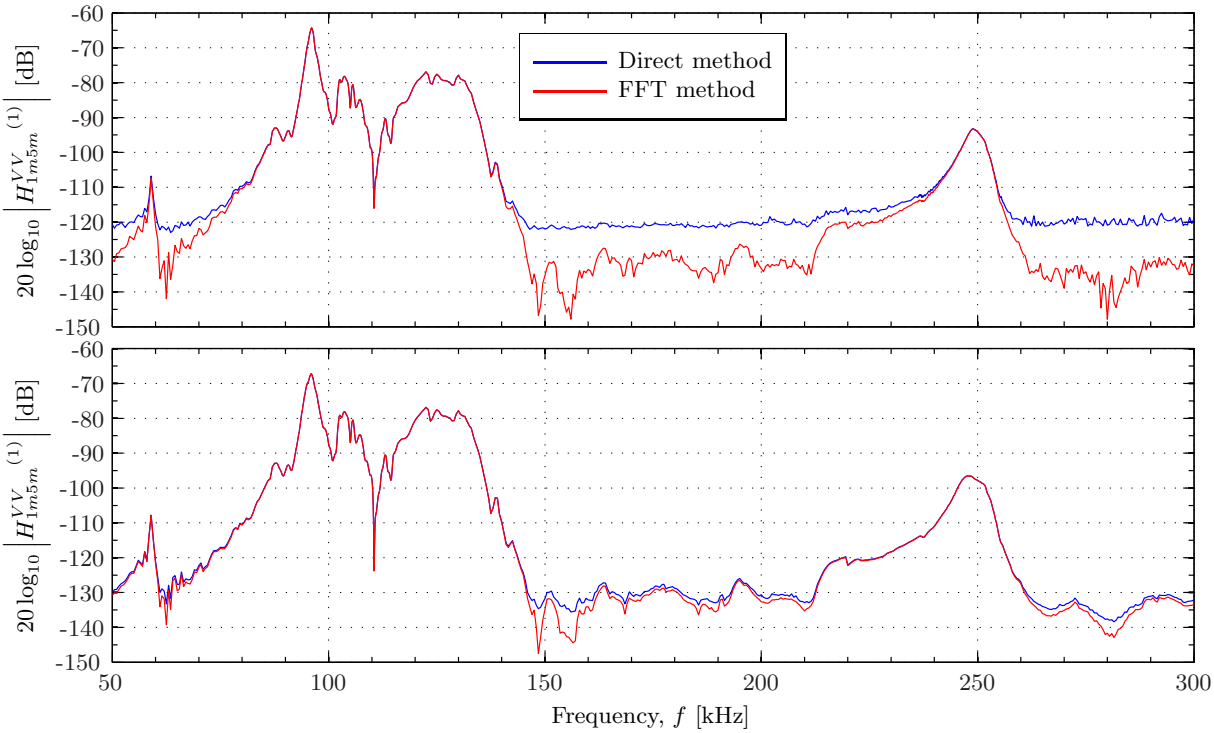


Figure 8.1: The measured $H_{1m5m}^{VV}$ of measurement No. 1, calculated using either the direct method or FFT method to determine the peak to peak voltage. The upper part is with a open-circuit generator voltage of $V_{pp}$ = 2 V, and the lower part is with $V_{pp}$ = 20 V.

### 8.1.2 SNR

The SNR for the measurement where Transducer No.2 transmits to Transducer No. 1, measurement No. 3 in Table 8.1, is shown in Fig. 8.2 for $V_{pp}$ = 2 V and $V_{pp}$ = 20 V. It is assumed that the SNR is representative for the measurements performed in the modified three-transducer reciprocity calibration discussed here.

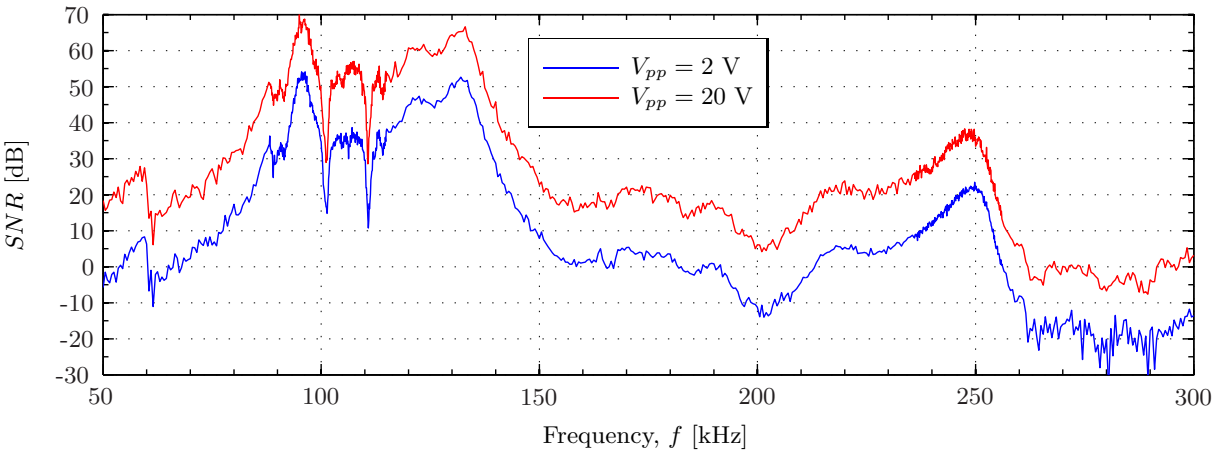


Figure 8.2: SNR for a measurement where Transducer No.2 transmits to Transducer No. 1, with a separation distance of 66 cm and an open-circuit generator voltage of $V_{pp}$ = 2 V and $V_{pp}$ = 20 V.

The SNR obtained for the two different generator voltages show similar behaviour, but with an SNR of the higher generator voltage increased by approximately 15 dB. The increase from $V_{pp} = 2$ V to $V_{pp} = 20$ V in the open-circuit generator voltage corresponds to an increase by 20 dB. It is assumed that this discrepancy is caused by an increase in the noise due to the increased generator voltage. The maximum SNR approaches 70 dB, and the level is above approximately 20 dB in the frequency ranges 70 kHz to 150 kHz and 214 kHz to 254 kHz for the higher generator voltage. Corresponding frequency ranges for the lower generator voltage are 84 kHz to 144 kHz and 247 kHz to 251.5 kHz. A frequency band extending from approximately 90 kHz to 140 kHz have an SNR exceeding 50 dB for the higher generator voltage, except for two distinct dips at approximately 100 kHz and 110 kHz.

In Fig. 8.3 the SNR obtained with the higher generator voltage is compared to the corresponding SNR for the measurements where elements are used as transmitters and receivers (see Fig. 7.11)).

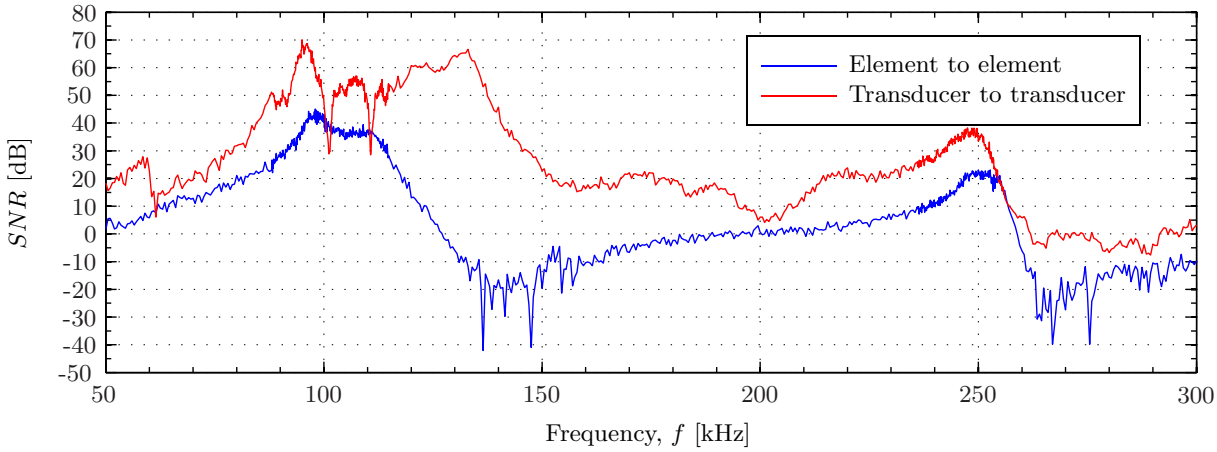


Figure 8.3: Comparison of the SNR obtained in the measurement with Transducer No. 2 to Transducer No.1 (Fig. 8.2) and with Element #16 to Element #6 (Fig. 7.11). The former at a separation distance of 66 cm, and the latter at a separation distance of 77 cm. Both with an open-circuit generator voltage $V_{pp} = 20$ V.

It is seen that the goal of increasing the SNR by constructing piezoelectric transducers has been accomplished, as the SNR is increased for all frequencies except the two distinct dips at R1. The piezoelectric transducers are designed for use at the first radial mode of the piezoelectric ceramic disk, and it is therefore expected that the increase in SNR is most significant around R1, with an increase of up to 70 dB. Note that a small part of the increase in SNR is due to the reduced separation distance.

There is still observed some rapid variations in SNR throughout the frequency range, and it is assumed that the cause of this is the variations in the noise described in 7.2.2.

### 8.1.3 Generator voltage

In Fig. 8.4 the measured voltage to voltage transfer function for measurement No. 1 is shown for open-circuit generator voltages of $V_{pp} = 2$ V and $V_{pp} = 20$ V. As seen in Fig. 8.1, but only considering the FFT method.

Some nonlinear effects are observed in the region around resonance for the generator voltage of $V_{pp} = 20$ V, compared to the $V_{pp} = 2$ V measurements. The effects are significantly smaller than those observed for the elements in Fig. 7.2.3, thus indicating that the construction of piezoelectric transducer decrease the nonlinear effects in the piezoelectric ceramic disks used. The decrease also indicates that the main contributor to the nonlinear effects observed at resonance is the piezoelectric material, and not air. This is because the nonlinear effects are diminished even though the energy transmitted from the transmitting piezoelectric transducer is higher than that transmitted from an element.

Outside resonance the nonlinear effects become negligible and a higher generator voltage is superior. A combination of measurements with the two different generator voltages are presented in the following, with the chosen demarcation frequencies in Table 8.2 shown by the symbol '×'.

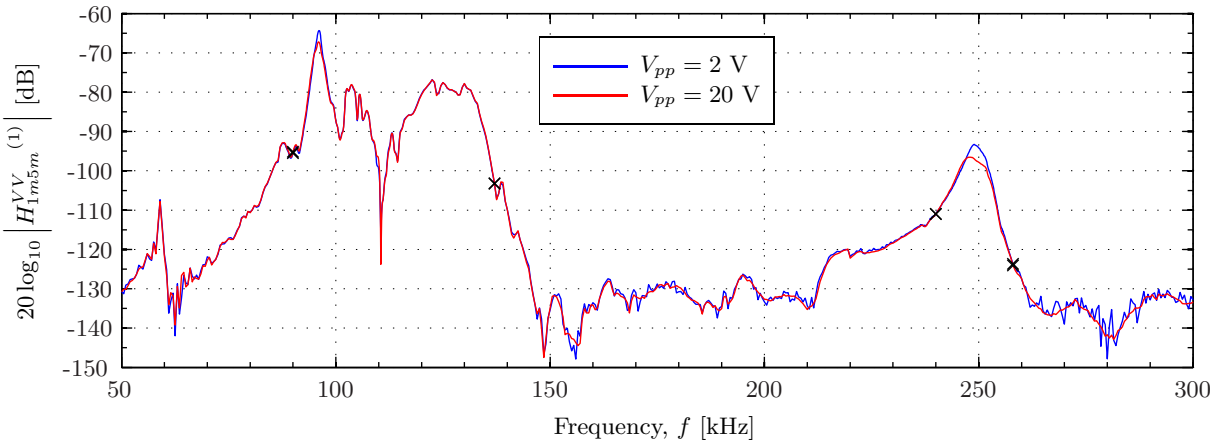


Figure 8.4: The measured $H^{VV}_{1m5m}$ of measurement No. 1, obtained with $V_{pp}$ = 2 V and $V_{pp}$ = 20 V open-circuit generator voltage. Demarcation frequencies, as given in Table 8.2, are indicated by the symbol '×'.

Table 8.2: Demarcation frequencies used when combining measurements with different open-circuit generator voltages.

| Frequency range | | | Open-circuit generator voltage |
|---|---|---|---|
| 50 kHz | - | 90 kHz | $V_{pp}$ = 20 V |
| 90 kHz | - | 137 kHz | $V_{pp}$ = 2 V |
| 137 kHz | - | 240 kHz | $V_{pp}$ = 20 V |
| 240 kHz | - | 258 kHz | $V_{pp}$ = 2 V |
| 258 kHz | - | 300 kHz | $V_{pp}$ = 20 V |

### 8.1.4 Effect of corrections

The effect of the corrections needed to to find $H^{VV}_{15}$ from the measurements, and in turn $S_V$ and $M_V$ for each transducer, are investigated in the following. The transmitting voltage response of Transducer No. 2 is used as an example.

In Fig. 8.5 the effect of attenuation correction, $C_\alpha$, on the calculated transmitting voltage response of Transducer No. 2 is shown. The effect is frequency (and distance) dependent, rising from below 0.5 dB at 50 kHz to above 5 dB at 300 kHz. The observed effect is smaller here than in Fig. 7.13 due to the shorter separation distance in the measurements performed with piezoelectric transducers compared to the measurements with piezoelectric disks.

The effective correction for the lack of far-field conditions (using diffraction correction) when on $S_V$ of Transducer No. 2 is determined is shown in Fig. 8.6. A larger effect of $C_{dif}$ is seen here than in Fig. 7.16, but it never exceeds 0.5 dB. The radius of the transmitting transducer's matching layer is used in the calculation of $C_{dif}$. The larger radius of the matching layers compared to the piezoelectric disks is one of the causes of the increased $C_{dif}$. The other cause is that the measurements with piezoelectric transducers are performed at shorter separation distances than the measurements where piezoelectric disks are used at both transmitters and receivers.

Fig. 8.7 shows the effect of the voltage to voltage transfer function for the receiving electronics, i.e. to account for the lack of open-circuit conditions, on $S_V$ of Transducer No. 2. The effective $H^{VV}_{5m5}$ depend on the measured admittance of the receiving transducers. Therefore a more complex behaviour is seen in Fig. 8.7 than in Fig. 7.14, as the measured admittance of the transducers are more complex than the admittance of the elements (see Sections 7.1 and 6.1.3). The effect of $H^{VV}_{5m5}$ is just exceeding 1.5 dB in the peaks for the transducer calibration, while it exceeded 5 dB in the element calibration. It is also seen that the effects are of similar magnitude at R1 and R2 in Fig. 8.7, while the effects at R2 were significantly smaller than at R1 in Fig. 7.14.

The effect of the $H^{VV}_{1m1}$, accounting for the cables between the oscilloscope and the transmitting transducer, on $S_V$ of Transducer No. 2 is shown in Fig. 8.8

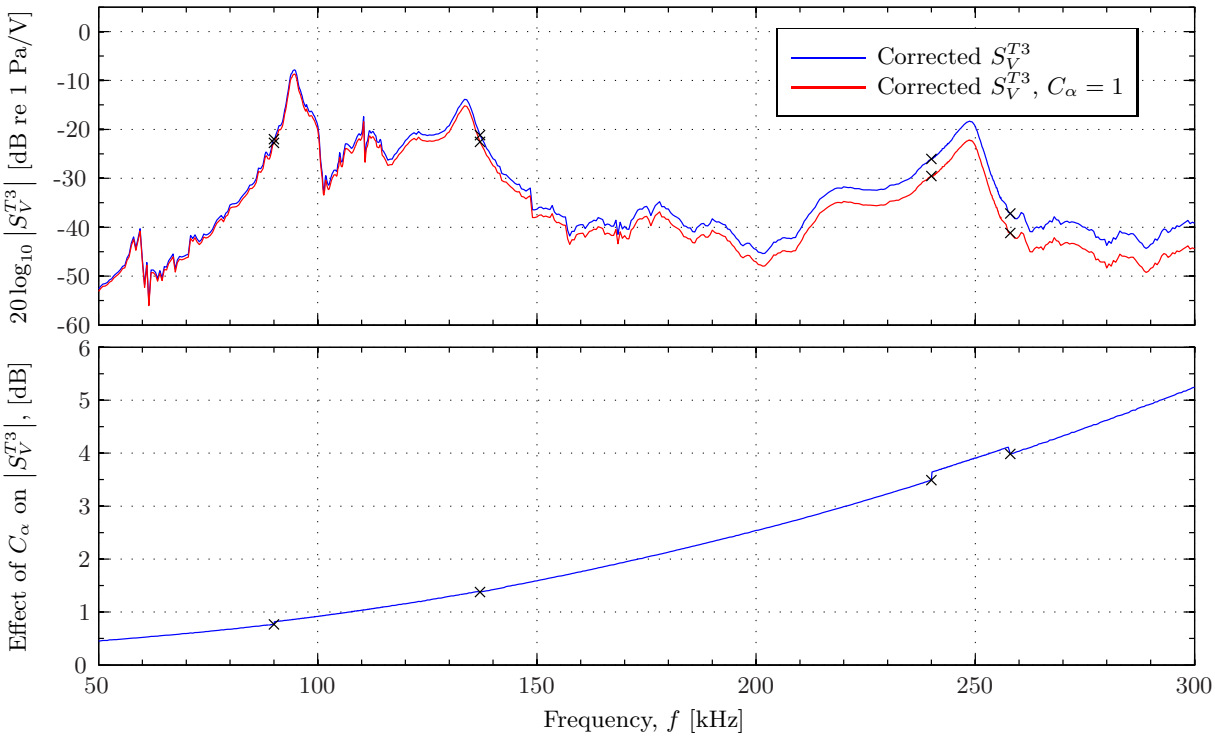


Figure 8.5: $S_V$ of Transducer No. 2 calculated with all corrections compared to $S_V$ calculated with all corrections, but with $C_\alpha = 1$. The effect of this is shown in the lower plot. The demarcation frequencies between the different generator voltages (see Table 8.2) are shown by the symbol '×'.

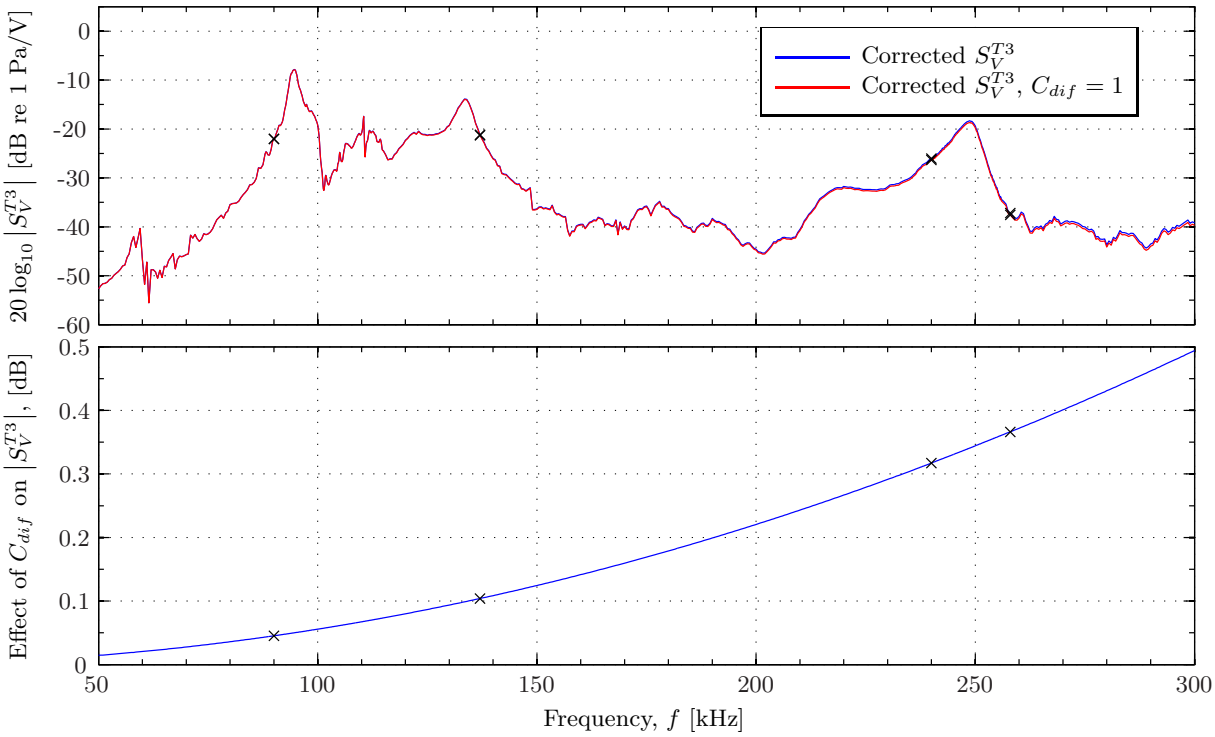


Figure 8.6: As Fig. 8.5, but for $C_{dif}$.

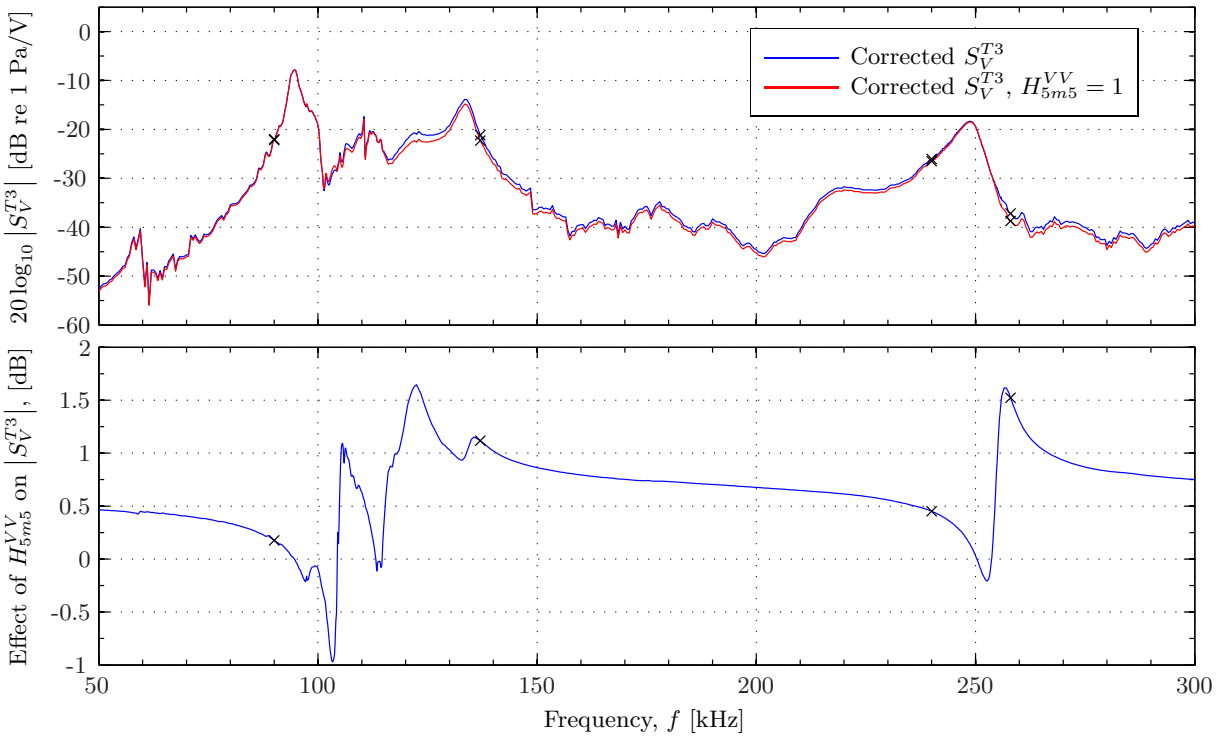


Figure 8.7: As Fig. 8.5, but for $H_{5m5}^{VV}$.

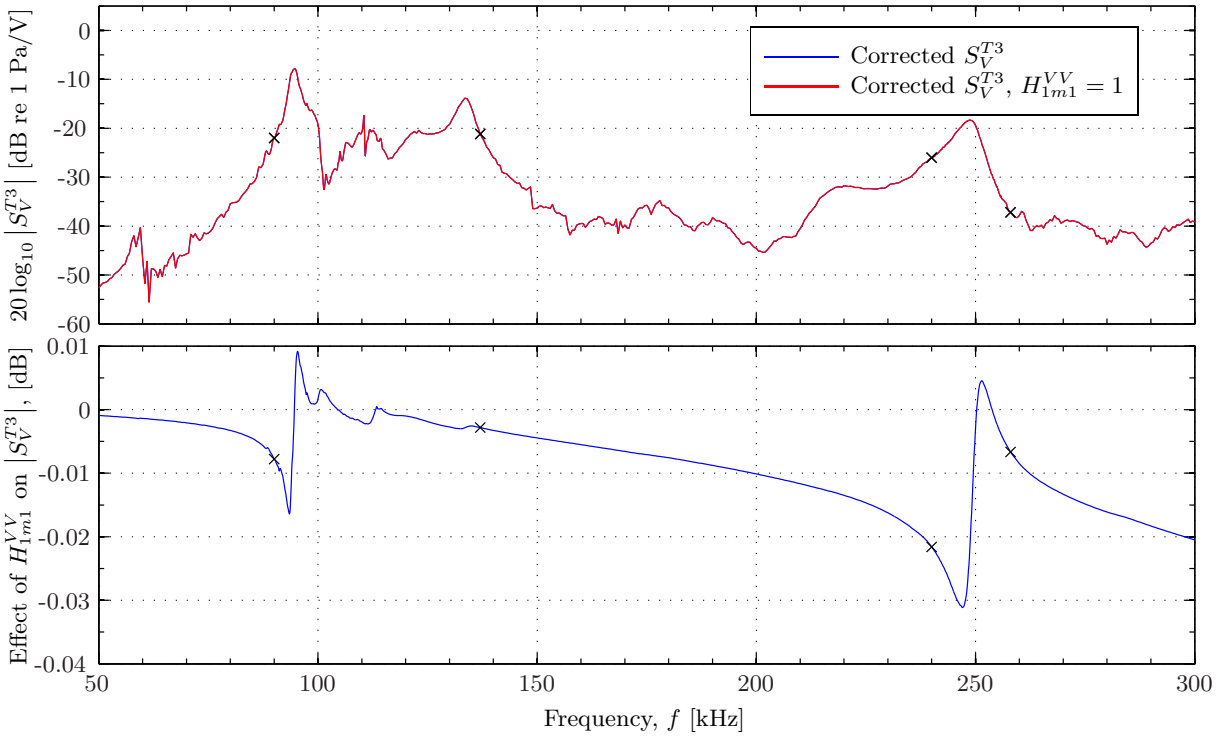


Figure 8.8: As Fig. 8.5, but for $H_{1m1}^{VV}$.

The admittance of the transmitting transducers effect $H_{1m1}^{VV}$, decreasing the maximum magnitude to just above 0.03 dB, compared to just below 0.06 dB in Fig. 7.15.

The dominant correction is the correction for absorption, especially at higher frequencies. It is followed by $H_{5m5}^{VV}$, which causes a frequency shift in the peaks of $M_V$ and generally increases the level magnitude of $S_V$ and $M_V$. The effect of $C_{dif}$ is observable in Fig. 8.6, except for lower frequencies. $H_{1m1}^{VV}$ is negligible compared to the other corrections. Overall the corrections have a slightly smaller impact on

the measurements performed with piezoelectric transducers compared to the measurements performed with piezoelectric disks.

### 8.1.5 Reciprocity check

A reciprocity check (see Sections 2.5 and 7.2.5) is performed for Transducer No. 2 and Transducer No. 3 and shown in Fig. 8.9. Open-circuit generator voltages of $V_{pp} = 2$ V and $V_{pp} = 20$ V are used. Two measurements are performed with the transmitter and receiver interchanged, i.e. measurement No. 2 and measurement No. 4 in Table. 8.1. The transducers are left in position, switching only the cables connecting them to the instrumentation.

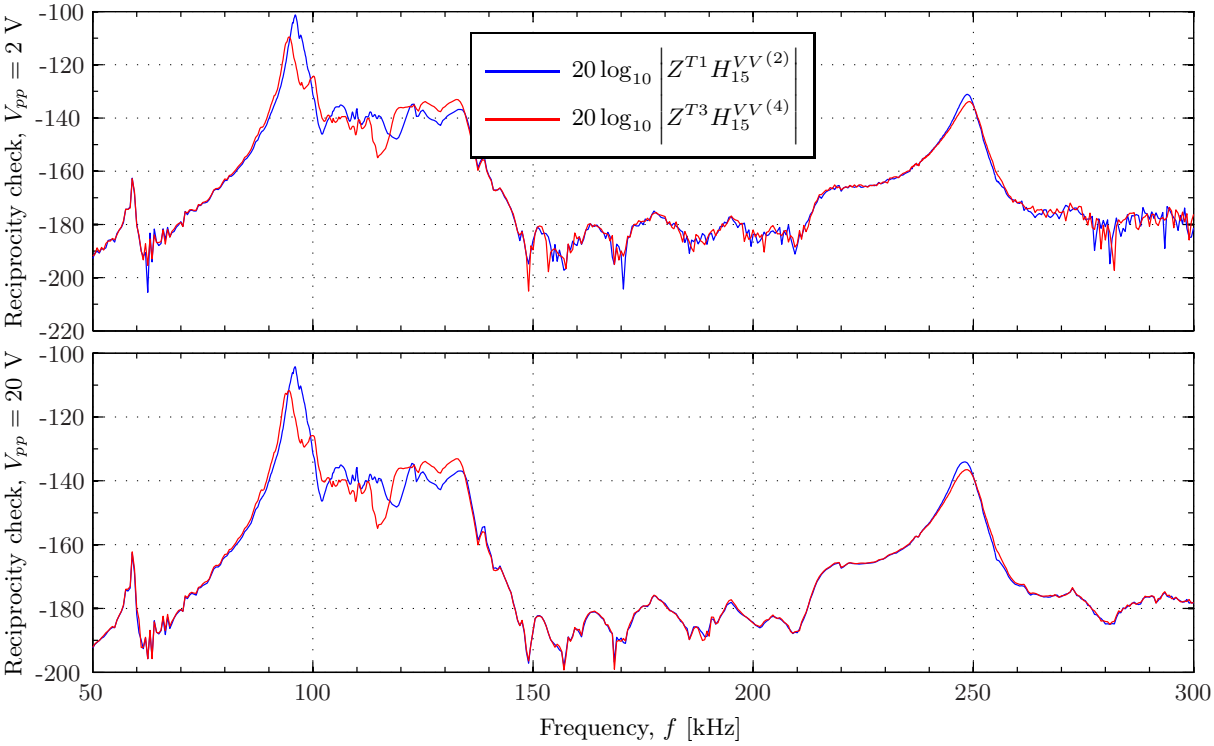


Figure 8.9: Reciprocity check of the transducer pair Transducer No. 2 and Transducer No. 3. Showing the electrical transfer impedances of two measurements performed with the transducers interchanged (See Eq. (2.70)). In the upper plot an open-circuit generator voltage of $V_{pp} = 2$ V is used, and $V_{pp} = 20$ V is used in the lower plot.

The measurement system is reciprocal if the two quantities plotted in Fig. 8.9 coincide. It is evident from the figure that the system containing Transducer No. 2 and Transducer No. 3 is not reciprocal at the peaks at R1 and R2, thus likely introducing an error in $S_V$ and $M_V$ obtained by the modified three-transducer reciprocity calibration method.

Deviations exceeding 15 dB are observed around the first peak at R1, but are generally lower. For the the higher generator voltage (lower plot) deviations within 2 dB are observed below 88 kHz and at frequencies between 135 kHz and 245 kHz. Similar frequency ranges apply for the lower generator voltage (upper plot), but with some larger deviations in the areas of relatively low SNR (see Fig. 8.2).

### 8.1.6 Measurement results and comparison with FE simulations

Results for $S_V$ and $M_V$ using the modified three-transducer reciprocity calibration method are obtained for Transducer No. 1, Transducer No. 2, and Transducer No. 3. All calculations rely on the reciprocity of Transducer No. 2. In addition must Transducer No. 1 be reciprocal in order to calculate its $S_V$, and likewise must Transducer No. 3 be reciprocal if its $M_V$ shall be determined. The calculations are performed as if all three transducers are reciprocal, although it does not appear to be the case (see Section 8.1.5).

In Fig. 8.10 the measured $S_V$ and $M_V$ of each transducer are compared.

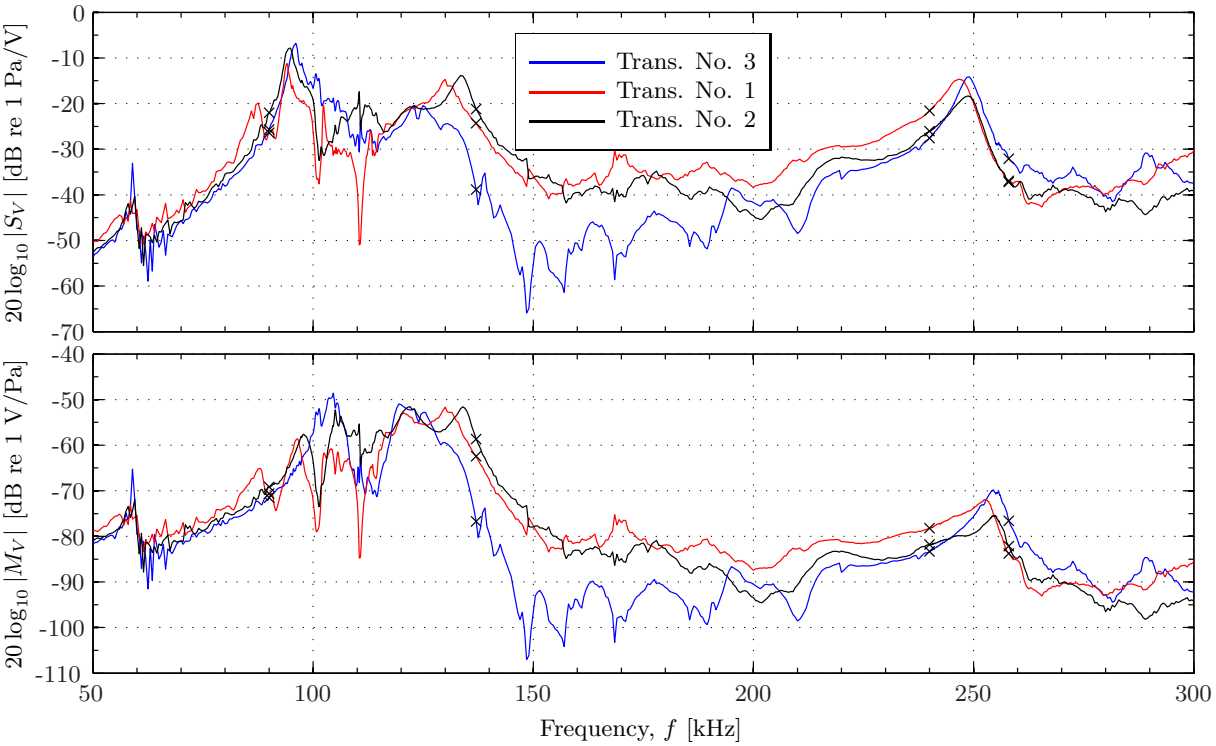


Figure 8.10: Comparison of $S_V$ and $M_V$ for the three piezoelectric transducers, found using the modified three-transducer reciprocity calibration method.

Qualitative agreement is observed between the transducers in Fig. 8.10, with best agreement for $S_V$ at and below the first peak at R1 (~95 kHz) and at the peak at R2 (~248 kHz). It is seen that Transducer No. 3 deviates from Transducer No. 1 and Transducer No. 2 for the frequencies between the second peak at R1 and the peak at R2

The three transducers are of identical design and with similar nominal dimensions. There are some minor differences in the measured dimensions, but not enough to account for the behaviour seen in Fig. 8.10. It is assumed that the main cause of the deviation between the transducers' $S_V$ and $M_V$ is the assembly process (see Section 6.2). Measurements of conductance and susceptance at several stages in the assembly process supports this assumption, as seen in Chapter 6. A possible reasons is the currently used silver conductive epoxy, which proved to be challenging to use due to its high viscosity. An even layer of silver conductive epoxy were not easily achieved, and the thickness of the epoxy layers may differ between the transducers. It is also possible that the variations between each mixed batch of silver conductive epoxy have impact on behaviour of the transducers. In the present design the backing layer is assumed kept in place by its fit in the housing, but this is not assured. A more carefully controlled assembly process as well as small changes in the transducer design may improve the predictability of the transducer construction. The modified two-transducer reciprocity calibration method (see Section 2.6) is not shown for the piezoelectric transducers, as it requires the use of two transducers with similar behaviour.

The measurement results are compared to FE simulations of the transducers in Figs. 8.11, 8.12 and 8.13. Different FEMP-structures are used to model the piezoelectric transducers. As described in Section 4.3, the computing power available does not enable simulations of the full transducers vibrating in air, and therefore a simplified structure is used with the length of the transducers reduced from approximately 8 cm to 2 cm. The full length of the transducers, but with some simplifications, are used when simulations are performed with the transducer vibrating in a vacuum. The commands `transducerfluid` and `transducervacuum` are used, respectively (see Section 4.3). When $S_V$ is calculated (and in turn $M_V$ by use of Eq. 2.4) with the transducer vibrating in vacuum, the hybrid FE/Rayleigh method is used, introducing simplifications as discussed in Section 2.8. Two different sets of material data are used for the matching layer Aptflex R3, as the simulations were performed at different stages in this work[1].

[1]The simulations with the transducer vibrating in air were performed on an earlier stage than those for vacuum. The air-simulations were performed using R3 alt. 2, while the vacuum-simulations were performed using R3 alt. 3. (see Section 4.4)

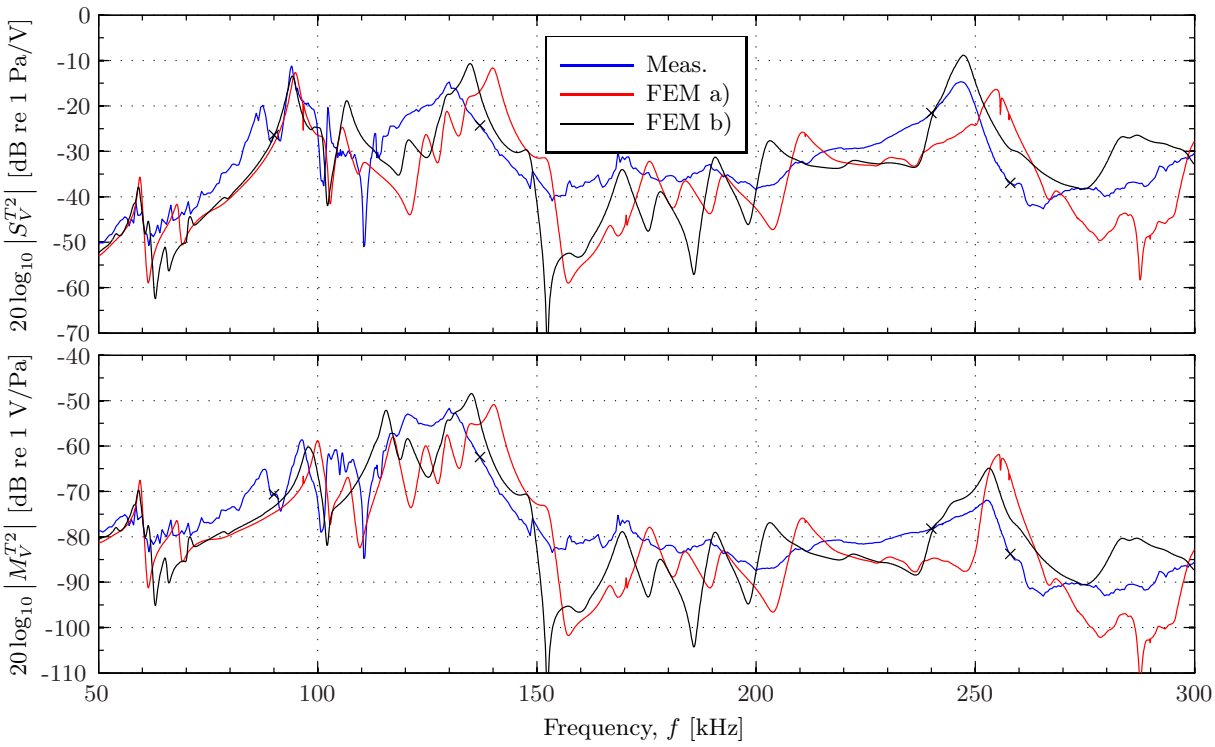


Figure 8.11: The magnitude of $S_V$ and $M_V$ of Transducer No. 1, obtained by the modified three-transducer reciprocity calibration method and compared with FE simulations. FEM a) is the transducer vibrating in air and FEM b) is the transducer vibrating in vacuum.

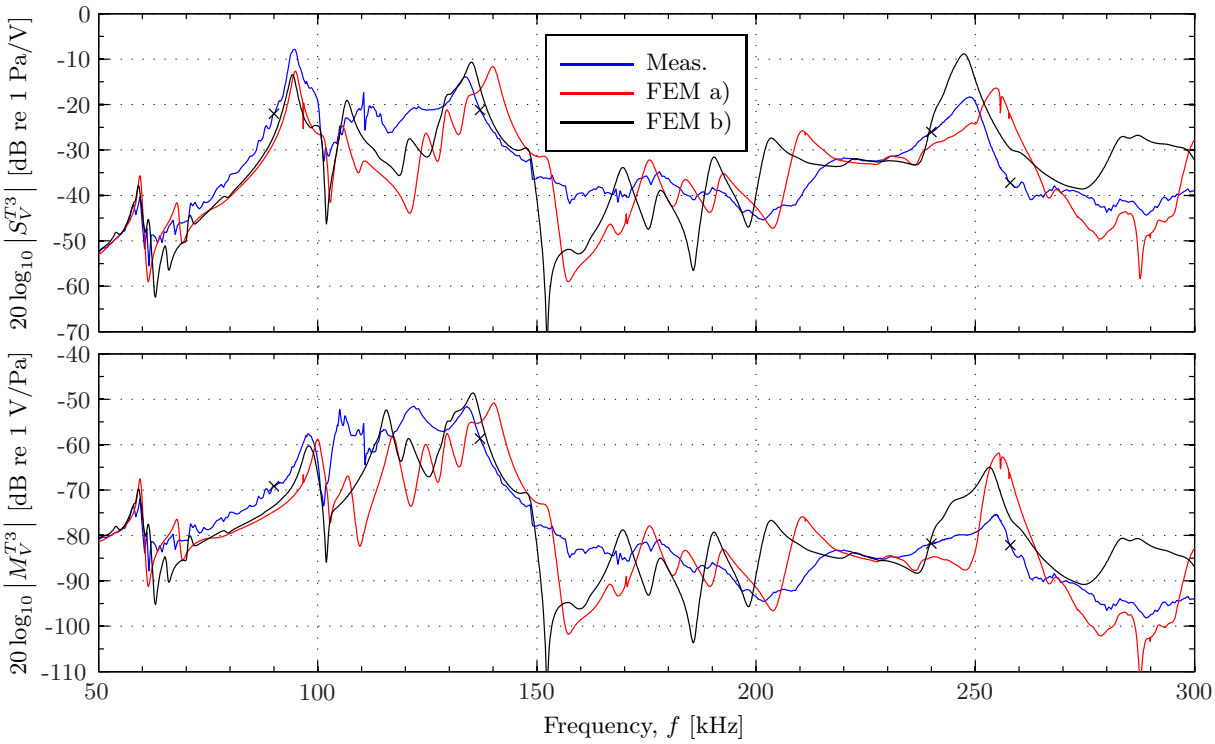


Figure 8.12: As Fig. 8.13, but for Transducer No. 2.

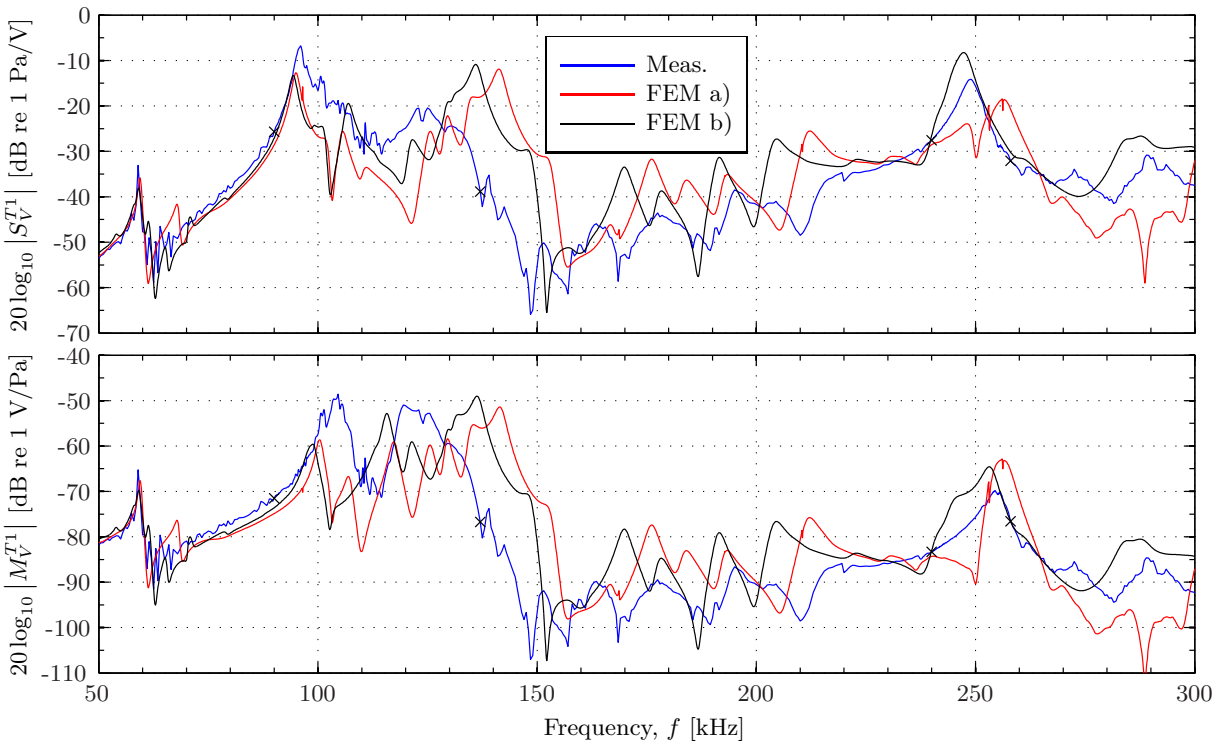


Figure 8.13: As Fig. 8.13, but for Transducer No. 3.

More rapid variations are observed in the FE simulations compared to the measured values, but no consistent deviation is seen. The difference between the measured values and the simulated values is expected, based on findings in Fig. 8.10 as well as on the electrical measurements in Section 6.1.3. Best agreement is seen at the peak at approximately 60 kHz, in the two main peaks in R1 and in the peak at R2. Transducers No.1 and No.2 show slightly better agreement with the simulations than Transducer No. 3. It is not easily determined which FE simulation should be preferred.

Note that the accuracy of the material parameters used in the FE simulations are essential to the final result. The material parameters used in the simulations shown in Figs. 8.11, 8.12 and 8.13 are given in Section 4.4. The material data available for some of the materials modelled are incomplete, and parameters must therefore be estimated based on information about similar materials. This increases the uncertainties in the FE simulations. For other materials nominal data are available, but more accurate data is of interest. The material parameters used for the Aptflex R3 [89] matching layer in the air-simulations are based on measurements performed in the present work (see Chapter 5) and values stated by the manufacturer. In the material data set used in the vacuum-simulations these values are adjusted to provide a better fit to electrical measurements (see Chapter 6). The material data set used for the piezoelectric material Pz27 (see Section 4.4) is also adjusted to provide a better fit to measurements [37].

## 8.2 Measurement with a calibrated microphone

Measurements are performed with a calibrated microphone for comparison with results obtained by use of the modified three-transducer reciprocity calibration method. Comparison is possible for frequencies up to 200 kHz, as this is the upper frequency limit of the calibration data supplied by the manufacturer [79]. $S_V$ are calculated for each of the measurements listed in Table 8.3 using Eq. (2.73). Only the B&K 4138-A-015 microphone system is used.

Table 8.3: Measurements on the piezoelectric transducer developed as part of the present work with calibrated microphones.

| Measurement parameters | | | |
|---|---|---|---|
| Transmitter | Receiver | Meas. distance | Burst length |
| T2 = Transducer No. 1 | B&K 4138-A-015 | 55 cm | 1.4 ms (~48 cm) |
| T3 = Transducer No. 2 | B&K 4138-A-015 | 55 cm | 1.4 ms (~48 cm) |
| T1 = Transducer No. 3 | B&K 4138-A-015 | 55 cm | 1.6 ms[2] (~55 cm) |

### 8.2.1 SNR

The SNR of the measurements where Transducer No. 3 transmits to B&K 4138-A-015 with a separation distance of 55 cm are shown in Fig. 8.14. A maximum level of approximately 70 dB is seen for the higher generator voltage between 90 kHz and 100 kHz. In general the highest SNR is observed for the lower frequencies, as is expected for the piezoelectric transducer designed for use at the first radial mode. The level difference between the lower and higher generator voltage is between 15-20 dB for the whole frequency range. The rapid variations in the SNR are probably caused by changes in the noise, described in Section 7.2.2.

Fig. 8.15 compares the SNR obtained when a piezoelectric transducer is used as transmitter to the SNR when a piezoelectric disk is used as transmitter. The results are shown for the higher generator voltage. It is seen that an increase in SNR is achieved around the first radial mode and up to 150 kHz. Upwards of this a reduction is observed. The element has a significantly more stable SNR between 150 kHz and 270 kHz. It seems that the development of piezoelectric transducers increased the SNR at for the frequencies of interest around R1, but also decreased the SNR at higher frequencies. It is therefore necessary to develop several different sets of transducers to increase the SNR for the whole frequency range. Note that the separation distance is longer for the transducer measurements than for the element measurements.

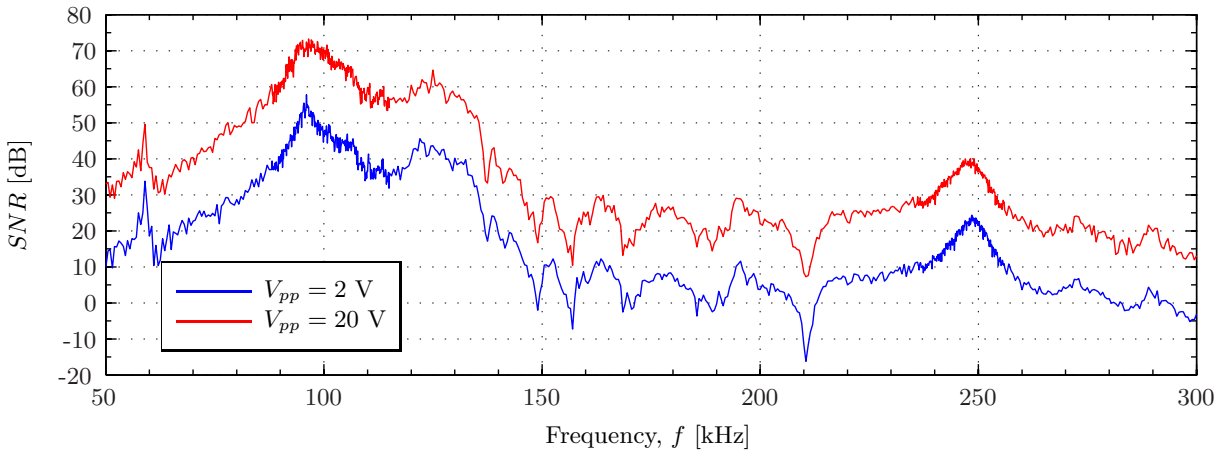


Figure 8.14: Signal to noise ratio for measurements performed with Transducer No.3 as transmitter and B&K 4138-A-015 as receiver, with a separation distance of 44 cm and an open-circuit generator voltage of $V_{pp}$ = 2 V and $V_{pp}$ = 20 V.

[2]A mistake in the initialization caused the burst length to be set to 1.6 ms instead of 1.4 ms.

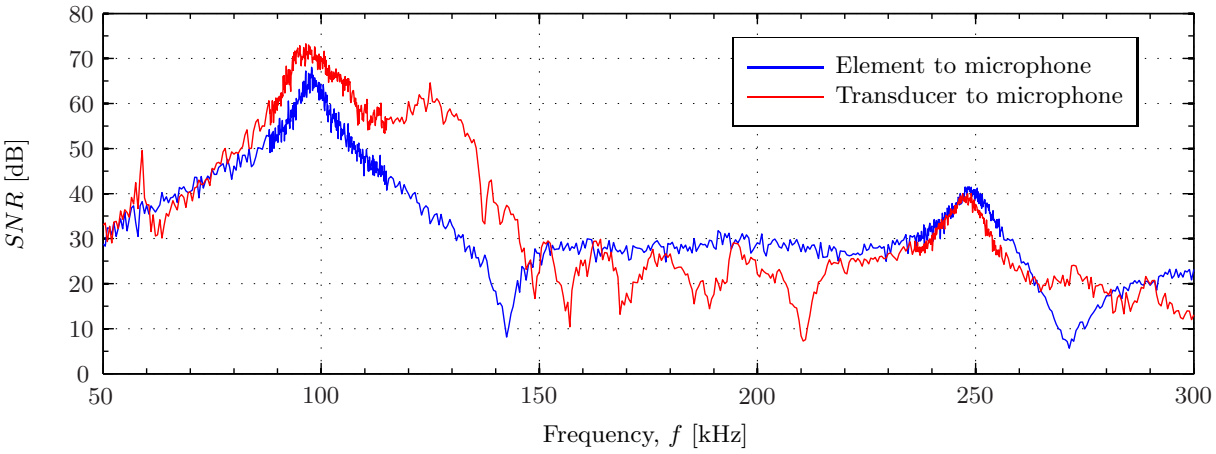


Figure 8.15: Comparison of the SNR obtained in measurements with Transducer No. 3 to B&K 4138-A-015 (Fig. 8.14) and Element #16 to B&K 4138-A-015 (Fig. 7.25). The former at a separation distance of 55 cm, and the latter at a separation distance of 44 cm. Both with an open-circuit generator voltage $V_{pp} = 20$ V.

### 8.2.2 Results and comparison

In Figs. 8.16, 8.17, and 8.18 the transmitting voltage response obtained by use of the modified three-transducer reciprocity calibration method is compared to the measurements performed with the calibrated B&K 4138-A-015. For the latter measurements only the lower generator voltage is used. This is because the measurements showed good agreement outside the resonances, while some nonlinear effects were observed in the peaks for the higher generator voltage.

It is seen from the figures that the results obtained through the modified three-transducer reciprocity calibration method yield similar results to those obtained by microphone measurements, but with increasing deviations for higher frequencies.

In Fig. 8.18, showing Transducer No. 3, the two measurements agree within approximately 1 dB for the larger part of the frequency range up to 135 kHz, but with some larger deviations for instance in the the frequency range 100 kHz to 115 kHz. The deviations increase upwards from 135 kHz, but is usually well below 5 dB.

Quite similar agreement as that seen for Transducer No. 3 is observed for Transducer No. 1 and Transducer No. 2, but not necessarily in the same frequency ranges. The increase in the deviation at higher frequencies does, however, not apply to Transducer No. 2.

Note that the possible effects caused by the differences observed in the reciprocity check of the piezoelectric transducers (see Section 8.1.5) are not determined from the figures.

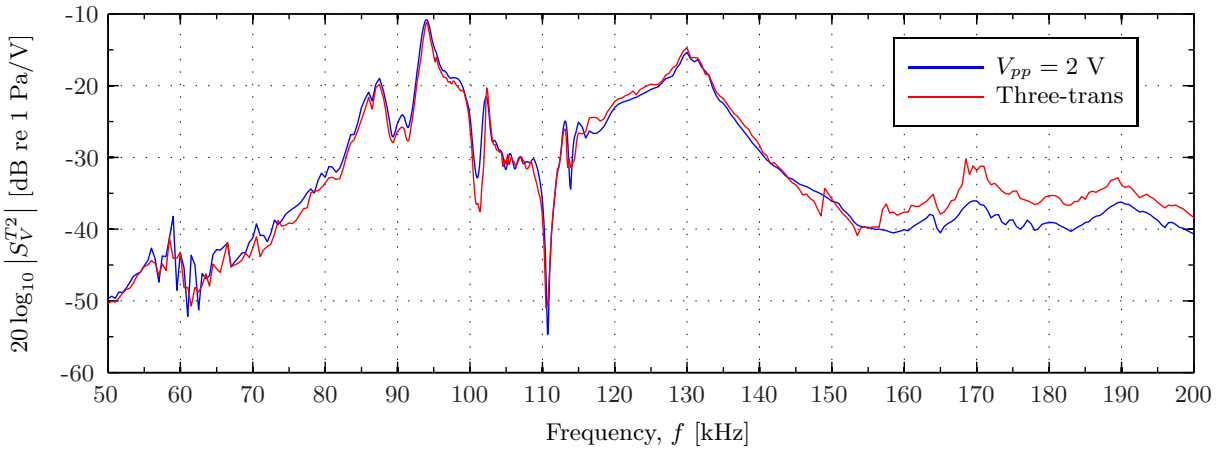


Figure 8.16: Transmitting voltage response of Transducer No. 1 (T2) measured by B&K 4138-A-015 for the frequency range 50 kHz to 200 kHz. Two different open-circuit generator voltages, $V_{pp}$ = 2 V and $V_{pp}$ = 20 V.

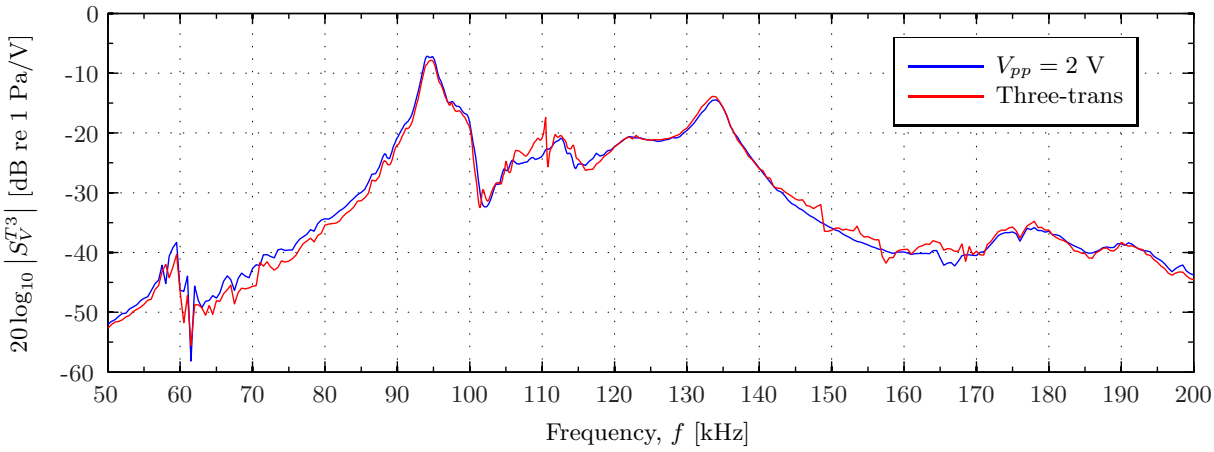


Figure 8.17: As Fig. 8.16, but for Transducer No. 2 (T3).

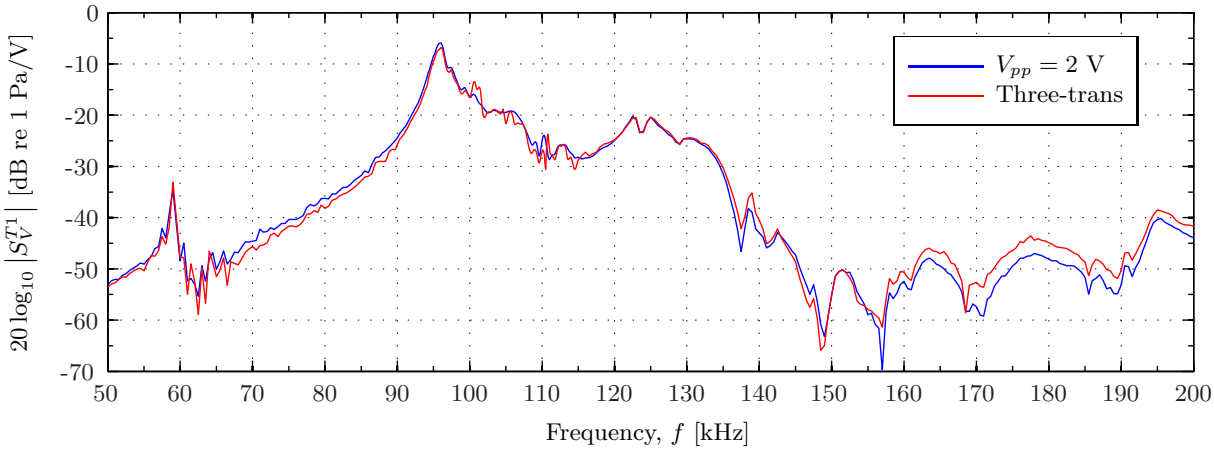


Figure 8.18: As Fig. 8.16, but for Transducer No. 3 (T1).

## 8.3 The modified method applied to the microphone system

The measurements conducted with the B&K 4138-A-015 microphone system, Transducer No. 3 and Transducer No. 2, listed in Table 8.4, are used in the modified three-transducer reciprocity calibration method to measure $M_V$ of B&K 4138-A-015.

Table 8.4: Three-transducer reciprocity calibration of B&K 4138-A-015.

| Measurement parameters | | | | |
|---|---|---|---|---|
| Meas. No. | Transmitter | Receiver | Meas. distance | Burst length |
| 1 | T1 = Trans. No. 3 | B&K 4138-A-015 | 55 cm | 1.6 ms (~55 cm) |
| 2 | T1 = Trans. No. 3 | T3 = Trans. No. 2 | 66 cm | 1.6 ms (~55 cm) |
| 3 | T3 = Trans. No. 2 | B&K 4138-A-015 | 55 cm | 1.4 ms (~48 cm) |

The results for measurements using open-circuit generator voltages of $V_{pp}$ = 2 V and $V_{pp}$ = 20 V are compared to the supplied calibration in Fig. 8.19. In Fig. 8.20 the results for the two generator voltages are combined.

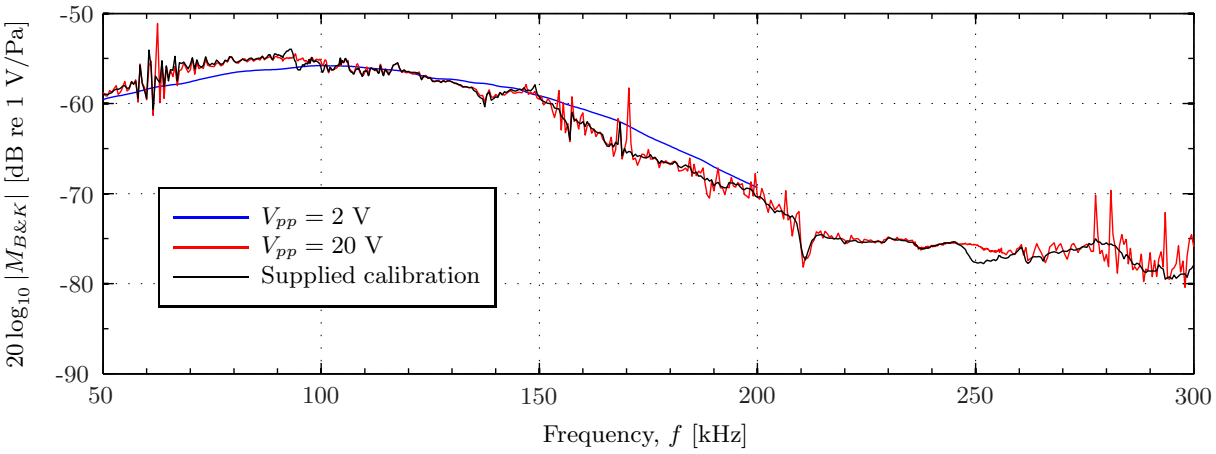


Figure 8.19: Free-field open-circuit receiving voltage sensitivity of B&K 4138-A-015, found by the three-transducer reciprocity calibration method with open-circuit generator voltage $V_{pp}$ = 2 V and $V_{pp}$ = 20 V, compared to $M_V$ supplied by B&K and calibrated by use of a pistonphone.

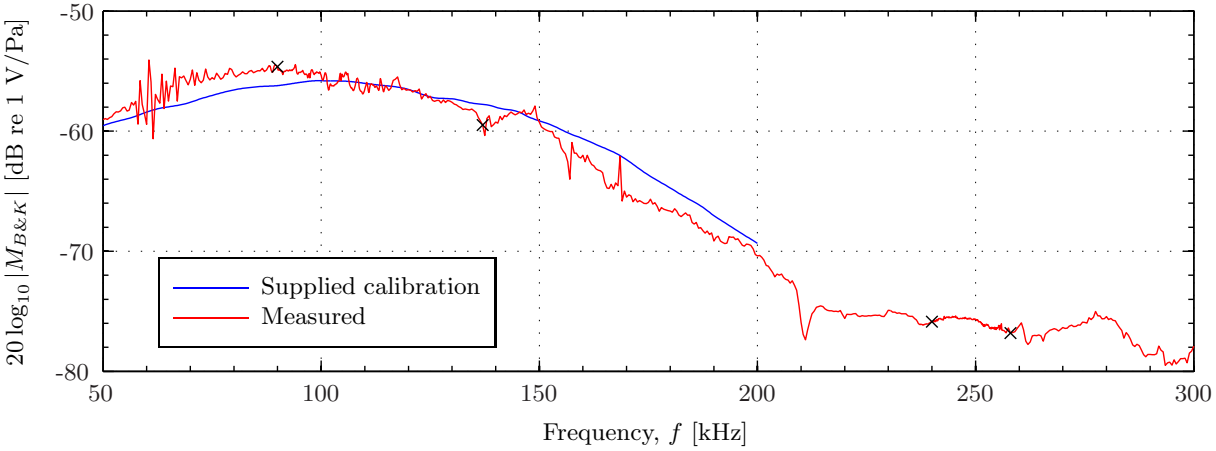


Figure 8.20: As Fig. 8.19, but with a combination of the two generator voltages. Transition between the different voltage are denoted by the symbol '×'.

For the combined results, an agreement within 1 dB is observed in the frequency range 94.5 kHz to 135 kHz, and within 2 dB for the frequency ranges 74.5 kHz to 94.5 kHz and 178 kHz to 200 kHz. It can be seen that the larger deviations, e.g. at approximately 60 kHz, is correlated to resonances in the responses of Transducer No. 2 and/or Transducer No. 3. This is not unexpected, as small frequency shifts in the resonances may cause comparatively large level differences in $S_V$ and $M_V$.

In Fig. 8.21 the graphs in Fig. 8.20 are compared to the results obtained by use of piezoelectric disks (see Fig. 7.30).

It is seen that the two measurement results show the same overall behaviour for the frequencies up to approximately 205 kHz, with deviations e.g. around 60 kHz for the piezoelectric transducers and in the frequency range centred at 140 kHz for the piezoelectric disks. The former is correlated with the a resonance in the piezoelectric transducer, while the the latter is caused by the low SNR in the measurement where piezoelectric disks are used as both transmitter and receiver. Best agreement with the supplied calibration is observed for the frequency range of approximately 100 kHz to 130 kHz for both measurements, where they agree within 1 dB. For the lower frequencies the measured values exceed the given calibration, while a the opposite is true for the higher frequencies.

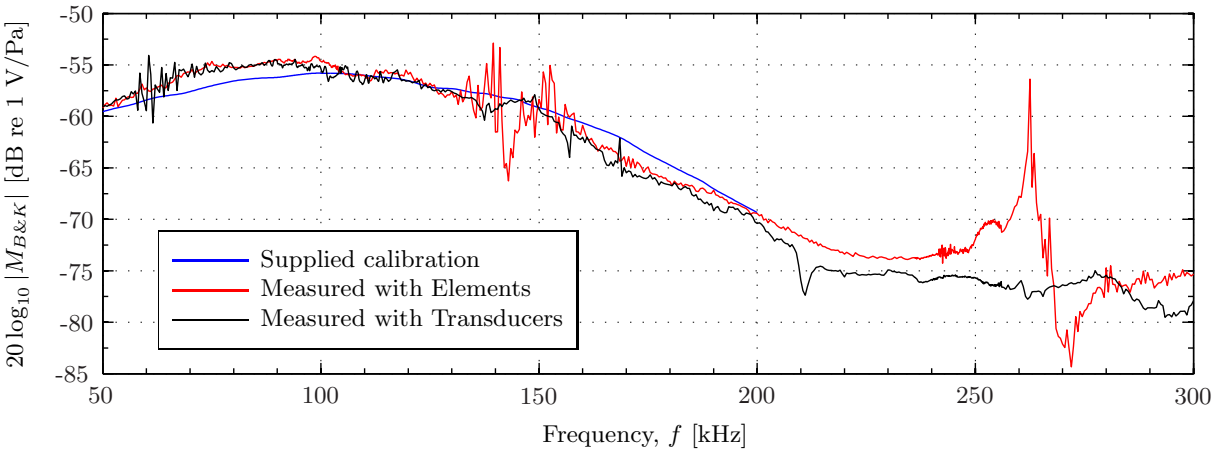


Figure 8.21: As Fig. 8.20, but compared to the results obtained from a modified three-transducer calibration method using piezoelectric disks.

There are a number of possible reasons for the deviations seen in the presented results, in addition to noise (see Section 7.2.2), challenges in the transducer construction (see Section 8.1.6), nonlinear effects (see Sections 7.2.3 and 8.1.3), reciprocity challenges (see Sections 7.2.5 and 8.1.5), and transducer alignment (see Section 7.2.6).

The transmitting transducers are suspended from metal rods mounted on a metal frame inside a measurement chamber (see Section 3.3.3). The separation distances and burst repetition rates are chosen so that standing waves between the transducers are avoided and that the reflections have been sufficiently dampened between each burst. It is, however, likely that sound waves are scattered from nearby surfaces such as the transducer mounting and chamber walls, and that these reflected sound waves interfere with the signal. It has been assumed that the effects of this are small, but it is of interest to investigate this future work and possibly reduce the reflections.

Correction factors are used in the calculations in the modified three-transducer reciprocity calibration method. These factor are not exact, and this will influence the final results. For instance are the cables modelled as ideal lossless transmission lines and the diffraction correction defined by Khimunin [40,41] is used. The effects of the frequency filter and measurement amplifier are neglected, and the correction for absorption is based on [47] which states an uncertainty of ± 10 %. The absorption is at present calculated using a default pressure of 1 bar in combination with the measured temperature and relative humidity.

The introduction of the electrical impedance $Z_T$ in the three-transducer reciprocity calibration method may also increase the uncertainties, depending on the accuracy of the impedance measurements.

The measurement of the separation distance is not ideal at present (see 3.3.3), with an estimated uncertainty of ± 2 mm. It can be shown that the impact of this is small when only the magnitudes are considered, if the estimated uncertainty is correct.

A better control of all these factors are needed in order to perform accurate measurements of the phase of $M_V$ and $S_V$, and to evaluate the measurement uncertainties in the present implementation. The construction of piezoelectric transducers designed for higher frequencies may be used in order to achieve a better SNR for the frequency range up to 300 kHz.

# Chapter 9

# Conclusions and further work

The three-transducer reciprocity calibration method [10, 11, 43] has been modified by introducing correction factors for absorption in air, diffraction effects, and receiving and transmitting electronics. The use of voltage and impedance measurements instead of current measurements are also included in the modifications. Measurements have been performed on piezoelectric ceramic disks of the material Pz27 and in-house constructed piezoelectric transducers, yielding the magnitude of the transmitting voltage responses, $S_V$, and free-field open-circuit receiving voltage sensitivities, $M_V$. The obtained results have been compared to measurements conducted with calibrated condenser microphones from Brüel & Kjær and to FE simulations. The frequency range studied is 50 kHz to 300 kHz, with emphasis on the frequencies around 100 kHz.

The use on the three piezoelectric ceramic disks and compared to measurement with the the calibrated B&K 4138-A-015 microphone system yielded agreement within 2 dB for the frequency range 80 kHz to 130 kHz.

The modified three-transducer reciprocity calibration method was also used on the B&K 4138-A-015 microphone system in combination with two of the piezoelectric ceramic disks. The results agreed with the supplied calibration of the microphone system within 1 dB for the frequency range 103 kHz to 130 kHz. When the piezoelectric ceramic disks where replaced by the in-house constructed piezoelectric transducers, the agreement with the supplied calibration was within 1 dB for the frequency range 94.5 kHz to 135.5 kHz.

Investigation of the different correction factors included in the modified three-transducer reciprocity calibration method have shown that the effects of absorption and the receiving electronics are dominant in the present measurement setup. The impact of the former on the calculated $S_V$ and $M_V$ approaches 6 dB, while the impact of the latter approaches 8 dB for the measurements with piezoelectric disks. The correction for receiving electronics causes a frequency shift of the peaks in $M_V$ of up to several kHz. This correction depends on the impedance of the receiving transducer. Thus the observed effects are smaller for the piezoelectric transducers than for the piezoelectric disks. The effects of correction for near-field effects are systematic, but below 0.5 dB for the separation distances used in the measurements. Its significance would increase at shorter distances and higher frequencies. The effects of the cable on the transmitting side are seen to be below 0.06 dB.

An SNR exceeding 30 dB is achieved in the frequency range 80 kHz to 140 kHz when measurements are performed with the in-house constructed piezoelectric transducers.

Good qualitative agreement where seen when comparing the measurements to FE simulations, but with significantly more challenges for the in-house constructed piezoelectric transducers than with only the piezoelectric elements.

## Further work

It is of interest to expand the modified three-transducer reciprocity calibration method up to 300 kHz by constructing multiple sets of piezoelectric transducers optimized for use at higher frequencies. Careful control of the construction process and accurate material data are needed to improve the correspondence between measurements and FE simulations.

Further work is also needed to extend the method to include measurements of phase response and to evaluate the measurement uncertainties in the modified three-transducer reciprocity calibration method.

# Bibliography


[1] E. Storheim, PhD thesis, Department of Physics and Technology, University of Bergen, Bergen, Norway (in preparation, 2013).

[2] Ø. S. Amundsen, "Material constants determination for piezoelectric disks, and influence on source sensitivity. Measurements and simulations.", Master thesis, Department of Physics and Technology, University of Bergen, Bergen, Norway (2011).

[3] R. Hauge, E. Mosland, E. Storheim, P. Lunde, M. Vestrheim, and J. Kocbach, "Finite element modeling of ultrasound measurement systems for gas. comparison with experiments in air.", in *Proceedings of the 36th Scandinavian Symposium on Physical Acoustics - Geilo 3rd February - 6th February* (2013).

[4] R. Hauge, "Finite element modeling of ultrasound measurement systems for gas. Comparison with experiments in air. ", Master thesis, Department of Physics and Technology, University of Bergen, Bergen, Norway (2013).

[5] "Regulations relating to measurement of petroleum for fiscal purposes and for calculation of CO2 tax", Norwegian Petroleum Directorate, Stavanger, Norway (2001).

[6] "AGA Report no. 9. Measurement of gas by ultrasonic meters. 2nd revision", American Gas Association, Transmission Measurement Committee, Washington DC, U.S.A. (2007).

[7] "Measurement of fluid flow in closed conduits - Ultrasonic meters for gas - Part 1: meters for custody transfer and allocation measurement. ISO 17089-1:2010", International Organization for Standardization, Geneva, Switzerland (2010).

[8] K.-E. Frøysa and P. Lunde, "Density and calorific value measurement in natural gas using ultrasonic flow meters", in *Proceedings of the 23rd International North Sea Flow Measurement Workshop, Tønsberg, Norway, 18-21 October 2005* (2005).

[9] K.-E. Frøysa, P. Lunde, A. Paulsen, and E. Jacobsen, "Density and calorific value measurement of natural gas using ultrasonic flow meters. Results from testing on various North Sea gas field data.", in *Proceedings of the 24th International North Sea Flow Measurement Workshop, St. Andrews, Scotland, 24-27 October 2006* (2006).

[10] "ANSI S1.10-1966 (R1976) - Method for the calibration of microphones", Acoustical Society of America, New York, NY, United States (1976).

[11] "IEC 61094-3 - Measurement microphones - Part 3: Primary method for free-field calibration of laboratory standard microphones by the reciprocity technique", International Electrotechnical Commission, Geneva, Switzerland (1995).

[12] S. Barrera-Figueroa, "New methods for transducer calibration: Free-field reciprocity calibration of condenser microphones", PhD-thesis, Technical University of Denmark (2003).

[13] W. Koidan, "Calibration of standard condenser microphones: Coupler versus electrostatic actuator", J. Acoust. Soc. Am. **44**(5), 1451–1453 (1968).

[14] A. Gachagan, G. Hayward, S. Kelly, and W. Galbraith, "Characterization of air-coupled transducers", IEEE Trans. Ultrason., Ferroelectr., Freq. Control **43**(4), 678–689 (1996).

[15] J. Hietanen and M. Oksanen, "Photoacoustic testing of ultrasonic air transducers", Measurement Science and Technology **5**(8), 960 (1994).

[16] M. J. Anderson and X. Liu, "Use of reciprocity to characterize ultrasonic transducers in air above 100 kHz", J. Acoust. Soc. Am. **103**(1), 446–453 (1998).

[17] M. Vestrheim, "Private communication", Department of Physics and Technology, University of Bergen, Bergen, Norway (2013).

[18] O. B. Matar, L. Pizarro, D. Certon, J. Remenieras, and F. Patat, "Characterization of airborne transducers by optical tomography", Ultrasonics **38**(1–8), 787 – 793 (2000).

[19] N. Bouaoua, "Free-field reciprocity calibration of condenser microphones in the low ultrasonic frequency range", PhD-thesis, Universität Oldenburg, Germany (2008).

[20] W. Galbraith and G. Hayward, "Development of a PVDF membrane hydrophone for use in air-coupled ultrasonic transducer calibration.", IEEE Trans. Ultrason., Ferroelectr., Freq. Control **45**(6), 1549–58 (1998).

[21] A. G. Bashford, D. W. Schindel, D. A. Hutchins, and W. M. D. Wright, "Field characterization of an air-coupled micromachined ultrasonic capacitance transducer", J. Acoust. Soc. Am. **101**(1), 315–322 (1997).

[22] A. Schroder, S. Harasek, M. Kupnik, M. Wiesinger, E. Gornik, E. Benes, and M. Groschl, "A capacitance ultrasonic transducer for high-temperature applications", IEEE Trans. Ultrason., Ferroelectr., Freq. Control **51**(7), 896–907 (2004).

[23] L. L. Thompson, "A review of finite-element methods for time-harmonic acoustics", J. Acoust. Soc. Am. **119**(3), 1315–1330 (2006).

[24] J. Kocbach, "Finite element modeling of ultrasonic piezoelectric transducers", PhD thesis, Department of Physics, University of Bergen, Bergen, Norway (2000).

[25] J. Kocbach, P. Lunde, M. Vestrheim, and R. Kippersund, "Finite element modeling of ultrasonic piezoelectric transducers: Extension of FEMP to 3D analysis", CMR Report no. CMR-06-A10046-RA-01, Christian Michelsen Research AS, Bergen, Norway (December 2006).

[26] W. R. MacLean, "Absolute measurement of sound without a primary standard", J. Acoust. Soc. Am. **12**, 140–146 (1940).

[27] I. Rudnick and M. N. Stein, "Reciprocity free field calibration of microphones to 100 Kc in air", J. Acoust. Soc. Am. **20**(6), 818–825 (1948).

[28] W. Wathen-Dunn, "On the reciprocity free-field calibration of microphones", J. Acoust. Soc. Am. **21**(5), 542–546 (1949).

[29] "IEC 486 - Values for the difference between free-field and pressure sensitivity levels for one-inch condenser microphones", International Electrotechnical Commission, Geneva, Switzerland (1974).

[30] "IEC 655 - Precision method for free-field calibration of one-inch condenser microphones by the reciprocity technique", International Electrotechnical Commission, Geneva, Switzerland (1979).

[31] E. W. Burnett and V. Nedzelnitsky, "Free-field reciprocity calibration of microphones", Journal of Research of the National Bureau of Standards **92(2)**, 129–151 (1987).

[32] K. Beissner, "Exact integral expression for the diffraction loss of a circular piston source", Acustica **49**, 212–217 (1981).

[33] M. J. Anderson, J. A. Hill, C. M. Fortunko, N. S. Dogan, and R. D. Moore, "Broadband electrostatic transducers: Modeling and experiments", J. Acoust. Soc. Am. **97**(1), 262–272 (1995).

[34] Ferroperm, "High quality components and materials for the electronic industry", Ferroperm Piezoceramics A/S (now a member of Meggitt's Sensing Systems division), Kvistgård, Denmark (2012).

[35] R. Fardal, "Endelig element analyse av elektriske egenskaper til piezoelektriske skiver", Master thesis, Department of Physics, University of Bergen, Bergen, Norway (2002), (in Norwegian).

[36] K. D. Lohne, "Undersøkelse og utnyttelse av svingemoder i ultralyd transduserkonstruksjoner", Master thesis, Department of Physics and Technology, University of Bergen, Bergen, Norway (2005), (in Norwegian).

[37] V. Knappskog, "Radiellmode svingninger i piezoelektriske ultralydstransdusere for luft. Målinger og endelig element analyse", Master thesis, Department of Physics and Technology, University of Bergen, Bergen, Norway (2007), (in Norwegian).

[38] M. Aanes, "Undersøkelser av piezokeramiske skiver. Målinger og endelig element analyser.", Master thesis, Department of Physics and Technology, University of Bergen, Bergen, Norway (2009), (in Norwegian).

[39] E. Storheim, M. Aanes, M. Vestrheim, and P. Lunde, "Ultrasonic piezoceramic transducers for air, - finite element analysis and measurements", in *Proceedings of the 33rd Scandinavian Symposium on Physical Acoustics, Geilo, Norway, 7-10 February 2010*, edited by U. Kristiansen (2010).

[40] A. S. Khimunin, "Numerical calculation of the diffraction corrections for the precise measurement of ultrasound absorption", Acustica **27**, 173–181 (1972).

[41] A. S. Khimunin, "Numerical Calculation of the Diffraction Corrections for the Precise Measurement of Ultrasound Phase Velocity", Acustica **32**, 192–200 (1975).

[42] E. Mosland, R. Hauge, E. Storheim, M. Vestrheim, P. Lunde, and J. Kocbach, "Reciprocity calibration method for ultrasonic, piezoelectric transducers in air, including finite element simulations", in *Proceedings of the 36th Scandinavian Symposium on Physical Acoustics - Geilo 3rd February - 6th February* (2013).

[43] "ANSI S1.20-1988 (R2003) - Proceedures for calibration of underwater electroacoustic transducers", Acoustical Society of America, New York, NY, United States (2003).

[44] "ANSI S1.1-1994 (R2004) - Acoustical terminology", Acoustical Society of America, New York, NY, United States (2004).

[45] M. Vestrheim, "PHYS 272 - Akustiske transdusere", Lecture notes, Department of Physics and Technology, University of Bergen, Bergen, Norway (2007), (in Norwegian).

[46] L. E. Kinsler, A. R. Frey, A. B. Coppens, and J. V. Sanders, *Fundamentals of Acoustics*, 4th edition (John Wiley & Sons, New York) (2000).

[47] "ANSI S1.26-1995 (R2009) - Method for calculation of the absorption of sound by the atmosphere", Acoustical Society of America, New York, NY, United States (2009).

[48] M. Vestrheim, "PHYS 373 - Akustiske målesystem", Lecture notes, Department of Physics and Technology, University of Bergen, Bergen, Norway (2008), (in Norwegian).

[49] E. Storheim, "Private communication", Department of Physics and Technology, University of Bergen, Bergen, Norway.

[50] S. Vervik, "Methods for characterization of gas-coupled ultrasonic sender-receiver measurement systems", PhD thesis, Department of Physics and Technology, University of Bergen, Bergen, Norway (2000).

[51] P. Lunde, K.-E. Frøysa, and M. Vestrheim, "Transient diffraction effects on ultrasonic flow meters for gas and liquid", in *Proceedings of the 26th Scandinavian Symposium on Physical Acoustics, Ustaoset, Norway, 26-29 January 2003* (2003).

[52] P. Lunde, R. A. Kippersund, M. Vestrheim, and K.-E. Frøysa, "Transient diffraction effects in piezoelectric ultrasonic transducers using finite element modelling", in *Proceedings of the 27th Scandinavian Symposium on Physical Acoustics, 25-28 January, 2004, Ustaoset, Norway* (2004).

[53] E. Storheim, P. Lunde, and M. Vestrheim, "Diffraction correction in ultrasonic fields for measurements of sound velocity in gas. Conventional and alternative methods", in *Proceedings of the 34th Scandinavian Symposium on Physical Acoustics, Geilo, Norway, 30th January - 2nd February 2011* (2011).

[54] R. W. P. King, H. R. Mimno, and A. H. Wing, *Transmission Lines, Antennas and Wave Guides* (Dover Publications, New York) (1965).

[55] R. J. Bobber, *Underwater electroacoustic measurements* (Naval Research Laboratory, Washington, D.C.) (1970).

[56] Hewlett-Packard Company, *Operation and service manual: 4192 LF impedance analyzer*, Palo Alto, CA, United States (1982).

[57] Vaisala, "Data sheet: HMI41 indicator and HMP42/HMP46 probes", Vaisala Oyj, Helsinki, Finland (2013).

[58] Brüel & Kjær, "Product data: Pistonphone - Type 4228", Brüel & Kjær Sound & Vibration Measurement A/S, Nærum, Denmark (1996).

[59] Agilent, "Product Data: Type 33220A signal generator", Agilent Technologies, Inc., Santa Clara, CA, United States (2007).

[60] Tektronix, "Product Data: Type DPO3012 digital oscilloscope", Tektronix, Inc., Beaverton, OR, United States (2010).

[61] Brüel & Kjær, "Product data: 1/8″ pressure-field microphone - Type 4138", Brüel & Kjær Sound & Vibration Measurement A/S, Nærum, Denmark (2008).

[62] Brüel & Kjær, "Product data: Microphone preamplifiers - Types 2633, 2639, 2645, 2660", Brüel & Kjær Sound & Vibration Measurement A/S, Nærum, Denmark (1993).

[63] Brüel & Kjær, "Product data: Falcon Range 1/4-inch microphone preamplifier - Type 2670", Brüel & Kjær Sound & Vibration Measurement A/S, Nærum, Denmark (2004).

[64] Physik Instrumente, "Operating manual MS 45E: C-842 DC-motor controllers", Physik Instrumente (PI) GmbH & Co. KG, Karlsruhe, Germany (1996).

[65] Physik Instrumente, "Product data - PI C-852 signal processor", Physik Instrumente (PI) GmbH & Co. KG, Karlsruhe, Germany (2012).

[66] Physik Instrumente, "Product data - PI M-531 linear stage", Physik Instrumente (PI) GmbH & Co. KG, Karlsruhe, Germany (2010).

[67] Physik Instrumente, "Product data - PI M-535 linear stage", Physik Instrumente (PI) GmbH & Co. KG, Karlsruhe, Germany (2010).

[68] Physik Instrumente, "Product data - PI M-037 rotational stage", Physik Instrumente (PI) GmbH & Co. KG, Karlsruhe, Germany (2010).

[69] Brüel & Kjær, "Product Data: Wide Range Measuring Amplifiers - Types 2610 and 2636", Brüel & Kjær Sound & Vibration Measurement A/S, Nærum, Denmark (1996).

[70] Krohn-Hite, "Product Data: Type 3940A bandpass filter", Krohn-Hite Corporation, Brockton, United States (2012).

[71] Vaisala, "Product data - Vaisala HMT310 series", Vaisala Oyj, Helsinki, Finland (2010).

[72] Vaisala, "Calibration certificate: Humidity and temperature transmitter HMT313, serial no. F4850018", Vaisala Oyj, Helsinki, Finland (2010).

[73] Mitutoyo, "Product data - Mitutoyo MDH-25H digital micrometer", Mitutoyo Corporation, Kanagawa, Japan (2012).

[74] Tesa, "Product data - Tesa digital caliper", TESA Technology UK Ltd., Telford, UK (2012).

[75] A. Erdal, *Elementær innføring i sannsynlighetsregning og problemløsninger ved analyse av måleresultater* (Alma Mater, Bergen, Norway) (1972), (in Norwegian).

[76] A&D, "GF Series precision balance - Instruction manual", A&D Company, Limited, Tokyo, Japan (2008).

[77] Brüel & Kjær, "Calibration data for 4138-A-015 microphone system serial no. 2795107", Brüel & Kjær Sound & Vibration Measurement A/S, Nærum, Denmark (2012).

[78] Brüel & Kjær, "Calibration data for Type 4138 microphone serial no. 1832479", Brüel & Kjær Sound & Vibration Measurement A/S, Nærum, Denmark (1995).

[79] Brüel & Kjær, "Calibration data for Type 4138 microphone serial no. 2784915", Brüel & Kjær Sound & Vibration Measurement A/S, Nærum, Denmark (2012).

[80] Brüel & Kjær, "Certificate of calibration No. C1201771 for B&K 4138-A-015 microphone system serial no. 2795107", Brüel & Kjær Sound & Vibration Measurement A/S, Nærum, Denmark (2012).

[81] Brüel & Kjær Sound & Vibration Measurement A/S, Nærum, Denmark, *Condenser microphones and microphone preamplifiers for acoustic measurements - Data handbook* (1982).

[82] Brüel & Kjær, "Calibration data for Type 4228 pistonphone serial no. 1918465", Brüel & Kjær Sound & Vibration Measurement A/S, Nærum, Denmark (1996).

[83] "The fundamentals of FFT-based signal analysis and measurement in LabVIEW and LabWindows/CVI", Available at URL http://www.ni.com/white-paper/4278/en (last viewed 21.05.2013) (2009).

[84] M.-A. Parseval, "Memoire sur les series et sur l'integration complete d'une equation aux differences partielle lineaires du second ordre, a coefficiens constans", Academie des Sciences (1806).

[85] H. Hobæk, "Private communication", Department of Physics and Technology, University of Bergen, Bergen, Norway (2013).

[86] J. P. Bentley, *Principles of measurement systems - 4th ed.* (Pearson Education Limited, England) (2005).

[87] J. Kocbach, "FEMP version 3.5 - Documentation", University of Bergen, Bergen, Norway.

[88] Andrew Hurrel, BSc (Hons), PhD, "Private communication", Precision Acoustics Ltd, Dorset, UK (2012).

[89] Precision Acoustics, "Syntactic foam, http://www.acoustics.co.uk/products/syntactic-foam", Precision Acoustics Ltd, Dorset, UK (Last reviewed 05.05.2013).

[90] MG Chemicals, "Silver conductive epoxy Cat. No. 8331-14G, packaging", MG Chemicals, Burlington, Ontario, Canada.

[91] MG Chemicals, "Silver conductive epoxy adhesive 8331 - Technical data sheet", MG Chemicals, Burlington, Ontario, Canada (2012).

[92] Onda Corporation, "Acoustic properties of solids", Onda Corporation, Sunnydale, CA, United States (2003).

[93] Atlas Steels, "Grade data sheet: 316, 316L, 316H", Atlas Steels, Australia (2011).

[94] M. Grujicic and H. Zhao, "Optimization of 316 stainless steel/alumina functionally graded material for reduction of damage induced by thermal residual stresses", Materials Science and Engineering: A **252**, 117–132 (1998).

[95] P. Norli, "Sound velocity cell for gas characterization", PhD thesis, Department of Physics and Technology, University of Bergen, Bergen, Norway (2007).

[96] DIAB Group, "Divinycell H, Technical data", DIAB Group, Laholm, Sweden (2012).

[97] H. Fosså, "Ultrasound phantom for myocardium", Master thesis, University of Bergen, Bergen, Norway (2011).

[98] N. Bilaniuk and G. S. K. Wong, "Speed of sound in pure water as a function of temperature", J. Acoust. Soc. Am. **93**(3), 1609–1612 (1993).

[99] N. Bilaniuk and G. S. K. Wong, "Erratum: Speed of sound in pure water as a function of temperature [j. acoust. soc. am. [bold 93], 1609–1612 (1993)]", J. Acoust. Soc. Am. **99**(5), 3257–3257 (1996).

[100] Olympus, "Olympus Immersion Transducers - V309-SU", Olympus NDT Inc., Waltham, United States, URL adress: "http://www.olympus-ims.com/en/ultrasonic-transducers/immersion/", Last viewed: 04.06.2013.

[101] Hanna Instruments, "HI 98509 - Checktemp 1", Hanna Instruments, Woonsocket, RI, United States, URL adress: http://www.hannainst.com/manuals/manHI_98509_98510.pdf, Last viewed: 04.06.2013.

[102] S. Vervik, "Transitt-tidsbestemmelse for ultralyd strømningsmetre. nullstrømningsforhold", (in norwegian), University of Bergen, Department of Physics and Technology, Bergen, Norway (1995).

# Appendix A

# MATLAB-scripts

Here the MATLAB-scripts used for electrical measurements, acoustical measurements, and signal processing are included.

## A.1 Electrical measurements

The acoustical measurements are performed with the MATLAB-script `impanal.m`, based on a similarly named script found in [38].

### A.1.1 impanal.m

```
%%%%%%%%%%%%%%%%%%%%%%%%%%%%%%%%%%%%%%%%%%%%%%%%%%%%%%%%%%%%%%%%%%%%%%%%%%%%
% impanal.m
%
% Performs admittance measurements.
% Based on work by Magne Aanes.
%
% Rune Hauge and Eivind Mosland, 2012/2013
%%%%%%%%%%%%%%%%%%%%%%%%%%%%%%%%%%%%%%%%%%%%%%%%%%%%%%%%%%%%%%%%%%%%%%%%%%%%

% Find a GPIB object.
% Computer EXP 2
%obj1 = instrfind('Type', 'gpib', 'BoardIndex', 0, 'PrimaryAddress', 17, 'Tag', '');
% Computer EXP 3
obj1 = instrfind('Type', 'gpib', 'BoardIndex', 1, 'PrimaryAddress', 17, 'Tag', '');

% Create the GPIB object if it does not exist
% otherwise use the object that was found.
if isempty(obj1)
    % Computer EXP 2
    %obj1 = gpib('NI', 0, 17);
    % Computer EXP 3
    obj1 = gpib('NI', 1, 17);
else
    fclose(obj1);
    obj1 = obj1(1);
end

% Connect to instrument object, obj1.
fopen(obj1);

tic

% Enables parametric measurements, with respect to
% impedance analyzer drive voltage.
for amplitudes = 0.3;

    %%%%%%%%%%%%%%%%%%%%%%%%%%%%%%%%%%%%%%%%%%%%%%%%%%%%%%%%%%%%%%%%%%%%%%%%%%%%
    % Specify object, environmental parameters and
    % frequency
    elnr = 'TransducerNo1';
    dimensjon = '20x2mm';
    temp = '24,7';
    hr = '29,5'; %luftfuktighet [%]
    p = '1013'; % lufttrykk [hPa]
```

```
45
46      % Osc. level [V]
47      amplitude = amplitudes;
48
49      % Frequency vector 5, corresponding to
50      % acoustical measurements.
51      f = [50e3:500:88e3,...
52      88.1e3:100:114.9e3,...
53      115e3:500:200e3,...
54      200.5e3:500:236e3,...
55      236.1e3:100:255.9e3,...
56      256e3:500:300e3]./1e3;
57
58      %%%%%%%%%%%%%%%%%%%%%%%%%%%%%%%%%%%%%%%%%%%%%%%%%%%%%%%%%%%%
59      ol = sprintf('%3.3f',amplitude);
60      % Set impedance analyzer to admittance mode
61      fprintf(obj1, ['A2C3F1OL',ol,'EN']);
62
63      % Timestring on the format yyyymmddHHMMSS
64      time = datestr(now, 'yyyymmddHHMMSS');
65      % Filename
66      title = [elnr,'_',dimensjon,'_freq_frekvensoppsett5',...
67          '_',temp,'_',hr,'_',p,'_',time,'_',num2str(amplitudes*10)];
68
69      i = 1;
70      ii = 1;
71      antal = length(f);
72      g = ones(1,antal);
73      b = ones(1,antal);
74      fr = ones(1,antal);
75      disp([num2str(antal),' frequencies.'])
76      disp('Starting measurement...')
77      for freq = f
78          percent = i/antal*100;
79          if percent >= ii*10
80              disp([num2str(ii*10),' %'])
81              ii = ii + 1;
82          end
83
84          s = sprintf('%3.3f',freq);
85          fprintf(obj1, ['FR',s,'ENEX']);
86          pause(0.25)
87          data1 = fscanf(obj1);
88          d=sscanf(data1,'%4c%f,%4c%f,%2c%f');
89          g(i)=d(5);b(i)=d(10);fr(i)=d(13);
90          i = i + 1;
91      end
92      disp('Measurement finished.')
93      disp('Saving...')
94      save(title,'g','b','fr')
95      disp('Done!')
96      stoptime = datestr(now, 'yyyymmddHHMMSS');
97
98  end
99
100 toc
```

## A.2 Acoustical measurements

The acoustical measurements are performed with the MATLAB-script `main.m`, which loads `measurement_parameters.m` and calls several subscripts.

### A.2.1 main.m

```
1   %%%%%%%%%%%%%%%%%%%%%%%%%%%%%%%%%%%%%%%%%%%%%%%%%%%%%%%%%%%%%%%%%%%%%%%
2   % main.m
3   % Main software for acoustic measurements in air.
4   % Espen Storheim, 2011 (v1.0)
5   % Based on work by Vidar Knappskog and Magne Aanes.
6   %
7   % Rune Hauge and Eivind Mosland, 2012/2013 (v2.0)
8   %%%%%%%%%%%%%%%%%%%%%%%%%%%%%%%%%%%%%%%%%%%%%%%%%%%%%%%%%%%%%%%%%%%%%%%
9
10  %% Version number.
```

```
airversion = '2.0';

%% Add the subfolders to MATLABs path, just in case.
% Change folder names to exclude spaces.
if (isunix || ismac)
    addpath([pwd '/User input'])
    addpath([pwd '/Kernel'])
    addpath([pwd '/Instrument control etc']);
else
    addpath([pwd '\User input'])
    addpath([pwd '\Kernel'])
    addpath([pwd '\Instrument control etc']);
end

% Load information about the measurement about to be performed.
measurement_parameters

% Initialization of the instruments prior to measurements.
init_instruments

% Read the electrical signal.
ch = 2;

% Adjust scaling according to input voltage.
voltage_scaling = [0.02 0.05 0.1 0.2 0.5 1 2 5 10];
for ii = 1:(length(voltage_scaling));
    if (4*voltage_scaling(ii) >= meas.voltage_in)
        fprintf(instrument.scope,['CH2:SCA ' num2str(voltage_scaling(ii))]);
        break;
    end
end

disp('Starting measurements of the electrical pulses.')
for ii = 1:length(meas.f)

    % Adjust the burst length to ensure temporal resolution.
    t = 16*100e-6;
    %     t = 14*100e-6;
    %     t = 10*100e-6;

    % Number if cycles is adjusted according to the given frequency so that
    % the burst length equals 1.4 ms.
    disp([num2str(meas.f(ii)/1000) ' kHz'])
    fprintf(instrument.generator,['BM:NCYC ', num2str(floor(meas.f(ii)*t))]);
    fprintf(instrument.generator,['FREQ ', num2str(meas.f(ii))]);

    % Record environmental data.
    [Temp RH] = VaisalaHMT313(instrument.humidity);
    results.temp_electric(ii) = Temp;
    results.humidity_electric(ii) = RH;
    results.electric_time(ii,:) = clock;
    clear Temp RH

    % Adjust time window.
    adjustTime('electric',instrument,meas)

    % Stop aquisition.
    fprintf(instrument.scope,'ACQ:STATE STOP');
    % Wait to ensure that the scope wipes its memory.
    pause(1)
    % Start aquisition.
    fprintf(instrument.scope,'ACQ:STATE RUN');
    % Wait for averaging.
    pause(meas.wait_scaling)

    % Read and save.
    [dum1 dum2 dum3] = DPO_les(ch,instrument.scope);
    results.electric_t(ii,:) = dum1;
    results.electric(ii,:) = dum2;
    results.electric_timescale(ii) = dum3;
    results.electric_Vscale(ii) = ...
    str2num(query(instrument.scope,['CH',num2str(ch),':SCA?']));
    results.electric_Termination(ii) = ...
    str2num(query(instrument.scope,['CH',num2str(ch),':TER?']));
    clear dum1 dum2 dum3

```

```
end

disp(' ')
disp('Finished reading the electrical signal.)
disp('Now readjusting the scope and continuing to acoustic...')

% Read the acoustic pulses.
ch = 1;

disp('Starting measurements of the acoustical pulses.')
for ii = 1:length(meas.f);

    % Adjust the bandwidth of the KH-filter
    pause(0.1)
    % Set the cutoff frequency for channel 1. (Not working properly)
    fprintf(instrument.filter,['F' num2str((meas.f(ii)/1000)/2) 'K']);
    pause(0.1)
    % Set the cutoff frequency for channel 2.
    fprintf(instrument.filter,['F' num2str((meas.f(ii)/1000)*2) 'K']);

    % Adjust the burst length to ensure temporal resolution.
    t = 16*100e-6;
    %     t = 14*100e-6;
    %     t = 10*100e-6;

    % Number if cycles is adjusted according to the given frequency so that
    % the burst length equals 1.4 ms.
    disp([num2str(meas.f(ii)/1000) ' kHz'])
    fprintf(instrument.generator,['BM:NCYC ', num2str(floor(meas.f(ii)*t))]);
    fprintf(instrument.generator,['FREQ ', num2str(meas.f(ii))]);

    % Record environmental data.
    [Temp RH] = VaisalaHMT313(instrument.humidity);
    results.temp_acoustic(ii) = Temp;
    results.humidity_acoustic(ii) = RH;
    results.acoustic_time(ii,:) = clock;
    clear Temp RH

    % Adjust time window.
    adjustTime('acoustic',instrument,meas)

    % Adjust amplitude scaling and read out signal.
    [dum1 dum2 dum3] = adjustAmplitude(1,instrument,meas);

    results.acoustic_t(ii,:) = dum1;
    results.acoustic(ii,:) = dum2';
    results.acoustic_timescale(ii) = dum3;
    results.acoustic_Vscale(ii) = ...
    str2num(query(instrument.scope,['CH',num2str(ch),':SCA?']));
    results.acoustic_Termination(ii) = ...
    str2num(query(instrument.scope,['CH',num2str(ch),':TER?']));
    clear dum1 dum2 dum3

end

%% Storing data

results.electric_f = meas.f;
results.acoustic_f = meas.f;

xx = strcat(meas.name,'_',datestr(now,'yyyymmddHHMMSS'));
save(xx,'results', 'meas', 'instrument');

%% Finishing touches.
% Close the instrument ports and clear device handles.
instrument_shutdown
```

### A.2.2 measurement_parameters.m

```
%%%%%%%%%%%%%%%%%%%%%%%%%%%%%%%%%%%%%%%%%%%%%%%%%%%%%%%%%%%%%%%%%%%%%%%%%%%%
% measurement_parameters.m
% Information about the calibration of the measurement microphone.
% Part of the software for acoustic measurements in air.
% Espen Storheim, 2011
% Based on work by Vidar Knappskog and Magne Aanes.
%
```

```
% Modified by Rune Hauge and Eivind Mosland, 2012/2013
%%%%%%%%%%%%%%%%%%%%%%%%%%%%%%%%%%%%%%%%%%%%%%%%%%%%%%%%%%%%%%%%%%%%%%%%%%%

% This file is designed to be tampered with prior to each measurement.

%% Define initial bandpass filter low and high cutoff frequency
meas.cutoff_1 = 20; % kHz
meas.cutoff_2 = 300; % kHz
% At present, cutoff_2 is adjusted for each measurement frequency in
% main.m. This is currently not done for cutoff_1.

%% General measurement info.
% Version of this software which was used to make the measurements.
% Should be taken from elsewhere.
% meas.version = 'Updated 20/7-2011.';

% Name of the person performing the measurement and date.
meas.name = '200,5kHzto300kHz_2Vpp';
TT = clock;
meas.date = [date ', ' num2str(TT(4)) ':' num2str(TT(5))];
clear TT

% Information about the transmitting transducer.
meas.source = 'Pz27 disk, D = 20.0 mm, T = 2.0 mm, Element No. 16 in batch 9/12.';

% Information about the receiving transducer.
meas.receiver = 'Pz27 disk, D = 20.0 mm, T = 2.0 mm, Element No. 6 in batch 9/12.';

% Additional notes regarding the specific simulation.
meas.notes = 'Elm 16 til elm 6.';

%% Distance from transmitter.
meas.distance = 0.77;
%meas.z

%% Frequency information [Hz]

% Frekvensoppsett 50-200 kHz elm 16 til elm 10.
meas.f = [50e3 100e3];

% meas.f = frequencies;

% meas.f = [50e3:500:88e3,...
%     88.1e3:100:114.9e3,...
%     115e3:500:236e3,...
%     236.1e3:100:255.9e3,...
%     256e3:500:300e3];

%% Input waveform data.
% Peak voltage out from the signal generator [V]
meas.voltage_in = 1;
% Number of periods in each burst [-]
% Only used in initialization of the generator. In main.m the number of
% cycles is adjusted to fit a certain burst length [ms] specified therein.
meas.cycles = 40;
meas.burst_cycles = meas.cycles;
% Burst repetition rate [Hz]
meas.burst_period = 40e-3;
meas.burst_rate = 1/meas.burst_period;

% Approximate time before the signal is steady after a voltage scaling change.
 meas.wait_scaling = 7;

% A note on the input voltage: The signal generator claims that the voltage
% specified above is the peak to peak voltage. This is the case when the
% generator is connected to a 50 Ohm load. However, the transmitting
% transducer typically has an electrical impedance in the kilo Ohm range and
% is connected directly to the generator. This causes a voltage division which
% depends of the impedance of the transducer, and hence an impedance mismatch.

%% Oscilloscope parameters.
% Number of pulses which the signal is averaged.
meas.average = 128;
% Number of data points recorded by the scope.
meas.samples = 1e5;
% Channel used for measurements.
```

```
%meas.channel = 1;

% Channel number where the signal generator is connected.
meas.channel_electrical = 1;
% Channel number where the oscilloscope is connected.
meas.channel_acoustical = 2;

%% Distance from transmitter to receiver [m].
%meas.distance = meas.z;

%% Total input gain in the B&K 2636 measurement amplifier [dB].
% Only recorded for later reference. Must be set manually.
meas.gain_in = 40;
meas.gain_out = 20;
meas.gain = meas.gain_in + meas.gain_out;
```

### A.2.3 init_instruments.m

```
%%%%%%%%%%%%%%%%%%%%%%%%%%%%%%%%%%%%%%%%%%%%%%%%%%%%%%%%%%%%%%%%%%%%%%%%%%%%
% init_instruments.m
% Initialize the instruments according to measurement_parameters
% Part of the software for acoustic measurements in air.
% Espen Storheim, 2011
% Based on work by Vidar Knappskog and Magne Aanes.
%%%%%%%%%%%%%%%%%%%%%%%%%%%%%%%%%%%%%%%%%%%%%%%%%%%%%%%%%%%%%%%%%%%%%%%%%%%%

% This script is used to initialize the instruments to the proper settings.
% Most of the values are taken from the "meas" structure specified by the
% user in the m-file "measurement_parameters.m".

instruments;

%% Initialize the oscilloscope.
% Code for the Tektronix DPO3012.
if strcmp(instrument.scope_name, 'Tektronix␣DPO3012.␣S/N:␣')
    % Set the acquisition mode to averaging.
    fprintf(instrument.scope,'ACQ:MOD␣AVE');
    % Set the number of cycles to average.
    fprintf(instrument.scope,['ACQ:NUMAV␣' num2str(meas.average)]);
    % Number of points which shall be read from the scope.
    fprintf(instrument.scope,['HOR:RECO␣' num2str(meas.samples)]);
    % Start point for the recorded signal
    fprintf(instrument.scope,'DAT:START␣1');
    % Stop point for the recorded signal
    fprintf(instrument.scope,['DAT:STOP␣' num2str(meas.samples)]);
    % Trigger specifications. Set to edge detection from external source.
    fprintf(instrument.scope,'TRIG:A:EDGE:SOU␣EXT');
    % Set the trigger type to positive edge.
    fprintf(instrument.scope,'TRIG:A:TYP␣EDG');
    % 2012.11.19 EM: Added additional initialization.
    % CH1
    % Set Offset to zero.
    fprintf(instrument.scope,'CH1:OFFS␣0');
    % Set position to zero.
    fprintf(instrument.scope,'CH1:POS␣0');
    % Set coupling to AC.
    fprintf(instrument.scope,'CH1:COUP␣AC');
    % CH2
    % Set Offset to zero.
    fprintf(instrument.scope,'CH2:OFFS␣0');
    % Set position to zero.
    fprintf(instrument.scope,'CH2:POS␣0');
    % Set coupling to AC.
    fprintf(instrument.scope,'CH2:COUP␣AC');
end

%% Initialize the bandpass filter.
% Code for Krohn-Hite 3940A filter.
if strcmp(instrument.filter_name, 'Krohn-Hite␣3940A.␣S/N:␣AM2626')
    % There seems to be an overflow when the commands are combined, so they
    % have been separated and a pause of 100 ms is set between each
    % command.
    %
    % Set the input and output gain on both channels to 0 dB.
    pause(0.1)
    fprintf(instrument.filter,'AL;0IG;0OG;B');
```

```
    pause(0.1)
    % Set channel 1 to high pass mode.
    fprintf(instrument.filter,'CH1.1;M2');
    pause(0.1)
    % Set the cutoff frequency for channel 1.
    fprintf(instrument.filter,['F' num2str(meas.cutoff_1) 'K']);
    pause(0.1)
    % Set channel 2 to low pass mode.
    fprintf(instrument.filter,'CH1.2;M1');
    pause(0.1)
    % Set the cutoff frequency for channel 2.
    fprintf(instrument.filter,['F' num2str(meas.cutoff_2) 'K']);
end

%% Initialize the signal generator.
% This code is for the Agilent 33*** series signal generators
if strcmp(instrument.generator_name, 'Agilent␣33220A.␣S/N:␣')
    fprintf(instrument.generator,'OUTP␣OFF');
    fprintf(instrument.generator,['APPL:SIN␣' num2str(meas.f(1)) ...
    '␣HZ,␣' num2str(meas.voltage_in) '␣VPP']);
    % Set the trigger to internal and positive slope.
    fprintf(instrument.generator,'TRIG:SOUR␣IMM');
    fprintf(instrument.generator,'TRIG:SLOP␣POS');
    % Set the number of periods in one burst.
    fprintf(instrument.generator,['BURS:NCYC␣' num2str(meas.burst_cycles)]);
    fprintf(instrument.generator,'BURS:STAT␣ON');
    % Set the burst rate, i.e. the frequency of the bursts.
    fprintf(instrument.generator,['BM:INT:RATE␣' num2str(meas.burst_rate)]);
    % Set the peak voltage.
    fprintf(instrument.generator,['VOLT␣' num2str(meas.voltage_in(1))]);
    % Activate the output.
    fprintf(instrument.generator,'TRIG:SLOP␣POS');
    fprintf(instrument.generator,'OUTP␣ON');
end
```

### A.2.4 instruments.m

```
%%%%%%%%%%%%%%%%%%%%%%%%%%%%%%%%%%%%%%%%%%%%%%%%%%%%%%%%%%%%%%%%%%%%%%%%%%%%
% Instruments.m
% Part of the software for acoustic measurements in air.
% Espen Storheim, 2011
% Based on work by Vidar Knappskog and Magne Aanes.
%%%%%%%%%%%%%%%%%%%%%%%%%%%%%%%%%%%%%%%%%%%%%%%%%%%%%%%%%%%%%%%%%%%%%%%%%%%%

% Initialization of the instrumens used in the measurement setup for air.
% Contains MATLAB-handles for the instruments used in the setup, both GPIB,
% serial, and the special functions used by the PI positioning equipment.
%
% This file contains information about many devices in the laboratory, many
% that are not in use on the setup for measurements in air. These are by
% default commented out in the code.
%
% Comment out instruments not in use!
%
% Notes about future updates.
% - Include a test to check for acoustic or impedance measurements.
% - Remove the _idn parameter since there is no common response.

instrument = {};

%% Signal generators.

% Signal Generator: Agilent 33220A. S/N:
%instrument.generator = gpib('find','DEV10');

instrument.generator = gpib('ni',0,10);
% fopen(instrument.generator)

% 14.09.2012 Rune Hauge: Include 'instrfind' for locating a GPIB object
% instrument.generator = instrfind('Type', 'gpib', 'BoardIndex', 0, ...
% 'PrimaryAddress', 10, 'Tag', '');

% if isempty(instrument.generator)
%     instrument.generator = gpib('NI', 0, 10);
% else
%     fclose(instrument.generator);
```

```
%     instrument.generator = instrument.generator(1);
% end

fopen(instrument.generator);

instrument.generator_name = 'Agilent 33220A. S/N: ';
instrument.generator_idn = query(instrument.generator,'*IDN?');

% Test the connection. Should be a command where the response can be
% verified.
if isempty(instrument.generator_idn)
    disp('Warning: The signal generator is not connected or configured properly.')
else
    disp('The signal generator is connected and appears to be working.')
end

%% Oscilloscopes.

% Digital oscilloscope: Tektronix DPO3012. S/N:
%instrument.scope =  gpib('ni',0,2);

% 14.09.2012 Rune Hauge: Include 'instrfind' for locating a GPIB object
instrument.scope = instrfind('Type', 'visa-usb', 'RsrcName', ...
'USB0::0x0699::0x0410::C010246::0::INSTR', 'Tag', '');

if isempty(instrument.scope)
    % Our oscilloscope
    instrument.scope = visa('NI', 'USB0::0x0699::0x0410::C010246::0::INSTR');
    % Magne Aanes's oscilloscope
    % instrument.scope = visa('NI', 'USB0::0x0699::0x0410::C011044::0::INSTR');
else
    fclose(instrument.scope);
    instrument.scope = instrument.scope(1);
end
% 20.09.2012 Rune Hauge: Set scope InputBufferSize to high enough value.
% Trying 1000000.
instrument.scope.InputBufferSize = 2000000;

fopen(instrument.scope)
instrument.scope_name = 'Tektronix DPO3012. S/N: ';
instrument.scope_idn = query(instrument.scope,'*IDN?');

% Old oscilloscope: LeCroy ###. S/N:

% Test the connection. Should be a command where the response can be
% verified.
if isempty(instrument.scope_idn)
    disp('Warning: The oscilloscope is not connected or configured properly.')
else
    disp('The oscilloscope is connected and appears to be working.')
end

%% Environmental parameters.

% % Temperature sensor: ASL F250. S/N:
% %instrument.temperature = gpib('ni',0,3);
% % 14.09.2012 Rune Hauge: Include 'instrfind' for locating a GPIB object
% instrument.temperature = instrfind('Type', 'gpib', 'BoardIndex', 0, ...
% 'PrimaryAddress', 3, 'Tag', '');
%
% if isempty(instrument.temperature)
%     instrument.temperature = gpib('NI', 0, 3);
% else
%     fclose(instrument.temperature);
%     instrument.temperature = instrument.temperature(1);
% end
% fopen(instrument.temperature)
% set(instrument.temperature,'EOSmode','read&write');
% set(instrument.temperature,'EOSCharCode',10); % Set terminator to LF.
% instrument.temperature_name = 'ASL F250 mk II. S/N: ';
% fprintf(instrument.temperature,'A0');
% instrument.temperature_idn = fscanf(instrument.temperature);

% % Test the connection. Should be a command where the response can be
% % verified.
% if isempty(instrument.temperature_idn)
```

```
%     disp('Warning: The thermometer is not connected or configured properly.')
% else
%     disp('The thermometer is connected and appears to be working.')
% end

% Pressure sensor: Paroscientific DigiQuartz 740. S/N:
%instrument.pressure = serial('COM2','Baudrate',4800,'Terminator', ...
%'cr','Databit',7,'Parity','even');;
instrument.pressure_name = 'Paroscientific DigiQuartz 740. S/N:';

% Relative humidity and temperature sensor: Vaisala HMT313. S/N:
instrument.humidity = serial('COM5','Baudrate',4800,'Terminator','cr',...
'Databit',7,'Parity','even');
instrument.humidity_name = 'Vaisala HMT313. S/N:';
fopen(instrument.humidity);


%% Signal processing.

% Bandpass filter: Krohn-Hite 3940A. S/N: AM2626.
%instrument.filter = gpib('ni',0,25);
% 14.09.2012 Rune Hauge: Include 'instrfind' for locating a GPIB object
instrument.filter = instrfind('Type', 'gpib', 'BoardIndex', 0, ...
'PrimaryAddress', 25, 'Tag', '');

if isempty(instrument.filter)
    instrument.filter = gpib('NI', 0, 25);
else
    fclose(instrument.filter);
    instrument.filter = instrument.filter(1);
end
fopen(instrument.filter)
instrument.filter_name = 'Krohn-Hite 3940A. S/N: AM2626';
instrument.filter_idn = query(instrument.filter,'*IDN?');


%% Impedance analyzer.

% Impedance analyzer: HP 4192 LF. S/N:
%instrument.impedance = gpib('find','DEV17');
%instrument.impedance_name = 'HP 4192 LF. S/N:';

% Impedance analyzer: Agilent 4294A. S/N:
%instrument.impedance2 = gpib('find','DEV17');
%instrument.impedance2_name = 'Agilent 4194A. S/N:';


%% Positioning equipment.
% Controlling the stages with MATLAB is not possible at present.

% Rotational stage: PI M-037

% Linear stage, horizontal: PI M-531

% Linear stage, vertical: PI M-535
```

### A.2.5 adjustAmplitude.m

```
%%%%%%%%%%%%%%%%%%%%%%%%%%%%%%%%%%%%%%%%%%%%%%%%%%%%%%%%%%%%%%%%%%%%%%%%%%%%
% adjustAmplitude.m
%
% [x wf timeDiv] = adjustAmplitude(ch,instrument,meas)
%
% Adjusts voltage scaling and records acoustic data.
%
% Rune Hauge & Eivind Mosland, 2012
%%%%%%%%%%%%%%%%%%%%%%%%%%%%%%%%%%%%%%%%%%%%%%%%%%%%%%%%%%%%%%%%%%%%%%%%%%%%

function [x wf timeDiv] = adjustAmplitude(ch,instrument,meas)

% Stop aquisition.
fprintf(instrument.scope,'ACQ:STATE STOP');
% Wait to ensure that the scope wipes its memory.
pause(1)
% Start aquisition.
fprintf(instrument.scope,'ACQ:STATE RUN');
```

```
% Wait for averaging.
pause(meas.wait_scaling)

% Read waveform.
[x wf timeDiv] = DPO_les(ch,instrument.scope);
maxV = max(wf);

% Get current scaling.
Scaling = str2num(query(instrument.scope,['CH',num2str(ch),':SCA?']));

% A minimum scaling of 10 mV/div is used to ensure that the noise prior to
% averaging is within the voltage range.
verticalScalings = [10e-3, 20e-3, 50e-3, 100e-3, 200e-3, 500e-3 1 2];
ind = find(Scaling==verticalScalings);
if isempty(ind)
    disp('ind er tom!')
    ind = 1;
    fprintf(instrument.scope,['CH',num2str(ch),':SCA ',num2str(verticalScalings(ind))]);

    [x wf timeDiv] = DPO_les(ch,instrument.scope);
    maxV = max(wf);
end

% Half the number of vertical division. 8 visible divisons on the screen
% and one additional above and below.
scrnRows = 5;

% Adjust vertical scaling and measure until no clipping.
finished = 0;
while ~finished
    %disp(['Current volt/div: ',num2str(verticalScalings(ind))])
    if maxV >= scrnRows*verticalScalings(ind)
        Scaling = verticalScalings(ind+1);
        fprintf(instrument.scope,['CH',num2str(ch),':SCA ',num2str(Scaling)]);
        ind = ind +1;

        % Wait for averaging to finish.
        pause(meas.wait_scaling)

        %disp('Measuring')
        [x wf timeDiv] = DPO_les(ch,instrument.scope);
        maxV = max(wf);

    elseif ind ~= 1 && maxV < scrnRows*verticalScalings(ind-1)
        %disp('Decreasing scaling')
        Scaling = verticalScalings(ind-1);
        fprintf(instrument.scope,['CH',num2str(ch),':SCA ',num2str(Scaling)]);
        ind = ind -1;

        % Wait for averaging to finish.
        pause(meas.wait_scaling)

        %disp('Measuring')
        [x wf timeDiv] = DPO_les(ch,instrument.scope);
        maxV = max(wf);
    else
        finished = 1;
    end
end

end
```

### A.2.6 adjustTime.m

```
%%%%%%%%%%%%%%%%%%%%%%%%%%%%%%%%%%%%%%%%%%%%%%%%%%%%%%%%%%%%%%%%%%%%%%%%%%%%
% adjustTime.m
%
% adjustTime(type,instrument,meas)
%
% Sets time scaling and adjusts window position.
%
% Rune Hauge & Eivind Mosland, 2012/2013
%%%%%%%%%%%%%%%%%%%%%%%%%%%%%%%%%%%%%%%%%%%%%%%%%%%%%%%%%%%%%%%%%%%%%%%%%%%%

function adjustTime(type,instrument,meas)
    import instrument
```

```
13
14      % Set scaling.
15      if ~strcmp(type,'noise')
16
17          % Get frequeny and number of cycles.
18          freq = query(instrument.generator,'FREQ?');
19          cycles = query(instrument.generator,'BURS:NCYC?');
20          % Compute appropriate scaling.
21          SignalLength = 1/str2num(freq)*str2num(cycles);
22          minScaling = SignalLength/10;
23
24          if minScaling <= 40e-6
25              Scaling = 40e-6;
26          elseif minScaling <= 100e-6
27              Scaling = 100e-6;
28          elseif minScaling <= 200e-6
29              Scaling = 200e-6;
30          elseif minScaling <= 400e-6
31              Scaling = 400e-6;
32          elseif minScaling <= 1e-3
33              Scaling = 1e-3;
34          end
35
36          % disp(['Desired scaling found to be ',num2str(Scaling),...
37          % ' Adjusting scope...'])
38          fprintf(instrument.scope,['HOR:SCA ',num2str(Scaling)]);
39      else
40          noise_Scaling = 40e-6;
41          fprintf(instrument.scope,['HOR:SCA ',num2str(noise_Scaling)]);
42      end
43
44      % Set window position.
45      if strcmp(type,'electric')
46          triggerDelay = Scaling*5;
47      elseif strcmp(type,'acoustic')
48          % Ensures that the onset of the acoustic signal is recorded.
49          triggerDelay = Scaling*5 + (meas.distance-0.01)/343;
50      elseif strcmp(type,'noise')
51          triggerDelay = (meas.distance+0.002)/343 - noise_Scaling*5;
52      end
53      fprintf(instrument.scope,['HOR:DEL:TIM ',num2str(triggerDelay)]);
54  end
```

### A.2.7 DPO_les.m

```
1   %%%%%%%%%%%%%%%%%%%%%%%%%%%%%%%%%%%%%%%%%%%%%%%%%%%%%%%%%%%%%%%%%%%%%%%%%%%%
2   % DPO_les.m
3   %
4   % function [x,wf,tidsskala] = DPO_les(ch,scope)
5   % Script that communicates with Tektronix DPO3012
6   % 8-bit unsigned characters. Windows version.
7   %
8   % Espen Storheim
9   %%%%%%%%%%%%%%%%%%%%%%%%%%%%%%%%%%%%%%%%%%%%%%%%%%%%%%%%%%%%%%%%%%%%%%%%%%%%
10
11  function [x,wf,tidsskala] = DPO_les(ch,scope)
12
13      fprintf(scope,'HOR:RECO 100000');
14
15      fprintf(scope,'DAT:SOUR CH1');
16      fprintf(scope,'DAT:START 1');
17      fprintf(scope,['DAT:STOP ' num2str(100000)]);
18
19      % Gating mode {SCREEN | CURSOR | NON}. Horizontal.
20      fprintf(scope,'SAV:WAVE:GATI NON');
21      fprintf(scope,['DAT:SOUR REF1']);
22      fprintf(scope,['SAV:WAVE CH' num2str(ch) ',REF1']);
23      pause(5);
24      fprintf(scope,['DAT:SOUR CH' num2str(ch)]);
25
26      fprintf(scope,'WFMO:XZE?');
27      xze = fscanf(scope,'%f');
28
29      fprintf(scope,'WFMO:XIN?');
30      xin = fscanf(scope,'%f');
31
```

```
    fprintf(scope,'WFMO:YOF?');
    YOF = fscanf(scope,'%f');

    fprintf(scope,'WFMO:YMU?');
    YMU = fscanf(scope,'%f');

    fprintf(scope,'WFMO:YZE?');
    YZE = fscanf(scope,'%f');

    fprintf(scope,['DAT:SOUR␣REF1']);

    fprintf(scope,'CURV?');

    b = fread(scope,100000,'int8');
    %disp('Finished reading')
    %%%wf = b(8:end-1);
    %x = xze:xin:(xze+9999*xin);
    %x = linspace(xze,100000*xze,length(wf));
    %wf = ((wf-YOF)*YMU) + YZE;

    fprintf(scope,'HOR:SCA?');
    tidsskala = fscanf(scope,'%f');

    wf = b(9:end-1);
    x = xze:xin:(xze+(length(wf)-1)*xin);

    wf = ((wf-YOF)*YMU) + YZE;
end
```

### A.2.8 instrument_shutdown.m

```
%%%%%%%%%%%%%%%%%%%%%%%%%%%%%%%%%%%%%%%%%%%%%%%%%%%%%%%%%%%%%%%%%%%%%%%%%%%%
% instrument_shutdown.m
%
% Shut down the instruments and clean up.
% Part of the software for the new measurement setup in air.
%
% Espen Storheim, 11/09-2012.
%%%%%%%%%%%%%%%%%%%%%%%%%%%%%%%%%%%%%%%%%%%%%%%%%%%%%%%%%%%%%%%%%%%%%%%%%%%%

% Close all the handles used for communication with the various
% instruments.

fclose(instrument.humidity)
%fclose(instrument.temperature)
%fclose(instrument.pressure)
fclose(instrument.generator)
fclose(instrument.scope)
fclose(instrument.filter)

delete(instrfindall)
```

### A.2.9 VaisalaHMT313.m

```
% VaisalaHMT313.m
% Script which reads the temperature and relative humidity from the Vaisala
% HMT313 temperature/humidity sensor. It uses serial communication.
% Warning! This script only works on Windows at present.
% There are two different operational modes:
% - 'single', used to do a spot reading. Warning: The command
% delete(instrfindall) is executed every time to delete existing instrument
% handles and prevent overflow.
% - 'cont', used for continuous reading. This requires the port handle s to
% be initialized in an external script.
%
% Espen Storheim, 18/05-2011
% function [T,RH] = VaisalaHMT313

function [T, RH] = VaisalaHMT313(handle)
    fprintf(handle,'send');
    a = fscanf(handle,'%f%f');
    %a = fscanf(handle);
    %a = strread(a,'%s',2);
    T = a(2);
    RH = a(1);
end
```

## A.3 Signal processing

In this section the essential MATLAB-scripts used in the signal processing of the recorded signals are given.

### A.3.1 Khimunin_diffractioncorrection.m

```
% Khimunin_diffractioncorrection.
%
% Calculate the diffraction correction for uniformly vibrating piston in a
% rigid baffle of infinite extent according to the expression given by Khimunin
% in A. S. Khimunin, "Numerical calculation of the diffraction corrections
% for the precise measurement of ultrasound absorption", Acustica 27(4),
% 173-181 (1972).
%
% There is a slight modification in the present script compared to the
% article. The output here is K = |p/p0| = A + iB, while the "output" in
% the article is |p/p0| = sqrt(A^2 + B^2). This allows the user to
% calculate both the magnitude and phase.
%
% Note: This version is limited to a fixed axial distance, z.
%
% Input variables:
% k : The wavenumber.
% a : The radius of the piston.
% z : The axial distance.
% N : Number of trapezoids in the numerical integration. 1000 is typically OK.
%
% Output variables:
% K : The complex diffraction correction.
%
% Espen Storheim (2009-2012).

function K = Khimunin_diffractioncorrection(k,a,z,N)

theta = pi*[0:1:N]/(2*N);    % Khimunins integration variable.
S = z/a^2*2*pi./k;           % Scaled axial distance.
ka = k*a;                    % ka number.

% Calculate the diffraction correction for the frequencies specified.
for ii = 1:length(ka)

    % Calculate the integrand for C and D in Eq. (3).
    CC = cos(sqrt(S(ii)^2*ka(ii)^4/(2*pi)^2 + 4*ka(ii)^2.*...
    (cos(theta)).^2)).*(sin(theta)).^2;
    DD = sin(sqrt(S(ii)^2*ka(ii)^4/(2*pi)^2 + 4*ka(ii)^2.*...
    (cos(theta)).^2)).*(sin(theta)).^2;

    % Numerical integration of C and D with the trapezoidal rule.
    C = theta(2)*(sum(CC(1:end)) - 0.5*(CC(1) + CC(end)));
    D = theta(2)*(sum(DD(1:end)) - 0.5*(DD(1) + DD(end)));

    % Calculate the real and imaginary part of the diffraction
    % correction.
    A = 1 - C*4/pi*cos(ka(ii)^2*S(ii)/(2*pi)) - D*4/pi*sin(ka(ii)^2*S(ii)/(2*pi));
    B = D*4/pi*cos(ka(ii)^2*S(ii)/(2*pi)) - C*4/pi*sin(ka(ii)^2*S(ii)/(2*pi));
    KK = A + 1i*B;

    % Store the complex diffraction correction for each ka number.
    K(ii) = KK;

    % Clear temp variables.
    clear CC DD C D A B

end

end
```

### A.3.2 absorpsjonluft.m

```
function korr_trykk = absorbsjonluft(frekvens,trykk,fukt,temp )

%Vidar Knappskog 2007
%Programmet regner ut absorbsjonskoeffisienten for hver frekvens
```

```
f=frekvens;
p=trykk;
h_rel=fukt;
T=temp;

%f=10000;                %Frekvens
%p=101.325;              %Atmosfaeretrykket
%h_rel=50;               %Relativ luftfuktighet
%T=253.15;               %Temperatur i Kelvin


T_01=273.16;     %Trippelpunkts isotermisk temperatur(0.01C)
p_ref=101.325;   % Referansetrykket i kPa( 1atm)
T_ref=293.15;    %Referanse temperatur Kelvin.(20 deg C)

%Finner foerst den molare konsentrasjonen av vann i luften
V=10.79586*(1-(T_01/T))-5.02808.*log10(T/T_01)+1.50474*...
    (10^-4)*(1-10^(-8.29692*(T/T_01-1)))+0.42873*(10^-3)*...
    (-1+10^(4.76955*(1-T_01/T)))-2.2195983;

h=h_rel*(10^V)*(p/p_ref)^-1;     %Molare luftfuktighet

%Relaksasjons frekvens for Oksygen
f_r0=(p/p_ref)*(24 + ((4.04*(10^4)*h)*(0.02+h)/(0.391+h)));

%Relaksasjonsfrekvensen for Nitrogen
f_rN=(p/p_ref)*(T/T_ref)^(-0.5)*(9+280*h*exp(-4.170*...
    ((T/T_ref)^(-1/3)-1)));

%Dempningskoeffisient
alfa=8.686*f^2*( (1.84*(10^-11)*(p/p_ref)^-1*...
    (T/T_ref)^(0.5))+ (T/T_ref)^(-5/2)*...
    (0.01275*(exp(-2239.1/T))*(f_r0/(f_r0^2+f^2))...
    + 0.1068*exp(-3352/T)*(f_rN/(f_rN^2+f^2))));

% Absorbsjon i dB/km
korr_trykk=alfa*1000;
```

### A.3.3 findPeakToPeak.m

```
% findPeakToPeak
%
% function peakToPeak = findPeakToPeak
%                   (signal,signal_f,sample_rate,l_lim,u_lim)
%
% Rune Hauge, 2012/2013

function peakToPeak = findPeakToPeak
                    (signal,signal_f,sample_rate,l_lim,u_lim)
    %% Acquire peak-to-peak values of the steady-state intervals
    signal = signal(:,l_lim:u_lim);

    for nn = 1:length(signal(:,1))
        %disp(['Freq: ',num2str(signal_f(nn))])
        zero = mean(signal(nn,:));
        cross = zero-signal(nn,:);
        found = find((sign(cross(2:end))-sign(cross(1:end-1)))==2 |...
            (sign(cross(2:end))-sign(cross(1:end-1)))==-2);
        samples = found(1);
        % Found first zero-cross, now continuing find the voltage
        % peak-to-peak on each periode

        step = round(1/signal_f(nn)*sample_rate(nn));

        ii = 1;
        while samples+step<length(signal(nn,:))
            maximum = max(signal(nn,samples:samples+step));
            minimum = min(signal(nn,samples:samples+step));
            peakToPeak_freq(ii) = (maximum-minimum);
            ii = ii + 1;
            samples = samples + step;
        end

        peakToPeak(nn) = mean(peakToPeak_freq);

    end
```

```
end
```

### A.3.4 findpeakToPeak_FFT.m

```
% findpeakToPeak_FFT
%
% Rune Hauge, 2013

function pp_FFT = findPeakToPeak_FFT
                (V_out,V_out_f,sample_rate,l_lim_ac,u_lim_ac)

    % Voltage out (acoustical signal) FFT
    signal = V_out(:,l_lim_ac:u_lim_ac);

    for nn = 1:length(signal(:,1))
        N = 2e5;
        Fs = sample_rate;
        sigL = length(signal(nn,:));
        sig_spect = fft(signal(nn,:),N)*2/sigL;
        sig_spect = fftshift(sig_spect);
        ff = -Fs/2:Fs/N:Fs/2-Fs/N;
        % Interpolate the measured frequencies upon the FFT spectra
        start = find(ff==0);
        stop = find(ff==V_out_f(end));
        spect_meas = interp1(ff(start:stop), ...
                        sig_spect(start:stop),V_out_f);
        pp_FFT(nn) = 2*abs(spect_meas(nn));
    end

end
```

### A.3.5 threeTransducerCalibration.m

```
% function res = threeTransducerCalibration(type,init)
%
% Eivind Mosland 2013

function res = threeTransducerCalibration(type,init)

%% Set reference distance, d_0
res.d_0 = 1;

%% Calculate Hvv_15 for measurement no. 1, T1 to T2
if strcmp(type,'piezo')
    [res.d_1 res.Hvv_15_1 res.f_1 res.TwoTrans_1] = ...
        calculateHvv(init.T1toT2_file, init, init.Y_T2_file, ...
        init.Y_T1_file, init.radius_T1);
elseif strcmp(type,'mic')
    tmp1 = init.l_lim_ac; tmp2 = init.u_lim_ac; tmp3 = ...
                init.l_lim_el; tmp4 = init.u_lim_el;
    %init.l_lim_ac = 50e3;init.u_lim_ac = 95e3;init.l_lim_el = ...
    % 50e3;init.u_lim_el = 95e3; % Elm to Mic
    init.l_lim_ac = 45e3;init.u_lim_ac = 68e3; % Trans to Mic
    init.l_lim_el = 45e3;init.u_lim_el = 68e3; % Trans to Mic
    [res.d_1 res.Hvv_15_1 res.f_1] = ...
        calculateHvvMic(init.T1toT2_file, init, init.Y_T1_file);
    init.l_lim_ac = tmp1; init.u_lim_ac = tmp2;
    init.l_lim_el = tmp3; init.u_lim_el = tmp4;
end

%% Calculate Hvv_15 for measurement no. 2, T1 to T3

[res.d_2 res.Hvv_15_2 res.f_2 res.TwoTrans_2] = ...
    calculateHvv(init.T1toT3_file, init, init.Y_T3_file, ...
    init.Y_T1_file, init.radius_T1);

%% Calculate Hvv_15 for measurement no. 3, T3 to T2

if strcmp(type,'piezo')
    [res.d_3 res.Hvv_15_3 res.f_3 res.TwoTrans_3] = ...
        calculateHvv(init.T3toT2_file, init, init.Y_T2_file, ...
        init.Y_T3_file, init.radius_T3);
elseif strcmp(type,'mic')
    tmp1 = init.l_lim_ac; tmp2 = init.u_lim_ac;
    tmp3 = init.l_lim_el; tmp4 = init.u_lim_el;
    %init.l_lim_ac = 50e3;init.u_lim_ac = 95e3; % Elm to Mic
```

```
    %init.l_lim_el = 50e3;init.u_lim_el = 95e3; % Elm to Mic
    init.l_lim_ac = 45e3;init.u_lim_ac = 68e3; % Trans to Mic
    init.l_lim_el = 45e3;init.u_lim_el = 68e3; % Trans to Mic
    [res.d_3 res.Hvv_15_3 res.f_3] = ...
        calculateHvvMic(init.T3toT2_file, init, init.Y_T3_file);
    init.l_lim_ac = tmp1; init.u_lim_ac = tmp2;
    init.l_lim_el = tmp3; init.u_lim_el = tmp4;
end

%% Calculate impedances

res.Z_T3 = 1 ./ calculateY(res.f_2,init.Y_T3_file);

if strcmp(type,'piezo')
    res.Z_T1 = 1 ./ calculateY(res.f_2,init.Y_T1_file);
    res.Z_T2 = 1 ./ calculateY(res.f_2,init.Y_T2_file);
end

%% Interpolation, if microphone calibration

if strcmp(type,'piezo')
    if isequal(res.f_1,res.f_2,res.f_3)
        res.f = res.f_1;
        res = rmfield(res,{'f_1','f_2','f_3'});
    else
        disp('The frequency vectors are not equal!')
        figure;
        plot(res.f_1,'b')
        hold on
        plot(res.f_2,'r')
        plot(res.f_3,'g')
    end
else
    res.f = res.f_1;
    res.Hvv_15_2 = interp1(res.f_2,res.Hvv_15_2,res.f,'linear');
    res.Z_T3 = interp1(res.f_2,res.Z_T3,res.f,'linear');
    res = rmfield(res,{'f_1','f_2','f_3'});
end

%% Determine the lossless spherical wave reciprocity parameter
res.J = calculateJ(res.f);

%% Calculate free-field open-circuit receiving voltage response

res.Mv_T2 = sqrt( res.J.*res.Z_T3 .* res.Hvv_15_1.*res.Hvv_15_3./ ...
    res.Hvv_15_2 * res.d_1*res.d_3/(res.d_0*res.d_2) );
res.Mv_T3 = sqrt( res.J.*res.Z_T3 .* res.Hvv_15_2.*res.Hvv_15_3./ ...
    res.Hvv_15_1 * res.d_2*res.d_3/(res.d_0*res.d_1) );

if strcmp(type,'piezo')
    res.Mv_T1 = sqrt( res.J.*res.Z_T1.^2./res.Z_T3 .* res.Hvv_15_1.* ...
    res.Hvv_15_2./res.Hvv_15_3 * res.d_1*res.d_2/(res.d_0*res.d_3) );
end

%% Calculate transmitting voltage response

res.Sv_T3 = sqrt( 1./(res.J.*res.Z_T3) .* res.Hvv_15_2.*res.Hvv_15_3./ ...
    res.Hvv_15_1 * res.d_2*res.d_3/(res.d_0*res.d_1) );
res.Sv_T1 = sqrt( 1./(res.J.*res.Z_T3) .* res.Hvv_15_1.*res.Hvv_15_2./ ...
    res.Hvv_15_3 * res.d_1*res.d_2/(res.d_0*res.d_3) );

if strcmp(type,'piezo')
    res.Sv_T2 = sqrt( res.Z_T3./(res.J.*res.Z_T2.^2) .* res.Hvv_15_1.* ...
    res.Hvv_15_3./res.Hvv_15_2 * res.d_1*res.d_3/(res.d_0*res.d_2) );
end

end
```

### A.3.6 calculateHvv.m

```
%%%%%%%%%%%%%%%%%%%%%%%%%%%%%%%%%%%%%%%%%%%%%%%%%%%%%%%%%%%%%%%%%%%%%%%%%%%%
%function [d Hvv_15 f TwoTrans] = calculateHvv...
%    (filename, init, receiver_admittance,...
%    transmitter_admittance, transmitter_radius)
%
% Calculates the corrected voltage to voltage transfer function.
```

```
%
% Mosland, E & Hauge, R, 2012/2013
% Based on work by Espen Storheim, Vidar Knappskog and Magne Aanes
%%%%%%%%%%%%%%%%%%%%%%%%%%%%%%%%%%%%%%%%%%%%%%%%%%%%%%%%%%%%%%%%%%%%%%%%%%%%

function [d Hvv_15 f TwoTrans] = calculateHvv...
    (filename, init, receiver_admittance,...
    transmitter_admittance, transmitter_radius)

%% Initialization

% Load measurement
load(filename,'meas','results')

% Measurement distance and reference distance
d = meas.distance;
d_0 = 1;

% Ambient pressure
pressure = init.pressure;

% Cable lengths
% Generator to oscilloscope
cable_length_osc = init.cable_length_osc;
% Generator to transmitting transducer
cable_length_trans = init.cable_length_trans;
% Receiving transducer to amplifier
cable_length_rec = init.cable_length_rec;


% Steady state limits
l_lim_ac = init.l_lim_ac;
u_lim_ac = init.u_lim_ac;
l_lim_el = init.l_lim_el;
u_lim_el = init.u_lim_el;

V_out = results.acoustic;       % Acoustical pulses.
V_out_f = results.acoustic_f;   % Corresponding frequencies.

V_in = results.electric;        % Electrical pulses.
V_in_f = results.electric_f;    % Corresponding frequencies.

%% Acquire peak-to-peak values of the steady-state intervals

% Voltage out (acoustical signal)
sample_rate = 100e3./(results.acoustic_timescale*10);
if strcmp(init.method,'FFT')
    voltage_out = findPeakToPeak_FFT
                (V_out,V_out_f,sample_rate,l_lim_ac,u_lim_ac);
else
    voltage_out = findPeakToPeak
                (V_out,V_out_f,sample_rate,l_lim_ac,u_lim_ac);
end

% Voltage in (electrical signal)
sample_rate = 100e3./(results.electric_timescale*10);
if strcmp(init.method,'FFT')
    voltage_in = findPeakToPeak_FFT
                (V_in,V_in_f,sample_rate,l_lim_el,u_lim_el);
else
    voltage_in = findPeakToPeak
                (V_in,V_in_f,sample_rate,l_lim_el,u_lim_el);
end

%% Save output and input voltage without any corrections

TwoTrans.voltage_out_raw = voltage_out;
TwoTrans.voltage_in_raw = voltage_in;

%% Amplifier correction

% Deduct gain
voltage_out = voltage_out/10^(meas.gain/20);

% Amplitude correction for frequencies above 200 kHz
% (Due to dampening in the B&K amplifier)
```

```
AmpCorr = calculate_AmpCorr(V_out_f);

%% Attenuation correction

% Calculate the attenuation coefficient according to
% ANSI S1.26 in dB per metre.
for kk = 1:(length(V_out_f))
    % Find temperature in Kelvin.
    temp = 273.15 + results.temp_acoustic(kk);
    % Find an approximate speed of sound the given temperature.
    results.acoustic_c(kk) = 331.4 + 0.6 *results.temp_acoustic(kk);
    % Calculate the attenuation coefficient.
    alpha_dB(kk) = absorbsjonluft(V_out_f(kk),(pressure/10),...
    results.humidity_acoustic(kk),temp)/1000;
end

% Absorption scaling.
C_alpha = 10.^((d*alpha_dB)/20);

%% Near-field correction by relative diffraction correction

C_dif = correctionDiffraction
    (transmitter_radius,V_out_f,d,results.acoustic_c);

%% Receiving electronics correction

H_VV_5m5 = correctionReceivingElectronics
    (cable_length_rec, V_out_f, receiver_admittance);

%% Transmitting electronics correction

H_VV_1m1 = correctionTransmittingElectronics
    (cable_length_osc,cable_length_trans,V_out_f,transmitter_admittance);

%% Calculate the voltage to voltage transfer function with corrections

voltage_out = voltage_out .* AmpCorr .* abs(C_dif) .* ...
    C_alpha .* abs(H_VV_5m5);

voltage_in = voltage_in .* abs(H_VV_1m1);

Hvv_15 = voltage_out./voltage_in;

f = V_out_f;

%% Calculate the transmitting voltage response
% and receiving voltage sensitivity

Y_rec = calculateY(f,receiver_admittance);
Y_trans = calculateY(f,transmitter_admittance);
J = calculateJ(f);

TwoTrans.Sv_rec = sqrt( Hvv_15 ./ J .* Y_rec * (d/d_0) );
TwoTrans.Sv_trans = sqrt( Hvv_15 ./ J .* Y_trans * (d/d_0) );
TwoTrans.Mv_rec = sqrt( Hvv_15 .* J ./ Y_rec * (d/d_0) );
TwoTrans.Mv_trans = sqrt( Hvv_15 .* J ./ Y_trans * (d/d_0) );

end
```

### A.3.7 calculateHvvMic.m

```
%%%%%%%%%%%%%%%%%%%%%%%%%%%%%%%%%%%%%%%%%%%%%%%%%%%%%%%%%%%%%%%%%%%%%%%%%%%%
% function [d Hvv_15 f] = calculateHvvMic(filename, init,
% transmitter_admittance_file)
% Calculates the corrected voltage to voltage transfer function for
% measurements with a calibrated microphone.
%
% Mosland, E & Hauge, R, 2012/2013
% Based on work by Espen Storheim, Vidar Knappskog and Magne Aanes
%%%%%%%%%%%%%%%%%%%%%%%%%%%%%%%%%%%%%%%%%%%%%%%%%%%%%%%%%%%%%%%%%%%%%%%%%%%%

function [d Hvv_15 f] = calculateHvvMic...
        (filename, init, transmitter_admittance_file)

%% Initialization

```

```
% Load measurement
load(filename,'meas','results')

% Measurement distance and reference distance
d = meas.distance;
d_0 = 1;

% Ambient pressure
pressure = init.pressure;

% Cable lengths
% Generator to oscilloscope
cable_length_osc = init.cable_length_osc;
% Generator to transmitting transducer
cable_length_trans = init.cable_length_trans;

% Steady state limits
l_lim_ac = init.l_lim_ac;
u_lim_ac = init.u_lim_ac;
l_lim_el = init.l_lim_el;
u_lim_el = init.u_lim_el;

V_out = results.acoustic;       % Acoustical pulses.
V_out_f = results.acoustic_f;   % Corresponding frequencies.

V_in = results.electric;        % Electrical pulses.
V_in_f = results.electric_f;    % Corresponding frequencies.

%% Acquire peak-to-peak values of the steady-state intervals

% Voltage out (acoustical signal)
sample_rate = 100e3./(results.acoustic_timescale*10);
if strcmp(init.method,'FFT')
    voltage_out = findPeakToPeak_FFT
            (V_out,V_out_f,sample_rate,l_lim_ac,u_lim_ac);
else
    voltage_out = findPeakToPeak
            (V_out,V_out_f,sample_rate,l_lim_ac,u_lim_ac);
end

% Voltage in (electrical signal)
sample_rate = 100e3./(results.electric_timescale*10);
if strcmp(init.method,'FFT')
    voltage_in = findPeakToPeak_FFT
            (V_in,V_in_f,sample_rate,l_lim_el,u_lim_el);
else
    voltage_in = findPeakToPeak
            (V_in,V_in_f,sample_rate,l_lim_el,u_lim_el);
end

%% Save output and input voltage without any corrections

results.voltage_out_raw = voltage_out;
results.voltage_in_raw = voltage_in;

%% Amplifier correction

% Deduct gain
voltage_out = voltage_out/10^(meas.gain/20);

% Amplitude correction for frequencies above 200 kHz
% (Due to dampening in the B&K amplifier)
AmpCorr = calculate_AmpCorr(V_out_f);

%% Attenuation correction

% Calculate the attenuation coefficient according to
% ANSI S1.26 in dB per metre.
for kk = 1:(length(V_out_f))
    % Find temperature in Kelvin.
    temp = 273.15 + results.temp_acoustic(kk);
    % Find an approximate speed of sound the given temperature.
    results.acoustic_c(kk) = 331.4 + 0.6 *results.temp_acoustic(kk);
    % Calculate the attenuation coefficient
    alpha_dB(kk) = absorbsjonluft(V_out_f(kk),(pressure/10),...
    results.humidity_acoustic(kk),temp)/1000;
```

```
end

% Absorption scaling.
C_alpha = 10.^((d*alpha_dB)/20);

%% Transmitting electronics correction

H_VV_1m1 = correctionTransmittingElectronics...
    (cable_length_osc,cable_length_trans,V_out_f,transmitter_admittance_file);

%% Calculate the voltage to voltage transfer function with corrections

voltage_out = voltage_out .* AmpCorr .* C_alpha;

voltage_in = voltage_in .* abs(H_VV_1m1);

Hvv_15 = voltage_out./voltage_in;

f = V_out_f;

end
```

### A.3.8 correctionReceivingElectronics.m

```
% function Hvv_5m5 = correctionReceivingElectronics
%                    (cable_length, f, filename)
% Eivind Mosland 2013

function Hvv_5m5 = correctionReceivingElectronics
                    (cable_length, f, filename)

%% Load the impedance measurement of the receiving transducer.
load(filename)

% Frequency
ind1 = find(fr == floor(min(f)/1e3));
ind2 = find(fr == ceil(max(f)/1e3));

fr = fr(ind1:ind2)*1e3;

%% Calculate the impedance of the receiving transducer.

% Determine the admittance
Y = (g(ind1:ind2)+1i*b(ind1:ind2));

% Perfrom interpolation if necessary
if length(f) == length(fr)
    if (f ~= fr)
        Y = interp1(fr,Y,f,'linear');
    end
else
    Y = interp1(fr,Y,f,'linear');
end

% Determine the interpolated impedance
Z_T = 1./Y;

%% Calculate the impedance of the B&K measurement amplifier, direct input
R = 1e6;
C = 90e-12;
Z_C = 1./(1i*2*pi*f*C);
Z_BK = R*Z_C ./ (R + Z_C);


%% Coaxial cable

% Characteristic cable parameters
Cx = 100e-12;
Lx = 250e-9;

Z_0 = sqrt(Lx/Cx);
k_em = 2*pi*f*sqrt(Lx*Cx);

% Cable length
l = cable_length;

```

```
Z_a = 1i*Z_0*tan(k_em*l/2);
Z_b = Z_0./(1i*sin(k_em*l));

%% Calculate Hvv_5m5

Hvv_5m5 = ( Z_BK.*(Z_a+Z_b) + (Z_a+Z_b).^2 - Z_b.^2 + ...
    Z_T.*(Z_a+Z_b+Z_BK) )./( Z_b.*Z_BK );

end
```

### A.3.9 correctionTransmittingElectronics.m

```
% function Hvv_1m1 = correctionTransmittingElectronics
%    (cable_length_osc, cable_length_trans, f, filename)
% Eivind Mosland 2013

function Hvv_1m1 = correctionTransmittingElectronics...
    (cable_length_osc, cable_length_trans, f, filename)

%% Load the impedance measurement of the transmitting transducer.
load(filename)

% Frequency
ind1 = find(fr == floor(min(f)/1e3));
ind2 = find(fr == ceil(max(f)/1e3));

fr = fr(ind1:ind2)*1e3;

%% Calculate the impedance of the receiving transducer.

% Determine the admittance
Y = (g(ind1:ind2)+1i*b(ind1:ind2));

% Perfrom interpolation if necessary
if length(f) == length(fr)
    if (f ~= fr)
        Y = interp1(fr,Y,f,'linear');
    end
else
    Y = interp1(fr,Y,f,'linear');
end

% Determine the interpolated impedance
Z_T = 1./Y;

%% Calculate the impedance of the oscilloscope
R = 1e6;
C = 11.5e-12;
Z_C = 1./(1i*2*pi*f*C);
Z_OSC = R*Z_C ./ (R + Z_C);


%% Coaxial cables

% Characteristic cable parameters
Cx = 100e-12;
Lx = 250e-9;

Z_0 = sqrt(Lx/Cx);
k_em = 2*pi*f*sqrt(Lx*Cx);

% Generator to transmitter
Z_a1 = 1i*Z_0*tan(k_em*cable_length_trans/2);
Z_b1 = Z_0./(1i*sin(k_em*cable_length_trans));

% Generator to oscilloscope
Z_a2 = 1i*Z_0*tan(k_em*cable_length_osc/2);
Z_b2 = Z_0./(1i*sin(k_em*cable_length_osc));

%% Calculate Hvv_1m1

Hvv_1m1 = ( (Z_b1.*Z_T)./(Z_b2.*Z_OSC) ) .* ( ...
    (Z_OSC.*(Z_a2+Z_b2) + (Z_a2+Z_b2).^2 - Z_b2.^2) ./ ...
    (Z_T.*(Z_a1+Z_b1) + (Z_a1+Z_b1).^2 - Z_b1.^2) ...
    );
end
```

### A.3.10 calculateJ.m

```
% function J = calculateJ(f,rho,c,d0)
%
% rho, c and d0 can be omitted. rho = 1.21, c = 343 and
% d0 = 1 will then be used.
%
% Eivind Mosland, 2013

function J = calculateJ(f,rho,c,d0)

switch nargin
    case 1
        rho = 1.21;
        c = 343;
        d0 = 1;
    case 2
        c = 343;
        d0 = 1;
    case 3
        d0 = 1;
end

% Wave number.
k = 2*pi*f/c;

% Spherical reciprocity parameter.
J = 2*d0./(1i*rho*f).*exp(1i*k*d0);

% figure;
% plot(f,20*log10(abs(J)))

end
```

### A.3.11 calculateY.m

```
% function Y = calculateY(f, filename)
%
% Eivinf Mosland 2013

function Y = calculateY(f, filename)

load(filename)

% Frequency
ind1 = find(fr == floor(min(f)/1e3));
ind2 = find(fr == ceil(max(f)/1e3));

fr = fr(ind1:ind2)*1e3;

% Admittance.
Y = (g(ind1:ind2)+1i*b(ind1:ind2));

if length(f) == length(fr)
    if (f ~= fr)
        Y = interp1(fr,Y,f,'linear');
    end
else
    Y = interp1(fr,Y,f,'linear');
end

end
```

### A.3.12 correctionDiffraction.m

```
% function C_dif = correctionDiffraction(a,f,d,c)
%
% Eivind Mosland 2013

function C_dif = correctionDiffraction(a,f,d,c)

% Far-field distance.
dff = 1000;
% Wavenumber
k = 2*pi*f./c;
N = 1000;
```

```
12
13  % Khimunin's diffraction correction
14  H_d = Khimunin_diffractioncorrection(k,a,d,N);
15  H_dff = Khimunin_diffractioncorrection(k,a,dff,N);
16
17  % Correction factor
18  C_dif = (dff/d) * (H_dff./H_d);
19
20  end
```

### A.3.13 performCalibrationElm.m

```
1   % Initializes and perform calculations for a three-transducer
2   % reciprocity calibration.
3   % EM 2013
4
5   % Calibration of disks: T1 = #6 ; T2 = #10 ; T3 = #16
6
7   clear all
8
9   %% Default ambient pressure
10  % 1000 hPa or 1013 hPa
11  init.pressure = 1000; % hPa
12
13  %% Measured admittances
14  init.Y_T1_file = 'dummy.mat';
15  init.Y_T2_file = 'dummy.mat';
16  init.Y_T3_file = 'dummy.mat';
17
18  %% Cables - Approximate lengths
19  % Generator to oscilloscope: 1 m
20  init.cable_length_osc = 1;
21  % Generator to transmitter: disk = 4.0 m, transducer = 3,0 m
22  init.cable_length_trans = 4.0;
23  % Receiver to amplifier: disk = 3.4 m, transducer = 2.2 m
24  init.cable_length_rec = 3.4;
25
26  %% Radius of the transmitting transducers
27  % Elm #6 = 10.125e-3 ; Elm #10 = 10.117e-3 ; Elm #16 = 10.12e-3;
28  % Trans 1 = 11.895e-3 ; Trans 2 = 11.895e-3 ; Trans 3 = 11.904e-3;
29  init.radius_T1 = 10.125e-3;
30  init.radius_T3 = 10.12e-3;
31
32  % Calculation method. 'Regular' or 'FFT'
33  init.method = 'Regular';
34
35  % Limits where 'steady-state' of the signal is found
36  init.l_lim_ac = 45e3;
37  init.u_lim_ac = 65e3;
38  init.l_lim_el = 45e3;
39  init.u_lim_el = 65e3;
40
41  %% Calibration.
42  % First argument is either 'piezo' or 'mic', depending on whether
43  % or not a microphone is used in the calibrations.
44
45  filename = 'ThreeTransElmsWithDirectMethod';
46
47  tic
48
49  % 50-200 kHz, 2 Vpp, Elements
50  init.T1toT2_file = 'dummy.mat';
51  init.T1toT3_file = 'dummy.mat';
52  init.T3toT2_file = 'dummy.mat';
53
54  res_2Vpp_part1 = threeTransducerCalibration('piezo',init);
55  toc
56
57  ...
58  ...
59
60  % Save
61  save(filename,'init','res_2Vpp_part1','res_2Vpp_part2', ...
62      'res_20Vpp_part1','res_20Vpp_part2');
```

### A.3.14 performCalibrationMic.m

```
% Initializes and perform calculations for a three-transducer reciprocity
% calibration.
% EM 2013

% Calibration of disks: T1 = #6 ; T2 = #10 ; T3 = #16
% Calibration of old microphone: T1 = #6 ; T2 = mic ; T3 = #16
clear all

%% Default ambient pressure
% 1000 hPa or 1013 hPa
init.pressure = 1000; % hPa

%% Measured admittances
init.Y_T1_file = 'dummy.mat';
init.Y_T3_file = 'dummy.mat';

%% Cables - Approximate lengths
% Generator to oscilloscope: 1 m
init.cable_length_osc = 1;
% Generator to transmitter: disk = 4.0 m, transducer = 3,0 m
init.cable_length_trans = 4.0;
% Receiver to amplifier: disk = 3.4 m, transducer = 2.2 m
init.cable_length_rec = 3.4;

%% Radius of the transmitting transducers
% Elm #6 = 10.125e-3 ; Elm #10 = 10.117e-3 ; Elm #16 = 10.12e-3;
% Trans 1 = 11.895e-3 ; Trans 2 = 11.895e-3 ; Trans 3 = 11.904e-3;
init.radius_T1 = 10.125e-3;
init.radius_T3 = 10.12e-3;

% Calculation method. 'Regular' or 'FFT'
init.method = 'FFT';

% Limits where 'steady-state' of the signal is found.
% ONLY FOR THE ELM TO ELM. ELM TO MIC IS SET IN
% threeTransducerCalibration()
init.l_lim_ac = 45e3;
init.u_lim_ac = 65e3;
init.l_lim_el = 45e3;
init.u_lim_el = 65e3;

%% Calibration.
% First argument is either 'piezo' or 'mic', depending on whether or not a
% microphone is used in the calibrations.

%% Old microphone

filename = 'ThreeTransOldMicElm';

tic

% 50-180 kHz, 2 Vpp, Elements
init.T1toT2_file = 'dummy.mat';
init.T1toT3_file = 'dummy.mat';
init.T3toT2_file = 'dummy.mat';

res_2Vpp_mic = threeTransducerCalibration('mic',init);
toc

% 50-180 kHz, 20 Vpp, Elements
init.T1toT2_file = 'dummy.mat';
init.T1toT3_file = 'dummy.mat';
init.T3toT2_file = 'dummy.mat';

res_20Vpp_mic = threeTransducerCalibration('mic',init);
toc

% Save
save(filename,'init','res_2Vpp_mic','res_20Vpp_mic');
```

### A.3.15 frequencyresponse_new.m

```
% Frequency response.

function M = frequencyresponse_new(f)

```

```
% Data sheet. Calibration of the microphone connected to the preamplifier.
f1 = [20.0 21.1 22.4 23.7 25.1 26.6 28.2 29.9 31.6 33.5 35.5 37.6 39.8 ...
    42.2 44.7 47.3 50.1 53.1];
AR1 = [20 17 18 17 13 14 12 10 10 10 7 7 8 7 6 6 5 5]*0.01;

f2 = [56.2 59.6 63.1 66.8 70.8 75.0 79.4 84.1 89.1 94.4 100.0 105.9 ...
    112.2 118.9 125.9 133.4 141.3 149.6 158.5 167.9 177.8 188.4 199.5 ...
    211.3 223.9 237.1 251.2 266.1 281.8 298.5 316.2 335.0 354.8 375.8 ...
    398.1 421.7 446.7 473.2 501.2 530.9 562.3 595.7 631.0];
AR2 = [4 4 3 4 3 4 3 3 3 3 2 2 2 2 1 1 2 1 0 3 2 0 1 1 0 2 1 0 0 0 0 ...
    0 0 0 0 0 1 -2 -1 -1 -1]*0.01;

f3 = [668.3 707.9 749.9 794.3 841.4 891.3 944.1 1000.0 1059.3 1122.0 ...
    1188.5 1258.9 1333.5 1412.5 1496.2 1584.9 1678.8 1778.3 1883.6 ...
    1995.3 2113.5 2238.7 2371.4 2511.9 2660.7 2818.4 2985.4 3162.3 ...
    3349.37 3548.1 3758.4 3981.1 4217.0 4466.8 4731.5 5011.9 5308.8 ...
    5623.4 5956.6 6309.6 6683.4 7079.5 7498.9];
AR3 = [2 1 2 3 1 3 2 3 3 3 1 2 2 2 2 2 3 3 3 3 3 3 2 3 6 6 6 4 2 2 0 0 ...
    2 2 1 2 3 3 0 -7 -4 -3 4]*-0.01;

f4 = [7943.3 8414.0 8912.5 9440.6 10000.0 10592.5 11220.2 11885.0 ...
    12589.3 13335.2 14125.4 14962.4 15848.9 16788.0 17782.8 18836.5 ...
    19952.6 21134.9 22387.2 23713.7 25118.9 26607.3 28183.8 29853.8 ...
    31622.8 33496.5 35481.3 37583.7 39810.7 42169.7 44668.4 47315.1 ...
    50188.7 53088.4 56234.1 59566.2 63095.7 66834. 70794.6 74989.4 ...
    79432.8 84139.8 89125.1];
AR4 = [1 -18 -13 -11 -10 -6 -5 -19 -6 -4 -2 -1 0 3 4 5 6 6 10 11 14 15 ...
    15 18 17 21 24 24 27 24 22 13 -1 -5 -3 -9 -25 -50 -79 -102 -122 ...
    -137 -163]*0.01;

f5 = [94406.1 100000.0];
AR5 = [-159 -151]*0.01;

% From calibration chart of the microphone only.
f_x = [10.0000   10.8059   12.0323   13.6685   15.3344   16.2827  ...
    17.9055   19.6900   22.1451   24.0496  27.1838   30.1935   32.7902 ...
    35.7887   39.3555   42.7402   44.8194   47.3536   50.4077   53.7932 ...
    56.5514   60.8038   64.8874   68.0441   72.0715   75.5776   79.4527 ...
    82.2829   86.9354   89.5830  92.7741   96.0788   98.7577  100.0000]*1e3;
AR_x = [-0.0067    0.0067    0.0202    0.0202    0.0337    0.0472  ...
    0.0607    0.0877    0.1147    0.1687  0.1822    0.2362    0.2767 ...
    0.3036    0.3306    0.3441    0.3441    0.2497    0.2362    0.1282 ...
    0.0067   -0.1012   -0.3981   -0.6545   -0.7355   -0.8165   -0.8974 ...
    -0.9784   -1.1403   -1.2348  -1.1943   -1.0999   -1.0189   -1.0054];

% Data for 100 to 200 kHz, read from the calibration chart. (99.5426
% -1.0150) is omitted.
f6 = [104.1380  105.9610  111.6240  114.3700  116.3720  118.8210 ...
    125.6080  128.6970  131.4060 134.1710  139.3940  141.3430  144.8190 ...
    148.3810  153.6230  158.4980  168.1320  170.4830  174.0710  179.5950 ...
    184.0130  187.2350  189.8530  191.8400  195.1990  197.2420  200.0000]*1e3;
AR6 = [-0.9398   -0.9023   -0.8835   -0.8271   -0.7707   -0.7143  ...
    -0.6955   -0.4699   -0.2068 -0.0000    0.5639    0.7707    1.2970 ...
    1.7857    2.4060    2.9135    3.0827    2.8196    2.2368  1.3534  ...
    0.6579    0.1692   -0.4323   -0.8459   -1.5038   -1.8985   -2.3872];

% Data on the pressure response curve for the given microphone.
%AR_f = [f1 f2 f3 f4 f5 f6];
%AR = [AR1 AR2 AR3 AR4 AR5 AR6];

AR_f = [f_x f6];
AR = [AR_x AR6];

% Free-field correction
FFC_f = [9.9907   12.3537   14.6509   17.6188   20.8949   24.0998 ...
    28.1860   33.3110   38.8235   46.0427  51.1101   56.3417   62.1088 ...
    67.5196   71.3862   74.6903   78.1474   81.1973   84.0730   86.1465 ...
    88.2711   90.4480   92.6787   94.3056   96.9683  100.7530  106.1520 ...
    109.9120  114.6000  119.0720  121.5850  126.3300  128.1010  130.8040 ...
    132.1770  134.9670  138.2950  140.7230  143.1930  145.2010  147.2360 ...
    150.3430  153.5160  156.7550  159.5070  162.8730  168.0560  174.0080 ...
    180.1710  186.5520  190.4880  200.0000]*1e3;
FFC = [0.4912    0.6366    0.7819    1.0727    1.4119    1.7753    2.3811 ...
    3.2048    4.1255    5.2643  6.0154    6.7423    7.6388    8.4383  ...
    8.9471    9.3833    9.7951   10.1101   10.3282   10.4736  10.5947 ...
    10.6916   10.7643   10.8128   10.8612   10.8370   10.6916   10.5220 ...
```

```
    10.2555    9.9163  9.6498    9.0683    8.8987    8.5595    8.3414 ...
    7.8811    7.3723    6.8634    6.3788    5.8943  5.2401    4.4405  ...
    3.6410    2.7203    2.0903    1.3634    0.6123   -0.0176   -0.3811 ...
    -0.7687   -0.9383   -1.3018];

response = interp1(AR_f,AR,f,'spline');
freefieldcorr = interp1(FFC_f,FFC,f,'spline');

M = response + freefieldcorr;

% Convert from dB
M = 10.^(M./20);

end
```

### A.3.16 frequencyresponse_old.m

```
% Frekvensresponsen til mikrofonen

function y = frequencyresponse_old(f)

FC = [1 629.3
2   631.3
3   635.3
4   637.3
5   638.7
6   639
7   639
8   640
9   640
10  640.7
20  623
30  601
40  583
50  568.5
60  603
70  675.5
80  677
90  692.5
100 678.3
110 668.3
120 638.7
130 596
140 551
150 437.3
160 273
170 205.7
180 311.3
190 491
200 664];
FC(:,1) = FC(:,1)*1000;

% Free-field correction
FFC_f = [9.9907   12.3537   14.6509   17.6188   20.8949   24.0998  ...
    28.1860   33.3110   38.8235   46.0427   51.1101   56.3417   62.1088 ...
    67.5196   71.3862   74.6903   78.1474   81.1973   84.0730   86.1465 ...
    88.2711   90.4480   92.6787   94.3056   96.9683  100.7530  106.1520 ...
    109.9120  114.6000  119.0720  121.5850  126.3300  128.1010  130.8040 ...
    132.1770  134.9670  138.2950  140.7230  143.1930  145.2010  147.2360 ...
    150.3430  153.5160  156.7550  159.5070  162.8730  168.0560  174.0080 ...
    180.1710  186.5520  190.4880  200.0000]*1e3;
FFC = [0.4912    0.6366    0.7819    1.0727    1.4119    1.7753    2.3811 ...
    3.2048    4.1255    5.2643  6.0154    6.7423    7.6388    8.4383  ...
    8.9471    9.3833    9.7951   10.1101   10.3282   10.4736  10.5947 ...
    10.6916   10.7643   10.8128   10.8612   10.8370   10.6916   10.5220 ...
    10.2555    9.9163  9.6498    9.0683    8.8987    8.5595    8.3414 ...
    7.8811    7.3723    6.8634    6.3788    5.8943  5.2401    4.4405  ...
    3.6410    2.7203    2.0903    1.3634    0.6123   -0.0176   -0.3811 ...
    -0.7687   -0.9383   -1.3018];

yint = interp1(FFC_f,FFC,f,'spline');

f1 = 20:10:100;
f2 = 200:100:900;

F = [f1 f2 FC(:,1)'];
```

```
dB = (619.5-FC(:,2))/52.5/2;
FCC = [zeros(1,length(f1)+length(f2)) dB'];

yint2 = interp1(F,FCC,f,'spline');

Mv = yint+yint2;

% Convert from dB
y = 10.^(Mv./20);

end
```

### A.3.17 calculateSNR.m

```
function [f SNR signalRMS noiseRMS] = calculateSNR(filename_signal,...
    filename_noise,l_lim_sig,u_lim_sig)

%% Calculate output voltage RMS

load(filename_signal,'meas','results')

V_out = results.acoustic;       % Acoustical pulses.
f_1 = results.acoustic_f;   % Corresponding frequencies.

method = 'FFT';

% Voltage out (acoustical signal)
sample_rate = 100e3./(results.acoustic_timescale*10);
if strcmp(method,'FFT')
    voltage_out = findPeakToPeak_FFT(V_out,f_1,sample_rate, ...
        l_lim_sig,u_lim_sig);
else
    voltage_out = findPeakToPeak(V_out,f_1,sample_rate, ...
    l_lim_sig,u_lim_sig);
end

signalRMS = voltage_out./(2*sqrt(2));

%% Calculate Noise RMS

load(filename_noise,'meas','results')

l_lim_noise = 50e3;
u_lim_noise = 90e3;

V_out = results.acoustic;       % Acoustical pulses.
f_2 = results.acoustic_f;   % Corresponding frequencies.

for ii = 1:length(f_2)
    signal = V_out(ii,l_lim_noise:u_lim_noise);
    %signal = signal - mean(signal);
%     mean(signal)
%     noiseRMS(ii) = sqrt(mean((signal-mean(signal)).^2));
% noiseRMS(ii) = sqrt(mean((signal).^2));
noiseRMS(ii) = rms(signal);
%     noiseMean(ii) = mean(signal);
%     noiseSignal(ii,:) = signal;
%     signal = signal - noiseMean(ii);
%     noiseRMS2(ii) = sqrt(mean((signal-mean(signal)).^2));
end

%% Calculate SNR

if isequal(f_1,f_2)
    f = f_1;
else
    noiseRMS = interp1(f_2,noiseRMS,f_1,'linear');
    f = f_1;
end

SNR = 20*log10(signalRMS./noiseRMS);
```

# Appendix B

# FEMP-structures

The FEMP-structures used in this work and not included in FEMP 5.0. Described in Section 4.3.

## B.1 piezodiskwidefrontglue

```
%! Piezoceramic disk with a wider front layer and a
%! glue layer, vibrating in vacuum.
%!
%! Based on work by Espen Storheim
%!
%! Eivind Mosland 2013

function [read]=read_inn_project(read,commands);

%%%%%%%%%%%%%%%%%%%%%%%%%%%%%%%%%%%%%%%%%%%%%%%%%%%%%%%%%%%%%%%%%%%%%%%%%%%
% read_inn_project.m which should be in the working directory
%
% Part of FEMP (Finite Element Modeling of Piezoelectric structures)
% Programmed by Jan Kocbach (jan@kocbach.net)
% (C) 2000 Jan Kocbach. This file is free software;  you can redistribute
% it and/or modify it only under the the terms of the GNU GENERAL PUBLIC
% LICENSE which should be included along with this file.
% (C) 2000-2010 Christian Michelsen Research AS
%%%%%%%%%%%%%%%%%%%%%%%%%%%%%%%%%%%%%%%%%%%%%%%%%%%%%%%%%%%%%%%%%%%%%%%%%%%

% Put a file read_inn_project.m in your project directory to define local
% FEMP input commands. Also include init_const_project.m in this directory
% and define the commands there.

global glob;
read = read;


if ~isempty(read.piezodiskwidefrontglue)
    read.points=[]; read.areas=[]; read.materials=[]; read.dof=[]; read.restraints=[];

    %! Read parameters from the inn-file.
    r = read.piezodiskwidefrontglue(1,1,:); %! Radius of the piezoceramic element.
    t = read.piezodiskwidefrontglue(1,2,:); %! Thickness of the piezoceramic element.
    elr = read.piezodiskwidefrontglue(1,3,:); %! Number of elements/wavelength in the
    % radial direction in the piezoceramic element.
    elt = read.piezodiskwidefrontglue(1,4,:); %! Number of elements/wavelength in the
    % thickness direction in the piezoceramic element.
    matnum = read.piezodiskwidefrontglue(1,5,:); %! Piezo materialnumber.
    rfront = read.piezodiskwidefrontglue(1,6,:); %! Radius frontlayer.
    tfront = read.piezodiskwidefrontglue(1,7,:); %! Thickness frontlayer.
    matnumfront = read.piezodiskwidefrontglue(1,8,:); %! Frontlayer materialnumber.
    tglue = read.piezodiskwidefrontglue(1,9,:); %! Thickness glue.
    matnumglue = read.piezodiskwidefrontglue(1,10,:); %! Glue materialnumber.

    for s=1:size(r,3)

        T(s) = t(s)+tglue(s)+tfront(s);

        %! Specify the points in the model.
        read.points(:,:,s) = [  1, 0, -T(s)/2;
                                2, r(s), -T(s)/2;
```

```
                                3, 0, -T(s)/2+t(s);
                                4, r(s), -T(s)/2+t(s);
                                5, rfront(s), -T(s)/2+t(s);
                                6, 0, -T(s)/2+t(s)+tglue(s);
                                7, r(s), -T(s)/2+t(s)+tglue(s);
                                8, rfront(s), -T(s)/2+t(s)+tglue(s);
                                9, 0, T(s)/2;
                                10, r(s), T(s)/2;
                                11, rfront(s), T(s)/2;
                                ];

        %! Set up the different areas in the model.
        read.areas(:,:,s) = [   %! Piezoceramic element.
                                1, 3, 1, 2, 4, elr(s), elt(s), 0, 0;
                                %! Glue layer.
                                3, 6, 3, 4, 7, elr(s), elt(s), 0, 0;
                                3, 7, 4, 5, 8, elr(s), elt(s), 0, 0;
                                %! Matching layer.
                                2, 9, 6, 7, 10, elr(s), elt(s), 0, 0;
                                2, 10, 7, 8, 11, elr(s), elt(s), 0, 0;
                                ];

        %! Define the various materials.
        read.materials(:,:,s) = [   1 glob.globvariables.piezo matnum(s);
                                    2 glob.globvariables.mechanic matnumfront(s);
                                    3 glob.globvariables.mechanic matnumglue(s);
                                ];

        %! "Ground" the front electrode of the transmitter.
        read.dof(:,:,s) = [-1e-9, r(s)+1e-9, -T(s)/2+t(s)-1e-9, ...
                           T(s)/2+t(s)+1e-9, glob.free.ep];

        %! Impose a 1 V electrical potential at the rear surface of the transmitter.
        read.restraints(:,:,s) = [-1e-9, r(s)+1e-9, -T(s)/2-1e-9, ...
                                  -T(s)/2+1e-9, glob.free.ep, 1];

    end
end
```

## B.2 transducervacuum

```
%! Set up the structure for the piezoelectric transducer developed during
%! this work, radiating in vacuum.
%!
%! Eivind Mosland 2013

function [read]=read_inn_project(read,commands);

%%%%%%%%%%%%%%%%%%%%%%%%%%%%%%%%%%%%%%%%%%%%%%%%%%%%%%%%%%%%%%%%%%%%%%%%%%%
% read_inn_project.m which should be in the working directory
%
% Part of FEMP (Finite Element Modeling of Piezoelectric structures)
% Programmed by Jan Kocbach (jan@kocbach.net)
% (C) 2000 Jan Kocbach. This file is free software;  you can redistribute
% it and/or modify it only under the the terms of the GNU GENERAL PUBLIC
% LICENSE which should be included along with this file.
% (C) 2000-2010 Christian Michelsen Research AS
%%%%%%%%%%%%%%%%%%%%%%%%%%%%%%%%%%%%%%%%%%%%%%%%%%%%%%%%%%%%%%%%%%%%%%%%%%%

% Put a file read_inn_project.m in your project directory to define local
% FEMP input commands. Also include init_const_project.m in this directory
% and define the commands there.

global glob;
read = read;

if ~isempty(read.transducervacuum)
    read.points=[]; read.areas=[]; read.materials=[]; read.dof=[]; read.restraints=[];

    %! Read parameters from the inn-file.
    r = read.transducervacuum(1,1,:); %! Radius of the piezoceramic element.
    t = read.transducervacuum(1,2,:); %! Thickness of the piezoceramic element.
    elr = read.transducervacuum(1,3,:); %! Number of elements/wavelength in
    % the radial direction in the piezoceramic element.
    elt = read.transducervacuum(1,4,:); %! Number of elements/wavelength in
    % the thickness direction in the piezoceramic element.
```

```
matnum = read.transducervacuum(1,5,:); %! Piezo materialnumber.
rfront = read.transducervacuum(1,6,:); %! Radius frontlayer.
tfront = read.transducervacuum(1,7,:); %! Thickness frontlayer.
matnumfront = read.transducervacuum(1,8,:); %! Frontlayer materialnumber.
rglue = read.transducervacuum(1,9,:); %! Radius glue.
tglue = read.transducervacuum(1,9,:); %! Thickness glue.
matnumglue = read.transducervacuum(1,10,:); %! Glue materialnumber.
lcasing = read.transducervacuum(1,11,:); %! Length of the casing.
tcasing = read.transducervacuum(1,12,:); %! Thickness of the casing.
matnumcasing = read.transducervacuum(1,13,:); %! Casing material number.
matnumbacking = read.transducervacuum(1,14,:); %! Backing material number.

for s=1:size(r,3)

    T(s) = lcasing(s);

    %! Specify the points in the model.
    read.points(:,:,s) = [  1, rfront(s) + rglue(s), -T(s)/2;
                            2, rfront(s) + rglue(s) + tcasing(s), -T(s)/2;
                            3, 0, T(s)/2 - tfront(s) - tglue(s) - t(s);
                            4, r(s), T(s)/2 - tfront(s) - tglue(s) - t(s);
                            5, 0, T(s)/2 - tfront(s) - tglue(s);
                            6, r(s), T(s)/2 - tfront(s) - tglue(s);
                            7, rfront(s), T(s)/2 - tfront(s) - tglue(s);
                            8, rfront(s) + rglue(s), ...
                               T(s)/2 - tfront(s) - tglue(s);
                            9, rfront(s) + rglue(s) + tcasing(s), ...
                               T(s)/2 - tfront(s) - tglue(s);

                            10, 0, T(s)/2 - tfront(s);
                            11, r(s), T(s)/2 - tfront(s);
                            12, rfront(s), T(s)/2 - tfront(s);
                            13, rfront(s) + rglue(s), T(s)/2 - tfront(s);
                            14, rfront(s) + rglue(s) + tcasing(s), ...
                                T(s)/2 - tfront(s);

                            15, 0, T(s)/2;
                            16, r(s), T(s)/2;
                            17, rfront(s), T(s)/2;
                            18, rfront(s) + rglue(s), T(s)/2;
                            19, rfront(s) + rglue(s) + tcasing(s), T(s)/2;

                            20, 0, -T(s)/2;
                            21, r(s), -T(s)/2;
                            22, rfront(s) + rglue(s), ...
                                T(s)/2 - tfront(s) - tglue(s) - t(s);
                            23, rfront(s) + rglue(s) + tcasing(s), ...
                                T(s)/2 - tfront(s) - tglue(s) - t(s);
                            ];

    %! Set up the different areas in the model.
    read.areas(:,:,s) = [   %! Piezoceramic element.
                            1, 5, 3, 4, 6, elr(s), elt(s), 0, 0;
                            %! Glue layer.
                            3, 10, 5, 6, 11, elr(s), elt(s), 0, 0;
                            3, 11, 6, 7, 12, elr(s), elt(s), 0, 0;
                            3, 12, 7, 8, 13, elr(s), elt(s), 0, 0;
                            3, 17, 12, 13, 18, elr(s), elt(s), 0, 0;
                            %! Matching layer.
                            2, 16, 11, 12, 17, elr(s), elt(s), 0, 0;
                            2, 15, 10, 11, 16, elr(s), elt(s), 0, 0;
                            %! Backing layer.
                            5, 3, 20, 21, 4, elr(s), elt(s), 0, 0;
                            5, 4, 21, 1, 22, elr(s), elt(s), 0, 0;
                            %! Casing wall.
                            4, 18, 13, 14, 19, elr(s), elt(s), 0, 0;
                            4, 13, 8, 9, 14, elr(s), elt(s), 0, 0;
                            4, 8, 22, 23, 9, elr(s), elt(s), 0, 0;
                            4, 22, 1, 2, 23, elr(s), elt(s), 0, 0;
                            ];

    %! Define the various materials.
    read.materials(:,:,s) = [   1 glob.globvariables.piezo matnum(s);
                                2 glob.globvariables.mechanic matnumfront(s);
                                3 glob.globvariables.mechanic matnumglue(s);
                                4 glob.globvariables.mechanic matnumcasing(s);
```

```
                                    5 glob.globvariables.mechanic matnumbacking(s);
                                ];

        %! "Ground" the front electrode of the transmitter.
        read.dof(:,:,s) = [-1e-9, r(s)+1e-9, T(s)/2-tfront(s)-tglue(s)-1e-9, ...
                           T(s)/2-tfront(s)-tglue(s)+1e-9, glob.free.ep];

        %! Impose a 1 V electrical potential at the rear surface of the transmitter.
        read.restraints(:,:,s) = [-1e-9, r(s)+1e-9, T(s)/2-tfront(s)-tglue(s)-t(s)-1e-9, ...
                                   T(s)/2-tfront(s)-tglue(s)-t(s)+1e-9, glob.free.ep, 1];
    end
end
```

## B.3 piezodiskwidefrontfluid

```
%! Piezoceramic disk with a wider matching layer, in a medium.
%! Espen Storheim, February 2013.
%! Updated 13/02-2013: Included support for parametric analysis.
%! Updated 12/02-2013: Fixed problem with the infinite elements.
%! Updated 2013 by RH & EM: Fixed meshing order.


function [read]=read_inn_project(read,commands);

%%%%%%%%%%%%%%%%%%%%%%%%%%%%%%%%%%%%%%%%%%%%%%%%%%%%%%%%%%%%%%%%%%%%%%%%%%%
% read_inn_project.m which should be in the working directory
%
% Part of FEMP (Finite Element Modeling of Piezoelectric structures)
% Programmed by Jan Kocbach (jan@kocbach.net)
% (C) 2000 Jan Kocbach. This file is free software;  you can redistribute
% it and/or modify it only under the the terms of the GNU GENERAL PUBLIC
% LICENSE which should be included along with this file.
% (C) 2000-2010 Christian Michelsen Research AS
%%%%%%%%%%%%%%%%%%%%%%%%%%%%%%%%%%%%%%%%%%%%%%%%%%%%%%%%%%%%%%%%%%%%%%%%%%%

% Put a file read_inn_project.m in your project directory to define local
% FEMP input commands. Also include init_const_project.m in this directory
% and define the commands there.

global glob;
read = read;


if ~isempty(read.piezodiskwidefrontfluid)
    read.points=[]; read.areas=[]; read.materials=[]; read.dof=[]; read.restraints=[];

    %! Read parameters from the inn-file.
    r = read.piezodiskwidefrontfluid(1,1,:); %! Radius of the piezoceramic element.
    t = read.piezodiskwidefrontfluid(1,2,:); %! Thickness of the piezoceramic element.
    elr = read.piezodiskwidefrontfluid(1,3,:); %! Number of elements/wavelength in the
    % radial direction in the piezoceramic element.
    elt = read.piezodiskwidefrontfluid(1,4,:); %! Number of elements/wavelength in the
    % radial direction in the piezoceramic element.
    matnum = read.piezodiskwidefrontfluid(1,5,:); %! Piezo materialnumber.
    rfront = read.piezodiskwidefrontfluid(1,6,:); %! Radius frontlayer.
    tfront = read.piezodiskwidefrontfluid(1,7,:); %! Thickness frontlayer.
    matnumfront = read.piezodiskwidefrontfluid(1,8,:); %! Frontlayer materialnumber.
    elfluid = read.piezodiskwidefrontfluid(1,9,:); %! Elements/wavelength in the fluid.
    rf = read.piezodiskwidefrontfluid(1,10,:); %! Rinf, i.e. radius of the finite elements.
    matnumfluid = read.piezodiskwidefrontfluid(1,11,:); %! Medium materialnumber.
    rinf = 2*rf; %! Radius of the infinite elements.
    zf = 0.6*rf; %! Square fluid region in front and to the rear.

    for s=1:size(r,3)
        %! Angles used to generate the curved finite and infinite areas.
        theta1 = atan(tfront(s)/rfront(s));
        theta2 = atan((tfront(s)+zf(s))/rfront(s));
        theta3 = atan((tfront(s)+zf(s))/r(s));
        theta4 = atan(t(s)/rfront(s));
        theta5 = atan((t(s)+zf(s))/rfront(s));
        theta6 = atan((t(s)+zf(s))/r(s));

        %! Specify the points in the model.
        read.points(:,:,s) = [  1, 0, -t(s);
                                2, r(s), -t(s);
```

```
                                3, 0, 0;
                                4, r(s), 0;
                                5, rfront(s), 0;
                                6, 0, tfront(s);
                                7, r(s), tfront(s);
                                8, rfront(s), tfront(s);
                                9, rfront(s), -t(s);
                                10, 0, -rf(s);
                                11, rf(s)*cos(theta5), -rf(s)*sin(theta5);
                                12, rf(s)*cos(theta4), -rf(s)*sin(theta4);
                                13, rf(s), 0;
                                14, rf(s)*cos(theta1), rf(s)*sin(theta1);
                                15, rf(s)*cos(theta2), rf(s)*sin(theta2);
                                16, rf(s)*cos(theta3), rf(s)*sin(theta3);
                                17, 0, rf(s);
                                18, 0, tfront(s)+zf(s);
                                19, r(s), tfront(s)+zf(s);
                                20, rfront(s), tfront(s)+zf(s);
                                21, 0, -rinf(s);
                                22, rinf(s)*cos(theta5), -rinf(s)*sin(theta5);
                                23, rinf(s)*cos(theta4), -rinf(s)*sin(theta4);
                                24, rinf(s), 0;
                                25, rinf(s)*cos(theta1), rinf(s)*sin(theta1);
                                26, rinf(s)*cos(theta2), rinf(s)*sin(theta2);
                                27, rinf(s)*cos(theta3), rinf(s)*sin(theta3);
                                28, 0, rinf(s);
                                29, 0, -t(s)-zf(s);
                                30, r(s), -t(s)-zf(s);
                                31, rfront(s), -t(s)-zf(s);
                                32, rf(s)*cos(theta6), -rf(s)*sin(theta6);
                                33, rinf(s)*cos(theta6), -rinf(s)*sin(theta6);
                                ];

        %! Set up the different areas in the model.
        read.areas(:,:,s) = [   %! Piezoceramic element.
                                1, 3, 1, 2, 4, elr(s), elt(s), 0, 0;
                                %! Matching layer.
                                2, 6, 3, 4, 7, elr(s), elt(s), 0, 0;
                                2, 7, 4, 5, 8, elr(s), elt(s), 0, 0;
                                %! Square fluid region.
                                3, 4, 2, 9, 5, elr(s), elt(s), 0, 0;
                                3, 18, 6, 7, 19, elr(s), elt(s), 0, 0;
                                3, 19, 7, 8, 20, elr(s), elt(s), 0, 0;
                                3, 2, 1, 29, 30, elr(s),elt(s), 0, 0;
                                3, 2, 30, 31, 9, elr(s), elt(s), 0, 0;
                                %! Finite fluid elements with a curvature.
                                3, 18, 19, 16, 17, elfluid(s), elfluid(s), 0, 3;
                                3, 19, 20, 15, 16, elfluid(s), elfluid(s), 0, 3;
                                3, 20, 8, 14, 15, elfluid(s), elfluid(s), 0, 3;
                                3, 8, 5, 13, 14, elfluid(s), elfluid(s), 0, 3;
                                3, 5, 9, 12, 13, elfluid(s), elfluid(s), 0, 3;
                                3, 9, 31, 11, 12, elfluid(s), elfluid(s),  0, 3;
                                3, 31, 30, 32, 11, elfluid(s),elfluid(s), 0, 3;
                                3, 30, 29, 10, 32, elfluid(s), elfluid(s), 0, 3;
                                %! Infinite elements.
                                4, 32, 10, 21, 33, elfluid(s), 1, 3, 3;
                                4, 11, 32, 33, 22, elfluid(s), 1, 3, 3;
                                4, 12, 11, 22, 23, elfluid(s), 1, 3, 3;
                                4, 13, 12, 23, 24, elfluid(s), 1, 3, 3;
                                4, 14, 13, 24, 25, elfluid(s), 1, 3, 3;
                                4, 15, 14, 25, 26, elfluid(s), 1, 3, 3;
                                4, 16, 15, 26, 27, elfluid(s), 1, 3, 3;
                                4, 17, 16, 27, 28, elfluid(s), 1, 3, 3;
                                ];

        %! Define the various materials.
        read.materials(:,:,s) = [   1 glob.globvariables.piezo matnum(s);
                                    2 glob.globvariables.mechanic matnumfront(s);
                                    3 glob.globvariables.fluid matnumfluid(s)
                                    4 glob.globvariables.infinitefluid matnumfluid(s)
                                ];

        %! "Ground" the front electrode of the transmitter.
        read.dof(:,:,s) = [-1e-9, r(s)+1e-9, 0-1e-9, 0+1e-9, glob.free.ep];

        %! Impose a 1 V electrical potential at the rear surface of the transmitter.
```

```
137         read.restraints(:,:,s) = [-1e-9, r(s)+1e-9, -t(s)-1e-9,-t(s)+1e-9, glob.free.ep, 1];
138
139     end
140 end
```

## B.4 transducerfluid

```
1  %! Transducer with piezoelectric element, matching layer, housing cylinder
2  %! and backing layer, radiating in a fluid.
3  %!
4  %! Based on a FEMP model of a Massa E188/220 transducer, as presented in
5  %! Norli (2007), with some minor adjustments, implemented by Espen Storheim.
6  %!
7  %! Some modifications performed by Rune Hauge, 2013
8
9  function [read]=read_inn_project(read,commands);
10
11 %%%%%%%%%%%%%%%%%%%%%%%%%%%%%%%%%%%%%%%%%%%%%%%%%%%%%%%%%%%%%%%%%%%%%%%
12 % read_inn_project.m which should be in the working directory
13 %
14 % Part of FEMP (Finite Element Modeling of Piezoelectric structures)
15 % Programmed by Jan Kocbach (jan@kocbach.net)
16 % (C) 2000 Jan Kocbach. This file is free software;  you can redistribute
17 % it and/or modify it only under the the terms of the GNU GENERAL PUBLIC
18 % LICENSE which should be included along with this file.
19 % (C) 2000-2010 Christian Michelsen Research AS
20 %%%%%%%%%%%%%%%%%%%%%%%%%%%%%%%%%%%%%%%%%%%%%%%%%%%%%%%%%%%%%%%%%%%%%%%
21
22 % Put a file read_inn_project.m in your project directory to define local
23 % FEMP input commands. Also include init_const_project.m in this directory
24 % and define the commands there.
25
26 global glob;
27 read = read;
28
29 if ~isempty(read.transducerfluid)
30     read.points=[]; read.areas=[]; read.materials=[]; read.dof=[]; read.restraints=[];
31     tb = read.transducerfluid(1,1,:); %! Not used.
32     td = read.transducerfluid(1,2,:); %! Not used.
33     elr = read.transducerfluid(1,3,:); %! El/lambda, radial dir. in piezoelectric element.
34     elt = read.transducerfluid(1,4,:); %! El/lambda, thickness dir. in piezoelectric element.
35     matnum = read.transducerfluid(1,5,:); %! Material number of the piezoelectric element.
36     tfr = read.transducerfluid(1,6,:);
37     tw1 = read.transducerfluid(1,7,:);
38     tw2 = read.transducerfluid(1,8,:);
39     afr = read.transducerfluid(1,9,:);
40     ad = read.transducerfluid(1,10,:);
41     elfluid = read.transducerfluid(1,11,:);
42     matnumfront = read.transducerfluid(1,12,:);
43     matnumfluid = read.transducerfluid(1,13,:);
44     matnumcasing = read.transducerfluid(1,14,:);
45     matnumside = read.transducerfluid(1,15,:);
46     matnumback = read.transducerfluid(1,16,:);
47     rf = read.transducerfluid(1,17,:);
48
49     rinff = 2*rf;
50     r1 = ad;
51     r2 = afr;
52     r3 = r2 + tw1;
53     r4 = r2 + tw2;
54     T = tb + td + tfr;
55     t1 = T/2;
56     t2 = T/2 - tfr;
57     t3 = t2 - td;
58     t4 = -T/2;
59
60 for s = 1:size(tb,3)
61     theta1 = atan(t1(s)/r1(s));
62     theta2 = atan(t1(s)/r2(s));
63     theta3 = atan(t1(s)/r3(s));
64     theta4 = atan(t1(s)/r4(s));
65     theta5 = atan(t2(s)/r4(s));
66     theta6 = atan(t3(s)/r4(s));
67     theta7 = atan(t4(s)/r4(s));
68     theta8 = atan(t4(s)/r3(s));
69     theta9 = atan(t4(s)/r2(s));
```

```
70      theta10 = atan(t4(s)/r1(s));
71
72      %! Specify the points in the model.
73          read.points(:,:,s) = [  1 0 t1(s);
74                  2 r1(s) t1(s);
75                  3 r2(s) t1(s);
76                  5 r4(s) t1(s);
77                  6 0 t2(s);
78                  7 r1(s) t2(s);
79                  8 r2(s) t2(s);
80                  10 r4(s) t2(s);
81                  11 0 t3(s);
82                  12 r1(s) t3(s);
83                  13 r2(s) t3(s);
84                  15 r4(s) t3(s);
85                  16 0 0;
86                  17 0 t4(s);
87                  18 r1(s) t4(s);
88                  19 r2(s) t4(s);
89                  21 r4(s) t4(s);
90                  22 0 rf(s);
91                  23 rf(s)*cos(theta1) rf(s)*sin(theta1);
92                  24 rf(s)*cos(theta2) rf(s)*sin(theta2);
93                  26 rf(s)*cos(theta4) rf(s)*sin(theta4);
94                  27 rf(s)*cos(theta5) rf(s)*sin(theta5);
95                  28 rf(s)*cos(theta6) rf(s)*sin(theta6);
96                  29 rf(s)*cos(theta7) rf(s)*sin(theta7);
97                  31 rf(s)*cos(theta9) rf(s)*sin(theta9);
98                  32 rf(s)*cos(theta10) rf(s)*sin(theta10);
99                  33 0 -rf(s);
100                 34 0 rinff(s);
101                 35 rinff(s)*cos(theta1) rinff(s)*sin(theta1);
102                 36 rinff(s)*cos(theta2) rinff(s)*sin(theta2);
103                 38 rinff(s)*cos(theta4) rinff(s)*sin(theta4);
104                 39 rinff(s)*cos(theta5) rinff(s)*sin(theta5);
105                 40 rinff(s)*cos(theta6) rinff(s)*sin(theta6);
106                 41 rinff(s)*cos(theta7) rinff(s)*sin(theta7);
107                 43 rinff(s)*cos(theta9) rinff(s)*sin(theta9);
108                 44 rinff(s)*cos(theta10) rinff(s)*sin(theta10);
109                 45 0 -rinff(s);
110                 ];
111
112     %! Set up the different areas in the model.
113         read.areas(:,:,s) = [
114                                 %! Matching layer.
115                                 2, 2,7,8,3, elr(s), elt(s), 0, 0;
116                                 2, 1,6,7,2, elr(s), elt(s), 0, 0;
117                                 %! Piezoceramic element.
118                                 1, 6, 11, 12, 7, elr(s), elt(s), 0, 0;
119                                 %! Side layer.
120                                 4, 7, 12, 13, 8, elr(s), elt(s), 0, 0;
121                                 %! Backing layer.
122                                 3, 11, 17, 18, 12,elr(s), elt(s), 0, 0;
123                                 3, 12, 18, 19, 13,elr(s), elt(s), 0, 0;
124                                 %! Casing.
125                                 5, 3, 8, 10, 5, elr(s), elt(s), 0, 0;
126                                 5, 8, 13, 15, 10, elr(s), elt(s), 0, 0;
127                                 5, 13, 19, 21, 15, elr(s), elt(s), 0, 0;
128                                 %! Curved fluid regions.
129                                 6, 1, 2, 23, 22, elr(s), elt(s), 0, 16;
130                                 6, 2, 3, 24, 23, elr(s), elt(s), 0, 16;
131                                 6, 3, 5, 26, 24, elr(s), elt(s), 0, 16;
132                                 6, 5, 10, 27, 26, elr(s), elt(s), 0, 16;
133                                 6, 10, 15, 28, 27, elr(s), elt(s), 0, 16;
134                                 6, 15, 21, 29, 28, elr(s), elt(s), 0, 16;
135                                 6, 21, 19, 31, 29, elr(s), elt(s), 0, 16;
136                                 6, 19, 18, 32, 31, elr(s), elt(s), 0, 16;
137                                 6, 18, 17, 33, 32, elr(s), elt(s), 0, 16;
138                                 %! Infinite elements.
139                                 7, 22, 23, 35, 34, elfluid(s), 1, 16, 16;
140                                 7, 23, 24, 36, 35, elfluid(s), 1, 16, 16;
141                                 7, 24, 26, 38, 36, elfluid(s), 1, 16, 16;
142                                 7, 26, 27, 39, 38, elfluid(s), 1, 16, 16;
143                                 7, 27, 28, 40, 39, elfluid(s), 1, 16, 16;
144                                 7, 28, 29, 41, 40, elfluid(s), 1, 16, 16;
145                                 7, 29, 31, 43, 41, elfluid(s), 1, 16, 16;
```

```
                                7, 31, 32, 44, 43, elfluid(s), 1, 16, 16;
                                7, 32, 33, 45, 44, elfluid(s), 1, 16, 16;
                                ];

    %! Define the various materials.
        read.materials(:,:,s) = [   1 glob.globvariables.piezo matnum(s);
                                    2 glob.globvariables.mechanic matnumfront(s);
                                    3 glob.globvariables.mechanic matnumback(s)
                                    4 glob.globvariables.fluid matnumside(s)
                                    5 glob.globvariables.mechanic matnumcasing(s)
                                    6 glob.globvariables.fluid matnumfluid(s)
                                    7 glob.globvariables.infinitefluid matnumfluid(s)
                                ];

    %! "Ground" the front electrodes (transmitter and receiver), and set the velocity
    %! potential at the edge of of the PML regions to zero.

        read.dof(:,:,s) = [-1e-9, r1(s)+1e-9, t3(s)-1e-9, t3(s)+1e-9, glob.free.ep;
                           ];

    %! Impose a 1 V electrical potential at the rear surface of the transmitter.
        read.restraints(:,:,s) = [-1e-9, r1(s)+1e-9, t2(s)-1e-9,t2(s)+1e-9, glob.free.ep, 1];

    glob.tfront(s) = T(s)/2;
    end
end
```

# Appendix C

# Paper submitted for the proceedings of the 36th Scandinavian Symposium on Physical Acoustics at Geilo, Norway, 3-6 February 2013

*36th Scandinavian Symposium on Physical Acoustics, Geilo, Norway, 3-6 February 2013*

# Reciprocity calibration method for ultrasonic, piezoelectric transducers in air, including finite element simulations

Eivind Mosland[a,b,*], Rune Hauge[a,b], Espen Storheim[a,b], Magne Vestrheim[a,b], Per Lunde[a,c,b], and Jan Kocbach[c,b]

[a] *University of Bergen, Department of Physics and Technology, P.O. Box 7803, N-5020 Bergen, Norway*
[b] *The Michelsen Centre for Industrial Measurement Science and Technology*
[c] *Christian Michelsen Research AS (CMR), P.O. Box 6031 Postterminalen, N-5892 Bergen, Norway*

**Abstract**

The conventional three-transducer reciprocity calibration method is modified and used to determine the transmitting voltage response of an ultrasonic piezoelectric transducer radiating in air at 1 atm. The transducer used in this work is a piezoelectric ceramic disk with first radial mode at approximately 100 kHz. The three-transducer reciprocity calibration is compared to measurement with a calibrated B&K 4138 condenser microphone and to finite element simulation. Preliminary results for a limited frequency band at the first radial mode of the piezoelectric ceramic disk demonstrate the feasibility of the method at high ultrasonic frequencies. Further work is needed to improve the accuracy and extend the calibrations to beyond the calibrated range of the B&K 4138 microphone.

## 1. Introduction

Accurate calibration data for ultrasonic transducers in gas at ultrasonic frequencies can be of importance in many applications, e.g. fiscal metering and gas characterization. For the 1/8 inch B&K 4138 condenser microphone, accurate calibration data are available from the manufacturer up to 140 kHz [1, 2]. However, frequencies up to 300 kHz and beyond may be of interest in certain applications [3].

A three-transducer reciprocity calibration method is considered here, which determines the transmitting voltage response and free-field open-circuit receiving voltage sensitivity of a transducer. In this work the method is discussed and preliminary results are shown for the transmitting voltage response of a piezoelectric ceramic disk at the first radial mode at approximately 100 kHz.

Measurements with the calibrated B&K 4138 microphone are performed to compare with the three-transducer reciprocity calibration method.

Piezoelectric ceramic disks are presently used as transducers to simplify finite element (FE) analysis, which is compared to the measurement results. FE analysis [4, 5] are expected to become even more important in further development of the method to higher frequencies and for also including phase response measurements.

## 2. Theory

The three-transducer reciprocity calibration method described in this work is based on the conventional method [6, 7]. It is modified to use measurements of input and output voltage and electric impedance, and some corrections are introduced to account for the lack of ideal measurement conditions. This includes corrections for receiver electronics, losses in the medium, and the use of diffraction correction to account for near-field effects. Linear theory is used.

The expressions needed in the calibration procedure are derived by combining the definitions of the transmitting voltage response, $S_V$, the free-field open-circuit receiving voltage sensitivity, $M$, and the spherical wave reciprocity parameter, $J$. All quantities are defined without losses in the medium. A harmonic time dependency of $e^{i\omega t}$ is assumed and suppressed.

*Corresponding author
*Email address:* eivmos@gmail.com (Eivind Mosland)

The transmitting voltage response of a transmitting transducer is defined as [8, 9]

$$S_V(f) \equiv \frac{p_3(z = d_0, f)}{V_1(f)}, \tag{1}$$

where $p_3(z = d_0, f)$ is the axial free-field pressure at the reference distance $z = d_0$. $V_1(f)$ is the input voltage to the transmitting transducer and $f$ is the frequency. If the reference distance is in the near-field, the pressure needs to be extrapolated back to $d_0$ from a pressure in the far-field.

The free-field open-circuit receiving voltage sensitivity of a receiving transducer is defined as [8, 9]

$$M(f) \equiv \frac{V_5(f)}{p_4(f)}, \tag{2}$$

where $p_4(f)$ is the free-field pressure at the position of the receiving transducer, assuming normal incidence and plane wavefronts at the transducer surface. $V_5(f)$ is the open-circuit output voltage from the receiving transducer.

For a given reciprocal transducer the spherical wave reciprocity parameter is defined as [7, 8]

$$J(f) \equiv \frac{M(f)}{S_V(f)Z(f)} = \frac{4\pi d_0}{i\omega\rho} e^{ikd_0} = \frac{2d_0}{if\rho} e^{ikd_0}, \tag{3}$$

where it is assumed that the transducer is linear, passive, reversible and electroacoustic. $Z(f)$ is the electrical input impedance of the transducer, $k = \omega/c$ is the wave number, $\omega = 2\pi f$ is the angular frequency and $\rho$ and $c$ are the density and the sound velocity in the medium, respectively.

Three measurements are needed in order to perform the three-transducer reciprocity calibration. In each measurement the transmitter and receiver are aligned coaxially. The transducers are denoted T1, T2 and T3, where T3 is reciprocal. In measurement #1 T1 transmits to T2 at axial distance $d_1$, in measurement #2 T1 transmits to T3 at axial distance $d_2$, and in measurement #3 T3 transmits to T2 at axial distance $d_3$. The input voltage to the transmitter, $V_1(f)$, and the output voltage from the receiver, $V_5(f)$, are measured and used to calculate the voltage to voltage transfer functions

$$H_{15}^{VV\,(1)}(f) \equiv \frac{V_5^{(1)}(f)}{V_1^{(1)}(f)}, \qquad H_{15}^{VV\,(2)}(f) \equiv \frac{V_5^{(2)}(f)}{V_1^{(2)}(f)} \qquad \text{and} \qquad H_{15}^{VV\,(3)}(f) \equiv \frac{V_5^{(3)}(f)}{V_1^{(3)}(f)}, \tag{4}$$

where the superscripts $^{(1)}$, $^{(2)}$ and $^{(3)}$ denote measurement #1, #2 and #3, respectively. The frequency dependency notation, $(f)$, is suppressed in the following.

Combining Eqs. (1) and (2) for each of the three acoustic measurements, and using Eq. (3) for the reciprocal transducer T3, yields [10]

$$S_V^{T3} = \left[ \frac{1}{JZ^{T3}} \frac{H_{15}^{VV\,(2)} H_{15}^{VV\,(3)}}{H_{15}^{VV\,(1)}} \frac{d_2 d_3}{d_0 d_1} e^{ik(d_2 + d_3 - d_0 - d_1)} \right]^{\frac{1}{2}}, \tag{5}$$

which is the transmitting voltage response of the transducer T3. Measurement of the electrical input impedance of T3, $Z^{T3}$, is needed in addition to the acoustic measurements.

If the transmitter and receiver are reciprocal and identical, a two-transducer reciprocity calibration can be performed with a single acoustic measurement [9, 11]. Solving for measurement #3 then yields

$$S_V^{T3} = \left[ \frac{H_{15}^{VV\,(3)}}{JZ^{T3}} \frac{d_3}{d_0} e^{ik(d_3 - d_0)} \right]^{\frac{1}{2}}. \tag{6}$$

An open-circuit receiver measuring the free-field sound pressure in the far-field of the transmitter in a lossless medium is impossible to achieve in a real measurement situation, but is assumed in Eqs. (5) and (6). Some of these conditions can be approximated using theoretical models to correct the measurements.

A diffraction correction can be used to account for near-field effects. In this work the diffraction correction defined by Khimunin [12] is used. This is based on theory for a uniform piston source in a rigid baffle of

infinite extent and is hence a simplification. A pressure, $p_{meas}(d)$, measured in the near-field at a distance $d$, is corrected to a far-field equivalent, $p_{corr}(d)$, by [10, 13]

$$\frac{p_{corr}(d)}{p_{meas}(d)} = \frac{H^{dif}(d_{ff})}{H^{dif}(d)} \frac{d_{ff}}{d}, \tag{7}$$

where $d_{ff}$ is a distance in the far-field and $H^{dif}$ is the diffraction correction. Details of the derivation can be found in [10]. This is used to correct the measured output voltage from the receiver as shown in Eq. (8).

It is also necessary to account for the effect of the coaxial cable connecting the receiving piezoelectric ceramic disk to the measurement amplifier [10]. This is done by including the coaxial cable when measuring the electric impedance of the receiving piezoelectric ceramic disk, denoted $Z'$.

The finite electrical termination of the receiver can be corrected for by using the measured electric impedance, $Z'$, in a Thévenin generator model [14] terminated in the signal amplifier with impedance $Z_{AMP}$ [10], see Eq. (8).

Losses in air are significant for the frequencies and distances of interest [10]. This is corrected for by $10^{(\alpha_{dB/m}d)/20}$ in Eq. (8), where $d$ is the measurement distance and $\alpha_{dB/m}$ is the attenuation coefficient in air calculated using [15]. The corrections are included in Eqs. (5) and (6) by replacing $Z$ with $Z'$ and $H_{15}^{VV}$ with $H_{15,corr}^{VV}$, where the latter is the corrected voltage to voltage transfer function and is given as

$$H_{15,corr}^{VV} = \frac{V_{5,corr}}{V_1} = \frac{V_5}{V_1} \frac{H^{dif}(d_{ff})}{H^{dif}(d)} \frac{d_{ff}}{d} \frac{Z' Z_{AMP}}{Z_{AMP}} 10^{(\alpha_{dB/m}d)/20}. \tag{8}$$

The reciprocity calibrations are to be compared with measurements using a calibrated B&K 4138 microphone. The magnitude of the transmitting voltage response of T3 is then given as

$$\left|S_V^{T3}\right| = \frac{\left|H_{15}^{VV}\right|}{|M_{B\&K}|} \frac{d}{d_0}, \tag{9}$$

where $M_{B\&K}$ is the free-field open-circuit receiving voltage sensitivity of the B&K 4138 microphone and $d$ is the separation distance between the coaxial transmitter and receiver.

## 3. Experimental setup

The piezoelectric ceramic disks were made of the material Pz27 [16] with approximate dimensions 20 mm × 2 mm. In addition a Brüel & Kjær 4138 1/8 inch pressure condenser microphone was used.

The electric impedance was measured using a HP 4192A impedance analyzer.

The acoustic measurement setup consisted of an Agilent 33220A waveform generator connected to a Tektronix DPO3012 oscilloscope and the transmitting transducer. Coaxial cables with a characteristic impedance of 50 Ω were used to connect the different components. The receiver was placed coaxially with the transmitter with a separation distance of 44 cm when the B&K 4138 was used as receiver and 77 cm otherwise. Pulsed sound waves were used in order to approximate free-field conditions. The separation distances were chosen to minimize electric crosstalk and acoustic reflections, while using sufficiently long signal bursts to reach steady-state. The receiver was connected to a Brüel & Kjær 2636 measurement amplifier, a Krohn-Hite 3940 frequency filter and finally to the Tektronix oscilloscope. Relative humidity and temperature were recorded using a Vaisala HMT313 probe. The measurements were performed in air at 1 atm.

## 4. FE simulation setup

The finite element simulations were performed using the simulation tool FEMP 5.0 [4, 5]. An adjusted material data set for Pz27 with complex loss [17] was used to model the piezoelectric disk radiating into air. The air was modelled without losses with $c = 343$ m/s and $\rho = 1.205$ kg/m$^3$. The meshing was performed with 5 elements per wavelength specified at 300 kHz, using 8 node isoparametric finite elements and 12 node infinite elements [4, 5]. The wavelength of shear waves was used in the piezoelectric material. $R_{inf} = 2.74$ cm (see [4, 5]). The transmitting voltage response was calculated at 1000 m and extrapolated spherically back to the reference distance $d_0 = 1$ m.

## 5. Preliminary results

Figure 1 shows preliminary results for the transmitting voltage response of the transducer T3 obtained by the modified three-transducer reciprocity calibration, compared to measurement with a calibrated microphone and FE simulation, for the frequency range 50 kHz to 180 kHz.

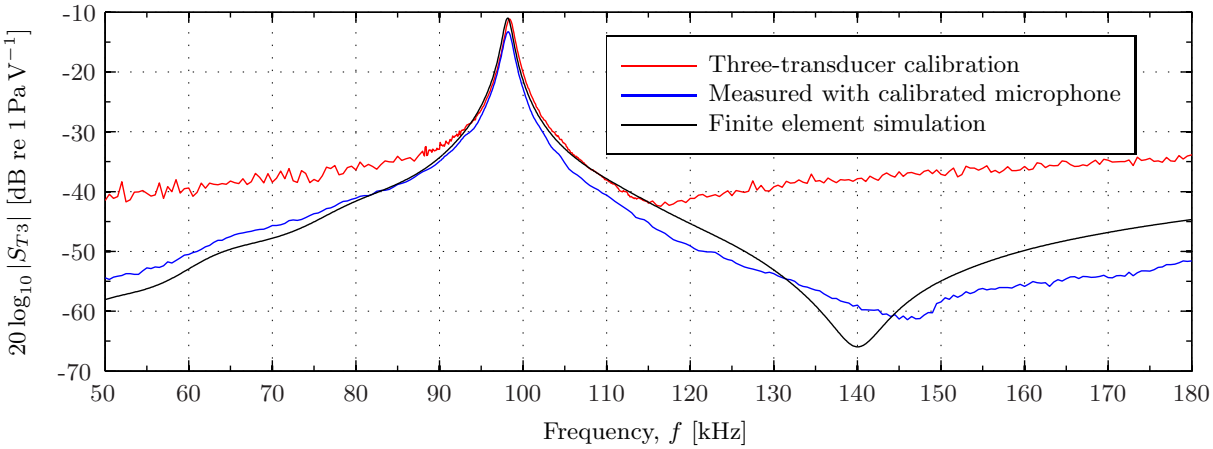


Figure 1: Magnitude of the transmitting voltage response of the piezoelectric ceramic disk T3 for the frequency range 50 kHz to 180 kHz. The measurements were performed with a 2 $V_{pp}$ drive voltage on the transmitter.

The magnitude of the transmitting voltage response when measuring with the B&K 4138 microphone is seen to be below that of the three-transducer calibration for the frequency range shown. In the frequency band 87 kHz to 115 kHz the measurements agree within 3.5 dB. The signal to noise ratio (SNR) is insufficient for the three-transducer reciprocity calibration method, even at the resonance, and needs to be improved.

The results from the FE simulation shows qualitative agreement with the results from three-transducer calibration at the first radial mode. The accuracy of the FE simulations depend on the accuracy of the material parameters.

## 6. Discussions and conclusions

Preliminary results have been shown for a three-transducer reciprocity calibration of a piezoelectric ceramic disk radiating in air at 1 atm. These have been compared to measurement with a calibrated B&K 4138 microphone and to FE simulations. The three-transducer reciprocity method shows promising results for a frequency band at the first radial mode.

The main limitation in the measurements is a low SNR. Other factors that affect the measurement is non-linearity, mainly in the piezoelectric material, distance measurements, reflections, and alignment of the transducers [10]. The use of a simplified diffraction correction model also affects the accuracy of the calibration.

The measurements shown here was performed with 2 $V_{pp}$ drive voltage, but measurements have also been performed with 20 $V_{pp}$ drive voltage. The higher voltage improves the SNR and expands the frequency band, but also increases the nonlinear effects, especially at resonance [10].

A more detailed analysis and additional results can be found in [10].

Further work is needed to improve the accuracy of the three-transducer reciprocity calibration method and extend the method to calibrations above the calibrated frequency range of the B&K 4138 microphone. Reduction of the noise level and improved signal processing, together with construction of more sensitive piezoelectric transducers with reduced nonlinear effects, are expected to be of importance in the further work.

## Acknowledgements

This work is done as part of a Master project by the first author [10], supported by The Michelsen Centre for Industrial Measurement Science and Technology.

**References**


[1] Bruel & Kjær, "Product data: 1/8″ pressure-field microphone - Type 4138", (2008).

[2] Brüel & Kjær, *Condenser microphones and microphone preamplifiers for acoustic measurements - Data handbook* (1982).

[3] M. J. Anderson and X. Liu, "Use of reciprocity to characterize ultrasonic transducers in air above 100 kHz", J. Acoust. Soc. Am. **103**(1), 446–453 (1998).

[4] J. Kocbach, "Finite element modeling of ultrasonic piezoelectric transducers", PhD thesis, Department of Physics, University of Bergen, Bergen, Norway (2000).

[5] J. Kocbach, P. Lunde, M. Vestrheim, and R. Kippersund, "Finite element modeling of ultrasonic piezoelectric transducers: Extension of FEMP to 3D analysis", CMR Report no. CMR-06-A10046-RA-01, Christian Michelsen Research AS, Bergen, Norway (December 2006).

[6] "ANSI S1.10-1966 (R1976) - Method for the calibration of microphones", American Institute of Physics (1976).

[7] "ANSI S1.20-1988 (R2003) - Proceedures for calibration of underwater electroacoustic transducers", American Institute of Physics (2003).

[8] "ANSI S1.1-1994 (R2004) - Acoustical terminology", American Institute of Physics (2004).

[9] M. Vestrheim, "PHYS 272 - Akustiske transdusere", Lecture notes, Department of Physics and Technology, University of Bergen, Bergen (2007).

[10] E. Mosland, Master thesis, Department of Physics and Technology, University of Bergen, Bergen, Norway (in preparation, 2013).

[11] R. J. Bobber, *Underwater electroacoustic measurements* (Naval Research Laboratory, Washington, D.C.) (1970).

[12] A. S. Khimunin, "Numerical calculation of the diffraction corrections for the precise measurement of ultrasound absorption", Acustica **27**, 173–181 (1972).

[13] M. Vestrheim, "Private communication", Department of Physics and Technology, University of Bergen, Bergen, Norway (2013).

[14] M. Vestrheim, "PHYS 373 - Akustiske målesystem", Lecture notes, Department of Physics and Technology, University of Bergen, Bergen (2008).

[15] "ANSI S1.26-1995 (R2009) - Method for calculation of the absorption of sound by the atmosphere", American Institute of Physics (2009).

[16] Ferroperm Piezoceramics A/S (now a member of Meggitt's Sensing Systems division), "High quality components and materials for the electronic industry", DK-3490 Kvistgård (2012).

[17] V. Knappskog, "Radiellmode svingninger i piezoelektriske ultralydstransdusere for luft. Målinger og endelig element analyse", Master thesis, Department of Physics and Technology, University of Bergen, Bergen, Norway (2007).